ELECTRON MICROSCOPY STUDIES OF INSOLUBLE INORGANIC MATERIALS GROWN IN GELS

by

JARIAH ABDULLAH

(B.Sc. al-Azhar, Cairo,

M.Sc. Fairleigh Dickinson, New Jersey)

THESIS SUBMITTED TO

THE UNTVERSITY OF GLASGOW

FOR THE DEGREE OF DOCTOR OF PHILOSOPHY

*** June 1988 ***

IN THE NAME OF GOD THE MOST COMPASSIONATE

THE MOST MERCIFUL

DECLARATION

This thesis is a record of the work carried out by me in the Department of Chemistry at Glasgow University under the supervision of Dr. Paul .S. Braterman and Dr. Thomas Baird. Some of the work described has appeared in the following papers:-

(1) Jariah Abdullah, Thomas Baird, and Paul S. Braterman (1986) "Precipitation Within Gels and the Morphology of Inorganic Colloids" J. Chem. Soc. Chem. Commun., 256-257.

(2) Jariah Abdullah, Thomas Baird, Paul S. Braterman, and Mehmet Kaya (1987) "Combining Two or More Techniques: Gel Growth, Gel Feedstock, and Precipitation from Homogeneous Solution" Journal of Crystal Growth, 83, 449-452.

Which are included at the end of this thesis. This work has not been submitted in any previous application for a degree.

ACKNOWLEDGEMENTS

This study was carried out in the Department of Inorganic Chemistry, the University of Glasgow, under the direction of Professor D.W.A. Sharp.

I would like to express my profound thankfulness and gratitude to my academic supervisors Dr. P.S. Braterman, for his learned guidance, help, and encouragement throughout the course of this study, and to Dr. T. Baird for his constant help, discussions, and useful guidance throughout this study especially in the employment of electron microscopic techniques (January, 1985 to June, 1988). Indeed, their advice and criticism have been a great value. However, whatever mistakes, if any, and unanswered questions are attributable to my own understanding of the problem.

I should also thank Dr. M. Kaya of Firat University, Turkey, for his preparing the precipitates of the metal carbonates and silicates. I also thank Mr. David Thom, a technician, for his valuable help. My thanks also extended to all Ph.D. colleagues.

My thank also goes to Johnson Matthey Chemicals Limited, U.K., for lending me Pt and Pd salts.

This study was made possible by the study award granted to me by Universiti Kebangsaan Malaysia and Malaysian Public Services Department.

I am very grateful to the authority of the Queen Mother´s Hospital for giving me facilities to use word processor during admitted there due to a complicated pregnancy.

To Miss Z. Abdullah, who from the outset of this work, took trouble but dedicated and patient in helping me looking after the children and doing some household works. May God bless and reward her with best rewards.

This work is dedicated to my beloved parents for their constant supports to pursue higher knowledge and truth of which this is a partial reflection.

Finally, I must thank my husband, a Ph.D. student at Edinburgh University, for his continuous support, encouragement, and keeping my spirit high without whom this work might not have been in the present form. I also thank all my children, who though still young, understand and appreciate the nature of my work. Indeed, their presence with me has made my stay, in this country, feel like home.

Jariah Abdullah

Glasgow,

18th June, 1988.

S U M M A R Y

The fascinating morphologies of metal oxides, oxyhydroxides, carbonates, silicates, and metals grown in gels have been observed in the present study. Morphologies resulting from some metal compounds grown in mobile solutions have been also studied for the purpose of comparison.

Silica, carrageenan and mixed gel were widely used as particle growth media. Several alkali sources have been used as the precipitating agent.

The colloidal particles from metal ions (Ag^{1+}, Al^{3+}, Ba^{2+}, Ca^{2+}, Cd^{2+}, Co^{2+}, Cu^{2+}, Fe^{3+}, Mg^{2+}, Mn^{2+}, Ni^{2+}, Pb^{2+}, Pd^{2+}, Pt^{2+}, Sr^{2+} and Zn^{2+}) grown in gels were observed and their morphologies and diffraction patterns studied by transmission (and in some cases, scanning) electron microscopy.

Hydrolysis of urea and hexamine solutions were used for homogeneous precipitation of metal salt solutions in silica gel at higher temperature (85-90°C).

Double diffusion at room temperature was used to grow precipitates from silver(I), copper(II) and iron(III) compounds.

Iron oxyhydroxide (ferrihydrite) was grown in the form of hair-like bundles under various conditions of gels and alkali source solutions, using 0.1M $NH_4Fe(SO_4)_2.12H_2O$ solution.

Seeding with ferrihydrite within the mixed gel gave long fibrils extending from the seeds (ferrihydrite). The possible mechanisms of bundle and fibril formation are discussed.

Goethite, α-FeOOH, seems to be produced only by transformation of ferrihydrite on aging within carrageenan gel, effect of heat, or hydrolysis of urea at 85° C.

Ferrihydrite and goethite associated with kaolinite were formed by aging ferrihydrite within carrageenan gel containing suspended kaolinite.

Bowtie, rod-like and crumpled sheet morphologies were observed from copper compounds grown in carrageenan gel, whereas rod-like structure obtained in mobile solutions developed to very thin sheets with serrated edges by aging in the solution. The possible mechanism of the bowtie formation is discussed.

Silver metal grew as dendritic crystals with open branches in silica gel, whereas cubic crystals were obtained in mobile solutions.

Loosely aggregated particles (semi-geometrical shapes) from platinum metal formed by homogeneous precipitation in silica gel, at room temperature, whereas some palladium particles had developed to well defined shapes at an early stage of precipitation.

Metal carbonates formed homogeneously in silica gel by hydrolysis of urea are comparatively large particles. Barium and strontium carbonates formed dendritic objects ($\sim$ 3mm long). Calcium carbonate (calcite) formed rhombohedral crystals. Cadmium oxide, identified by diffraction was probably formed by decomposition of carbonate in the beam; it showed small crystals. Basic lead carbonate crystals exhibited thin platelets $\sim 4\mu m$ with twin boundaries and many intensity contour lines. Zinc compounds showed a crumpled sheet morphology identification of the compounds was not possible as only diffuse diffraction patterns were obtained.

Morphologies of metal silicates formed in silica gel by hydrolysis of hexamine are as follows:

Circular arrays of dendritic $PbSiO_3$ formed in silica gel. Co_2SiO_4 and Ni_2SiO_4 form a crumpled sheet morphology. Aluminum silicate shows oval shaped crystals consisting of a network of small particles. $MgSiO_3$ is a thin rhombus crystal. Zn_2SiO_4 gave a parallelogram morphology which has the electron diffraction of a single crystal, together with unidentified rings.

Small crystals of ρ-MnO_2 were obtained by hydrolysis of urea or hexamine in the presence of Mn^{2+} and air, whereas wide ranges of crystals were formed by oxidation with $KHSO_5$ solution and small crystals associated with silica gel are formed by oxidation with $NaIO_4$ solution.

CONTENTS

page

DECLARATION i

ACKNOWLEDGEMENTS ii

SUMMARY iv

Chapter One: Introduction

1.1 Purposes of the Present Study 1

1.2 Gel Method 2

1.3 Gel Materials 4

1.4 Crystallisation 13

1.5 Hydrolysis of Metal Salts 21

Chapter Two: Experimental

2.1 Transmission Electron Microscope (TEM) 28
2.1.1 Image Formation and Contrast 29
2.1.2 Factors Limiting Retrieval of Formation 31
2.1.3 Electron Diffraction 36

2.2 Materials Used 39

2.3 Preparation of Gels 40

2.4 Gel Plug Preparation 42

2.5 Double Tube Diffusion Method 42

2.6 Preparation of Solutions 42

2.7 Preparation for Precipitation 43

2.8 Heat Effect on Iron Oxyhydroxide within Gels 51

2.9 Homogeneous Precipitation within Silica Gel by Hydrolysis of Hexamine or Urea 52

2.10 MnO_2 within Silica Gel Using Peroxomono-Sulphuric Acid (mono K salt) and Periodate 53

2.11 Specimen Preparation for TEM 54

2.12 Specimen Preparation for Scanning Electron Microscopy (SEM) 58

Chapter Three: Precipitation of Iron Oxyhydroxides

3.1 Iron Oxyhydroxide in Gels 59

3.2 Iron Oxyhydroxide in Mobile Solutions 75

3.3 Iron Oxyhydroxide in Mixed Gel; Effect of Ferrihydrite Seeds 76

3.4 Iron Oxyhydroxide in Carrageenan Gel Containing Kaolinite 78

3.5 Dissolving Goethite in a Sample Containing Kaolinite 82

3.6 Homogeneous Precipitation of Iron Oxyhydroxide within Silica Gel by Hydrolysis of Urea 83

Chapter Four: Precipitation of Copper Compounds

4.1 Precipitation in Carrageenan Gel 84

4.2 The Morphology Formed within the Gel ... 85
4.2.1 Rod-Like Morphology 85
4.2.2 Crumpled Sheets Morphology 86
4.2.3 Bowtie Morphology Formation 87
4.2.4 Dendritic Morphology 90

4.3 Copper (II) Perchlorate in NaOH Solution 91

Chapter Five: Precipitation of Ag, Pt and Pd Metals

5.1 Silver Particles in Silica Gel 93

5.2 Silver Particles in NaOH Solution ... 94

5.3 Platinum Particles in Gels 95

5.4 Palladium Particles in Gels 98

Chapter Six: Miscellaneous Precipitations in Silica Gel

6.1 Precipitation of Metal Carbonates within the Gel by Hydrolysis of Urea 102

6.2 Precipitation of Metal Silicates within the Gel 106

6.3 Precipitation of MnO_2 within Silica Gel 110

Chapter Seven:

Conclusion 114

Further Work in Gels 119

References 120

CHAPTER ONE

INTRODUCTION

page

1.1 PURPOSES OF THE PRESENT STUDY 1

1.2 GEL METHOD 2

1.3 GEL MATERIALS 4

1.3.1 Types of Gels 4
(a) Silica Gel 5
(b) Carrageenan Gel 8

1.3.2 Growth in Gels 8

1.3.3 Growth Mechanisms in Gels 12

1.4 CRYSTALLISATION 13

1.4.1 Solubility and Supersaturation 13

1.4.2 Nucleation and Growth 15
(a) Crystal Formation 18
(b) Crystal Growth 18

1.4.3 Dendrites 19

1.5 HYDROLYSIS OF METAL SALTS 21

1.5.1 Metal (Hydrous) Oxides 21

1.5.2 Hydrolysis of Iron (III) Salts 23

1.5.3 Iron (Hydrous) Oxides 25

1.5.4 Ferrihydrite 25

1.1 PURPOSES OF THE PRESENT STUDY

The purpose of this work is to study the effect of gels (controlling mixing and suppression of nucleation especially heteronucleation) in the development of the structures and morphologies of highly insoluble inorganic materials by hydrolysis mainly at room temperature. Braterman & Baird (1984) precipitated hydrous Fe(III) oxide in silica gel; they expected the results would be similar to Matijevic's report or other reports. But the actual results has more surprising and interesting phenomena. From this important point, this present study started.

Morphologies of highly insoluble inorganic materials are interesting, because of their possible relevance to the earliest stages of evolution (Cairns-Smith, 1982), as well as their importance in sol-gel technology (Woodhead & Segal, 1984; Woodhead, 1980), catalyst preparation (Trimm, 1978), serving to explain the genesis of minerals and the growth processes which take place in nature (Barta et al., 1971), and materials science generally.

1.2 GEL METHOD

The crystallisation apparatus for the gel method is usually a simple test-tube, double test-tube, tube with fritted bottom, a U-form tube, or a modified U-tube.

The formation of crystals is accomplished by the reaction between two reagents (diffusion) in gels (sodium metasilicate gels, agar, gelatin, etc.). The basic procedures are:

(1) The gel itself contains one of the reagents. The gel is usually prepared from an aqueous solution of sodium metasilicate by adjusting the pH to between 7 and 8 with acetic acid. After the gel has set, an excess of the second reagent is placed gently on top of it without damaging its surface and allowed to diffuse, usually in a simple test-tube as shown in Fig.1.1. In addition, in order to avoid damage, the supernatant solution should be added dropwise with a pipette, allowing the drops to fall on the side of the test tube (Henisch, 1970). Clearly, the amount of product formed is fixed by the concentration of the first solution in the gel. Crystals are usually near the upper boundary of the gel and their ultimate sizes depend on the initial concentration of the first solution and the number nucleated.

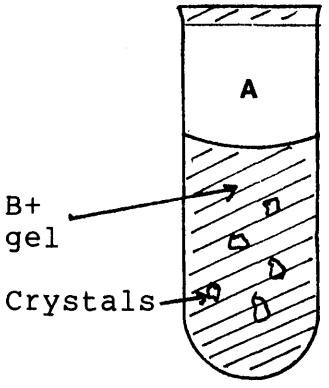

Fig. 1.1.

Test-tube

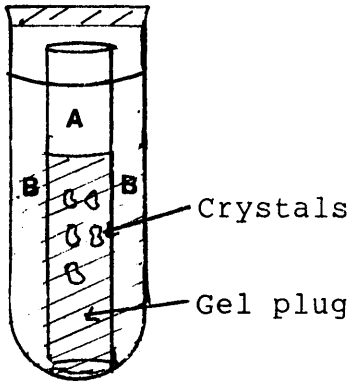

Fig. 1.2.

Double test-tube

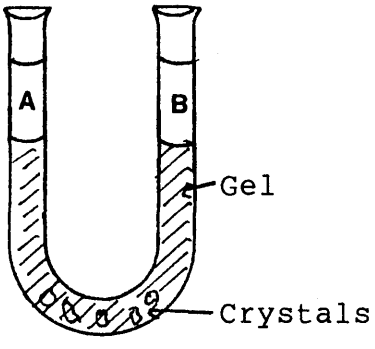

Fig. 1.3.

U-tube

Basic growth procedures. (After Henisch, 1970).
(A: 1st reagent, B: 2nd reagent).

(2) The neutral gel (free from any reagent) is set in a tube (double test tube, U-tube, or modified U-tube). The two reagents diffuse into it from two sides and precipitates form where they meet, as shown in Fig. 1.2-1.6.

The technique in Fig. 1.5 is suitable for growing cuprous halides (O´Connor et al.,1966). The advantage of this technique is to attain the steady state; the water reservoir can minimise the acidity produced by the liberated HCl, which tends to dissolve the crystals. Another advantage is for growing larger crystals in gels (O´Connor & Armington, 1967).

The modified double diffusion system illustrated in Fig. 1.6 has advantages over the U-tube; growing larger crystals in the shorter period, easy to clean the tube and eliminating of the blockage at the gel-feed solution interface (Armington & O´Connor, 1968).

Fig. 1.7 & 1.8 are two examples of hybrid gel methods which were carried out to grow calcite by Nickl & Henisch (1969). In the test tube system (Fig.1.7), sodium metasilicate solution is floated on a concentrated solution of NH_4Cl and allowed to gel before adding the supernatant $CaCl_2$ solution; the crystals grow primarily in the solution belt. In the system in Fig.1.8, the regents diffused through separate gel columns, and the entire growth medium is filtered in

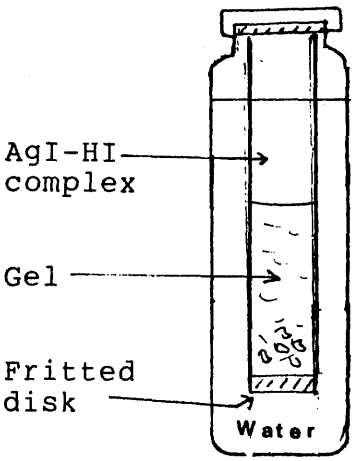

Fig. 1.4.

Double diffusion system with fritted disk.
(After Nickl & Henisch, 1969).

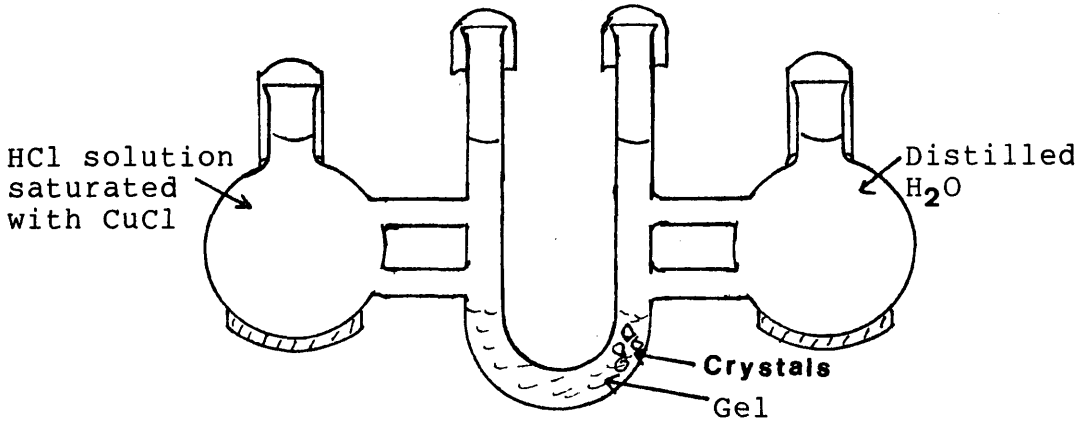

Fig. 1.5.

Reservoired U-tube apparatus for the growth of cuprous chloride crystals. (After O´Connor & Armington, 1967).

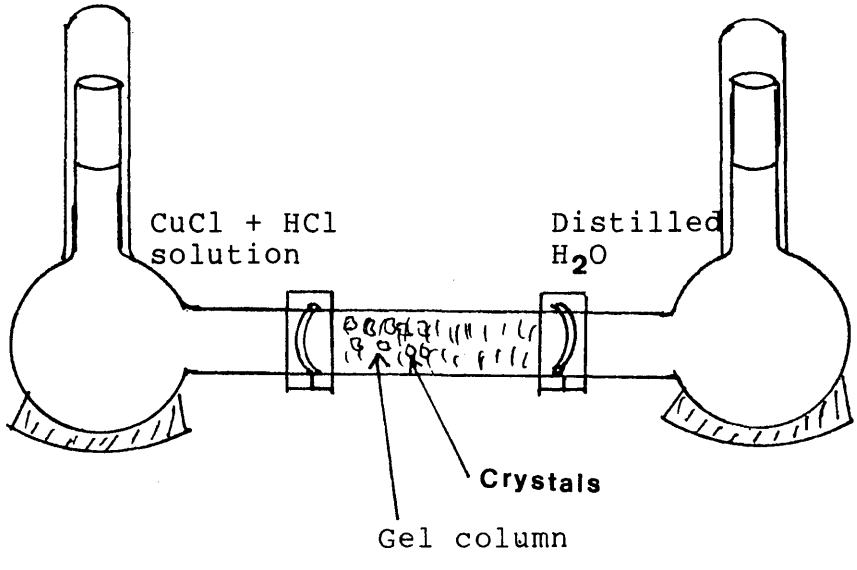

Fig. 1.6.

Modified double diffusion system with reagent reservoirs and straight diffusion column; column diameter 20 cm, length 25 cm. (After Armington & O´Connor, 1968).

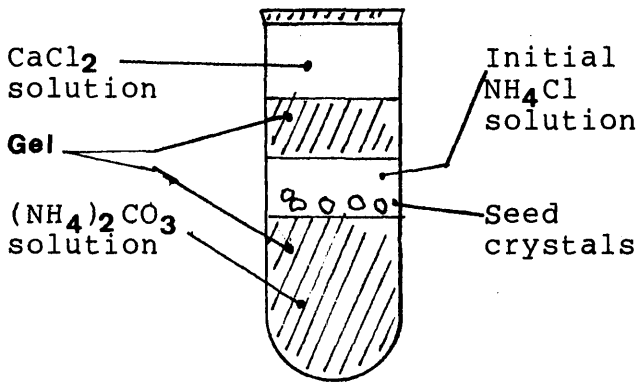

Fig. 1.7.

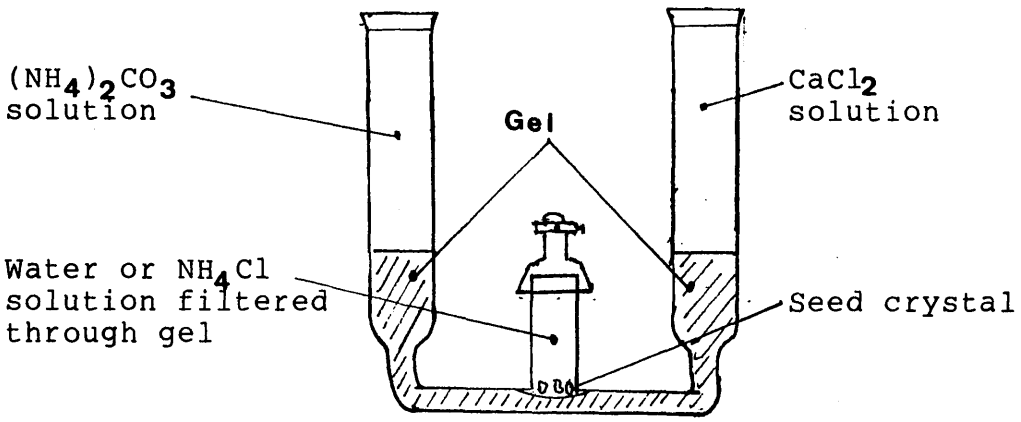

Fig. 1.8.

Systems for calcite growth by hybrid gel method. (After Nickl and Henisch, 1969).

this way. This system has the advantage that seed can be placed in the solution. They obtained clear new layers by epitaxial growth and weight increases by factors up to 10 were easily achieved.

The most important requirement is a constant ambient temperature because its variations will cause changes in the supersaturation which leads to excessive undesired nucleation. The presence of foreign nuclei in the solution used in gels may also cause of excessive nucleation. Glass, and particularly plastic, materials easily absorb ions which are released rather slowly. Brice (1986) suggested that when purity is important, reactors (test tube, U-tube, or modified U-tube) should be use for one product only.

1.3 GEL MATERIALS

1.3.1 Types of Gels

A variety of gels may be used to influence the formation of crystalline products. The usual gels (agar, gelatine and silicic acid) were employed in earlier investigations, but in general the crystals grow larger in silicic acid than the others. (Hatschek, 1912a & b; Liesegang, 1926a and Holmes, 1926). Silica gel is usually prepared from sodium metasilicate solution, agar is a carbohydate polymer derived from seaweed, and

gelatin is a substance closely related to proteins. Other gels can be formed from a variety of oleates and stearates, polyvinyl alcohol, and various hydroxides in water. (Henisch, 1970). It was Marriage (1891) who first grew crystals of lead iodide in various fruit gels and jams. Arend & Connelly (1982) reported that gel prepared from tetramethoxysilane ($Si(OMe)_4 + 2H_2O \longrightarrow SiO_2 + 4MeOH$) has several advantages of growing the crystals, for example, deuterated crystals: $KC_4H_4O_6$, (primary potassium tartrate), $(NH_4)_2ZnCl_4$, $Pb(H_{1-x}D_x)PO_4$, and $(C_{10}H_{21}NH_3)_2CdCl_4$.

The structures closest to the gels are sols but these resemble liquid more than solids, and consist of small jelly- like particles seperated by liquid phase (coagels). Gels are formed in a three-dimensional system of cross-linkages as loosely interlinked polymers. Hydrogel is the term used for a gel formed from solutions in water. The gelling process takes various times, from minutes to many days, depending on the nature of the material, concentration, temperature, etc. (Hanisch, 1970).

(a) Silica Gel

Silica gel is as adsorbent but adsorption decreases with increasing temperatures. It is highly porous in structure with enormous surface area which is ideal as

carrier (eg. for Pt) for catalysts; its surfaces can be impregnated with many metals or metal oxides. It is also chemically inert, stable in air and at high temperatures, and resistant to mechanical action. (Miller, 1931). It was at one time considered that the silicic acid gels offered the best laboratory parallel to the gel processes in nature (Holmes, 1917). However, silica gel does not resemble natural sedimentation conditions because natural muds consist of discrete clay minerals mixed with find sand, other minerals and organic constituents (Cody & Shanks, 1974).

The formation of silica gel can be regarded as initially formed $Si(OH)_4$ or a monosilicic acid (H_4SiO_4) from sodium metasilicate solution,

$$Na_2SiO_3 + 3H_2O = H_4SiO_4 + 2NaOH$$

On dilution of viscous concentrated alkaline solutions (H_4SiO_4/NaOH), smaller oligomers are formed. The species present are monomeric at concentrations below 1mM. Acidification of sodium silicate gives the hydrated oxide in the form of silica sol or silica gel. At room temperature, silica sols may remain metastable for long periods of time; often they develop into gels of $SiO_2 . nH_2O$. But on laboratory time scales at room temperature, they never arrive at the thermodynamic ideal_quartz. (Cairns-Smith, 1982, p.181).

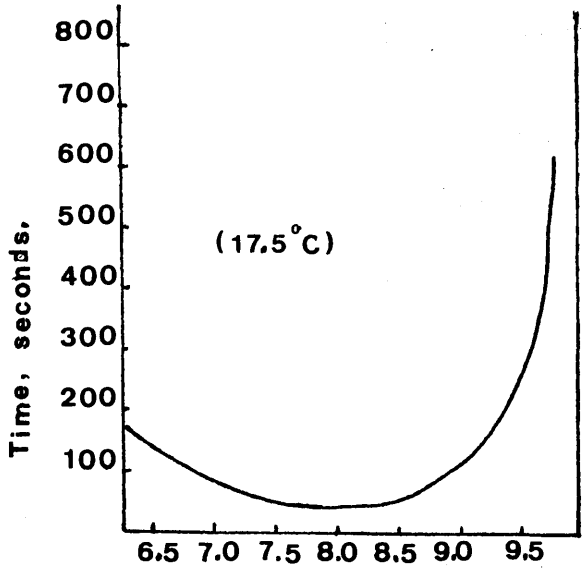

Fig. 1.9.

The effect of pH on gel time.
(After Plank, 1947).

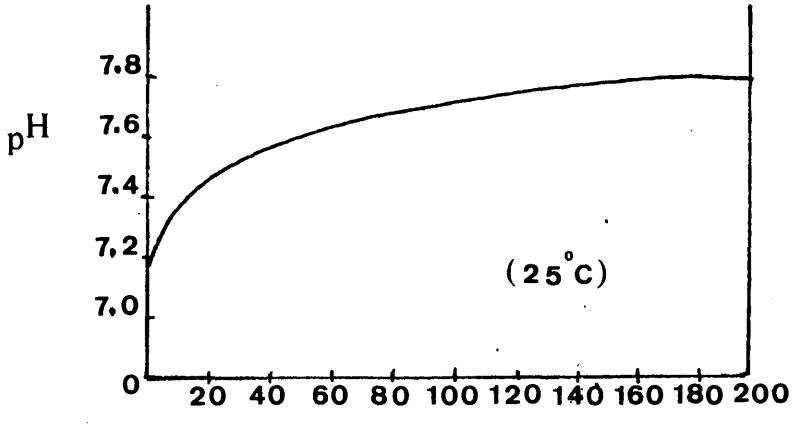

Fig. 1.10.

Syneresis time (hrs).
(After Plank, 1947).

Polymerisation of the monomers leads to a rigid, highly porous, tangled network of branching chains. Therefore, three stages are recognised:

(1) Polymerisation of monomer to form particles;

(2) Growth of particles; and

(3) The particles linking together into branched chains, then networks, and extending throughout the liquid medium, finally thickened to a gel (Iler, 1979).

The effect of pH on gelling time can be observed in Fig.1.9. which shows a minimum at about a pH of 8. Fig.1.10. shows how the pH of an initially neutral gel increases during syneresis which is probably resulting from the progressive and stabilizing hydroxyl substitution for oxygen in the polymerised structure:

$$-\overset{|}{\underset{|}{Si}}-O^- + H_2O \longrightarrow -\overset{|}{\underset{|}{Si}}-OH + OH^- \quad \text{(Plank, 1947).}$$

In addition, the most suitable consistence of the gel occurs at a water glass density of 1.04-1.06 g/cm^3, at pH of 7-8 (Barta et al., 1971).

(b) Carrageenan Gel

Carrageenan is one of the intercellular matrix polysaccharides of red seaweeds. The κ-carrageenan molecule consists of alternating D-galactose 4-sulphate and 3,6-anhydro-D-galactose 2-sulphate monomers which are occasionally interrupted with a D-galactose 2,6-disulphate or 6-sulphate (Fig.1.11). The gelling properties are due to the regular stretches which twist together to form double helices which are stabilised by hydrogen bonding between the chains. Thus, the molecules become tied together into an open three-dimensional network which may entrain more than 99% of water (Fig.1.12). The gel can be melted and reformed by heating and cooling; due to the action of the double helical tie-points in agars. (Cairns-Smith, 1982).

1.3.2 Growth in Gels

A gel in crystal growth can be characterised as a system consisting of a more or less regular and rigid three-dimensional network formed by polymerisation or polycondensation.

The principal role of the gel appears to be suppression of turbulence, nucleation, and the effect of gravity (Arend and Connelly, 1982). It is also advantageous in the gel method, it could be used to grow

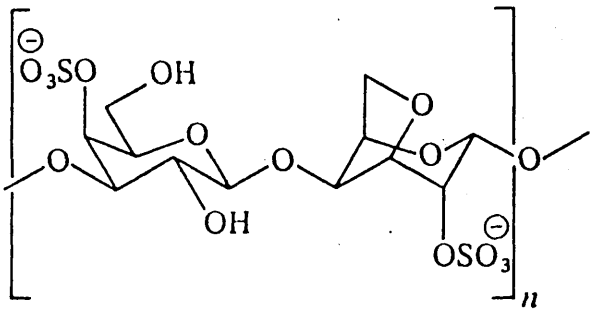

Fig. 1.11.

A regular sequence in an ι-carrageenan molecule gives rise to a double helix with a similar stretch in another molecule. (From Cairns-Smith, 1982).

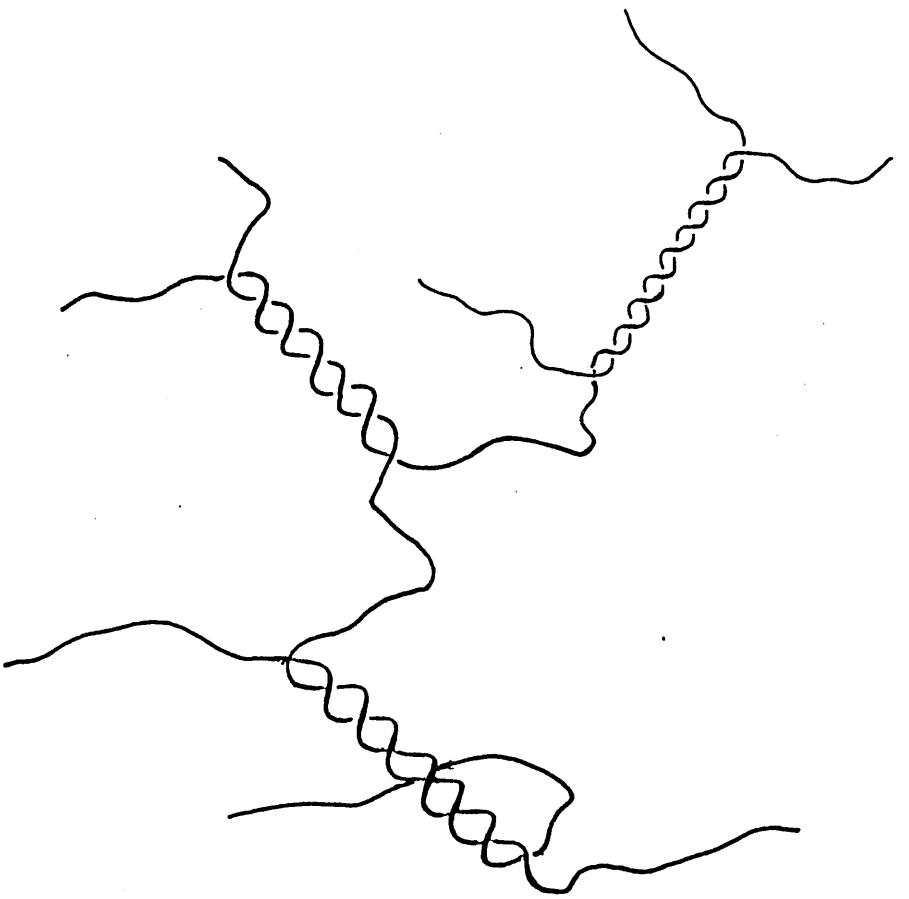

Fig.1.12.

Stretched intermolecular double-helices of ι-carrageenan form an open three-dimensional network which may entrain more than 99% water. (After Cairns-Smith, 1982).

various sorts of crystals - ionic, organic and even metallic crystals - at ambient temperatures (Barta et al., 1971). In addition, the apparatus and methods are very simple, convenient, and cheap (Armington & O´Connor, 1980).

The growth of crystals in gels was recorded since the earlier nineteen centuries or even before that by Marriage (1891) but it was greatly stimulated after the work of Henisch and co-workers in 1969-1970.

In the early work, the growth in gels became interesting subject due to the formation of rhythmic banding of precipitates (Liesegang ring) ; named after the German colloid chemist and photographer (Raphael Eduard Liesegang), who described them in 1896. Liesegang observed that concentric rings of silver dichromate were formed when he added a drop of strong silver nitrate solution on a glass plate coated with moist gelatin impregnated with potassium dichromate (Bradford, 1926). The formation of Liesegang rings has been studied widely by many scientists: Liesegang (1914), Bradford (1926), Holmes (1926). Diffusion with chemical transformation giving rise to rhythmical precipitation (Liesegang, 1926a). For details of Liesegang rings see Henisch (1988).

The formation of banded precipitates was regarded as the important matter because it may explain the veins in the quartz. The beautiful bands of gold in silica

gels are regarded as typical of the development of banded gold in quartz (Hatschek, 1911; Hatschek & Simon, 1912). Holmes (1917) obtained rainbow bands of red, blue and green colliodal gold, grown in silicic acid gel. It was formerly thought probable that almost all earth's quartz (except igneous quartz) was formed from gelatinous silicic acid (Holmes, 1926). For example, the natural growth of tourmaline and rutile in a single crystal of quartz as needles (Fig.1.13a & 1.13b). The needles were proposed to grow first when the medium was a gel. But current opinion among geologists and mineralogists is that the particular form is due to the outcome of hydrothermal growth (Henisch, 1988). The bands in agates have been predicated as a rhythmic precipitation of iron hydroxide in a pre-existant silicic acid gel, which was ageing from sol via jelly, opal, chalcedony, to quartz by the process of syneresis (Liesegang, 1926b). In addition, Liesegang (1912) observed from the experiment (gelatinisation of the silicic acid obtaining from mixing soda or aragonite crystals with diluted neutralised water glass solution) that he suggested this phonomenon as a explanation of the formation of Queensland opals, which are found in the cracks of limestone, and various other mineralogical occurrences, agate, etc.

Gel media allows crystals to grow at ambient temperature in some compounds which are difficult to

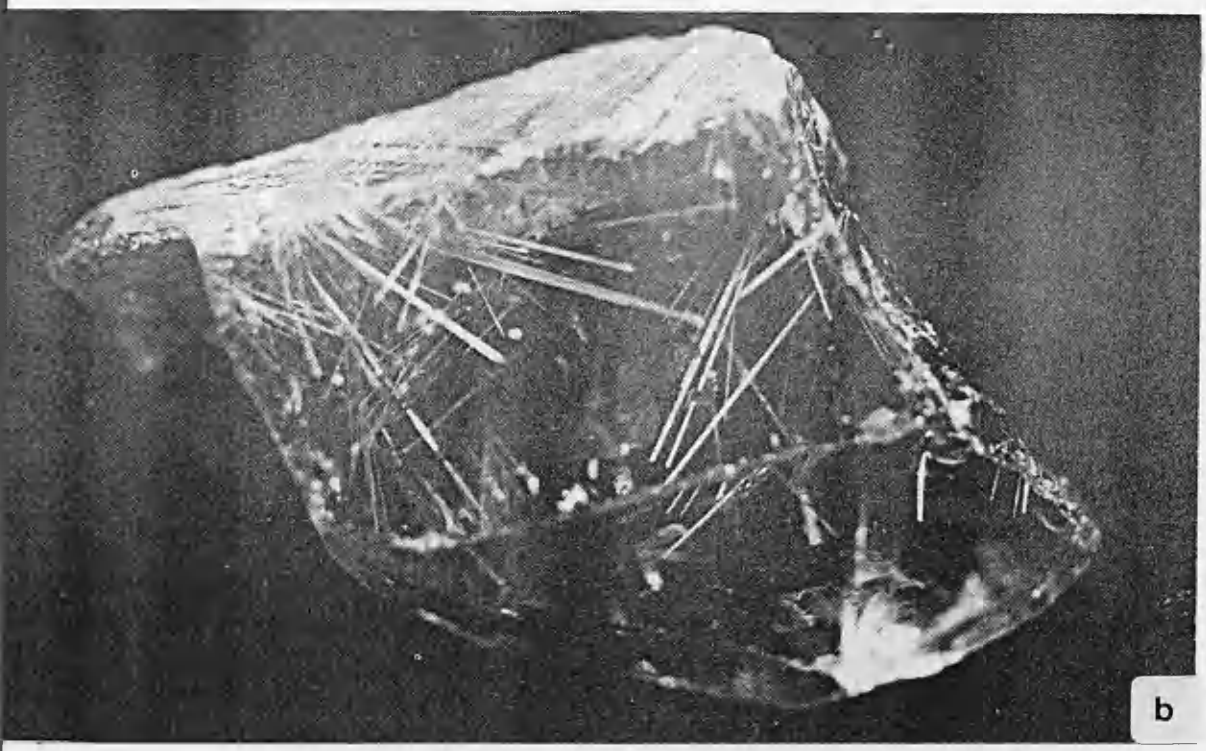

Fig. 1.13.

Natural growth in a single crystal of quartz as needles of (a) tourmaline, and (b) rutile. After Henisch (1988).

crystallise in solutions, for example, sulphide crystals are usually grown by vapour transport (Parker & Pinnell, 1968; Lendvay, 1971) and solidification from the melt (Kume et al., 1972; Steinberger et al., 1972). In spite of these methods, the crystals produced are not always good stoichiometric crystals, whereas Abdulkhadar & Ittyachan (1981) succeeded in growing the single crystals, of ZnS and PbS in silica gel from inorganic sulphur compounds with great ease at ambient temperature and they grew also AgI crystals in U-tube from silver and iodine sols, agar and silica gel were used.

There are many examples of inorganic crystals grown presently in gels: metals (gold, lead, etc.), metal carbonates, sulphates, dichromates, molybdates, halides, etc. Some examples of crystal growth in gels are as follows: Calcium tartrate, lead and silver iodide crystals were grown by Halberstadt & Henisch (1968). Silver iodide crystals were grown by Suri et al.(1970) and Caslavsky & Suri (1970). Silver acetate crystals were grown by Boulin & Ellis (1970). Cuprous halide crystals were grown by Armington & O'Connor (1968). Calcium sulphate crystals were grown by Cody & Shanks (1974). Crystals of Calcium phosphate (brushite, $CaHPO_4 . 2H_2O$) were grown by LeGeros & LeGeros (1972). Lead carbonate crystals were grown by Franke et al. (1981). Lead dendrites were grown by Liaw & Faust (1972). Group II-VI crystals were grown by Blank & Brenner (1971).

Calcium carbonate by Nickl & Henisch (1969). Barium molybdate and carbonate were grown by Cho et al. (1977). Barium and strontium sulphates were grown by Patel & Bhat (1972). Henisch (1988) gives many other examples. The most interesting observation from the crystal growth's habit is that of García-Ruiz & Amorós (1981), who grew the barium and strontium carbonates in silica gel at higher pH (10.2) at 20°C. After dissolving the gel, they observed the crystals impregnated in a polysilicate membrane that acts as a template for the crystal growth. It is postulated that the membrane determines the morphology of the aggregate, and this phenomenon is relevant to some theories of the origins of life (see also Cairns-Smith, 1982).

1.3.3 Growth Mechanism in Gels

The process involves the creation of a supersaturation of the product by diffusion of two reagents into gels. In this method, diffusion control sets up concentration gradients of all ions involved. For example, in the case of only one type metal ion and one type alkali source have been used; as in the present study. Then, the concentration gradients of the metal ion from the top of the tube, and hydroxide ion at the bottom (Fig. 1.14a & 1.14b).

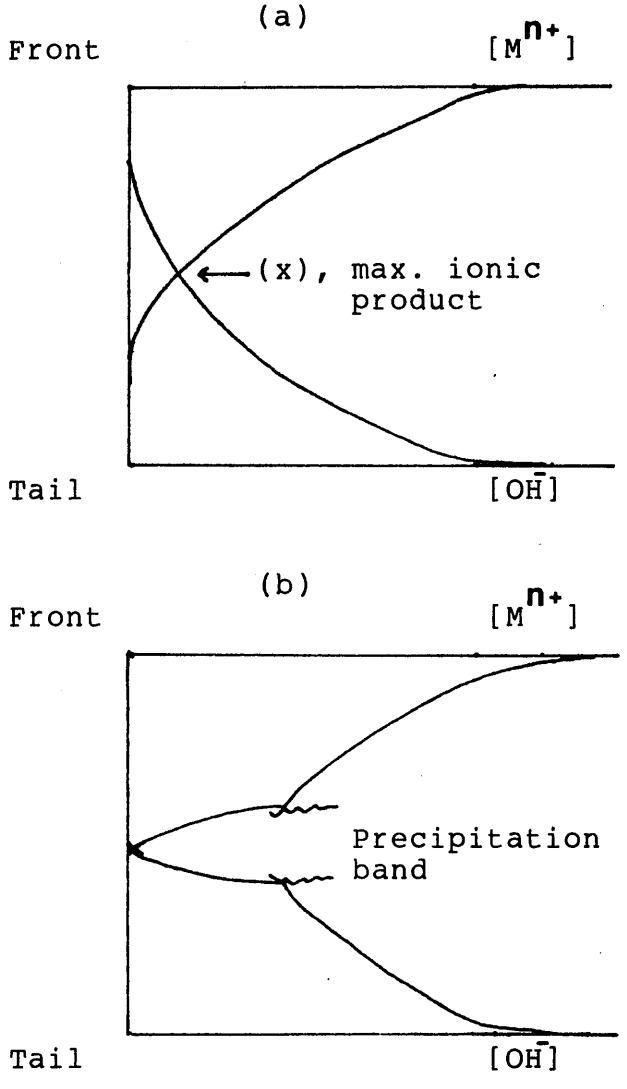

Fig. 1.14.

Concentration gradients due to controlled diffusion in the gel plug.

Fig. 1.14a, point (x) represents the position in the gel plug where there is maximum ionic product (before nucleation). A considerable degree of supersaturation may exist but nucleation has not occurred. In Fig. 1.14b, nucleation has occurred and subsequent growth lowers the concentrations in the local area of the band of nuclei.

1.4 CRYSTALLISATION

The deposition of a solid crystalline phase mainly relies on the degree of supersaturation or supercooling in the system. The crystallisation operation may comprise in three basic steps:

(1) supersaturation or supercooling;

(2) formation of crystal nuclei; and

(3) growth of the crystals. (Mullin, 1961).

1.4.1 Solubility and Supersaturation

The state of supersaturation is an essential feature of all crystallisation operations. Ostwald (1897) first introduced the term labile (unstable) and metastable (supersaturation). A supersaturated solution contains more dissolved solid than a saturated solution. Ostwald (1900) first introduced the relationship between

particle size and solubility in form of a thermodynamic equation which was later corrected by Freundlich (1909) as shown below

$$\ln \frac{c_1}{c_2} = \frac{2 M \sigma}{RT \rho} \left(\frac{1}{r_1} - \frac{1}{r_2}\right)$$

where

c_1 and c_2 = solubilities of spherical particles of radius r_1 and r_2, respectively

R = gas constant

T = absolute temperature

ρ = density of the solid

M = molecular weight of the solid in solution

σ = surface energy of the solid particle in contact with the solution.

A coefficient or degree of supersaturation S can be expressed by

$$S = \frac{c}{c^*}$$

Where c is the concentration of the solution and c^* is the equilibrium saturation concentration at the same temperature. Therefore, $S > 1$ indicates supersaturation, $S = 1$ denotes a saturated solution, and $S < 1$ indicates undersaturation. (Mullin, 1975).

The initial rate of precipitation correlates with relative supersaturation as given by von Weimarn's equation:

$$W = k \frac{(Q-S)}{S} = k R_s$$

where k = constant

Q = the instantaneous concentration of solute

S = the equilibrium solubility

R_s = relative supersaturation (von Weimarn, 1925).

1.4.2 Nucleation and Growth

A cluster (crystals, aggregates, dendrites, etc) is formed initially by a process of nucleation and growth from individual atoms or molecules. As time progresses, more clusters are nucleated and then clusters grow, coalesce, aggregate, and finally the clusters are formed in different shapes and types according to the nature of atoms or molecules, condition in the system, and the technique used.

Nucleation and growth process of metals have been studied by depositing atoms (vapour or solution) on the substrates. An example is the nucleation of gold metal on alkali halide (NaCl), as a substrate at high temperature (250° C). (Venables & Price , 1975). The nucleation and growth processes can be illustrated as below:

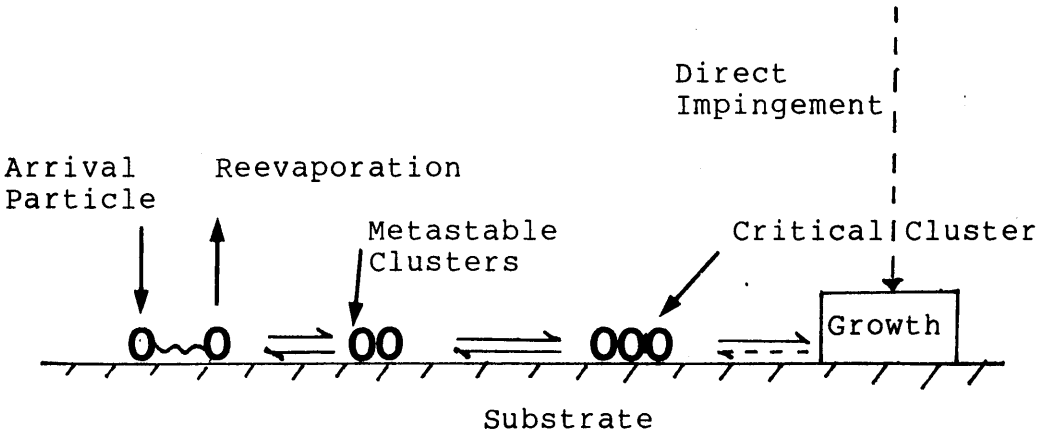

Fig.1.15. Processes in the nucleation and Growth of crystals on a substrate. (From Venables & Price, 1975).

These processes can be compared with the nucleation and growth in gels; gels act as substrates which are mechanically strong enough to support the crystals.

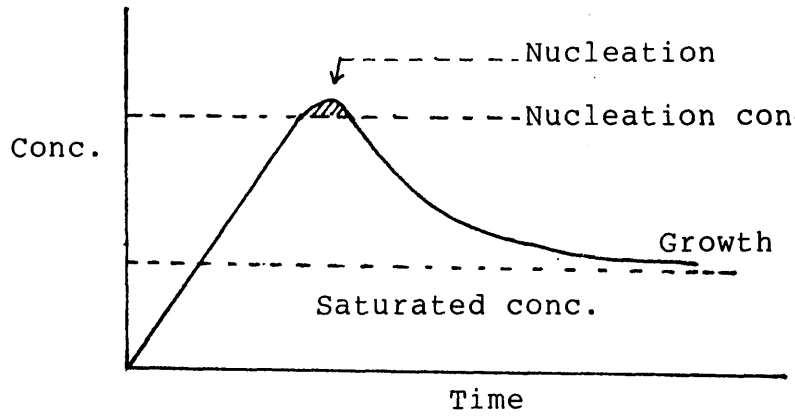

Fig.1.16. The separation of nucleation and growth period leads to a monodisperse sol.

Fig.1.16 based on La Mer's work (1950) shows that if the material for the particles is supplied continuously (slow rate flow) and the nucleation concentration is sufficiently far above the saturation concentration, a short burst of nucleation may rapidly lower the concentration below the supersaturation needed for nucleation; further material will only cause growth of the existing particles, without any new ones being formed. This process has been illustrated in the present study by growing ferrihydrite on ferrihydrite seeds within mixed gel. (Sec. 3.3.1 & 3.3.2).

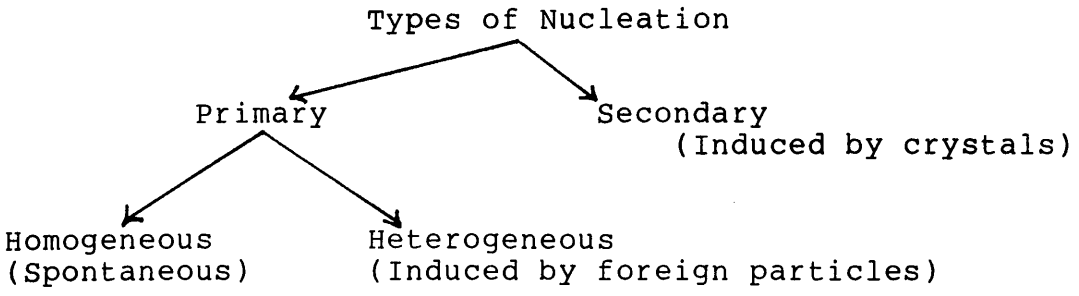

Fig.1.17. Types of nucleation (From Mullin, 1975).

The classical theories of nucleation based on homogeneous systems (Fig.1.17) can be expressed the rate of nucleation, J, as

$$J = A \cdot \exp\left[-K (\log S)^{-2}\right]$$

where A and K are constants and S is the supersaturation but they are inapplicable to industrial conditions (predominantly heterogeneous nucleation). Thus, the rate of nucleation from simple empirical relationships can be simplified to

$$J = K_n (\Delta c)^m$$

where K_n is a constant, m (>2 & ≤9) is the order of the nucleation process depending on the physical properties and hydrodynamics of the system, and $\Delta c = c - c^*$. (Mullin, 1975).

A diagram of the nucleation rates and particle growth depend on relative supersaturation as

shown in Fig.1.18. below:

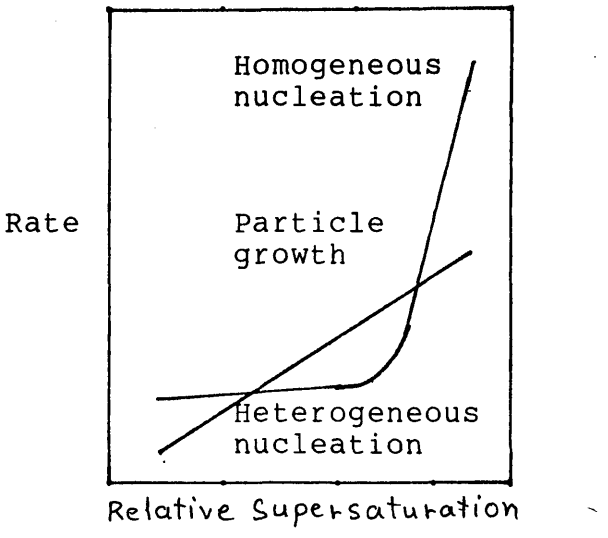

Fig.1.18. The dependence of the rates of nucleation and particle growth on relative supersaturation. (After van Rheenen et al., 1987).

(a) Crystal Formation

It is known that crystals can be classified to the seven general systems. These systems (structures) may be distorted (modified) according to the rate of growth and other factors (impurity, degree of supersaturation, solvent, etc). For example, the crystals may grow more rapidly in one direction giving a needle-shaped crystal (acicular morphology), while a stunted growth gives a flat plate-like crystal (tabular, platy or flaky morphology). Rapid crystallisation, which may produced by the sudden cooling or seeding of a supersaturated solution, generally leads to the formation of needle crystals. (Mullin, 1965).

(b) Crystal Growth

The particles larger than the critical size (as stable nuclei) formed in a supersaturated or supercooled

system will begin to grow into crystals of visible size. The larger particles will grow at the expense of the smaller ones (Oswald ripening), which have a higher solubility and vapour pressure.

The mass rate of crystallisation, R is as below:

$$R = K_g (\Delta c)^g$$

where g (≈1→2) is the order of the growth process and K_g is the growth rate constant. (Mullin, 1975).

1.4.3 Dendrites

The term dendrite, "tree-like", was first introduced to the world of crystal growth by Tschernoff, 1879 (see Smith 1965); this morphology was found in the centre of metal ingots, as in Fig.1.19. The dendritic morphology is frequently produced by the processes of rapid crystallisation from supercooled melts, supersaturated solutions and vapours. The main stem grows rapidly in a seeded-supercooled system, and primary branches grow at a slower rate out of the stem at a later stage, at some regular angles. In some cases, small secondary branches may grow slowly out of the primaries. The branches may cease and the pattern becomes crystalline material. (Mullin, 1961; see also Ch.V, Plate 5.1).

The dendritic phenomenon is suggested as irreversible aggregation of many separate small elements to form large clusters, which can be seen in many

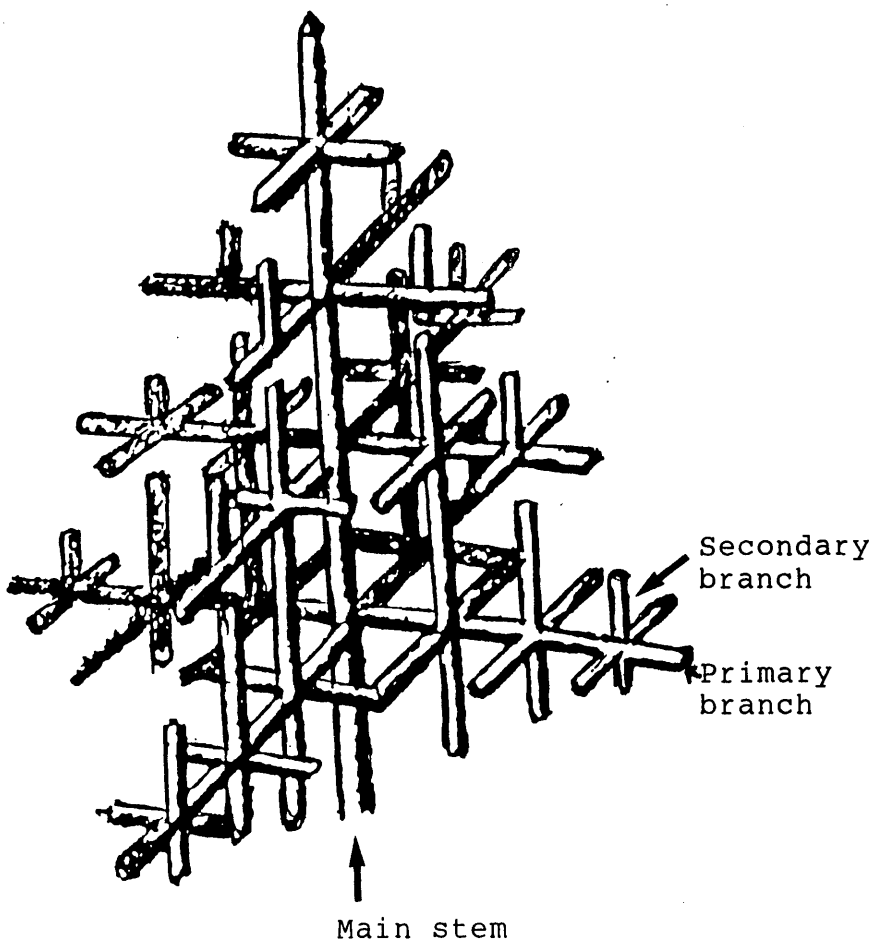

Fig.1.19.

Original sketch of a dendrite in a cast metal ingot by Tschernoff (1879). [After Smith, 1965].

fields; aerosol and colloidal physics, polymer science, material science, immunology, phase transitions, etc. (Matsushita et al., 1984).

Aggregation is an irreversible physical process in which initially dispersed particles or microaggregates stick together by attractive forces, so that the size of the aggregate increases with time.

Recently (~last 7 years) much work has been explored in this type of aggregation using the diffusion-limited-aggregation processes (DLA) by computer simulations. (Witten & Sander, 1981,1983 and Meakin, 1983). The patterns produced by DLA processes are characterized by the open, random, and chain-like structure are described as fractals (Matsushita et al., 1984; Brady & Ball, 1984 and Mandelbrot, 1982). The mathematical concept of fractal permitted a quantitative description of the aggregated structure, generally considered as too complicated in the past. (Julien & Botet, 1987).

1.5. HYDROLYSIS OF METAL SALTS

Hydrolysis of metal salt solutions has been studied for many years, as early as 1907 by Werner & Pfeiffer. They recognised that the hydrolysis of metal ions was the result of deprotonation of the co-ordinated water molecules. The process of hydrolysis may produce metal oxides, hydrous oxides, oxyhydroxides or hydroxides depending on temperature and pH.

1.5.1 Metal (Hydrous) Oxides

Metal (hydrous) oxides are accounted as great significance in the families of inorganic compounds which appear in nature as many minerals. The large surface areas of metal (hydrous) oxides may be used as catalyst supports (Britz & Nancollas, 1969). They are used in numerous applications such as catalysts, catalyst carriers, pigments, coatings, fillers, etc. The end product of metal corrosions consist of metal (hydrous) oxides with various compositions and morphologies due to their sensitivities to a number of parameters; the temperature, pH, and the presence of different anionic species. Therefore, these compounds have been continuously investigated by chemists and colloid scientists.

In order to generate the colloidal metal (hydrous) oxides, it is necessary to control the process of hydroxylation of metal ions. The common written equation is as follow:

$$M^{z+}(aq) + z\,OH^{-}(aq) = M(OH)_z(s)$$

Among the examples for the formation of the complex precursors to nucleation of metal (hydrous) oxides are as follows:

(1) When assuming only hydroxide ions present in hydroxylation, the mechanism of precipitation would be

$$n[M(H_2O)_p]^{z+} \xrightarrow{OH^-} [M_n(H_2O)_{np-m}(OH)_m]^{(nz-m)+} \xrightarrow{OH^-} nM(OH)_z$$

The complexes act as precursors to nucleation and consequently to the particle growth. But not all complexes in solution need to participate in the formations of the solid phase.

(2) Temperatures accelerate the process of hydroxylation which involve deprotonation of hydrated metal ions according to

$$n[M(H_2O)_p]^{z+} \longrightarrow [M_n(H_2O)_{np-m}(OH)_m]^{(nz-m)+} + mH^+$$

Thus, by adjusting the initial pH of the solution and the temperature, it is proposed the possibility to

generate the complexes. The hydroxylation process can (sometimes) be accelerated by the homogeneous generation of hydroxide ion (decomposition of urea) (Matijević, 1981).

1.5.2 The Hydrolysis of Iron (III) Salts

Hydrolysis of ferric ions at room temperature produces $Fe(OH)^{2+}$, $Fe(OH)_2^{+}$, $Fe_2(OH)_2^{4+}$ and $Fe_3(OH)_4^{5+}$ (Lamb & Jacques, 1938; Biedermann & Schindler, 1957; Feithnecht & Michaelis, 1962). It has been reported that ferric hydroxide has a strong tendency to form supersaturated solutions; precursors to solid phases

$$Fe^{3+} + 2H_2O \rightleftharpoons FeOOH(s) + 3H^{+}$$

For example, the precipitation reaction attains a steady state after about 200 hours; no Fe^{3+} and H^{+} could be detected (Biedermann & Schindler, 1957; Sylva, 1972).

The solid phase may commonly contain the original anion; for instance, ferric nitrate solutions give $Fe(OH)_{2.35}(NO_3)_{0.65}$. Sulphate, however, is an exception (fortunately for this work) (Fox, 1988).

Iron complexes (and from other metal complexes) commonly are considered to dimerise via oxo (a) or hydroxo (b) bridging (water molecules are not shown) for example,

(a) (b)

(Schugar et al., 1967).

The probable structure of a diamagnetic dimer is proposed by Mulay & Selwood (1955) as

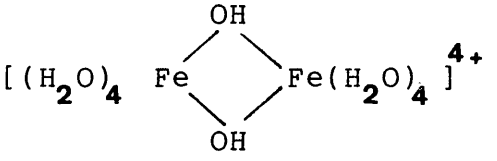

Addition of NaF and subsequent titration with HCl to the hydrolysis of Fe(III);

$$8Fe(NO_3)_3 + 11Na_2CO_3 + 5\,H_2O \longrightarrow$$
$$2[Fe_4O_3(OH)_5]NO_3 + 22NaNO_3 + 11CO_2$$

demonstrated the production of 5 moles of NaOH per mole of tetramer. Therefore, Schugar et al. (1967) interpreted that the tetramer contained 5 hydroxyl groups in the coordination sphere as:

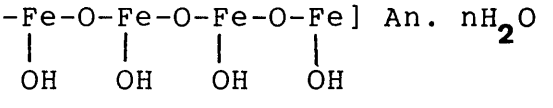

where An is a monoanion.

It is well known that heating salts solutions accelerates metal hydrolysis and promotes polynuclear complex formation (Matijević et al., 1975).

1.5.3 Iron (Hydrous) Oxides

There are various forms of iron (hydrous) oxides that appear in nature. They are used as pigments, catalysts, coatings, flocculents, etc. (Matijević & Scheiner, 1978). Iron oxyhydroxide (FeOOH) alone consists of many phases (alpha, beta, gama) and ferrihydrite (Fe_2O_3. 2FeOOH. 2.6 H_2O). Delta-FeO(OH) is obtained by synthesis, named feroxyhyte (Chukhrov et al., 1976).

There are many pieces of evidence showing that the solid phase formed in solutions of ferric salts vary considerably in chemical and structural composition, morphology, particle size, colour, surface and magnetic properties, and other characteristics. The final precipitated product depends on the concentration of ferric ions, pH, temperature, aging time, the nature of the anions present, and other topochemical transformations. Thus, a small change in conditions may yield an entirely different precipitate (Matijević & Scheiner, 1978; Music et al., 1982; Murphy et al., 1976; Lewis & Schwertmann, 1979; Gildawie, 1977; Prasad & Rao, 1984).

1.5.4 Ferrihydrite

The most poorly crystalline form among the iron (hydrous) oxides is ferrihydrite, which is a product of

the hydrolysis of ferric ion in water (Towe & Bradley, 1967). Ferrihydrite is thermodynamically unstable. It transforms to more stable Fe-oxides, usually goethite under a temperature or cool humid climate. Therefore, ferrihydrite is considered as a young Fe-oxide form (Carlson & Schwertmann, 1981).

A number of occurrences discovered in Finland cover a range of crystallinities of ferrihydrite, which contained significant amount of Si (Carlson & Schwertmann, 1981). Adsorbed silica may retard the transformation of ferrihydrite to more stable goethite in nature (Cornell & Glovanoli, 1987; Carlson & Schwertmann, 1981).

The most important property of any iron oxide in a soil appears to be its surface area (Borgg^aard, 1984). It has been proposed that the small particle size of ferrihydrite with its large surface area is likely to play an important part to influence soil properties. The properties of ferrihydrite itself are still imperfectly understood. Therefore, Saleh & Jones (1984) proposed to conduct further study the relationship of ferrihydrite to the surface of soil mineral (kaolinite).

The formula of ferrihydrite has been written as earlier workers as $Fe_5HO_8 \cdot 4H_2O$ (for a synthetic product) (Towe & Bradley, 1967); $Fe_5(O_4H_3)_3$, $5Fe_2O_3 \cdot 9H_2O$ for a natural one (Chukhrov et al., 1972; 1973) respectively. No bands of hydroxyl were noted from IR spectrum before

the year 1979. A recent important report by Russell (1979) suggested OH to be an essential part of the structure; based on infrared spectroscopy. Then, the formular is re-written as Fe_2O_3. 2FeOOH. 2.6H_2O. Prasad et al. (1984) identified the composition of ferrihydrite by TG data as Fe_2O_3.1.8H_2O in agreement with the formula suggested by Russell (1979).

X-ray diffraction and infrared spectroscopy show the decomposition of ferrihydrite by thermal analyses as follows:

$$Fe_2O_3.2FeOOH\ .2.6H_2O \xrightarrow{30\text{-}200^{\circ}C} 2Fe_2O_3.H_2O$$

$$2Fe_2O_3.H_2O \xrightarrow{200\text{-}450^{\circ}C} 6Fe_2O_3.H_2O$$

$$\xrightarrow{450\text{-}600^{\circ}C} \alpha\text{-}Fe_2O_3 \quad \text{(Prasad et al., 1984).}$$

The structure of ferrihydrite has been proposed as a hexagonal cell with a = 5.08, c = 9.4 A° containing FeO_6 -octahedra (Chukhrov et al. ,1973). Murad & Schwertmann (1980) considered ferrihydrite's structure , Fe^{3+}surrounded by six O, OH, and / or OH_2, analysed by Mössbauer spectroscopy.

CHAPTER TWO

EXPERIMENTAL

page

2.1 TRANSMISSION ELECTRON MICROSCOPE (TEM) ... 28

2.1.1 Image Formation and Contrast 29

2.1.2 Factors Limiting Retrieval of Information 31

2.1.2.1 Spherical Aberration 31

2.1.2.2 Chromatic Aberration 33

2.1.2.3 Astigmatism 34

2.1.2.4 Coherence 34

2.1.2.5 Specimen Contamination 34

2.1.2.6 Specimen Stability 35

2.1.3 Electron Diffraction 36

2.1.3.1 Selected Area Diffraction 38

2.2 MATERIALS USED 39

2.3 PREPARATION OF GELS 40

2.3.1 Silica Gel 40

2.3.2 Carrageenan Gel 40

2.3.3 Mixed Gel 41

2.3.4 Carrageenan Gel Containing Kaolinite ... 41

2.4 GEL PLUG PREPARATION 42

2.5 DOUBLE TUBE DIFFUSION METHOD 42

2.6 PREPARATION OF SOLUTIONS 42

2.6.1 HEPPS Buffer 42

2.6.2 HEPES Buffer 43

2.6.3 Acid Oxalate Extractant 43

2.7 PREPARATION FOR PRECIPITATION 43

2.7.1 Iron Oxyhydroxide in Gels 43

2.7.1.1 Urea Solution Added to the Gel 44

2.7.1.2 Aging in Distilled Water 44

2.7.1.3 Effect of Ionic Strength 45

2.7.1.4 Effect of Chloride Ion 45

2.7.2 Iron Oxyhydroxide in Mobile Solutions ... 45

2.7.2.1 Simulation of Initial Precipitate ... 45

2.7.2.2 Simulation of Metal-Rich Zone 46

2.7.3 Iron oxyhydroxide in the Mixed Gel Containing Ferrihydrite Seeds 46

2.7.4 Iron Oxyhydroxide in the Carrageenan Gel Containing Kaolinite 47

2.7.5 Disolving a Sample Containing Goethite-Kaolinite by Acid Oxalate Extractant ... 48

2.7.6 Copper Compounds in The Carrageenan Gel 48

2.7.7 Copper Compounds in the Carrageenan Gel Containing Kaolinite 48

2.7.8 Copper Compounds in Mobile Solutions ... 49

2.7.9 Silver Compounds in The Silica Gel ... 49

2.7.10 Silver Compounds in Mobile Solutions 49

2.7.11 Preliminary Reactions with Platinum and Palladium Complexes 50

2.7.11.1 In Mobile Solutions 50

2.7.11.2 In Silica Gel 50

2.7.12 Platinum and Palladium Metals in Silica Gel 50

2.7.12.1 Containing HEPPS 50

2.7.12.2 Containing NaHCO 51

2.8 HEAT EFFECT ON IRON OXYHYDROXIDE WITHIN GELS 51

2.8.1 In Silica and Mixed Gel 51

2.9 HOMOGENEOUS PRECIPITATION WITHIN SILICA GEL BY HYDROLYSIS OF HEXAMINE OR UREA ... 52

2.10 MnO_2 WITHIN SILICA GEL USING PEROXOMONO-SULPHURIC ACID AND PERIODATE 53

2.10.1 MnO_2 by Peroxomonosulphuric Acid 53

2.10.2 MnO_2 by Periodate 54

2.11 SPECIMEN PREPARATION FOR TEM 54

2.11.1 Carbon Film Specimen Support Preparation 54

2.11.2 Specimen Preparation Via The Droplet Method 55

2.11.3 Specimen Preparation Using the Spray Method 56

2.11.4 Thin Sections 57

2.11.5 The Freeze-Drying Method 57

2.12 SPECIMEN PREPARATION FOR SCANNING ELECTRON MICROSCOPY (SEM) 58

2.1 THE TRANSMISSION ELECTRON MICROSCOPE (TEM)

Bush (1926) was the first to demonstrate the ability of a magnetic lens to focus an electron beam. The first electron microscope was constructed by Knoll and Ruska (1932) and a commercial model became available in 1938 (Von Borries and Ruska).

The short wavelength of an electron beam allows higher resolution than that obtainable in optical microscopes. The development of electron optical theory and instrumentation has advanced remarkably since then (Zworykin et al., 1945 and Agar et al., 1974).

Modern commercial high resolution electron microscopes can now achieve resolution at the molecular and atomic levels (Hashimoto et al., 1977 and Smith et al., 1981).

Ray diagram for image formation in the electron microscope was described by Andrews et al. (1967) as shown in Fig. 2.1a, 2.1b, and 2.1c.

A J.E.O.L JEM 100C transmission electron microscope was used throughout the present work. Acceleration potentials up to a limit 100 keV are possible with this instrument. The instrument was normally operated with a hairpin tungsten filament. Increased brightness and coherence could, however, be achieved by use of pointed filaments (Hibi, 1954 and Wolf & Joy, 1971) or single

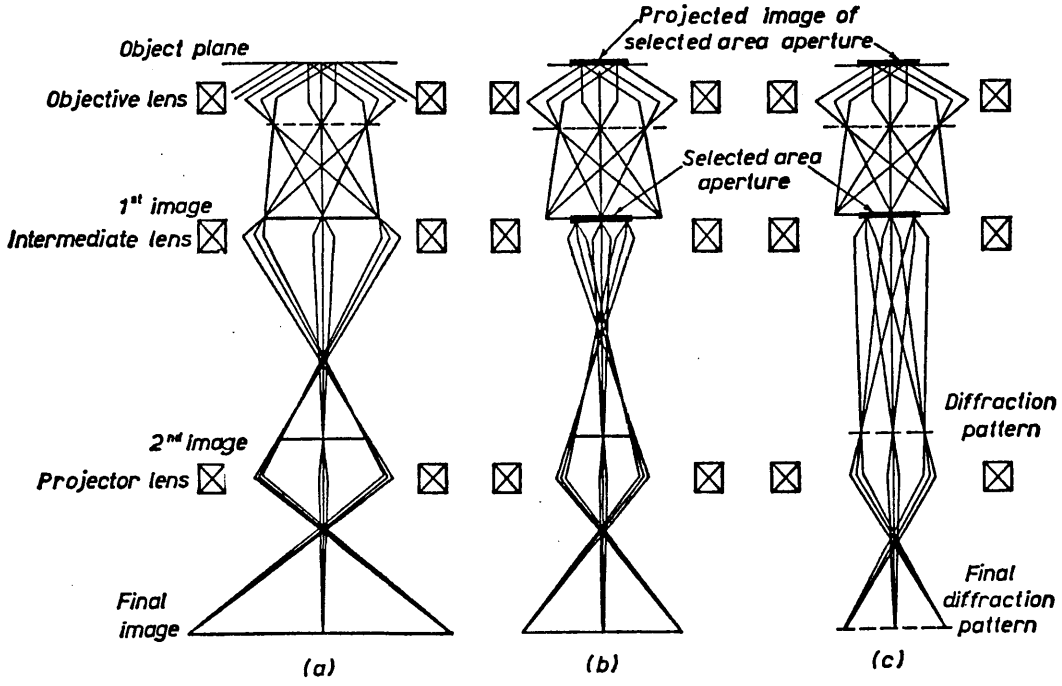

Fig. 2.1.

Ray diagram for image formation in the electron microscope.

(a) Normal image formation.
(b) Selected-area image formation.
(c) Selected-area diffraction pattern.
(After Andrew et al., 1967).

crystal lanthanum hexaboride (LaB_6) filaments (Ahmed & Broers, 1972). Some filament specifications are given in Fig.2.2.

When the beam current is increased, the current density on to the specimen is increased and hence the intensity of the illumination on the fluorescent screen. A high beam current is usually necessary for operation at very high magnification, or for the penetration of thick samples. In general it is desirable to keep the irradiation as low as possible, and the current should be as small as is consistent with operating convenience (Agar, 1965). In this study a beam current of 50-80 μA was used throughout.

Condenser lenses focus the electron beam on to the specimen down to spot sizes of 2-3 μm in diameter.

2.1.1 Image Formation and Contrast

The image is formed by the objective lens and subsequently magnified by intermediate and projector lenses. The image is then projected on to a fluorescent sceen for viewing or for recording via a photographic film.

The quality of the objective lens is of major importance in determining the performance of the microscope. Therefore, a high quality objective lens is crucial for high resolution purposes. Subsequent lenses

	Brightness β A/cm/sr at 25kV	Source Diameter d_s	Surface Current Density J_o, A/cm^2	Energy Spread Fwl/e M	Life hours	Vacuum torr
Tungsten Hairpin	1.5×10^{5}	25μm	5-10	2-4	10-15	10^{-4}
LaB_6 (20μm point)	$1.\times10^{6}$	~20μm	100-200	3	100-200	10^{-5}
LaB_6 (1μm point)	5×10^{6}	~1μm	100-200	3	50-100	10^{-6}
310 Tungsten	3×10^{8} -2×10^{11}	10-50Å	10^{4} -5×10^{6}	0.25	>1000 possible	5×10^{-10} to<< 10^{-10}

Figure 2.2. Figures based mainly on (Broers, 1972).

such as the intermediate and projector are less important in terms of performance.

The final magnified image, M, is the product of the magnification of the individual lenses; $M = M_{ob}\ M_{p1}\ M_{p2}$ where M_{ob} = magnification of the objective lens.

M_{p1} = magnification of the first projector lens (intermediate)

M_{p2} = magnification of the second projector lens.

Typical values of these lens magnifications are $M_{ob} = 40$, $M_{p1} = 20$ and $M_{p2} = 200$, giving M = 160,000 (Fryer, 1979).

Image contrast in an electron microscope arises from interactions between the electron beam and the specimen.

Elastic scattering is produced when electrons interact with the nuclei of the specimen without any loss of energy. Elastic scattering increases with atomic number and thickness of the specimen. The resulting scattered beams are deflected from the optic axis. In a crystalline specimen, the angles through which electrons are elastically scattered can be determined by the Bragg Law.

$$\lambda = 2d_{hkl} .\sin \theta$$

λ = electron beam wavelength

θ = scattered angle

d_{hkl} = interplanar spacing for hkl planes.

In contrast, inelastic scattering can occur when electrons in the beam encounter or collide with orbital electrons in an atom of a thin specimen resulting in a change in their energy and wavelength . When these inelastic scattered waves interact with other beams phase relationships develop which give rise to contrast in the image (but not at perfect focus).

A thick specimen produces much scattering of the electron beam, but if the scattered electrons are inhibited from contributing to the final image, via an aperture the thick parts of the specimen and/or areas containing heavy atom will be imaged as dark contrast.

2.1.2 Factors Limiting Retrieval of Information

2.1.2.1 Spherical Aberration

This is caused by stronger refraction of rays at increasingly larger angles from the optic axis and gives rise to a disc of confusion about the Gaussian image point (Fig.2.3). The disc diameter for a point object, d_s can be expressed by:

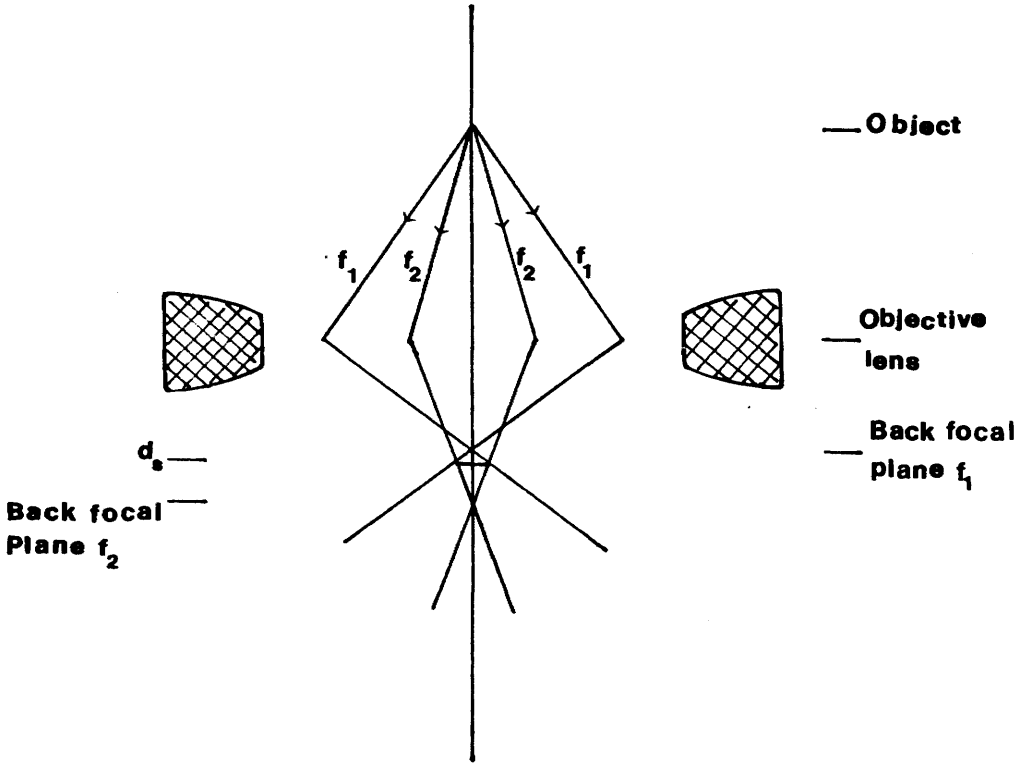

Fig. 2.3.

Spherical aberration in the objective lens giving rise to a different focal length for peripheral rays (f_1) compared with axial rays (f_2). d_s is the smallest resolvable diameter. (After Fryer, 1979).

$$d_s = 1/2 \; C_s \alpha^3$$

where C_s is the spherical aberration coeffient and α is the semi-angular aperture of the lens.

For a periodic object, the scattering angle of the widest diffracted beam replaces α in the above expression.

However, the effect of spherical aberration can be minimised by reducing the aperture of the lens.

Unfortunately, reduction of the objective aperture will give rise to an interference effect in terms of diffraction.

This effect at the edge of the aperture for a point object is shown by:

$$d_d = \frac{0.61\lambda}{\alpha}$$

where d_d is the disc diameter of minimum confusion caused by diffraction. λ is the electron beam wavelength, and α is the semi-angular aperture.

A combination of both effects leads to a theoretical resolution limit of the lens (d_{min}), for a point object given by:

$$d_{min} = B \; C_s^{1/4} \; \lambda^{3/4}$$

where B is a constant, for phase contrast = 0.65 and for a periodic object given by:

$$d_{min} = C_s \theta^3$$

For an optimum objective aperture size,

$$\alpha_{opt} = C_s^{-1/4} \lambda^{1/4}$$

(Fryer, 1979).

2.1.2.2 Chromatic Aberration

Chromatic aberration arises from spreading of variations of the electron energy passing through the objective lens and results in a disc of confusion at the image plane. The limit of resolution as a disc diameter of confusion, d_c given by:

$$d_c = C_c \alpha (\Delta V/V - 2 \Delta I/I)$$

where C_c is the chromatic aberration coefficient, V is the accelerating voltage relativistically corrected, I is the lens current and α is the objective semi-angular aperture.

2.1.2.3 Astigmatism

This is caused by asymmetry of the objective lens and arises from inaccuracies in manufacture or inhomogeneities in the iron pole pieces. Furthermore, astigmatism can result from a contamination layer that has formed on an objective aperture; this builds up a charge which modifies the lens properties as the aperture is moved. This defect causes a point object to be imaged as two mutually perpendicular lines at different levels in image space causing a directional structure in the image. However, this can be corrected via compensation by an elliptical lens field.

2.1.2.4 Coherence

Coherence is the condition of an illuminating electron wave as it approaches an object. Coherent illumination arises when all waves in the incident beam are in phase. Increased coherence can be obtained by using a small condenser aperture and a pointed filament.

2.1.2.5 Specimen Contamination

Contamination of objective and other apertures in the microscope occurs during operation. A brown deposit forms from polymerisation of hydrocarbon vapours (Ennos,

1954). The source of these adsorbed molecules are from the various vacuum fluids and greases used in the microscope and sometimes from the specimen itself.

The contamination can affect image formation, resulting in poor resolution, loss of intensity for viewing and photography, and the creation of mechanical stress (Hart et al., 1970 and Hren, 1979). In extreme cases loss of diffraction data from crystalline specimens arises (Halliday, 1965).

However, such contamination can be minimised by thorough cleaning of the microscope as well as the specimen. In addition, modern microscopes use liquid-nitrogen cold-traps around the specimen which prevent contamination (Spence, 1981). Careful handling (using gloves) of microscope components during specimen mounting also helps to minimise contamination.

2.1.2.6 Specimen Stability

The process of radiation damage to the specimen by the electron beam is accompanied by many energy transfer processes. The generation of heat can change the physical structure as well as the chemical composition of the specimen.

Beam damage readily occurs in organic materials and results in molecular ionization leading to chemical bond dissociation, structural damage, specimen etching and mass loss (Isaacson, 1977 and Cosslett, 1978).

2.1.3 Electron Diffraction

When electrons pass through a crystalline specimen in the microscope a diffraction pattern is formed in the back focal plane of the objective lens as illustrated in Fig. 2.4.

This diffraction pattern can be observed by increasing the focal length of the intermediate lens so that the back focal plane of the objective lens is imaged on the fluorescent screen. In diffraction, rays travelling in specified directions from all object points are focused to form the diffraction pattern. In normal bright field, microscopy rays travelling in all directions from every object point are focused to form the magnified image points. Ray path diagrams for the two cases are shown in Fig. 2.5.

The diffraction pattern contains structural data about the specimen. Diffraction only arises from lattice planes parallel or nearly parallel to the electron beam and can be used to determine the orientaion of the specimen.

A single crystal will give a spot pattern corresponding to the planes parallel to the electron beam. A polycrystalline specimen will give a series of rings which are composed of large numbers of spots arising from randomly oriented crystals; the spots from any specific hkl reflection form a ring.

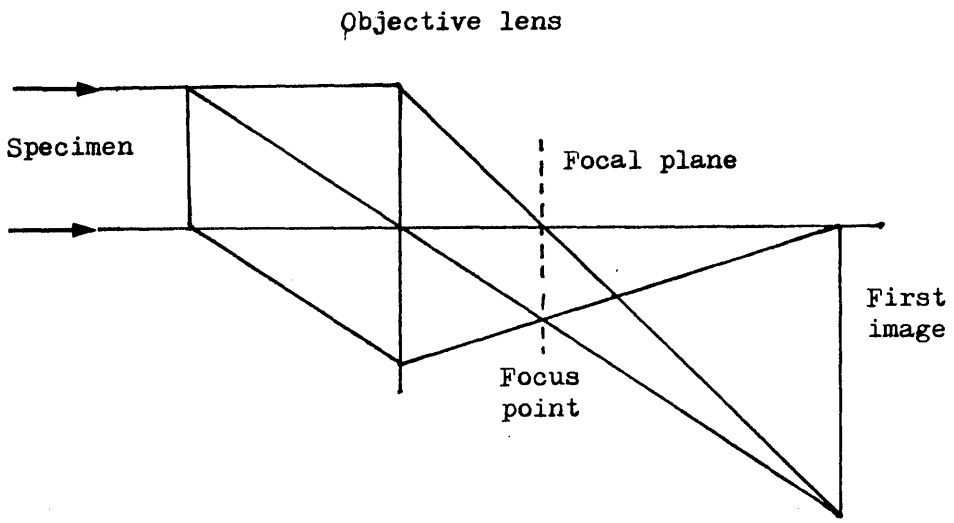

Fig. 2.4.

Elementary geometrical optics of the objective lens (After Alderson and Halliday, 1965).

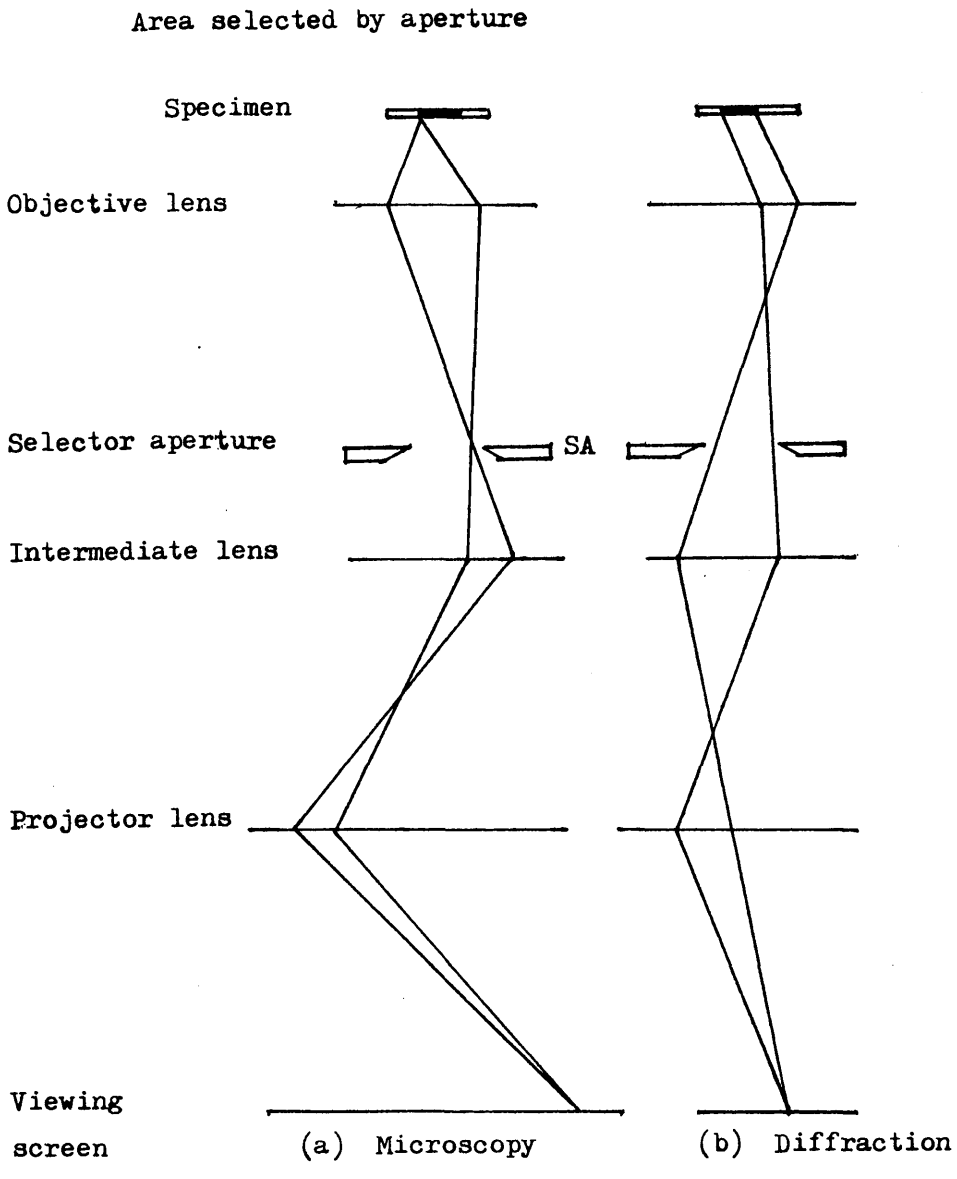

Fig. 2.5.

Ray paths in a three-stage electron microscope for (a) microscopy and (b) diffraction (After Alderson and Halliday, 1965).

The interplanar spacing, d, of the crystal lattice can be derived from the electron diffraction pattern (Fig.2.6) as follows:

$$D / 2 L = \tan 2\theta$$

where D/2 is the distance between the diffracted beam and the primary beam at the plane of the photographic plate, and L is the effective camera length which is referred to other factors as shown below:

$$L = f_o \times m \times M$$

where f_o is the focal length of the objective lens, m and M are magnification of the intermediate and projector lenses respectively (Andrews et al., 1967).

Moreover, $\lambda L = \lambda f_o \times m \times M$, where L known as the camera constant. For accurate diffraction, therefore, λL must be determined for almost each spot or ring on the diffraction pattern.

The value of 2θ is very small and hence $\tan 2\theta \simeq \sin 2\theta \simeq 2\sin\theta \simeq 2\theta$. The Bragg relationship of the first order diffraction, $\lambda = 2 d \sin\theta$, can be applied where d is the interplanar spacing of the crystal lattice.

Therefore by substitution,

$$D\, d/2 = \lambda L = K$$

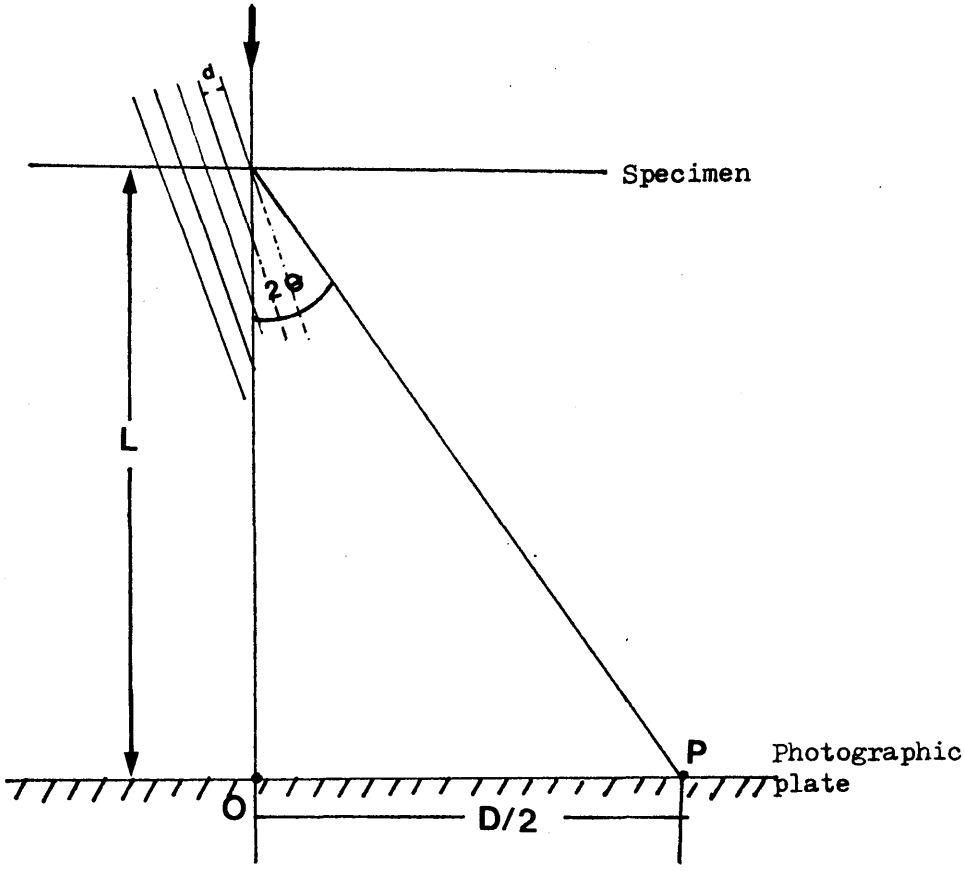

Fig. 2.6.

Formation of the diffraction pattern.

2θ : Scattering angle (very small).
P : Diffraction spot.
O : Central spot.
d : Interplanar spacing.
L : Camera length.

where K is the " camera constant ". The camera constant can be obtained by calibration with a standard. In practice thallous chloride or evaporated metal films are often used as a standard specimen (Fryer 1979). In the present study graphite was used as a standard as it is invariably present on specimen grids covered with a carbon film. The camera constant was calculated each time the microscope was used.

Thus,

d (unknown) = K (graphite) / D (measured).

Thus a diffraction pattern can be used to identify a substance by comparing its spacings with tabulated X-ray spacings given in the A.S.T.M. index.

2.1.3.1 Selected Area Diffraction

This technique allows a diffraction pattern to be obtained from a specific area of specimen (Le Poole, 1947). A selector aperture is inserted in the image plane of the objective lens where the specimen is magnified approximately fifty times. Thus an aperture of 50 μm diameter in the intermediate aperture plane can define 1 μm diameter region at the specimen. The minimum selected area in the JEOL JEM 100C is 0.23 μm (Gildawie, 1977). Spherical aberration of the objective lens is the major source of error in the selected area technique. (Agar, 1960; Riecke, 1961 and Hirsch et al., 1965).

2.2 MATERIALS USED

K_2PdCl_4 and K_2PtCl_4 were loaned by Johnson Matthey Chemicals Ltd.

Aluminium(III), cobalt(II), copper(II), manganese (II), and magnesium(II) sulphates were Analar grade BDH.

Barium(II), calcium(II), cadmium(II), strontium(II) chlorides and barium nitrate were Analar grade BDH.

Sigma Carrageenan Type I (predominantly kappa, with some lambda; K^+, Ca^{2+}, and Na^+ counter-ions) was supplied by SIGMA Chemicals Company.

$NH_4Fe(SO_4)_2.12H_2O$ was supplied by Hopkin & Williams Ltd.

The materials that were purchased from BDH Ltd. are as follows:

Resin: Dowex 50w-x8(H), particle size 0.39-1.00 mm,

Sodium silicate stock solution, 12% Na_2O & 30% SiO_2;

(H)EPPS: (N-(2-Hydroxyethyl) piperazine-N'-3-propane-sulphonic acid),

HEPES: N-2 – Hydroxyethyl piperazine-N'-2-ethane sulphonic acid and

HEPES monosodium salt: N-2-hydroxyethyl piperazine-N'-2-ethane sulphonic acid monosodium salt were purchased from BDH Ltd.

Kaolinite was supplied by Department of Geology, University of Missouri, batch KGR-1, described as well-crystallised Kaolin from Washington County, Georgia,USA.

$AgNO_3$ (crystalline) was purchased from Johnson Matthey. Other chemical reagents were Analar grades and all the chemicals were used without further purification.

2.3 PREPARATION OF GELS

2.3.1 Silica Gel

Ion-free silica hydrogel was prepared by a rough titration of sodium silicate solution with a strong acid cation exchanger (Dowex 50W-X8 (H)) to pH 2.5-3.0 or pH 5-6 according to the experimental conditions needed using external indicator paper. The sodium silicate solution as supplied by BDH was diluted to 10 % proportion with distilled water (ca 4.5 % SiO_2) (Abdullah et al., 1986). This solution was allowed to set at room temperature for 24 hours. The freshly prepared gel became mobile if heated to about 95° C.

2.3.2 Carrageenan Gel

This was prepared by dissolving 1 % proportion of Sigma Carrageenan type I with boiling distilled water

and heating until all the carrageenan dissolved using magnetic stirring. The gel solution was allowed to cool and set at room temperature for 24 hours.

2.3.3 Mixed Gel

The gel was prepared by mixing a neutralized silica gel solution at pH 5-6 with the carrageenan gel solution both as described above. The ratio was one part of the silica gel to ten parts of the carrageenan gel. The silica gel was added with stirring to the carrageenan gel while it was warmed at about 70° C. The gel was allowed to cool and set at room temperature for 24 hours. The mixed gel became mobile if heated to about 60-65° C.

2.3.4 Carrageenan Gel Containing Kaolinite

About 0.001 M kaolinite suspension was carefully prepared by mixing kaolinite with distilled water in a fume cupboard. The suspension was dispersed using an ultrasonic agitator, BLT, and a Micro Angle-Ultrasonics Centrifuger, KERRY. This suspension was used instead of water to prepare carrageenan gel as above. The mixture was allowed to cool and set at room temperature for 24 hours.

2.4 GEL PLUG PREPARATION

Gel plugs were prepared by placing a bundle of 1cm diameter by 10cm long transparent plastic Tygon clear PVC tubes in a beaker containing about 6 cm depth of gel solution. After 24 hours at room temperature the tubes could be dissected out with care using a spatula.

2.5 DOUBLE TUBE DIFFUSION METHOD

A gel plug was placed in a 17 mm×150 mm test tube. About 0.5 ml of metal ion solution was added on top of the gel dropwise on the wall of the gel plug to about 2.5 cm depth using a Pasteur pipette.

About 12 ml of alkali source solution was then added to the test tube outside the gel plug (6 cm depth) until it reached the same level with the metal ion solution, and the tube stoppered with a rubber bung as shown in Fig.2.7.

2.6 PREPARATION OF SOLUTIONS

2.6.1 HEPPS Buffer

This was prepared from equal volumes of 0.4 M of HEPPS and 0.3 M of NaOH solutions.

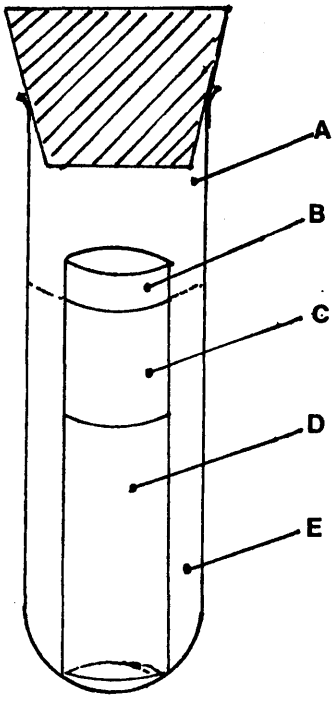

Fig. 2.7.

Double tube diffusion method.

A : The stoppered test tube (17mm × 150mm).
B : The plastic tube (1cm × 10cm).
C : The metal ion solution (0.5ml).
D : The gel plug (6cm depth).
E : The hydroxyl ion solution (12ml).

2.6.2 HEPES Buffer

This solution was made up from equal volumes of 0.1M of HEPES-H^+ solution and 0.3 M of HEPES-Na^+ solutions.

2.6.3 Acid Oxalate Extractant

0.175 molar or 2.49 gram ammonium oxalate (hydrate) and 0.1 molar or 1.26 gram oxalic acid (dihydrate) were dissolved in 100 ml of distilled water.

2.7 PREPARATION FOR PRECIPITATION

2.7.1 Iron Oxyhydroxide in Gels

A general survey of the growth of particles of iron oxyhydroxide by the double tube method was carried out using various alkali source solutions and gels. 0.1 M Fe(III) (as ammonium sulphate double salt), $NH_4\ Fe(SO_4)_2 .12\ H_2O$ and 0.1 M alkali source solutions were used throughout.

The alkali solutions were:

$NaHCO_3$, HEPPS buffer, HEPES buffer, NaOH and hexamine.

The growth media were:

The silica, the carrageenan and the mixed gel.

In general case, samples were taken from the

main precipitation zone after two weeks of reaction for particle growth comparison. But in the mixed gel, samples were examined at various stages and from three zones of the precipitates. At the same time the pH was taken using pH papers, Whatman Test Paper Books for ranges; 1.0-3.5, 3.6-5.1, 5.2-6.7, 6.8-8.3, and 8.4-10 were used in this experiment by inserting vertically at the middle of gel plug at every stage and every zone in order to understand the detailed growth of the particles.

2.7.1.1 Urea Solution Added to the Gel

0.2 M urea solution was used in place of water to dilute the silica gel solution in order to see if any morphologies changed. When the gel was set, the double tube diffusing method was carried out using 0.1 M Fe(III) and 0.1 M $NaHCO_3$ solution.

2.7.1.2 Aging in Distilled Water

The yellow-orange precipitate from the main precipitation zone was removed from the gel plug, separated using the Ultrasonics Centrifuge and kept in distilled water for more than eight months.

2.7.1.3 Effect of Ionic Strength

About 0.5 ml of 0.1 M Fe(III) solution was added on top of the mixed gel. 1 ml of 1 M $NaClO_4$ solution was added to about 11 ml of 0.1 M $NaHCO_3$ solution and then added below the gel plug in the double tube. The final concentration of $NaClO_4$ solution was about 0.083 molar solution.

2.7.1.4 Effect of Chloride Ion

1ml of 1 M NaCl solution was added to about 11 ml of 0.1 M $NaHCO_3$solution and then the solution was added below the gel plug in the double tube. The final concentration of NaCl solution was about 0.083 molar solution. 0.1 M Fe(III) solution was added on top of the mixed gel.

2.7.2 Iron Oxyhydroxide in Mobile Solutions

2.7.2.1 Simulation of Initial Precipitate

0.01 M $NaHCO_3$ solution saturated with CO_2 (by dropping CO_2 ice) was slowly added to 0.05 M Fe(III) solution until enough precipitate formed to collect and examine. The yellow- orange precipitate was washed as soon as it formed to minimise further reactions.

2.7.2.2 Simulation of Metal-Rich Zone

0.01 M $NaHCO_3$ solution saturated with CO_2 (by dropping CO_2 ice) was slowly added to a slight excess of 0.05 M Fe(III) solution. Some yellow-orange precipitate was collected and the rest was left in the solution for seven days to see the effect of aging.

2.7.3 Iron Oxyhydroxide in the Mixed Gel Containing Ferrihydrite Seeds

This experiment was carried out in the double tubes. Fe(III) and $NaHCO_3$ solutions were used through out the experiment. Two weeks aged precipitate was used as seeds and were taken from the main precipitation region as the first generation seeds, whereas, from metal-rich zone as the second generation seeds. At the same time a test of null hypothesis was set up in parallel by the following steps:

(A) Real Experiment	(B) Control Experiment
a. Seeds were made up as mentioned above.	The mixed gel was made up as an old gel.
b. The washed seeds were transfered to a new mixed gel.	The old gel was transfered to a new mixed gel.

c. Ferrihydrite was grown in the new (seeded) gel.	Ferrihydrite was grown in the new gel that contained some old gel.
d. Main precipitation region was taken as a sample.	Main precipitation region was taken as a sample.
e. Seeded growth region i.e. metal ion rich zone was taken as a sample.	Same region which in (A) contained seeded growth was taken as a sample.

In addition to the control experiment, a lower concentration of Fe(III) was made up as follows:

0.05 M $Fe(NH_4)(SO_4)_2$ + 0.1 M $(NH_4)_2SO_4$

and 0.01 M $Fe(NH_4)(SO_4)_2$ + 0.18 M $(NH_4)_2SO_4$

0.1 M $NaHCO_3$ solution was diffused to the lower end of the gel plug in the double tubes of the silica gel.

2.7.4 Iron Oxyhydroxide in the Carrageenan Gel Containing Kaolinite

Fe(III) solution and HEPES buffer solution were used to diffuse from the opposite ends of the gel in the double tubes. This experiment was carried out in order to see the role of kaolinite in the particle growth. Precipitates were examined at the period of nine days diffusion, eight months diffusion, and nine days diffusion followed by eight months in distilled water.

2.7.5 Dissolving a Sample Containing Goethite-Kaolinite by Acid Oxalate Extractant

The sample was stirred well with the extractant solution (Sec. 2.6.3) for 15 minutes in order to dissolve the goethite. It was then centrifuged using the Ultrasonics Centrifuger, washed twice with the extractant and twice with distilled water.

2.7.6 Copper Compounds in the Carrageenan Gel

0.1 M $CuSO_4$ or $Cu(ClO_4)_2$ solution was used as the metal ion solutions. HEPES buffer, HEPPS buffer or 0.3 M NaOH solution was used as the alkali source solution. Both solutions were diffused from the opposite ends of the gel plugs in the double tubes. But the alkali solution diffuses much more quickly than the metal ion, so the latter was allowed to diffuse for four days before the reaction was carried out.

2.7.7 Copper Compounds in the Carrageenan Gel Containing Kaolinite

0.1 M $CuSO_4$ or $Cu(ClO_4)_2$ solution and only HEPES buffer solution were used to diffuse from the opposite ends of the gel plugs in the double tubes. This experiment was carried out in order to see the effect of kaolinite on the particle growth.

2.7.8 Copper Compounds in Mobile Solutions

About 0.1 g of $Cu(ClO_4)_2$ solid was slowly added into 6 ml of 0.3 M NaOH solution and stirred well. Excess NaOH was used in order to complete the reaction of Cu(II) and avoid double salt formation. Precipitates were collected at various ages.

2.7.9 Silver Compounds in The Silica Gel

0.1 M Ag(I) nitrate solution and HEPES buffer or HEPPS buffer solution were diffused from the opposite ends of the gel in the double tubes. All tubes were wrapped with aluminium foil and kept in the dark to avoid any photochemical reaction. Fresh and aged precipitates were taken as samples for examination.

2.7.10 Silver Compounds in Mobile Solutions

0.1 M NaOH solution was slowly added to 0.1 M Ag(I) nitrate solution until enough precipitate formed to collect and examine. Fresh and aged precipitates were collected as samples. All the rubber stoppered tubes were wrapped well with aluminium foil and kept in a dark place.

2.7.11 Preliminary Reactions with Platinum and Palladium Complexes

2.7.11.1 In Mobile Solutions

0.01 M Pt(II) or 0.1 M Pd(II) (as K_2PtCl_4 or K_2PdCl_4) was added to either one of 0.1 M $NaHCO_3$, HEPES buffer or HEPPS buffer solution.

2.7.11.2 In Silica Gel

0.1 M Pt(II) or Pd(II) solution and 0.1 M $NaHCO_3$ solutions were diffused from the opposite ends of the gel in double test tubes.

Also 0.2-0.01 M Pt(II) or Pd(II) and HEPES or HEPPS buffer solution were diffused in the double test tubes.

2.7.12 Platinum and Palladium metals in Silica Gel

2.7.12.1 Containing HEPPS

Solid HEPPS was added to 10% diluted sodium silicate stock solution to make up 0.1 M. The solution was brought to pH 8.0 with a strong acid cation exchanger. 10 ml of this solution was mixed with 5 ml Pt or Pd solutions in the test tubes. These mixtures set

after five minutes. After 30 minutes, a few drops of distilled water was added to the set gel to avoid drying out, and the tubes stoppered. The Pt and Pd solutions used here contained from various of 0.05 M K_2PdCl_4 to 0.1 M KCl, so that cation concentration was constant. (Table 2.1).

2.7.12.2 Containing $NaHCO_3$

5 ml solutions containing various ratios of 0.05 M Pt(II) or Pd(II) to 0.1 M KCl solution were prepared. The solution was added to 10 ml of the diluted solution for silica gel formation at pH 5-6 in the stoppered test tubes. Finally solid $NaHCO_3$ enough to give a 0.1 M solution was added to the above solution and mixed well before it set. A few drops of water were added to the set gel to prevent drying out.

Note: All the experiments for Pt(II) and Pd(II) were carried out in tubes wrapped with aluminium foil and kept in the dark to avoid any reaction from the light.

2.8 HEAT EFFECT ON IRON OXYHYDROXIDE WITHIN GELS

2.8.1 In Silica and Mixed Gel

After 2 weeks of precipitation, both solutions were decanted off in the double tube and distilled water was added instead. Distilled water had been changed every

TABLE 2.1

Various Ratios Concentration of K_2PtCl_4 in KCl Solutions (Sec.2.7.12.1)

A ml	B ml	(A+B) ml	Conc.of A in (A+B) Molar
5	0	5	0.05
4	1	5	0.04
3	2	5	0.03
2.5	2.5	5	*0.025
2	3	5	0.02
1	4	5	0.01

* : Conditions used in the most extensive studies.
A : Volume of 0.05M K_2PtCl_4 or K_2PdCl_4 solution.
B : Volume of 0.1M KCl solution.
(A+B) : Total volume of (A+B).

day as washing process for 5 days in order to remove all the solutions from the precipitate and to minimise further reaction during heating process. The tubes were loosely plugged by rubber stoppers and were then heated in a water bath maintained at 85-90°C and 98-100° C for various hours.

2.9 HOMOGENEOUS PRECIPITATION WITHIN SILICA GEL BY HYDROLYSIS OF HEXAMINE OR UREA

These reactions were carried out by Dr. M. Kaya (visitor from Firat University, Turkey) as follows:-

The silica gel solution containing hexamine or urea was prepared by bringing the solution to pH 5-6 with a strong acid cation exchanger. It was allowed to set to 2cm depth at room temperature for 24 hours in 17 mm x 150 mm test tubes except for Mn(II) with urea for which a B14/23 quick^fit test tube was used to reduce the oxidation of the manganese sample with air in the heating process. After that a solution containing equal volumes of solutions A and B (see Tables 2.2 & 2.3) and a small amount of solution C, was added on top of the gel at about 10 cm depth. Solution C was added in order to adjust pH. Afer diffusion for some days (see Tables 2.2 & 2.3), the solution was decanted off and a few drops of distilled water were added to prevent drying

TABLE 2.2

Hydrolysis of Metal Solutions by Urea at 85-90° C

silica gel +	soln.A, (M)	soln.B, (M)	soln.C	pH of A+B	diff., days	hrs.	colour ppts.
none	0.1Fe(III)	0.2urea	dil.H_2SO_4	2.5-3	3.5	2	yel-orange
0.6M	0.2Mn(II)	0.6urea	" "	3.9-4.2	11	10	pl-brn.
urea	0.2Zn(II)	" "	" "	3.9-4.2	6	120	col.
"	0.2Ba(II)	" "	HCl	2.5	5	24	wh.dr.
"	0.2Ca(II)	" "	"	2.5	5	24	rbhd.
"	0.2Sr(II)	" "	"	2.5	5	24	wh.dr.
"	0.2Cd(II)	" "	"	3.0	5	12	wh. cr.
"	0.2Pb(II)	" "	CH_3COOH	4.5-4.8	5	12	shiny cr.

Key word:

brn.: brown, col.: colorless, cr.: crystal, diff.: diffusion, dr.: dendritic, hrs,: hours, M: molarity, pl.: pale, ppts.: precipitates, rbhd.: rhombohedral, wh.: white, yel.: yellow.

TABLE 2.3

Hydrolysis of Metal Solutions by Hexamine at 85-90° C

silica gel +	soln.A, (M)	soln.B (M)	soln.C	pH of soln.B	diff., days	hrs.	colour ppts.
0.15M hexa.	0.2Mn(II)	0.15	dil.H_2SO_4	4-6.5	4	10	dk.-brn.
"	0.2Cu(II)	hexa.	" "	4.5-5	4	10	pl.gr-bl.
"	0.2Co(II)	"	" "	4-6.5	4	10	pink
"	0.2Ni(II)	"	" "	4-6.5	4	10	pl.gr.
"	0.2Zn(II)	"	" "	4-6.5	4	10	col.
0.2M hexa.	0.2Al(III)	0.2 hexa.	" "	5.0	5	48	wh.
"	0.2Mg(II)	"	———	~7.0	5	96	wh.
"	0.2Pb(II)	"	CH_3COOH	5.0	5	24	wh.

Key Word :

brn.: brown, bl.: blue, col.: colorless, diff.: diffusion, dk.: dark, gr.: green, hexa.: hexamine, hrs.: hours, M : molarity, pl.: pale, ppts.: precipitates, wh.: white.

out. All the tubes were lossely plugged by rubber stoppers and were then heated in a water bath maintained at 85-90°C for various times. Full experimental details are shown in Tables 2.2 & 2.3.

2.10 MnO_2 WITHIN SILICA GEL USING PEROXOMONOSULPHURIC ACID AND PERIODATE

2.10.1 MnO_2 by Peroxomonosulphuric Acid

These reactions were carried out by Dr. M.Kaya (Firat University) as follows:-

The first layer of the silica gel solution was prepared by bringing the gel solution to pH 2.5-3.0 with the strong acid cation exchanger. This solution was allowed to set at room temperature for 24 hours in crystallisation dishes which have 5 cm depth and 9 cm diameter, in the hope of observing pattern formation (see Discussion).

Equal volumes of 0.02 M Mn(II) and acetate buffer (pH 4.3-4.6, I = 0.5; 0.5 M CH_3COONa and 0.8 M CH_3COOH) was added on top of the first gel to 7.7 mm depth. After five days, the solution was decanted off and a second gel solution prepared as above was allowed to set on top of the first gel to 2 mm depth. After that equal volumes of 0.2 M $KHSO_5$ and the acetate buffer was added on top of it to 7.7 mm depth.

In this experiment, the second layer of the gel was introduced in order to avoid high nucleation density near the interface of the gel with the second solution. It was noted that the concentration of Mn(II) was changed to 0.01M and 0.1 M for $KHSO_5$ solution after mixing with the acetate buffer.

2.10.2 MnO_2 by Periodate

The first layer of silica gel containing 0.02 M $NaIO_4$ was neutralized with a strong acid cation exchanger to pH 5-6. This gel solution was allowed to set in the crystallisation dishes to 5 mm depth at room temperature for 24 hours. After the first gel was set, a second gel solution which was prepared as above was allowed to set on top of it to 2 mm depth. After that the solution of equal volumes of 0.04 M Mn(II) and the acetate buffer was added on top of the second gel to 7.7 mm depth.

The experiment was conducted at room temperature.

2.11 SPECIMEN PREPARATION FOR TEM

2.11.1 Carbon Film Specimen Support Preparation

The carbon-filmed copper grids were prepared as follows:

(a) Mica sheets were cleaved into thin sheets and placed on the base-plate of a vacuum coating unit

(Edwards 12E6). After evacuation ($\sim$10 Torr) a high current was passed through carbon (graphite) rods connected to electrodes to produce a thin layer of evaporated carbon on the mica (Fig. 2.8).

(b) A cleaned copper gauze was placed into a Petri dish filled with distilled water. Copper grids were placed on top of this and the carbon film on the mica was floated onto the surface of the water by careful immersion of the mica under the surface. The resultant carbon film was lowered onto the grids by slowly draining off the water. The grids were then dried in an oven (30°C).

3.05 mm, 400/200 square mesh copper grids coated with carbon films were used throughout this work as specimen supports.

2.11.2 Specimen Preparation via the Droplet Method

A fine suspension of washed specimen material from gels was dropped onto the coated copper grid (on the opposite side to the carbon film to avoid destroying the carbon support film) using a Pasteur pipette drawn out to a fine point in a Bunsen flame. Samples were allowed to dry in the oven at 30°C.

Reaction solutions containing metal and hydroxyl ions were decanted off from the double test tubes. The remaining bands of precipitate were washed within the

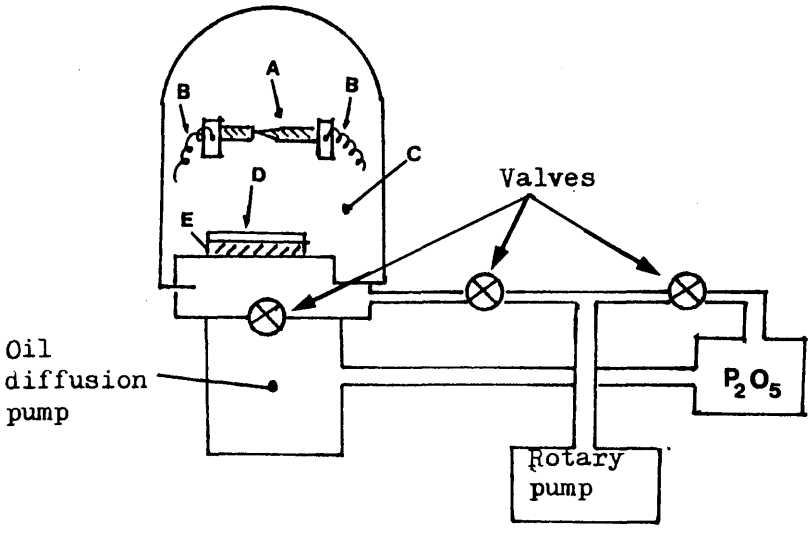

Fig. 2.8.

Apparatus used in the preparation of amorphous carbon films.

A : Crystalline graphite rods.
B : Electrodes.
C : Vacuo.
D : Amorphous carbon films.
E : Mica sheets.

tube with distilled water to avoid the possibility of metal and hydroxyl ions co-precipitating from solution during this process.

After that sections approximately 3 mm wide within a band were dissected out with a razor blade and placed in separate tubes.

Unless otherwise stated all the specimens were then washed with distilled or deionised water and centrifuged down 6-7 times to remove any excess material which would crystallise out on the specimen grids and confuse the subsequent electron microscopic examination.

2.11.3 Specimen Preparation Using the Spray Method

A section of gel containing precipitate was cut and placed in a specimen tube without any washing or centrifuging in order to examine the original morphology of particles. The sample was broken up in distilled water to make a fine suspension. A plastic atomiser was filled up with the suspension and sprayed several times onto the coated grids. The specimen could be examined immediately in an electron microscope as it dried very quickly at room temperature, avoiding any morphology changes caused by drying in the oven, or by excessive handling.

2.11.4 Thin Sections

Thin sections were prepared from dried gels embedded in resin in further attempts to examine the original morphology of precipitates.

Araldite resin was used in the present experiments. Blocks were prepared by the Zoology Department, University of Glasgow, using the following proportions:

Araldite CY 212	23.0ml
DDSA or HY 964 (dodecenyl succinic anhydride)	27.0ml
DMP 30 or DY 064 (tridimethylaminomethyl phenol)	0.75ml

The procedure used was similar to that recommended by Luft (1961). The resulting hard block was then cut into ~500 Å sections with a diamond knife in an ultramicrotome (LKB) and the sections picked up on copper grids.

2.11.5 The Freeze-Drying Method

This method of specimen preparation was employed to minimise morphological changes which might occur on drying down a specimen.

A metal bar was immersed in liquid nitrogen for 10 minutes and then placed in a coating unit. A fine suspension of the specimen was prepared on carbon-coated

grids which were then placed on a sheet of mica. The specimen was then frozen by placing the mica on top of the frozen metal surface. Sublimation of the ice from the sample was then achieved by evacuation of the coating unit.

2.12 SPECIMEN PREPARATION FOR SCANNING ELECTRON MICROSCOPY (SEM)

The precipitate within a gel was dissected out and dried in air and mounted on an aluminium stub. The surface of the aluminium specimen holder was precoated with a carbon paint (CCC LEIT-C) to act as a conductor. The paint was left until half dry and then the sample was placed on it. Subsequently the sample was coated with gold-platinum in a sputter-coater to deposit a conducting layer on the outer surfaces of the specimen.

Samples were examined at the Department of Veterinary Anatomy, and Physiology, Glasgow University using the Philips 501B SEM , fitted with microanalysis facilities and operated at 15 kV.

CHAPTER THREE

PRECIPITATION OF IRON OXYHYDROXIDE

page

3.1 IRON OXYHYDROXIDE IN GELS 59

3.1.1 Various Gels and Alkali Sources 59

3.1.1.1 Change of pH 61

3.1.1.2 Hydroxide-Rich Zone 62

3.1.1.3 Main Precipitation Zone 62

3.1.1.4 Metal-Rich Zone 63

3.1.1.5 D Zone 63

3.1.1.6 Mechanism of Formation of Bundles ... 64

3.1.1.7 Confirmation of Ferrihydrite's Morphology 65

3.1.2 Effects of Aging on the Precipitates ... 66

3.1.2.1 In Carrageenan Gel 66

3.1.2.2 In Silica Gel 69

3.1.2.3 In Mixed Gel 70

3.1.3 Urea Added to the Silica Gel 70

3.1.4 $NaClO_4$ Solution Added to $NaHCO_3$ Solution 71

3.1.5 NaCl Solution Added to $NaHCO_3$ Solution ... 72

3.1.6 Effect of Heat 73

3.1.6.1 In Silica Gel 73

3.1.6.2 In Mixed Gel 74

3.2 IRON OXYHYDROXIDE IN MOBILE SOLUTIONS 75

3.3 IRON OXYHYDROXIDE IN MIXED GEL; EFFECT OF FERRIHYDRITE SEEDS 76

3.3.1 Metal Ion Rich Zone; Seeded 76

3.3.2 Main Precipitation Zone; Seeded 76

3.3.3 Low Concentration of Fe(III) Solution (0.05 & 0.01M); Unseeded 77

3.4 IRON OXYHYDROXIDE IN CARRAGEENAN GEL CONTAINING KAOLINITE 78

3.4.1 Kaolinite, $Al_2Si_2O_5(OH)_4$ 78

3.4.2 Nine Days Diffusion 79

3.4.3 Eight Months Diffusion 80

3.4.4 Nine Days Diffusion Followed by Eight Months in Distilled Water 81

3.5 DISSOLVING GEOTHITE IN A SAMPLE CONTAINING KAOLINITE 82

3.6 HOMOGENEOUS PRECIPITATION OF IRON OXYHYDROXIDE WITHIN SILICA GEL BY HYDROLYSIS OF UREA ... 83

3.1 IRON OXYHYDROXIDE IN GELS

The main reactions expected from metal cations are as follows:

1. HEPES or HEPPS Solution:

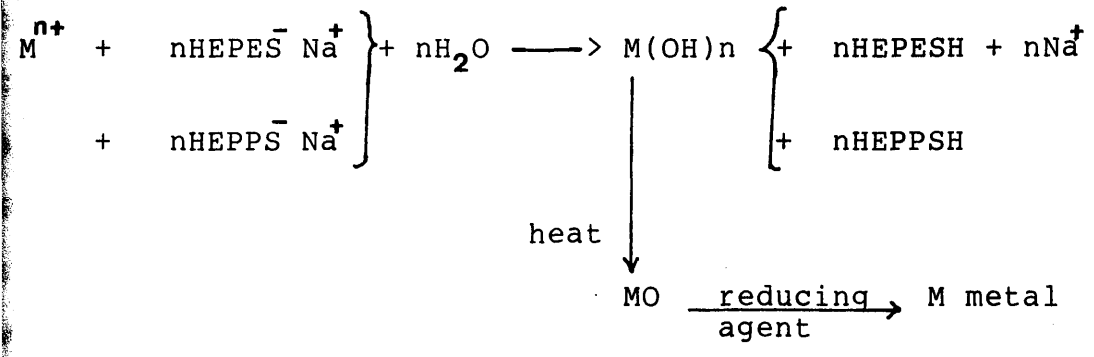

2. $NaHCO_3$ Solution:

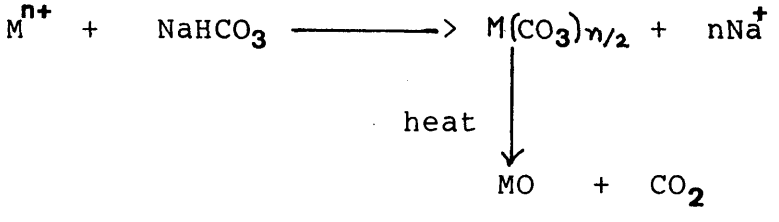

3.1.1 Various Gels and Alkali Sources

Particles do grow in a variety of gels, but for practical purposes, the growth media which concern us are as mentioned in Chapter 2: 2.7.1.

Preliminary work by Baird and Braterman (1984, which was included in Abdullah et al., 1986) had shown that elongated ferrihydrite bundles were formed by diffusion in silica gel.

After precipitation, it was evident that the precipitate was formed more rapidly in mixed gel than in carrageenan alone. The precipitate appeared mainly in

two zones; a red-brown precipitate at zone A and a yellow-orange precipitate at zone B (Fig. 3.1). The former zone increased only to about 7 mm depth and its colour fades away downwards along the tube; occasionally brown Liesegang rings formed instead. This zone is called the hydroxide-rich zone, whereas the precipitate at zone B increased rapidly until it reached zone C. Precipitate at zone B thickened by aging and it is called the main precipitation zone. Precipitate zone C was formed after zone B had been formed and its colour fades away to light yellow; it is called the metal-rich zone.

The main precipitation zone from various gels was examined under the electron microscope. Plate 3.1 shows a clear example of particle growth in mixed gel as elongated hair-like bundles. Plate 3.2 shows material grown in silica gel, which has interfered with the formation of bundles. Plate 3.3 shows bundles grown in carrageenan in the absence of silica gel; growth is slower and the form less well-developed than in the mixed gel.

Thus, silica gel has an important role in gel media but the details depend on the ratio to other gelling media.

Despite their different morphologies, all three kinds of material gave similar electron diffraction patterns (Plate 3.4) with two strong spacings, 0.153 nm

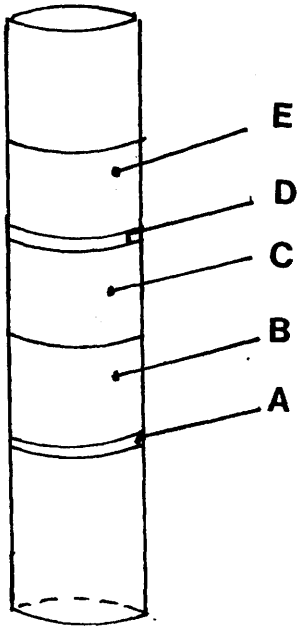

Fig. 3.1.

Precipitation zones of ferrihydrite in the gel plug.

A : The hydroxyl ion rich zone.
B : The main precipitation zone.
C : The metal ion rich zone.
D : The surface of gel plug.
E : The metal ion solution.

and 0.256 nm characteristic of ferrihydrite (a comparison with the standard spacings, A, B, and C is given in Table 3.1).

Since silica gel interfered in imaging the ferrihydrite morphology, and carrageenan gel alone slowed the particle growth, the mixed gel was chosen to grow ferrihydrite.

After diffusion reaction for two weeks within mixed gel, two zones of precipitate appeared at zones A and B (Fig. 3.1). The yellow-orange precipitate was examined from all the different conditions of alkali source (Chapter 2 : 2.7.1); its typical morphology is shown in Plate 3.1 and its diffraction patterns (2 strong rings) is shown in Plate 3.4.

Thus, it seems that any alkali source can be used to grow ferrihydrite.

Therefore, mixed gel and $NaHCO_3$ solution were chosen for detailed growth studies of ferrihydrite; this solution has the advantages of low pH and cheapness.

3.1.1.1 Change of pH

The pH of the region surrounding the precipitate increased with time at every zone as the result of diffusion (Table 3.2).

At the metal-rich zone, it was observed that precipitate formed after about 26 days, and started at pH 3.0.

TABLE 3.1

Electron Diffraction Result of Ferrihydrite in Gels,

Sec. 3.1.1

Pl 3.4 nm	A nm	B nm	C nm	Ferrihydrite nm	hkl
...	...	0.270	...	...	...
0.255	0.255	0.256	0.250	*0.254	100
...	0.225	0.227	...	*0.224	112
...	...	0.192	...	0.198	113
...	...	0.170	...	0.173	114
0.150	...	0.153	0.150	*0.151	115
...	0.147	0.147	...	*0.147	300,213

* : Indicates the strong rings.
Pl3.4 : The spacings from hair-like bundles in Plate 3.3.
A & B : d spacing of ferrihydrite reported by M. Kassim (1982).
C : d spacing of ferrihydrite reported by Chukhrov, et al. (1973).
Ferrihydrite : Standard d spacing (Towe & Bradley, 1967; Brown, 1953).

TABLE 3.2

pH Measurement of Precipitates at Various Zones by Aging of Iron Oxyhydroxide in Mixed Gel Using $NaHCO_3$ Solution. (Sec. 2.7.1)

Age (days)	pH A	pH B	pH C	pH D
6	...	3.0	3.0	6.8
8	...	3.0	3.0	6.8
10	...	3.0	3.0	6.8
12	...	3.0	3.0	6.8
14	...	3.0	3.5	6.8
16	...	3.0	3.6	6.8
18	...	3.0	4.8	7.1
20	...	3.9	4.8	7.1
26	3.0	5.1	6.8	7.7
30	3.0	5.1	7.1	7.7
34	3.6	7.7	7.7	7.7
37	3.6	7.7	7.7	7.7
40	7.1	7.7	8.0	8.3
44	7.4	7.7	8.0	8.3
47	7.7	8.0	8.0	8.3

A : Metal ion rich zone.
B : Main precipitation zone.
C : Hydroxide ion rich zone.
D : Below hydroxide ion rich zone.

In all other zones, precipitate formed after 6 days of diffusion and pH increased until it reached a constant value of between 7.7-8.3.

Hence, it was observed that the increase of pH at different zones did not give much information concerning the particle growth. For example, the precipitate at zones A and B (Fig. 3.1) are at the same pH of 8.0 but gave rise to size differences (Plate 3.5 & 3.7).

Therefore, the growth of ferrihydrite in gel would seem to be independent of the pH range.

3.1.1.2 Hydroxide-Rich Zone

The precipitate at this zone did not increase much over a period of days, and its morphology was in the form of small bundles throughout (Plate 3.5). The electron diffraction pattern was the same as that observed in Plate 3.4. It could be that metal ion was used up in zones B and C rather than moving further downwards.

3.1.1.3 Main Precipitation Zone

At this zone the yellow-orange precipitate increased and thickened by aging. Furthermore, transmission electron microscope images show bundles of fine fibrils after 8 days aging (Plate 3.6). These

bundles slowly thickened by the growth of new fibres after 47 days aging (Plate 3.7). The average diameter of a single fibril is about 0.7 nm (Plate 3.8). The electron diffraction pattern from material at this zone also resembled Plate 3.4. Long fibrils and cross-linkages of fibrils could be seen embedded in the gel (Plate 3.9) when the sample from the main precipitation zone was examined by SEM.

3.1.1.4 Metal-Rich Zone

At this zone the precipitate appeared as pale yellow and was imaged by transmission electron microscopy as long fibrils and rarely observed as bundles even after aging (Plate 3.10). A possible explanation is that once the nucleus had formed at the main precipitation zone, further precipitation in the metal-rich zone led only to a lengthening of the fibrils.

3.1.1.5 D Zone

In addition, when hydroxide ion diffused further and reached the uppermost part of the gel at region D (Fig. 3.1), yellow precipitate started to form at the surface of the gel. An electron micrograph of the precipitate is shown in Plate 3.11; its diffraction data

corresponded to ferrihyrite. It was noticed that two morphologies formed at this region; long fibrils similar to those found at the metal-rich zone (compare Plate 3.10) probably from the surface of the gel, and agglomerated, loosely aggregated particles of the same morphology as in Plate 3.26, prepared in mobile solutions (Chapter 2: 2.7.2).

3.1.1.6 Mechanism of Formation of Bundles

The formation of bundles and long fibrils of ferrihydrite within gels could be explained as follows:

Growth of New Fibrils: For a new fibril to form on the surface of an existing bundle, it is suggested that it is necessary for two particles to be present (Fig.3.2). Then both particles will move randomly until they collide or attract each other to form a new layer on top of the old one, and so forth (Fig. 3.2).

Tip Growth: At low concentration, growth of an existing layer could be explained as follows: if one particle reaches the surface, it will move randomly up and down along it until it reaches the most stable position, probably at either one end, and similarly with the next particle. Since concentration is low, there is little chance of it meeting another particle during this process. Thus a long fibril will form (Fig. 3.3).

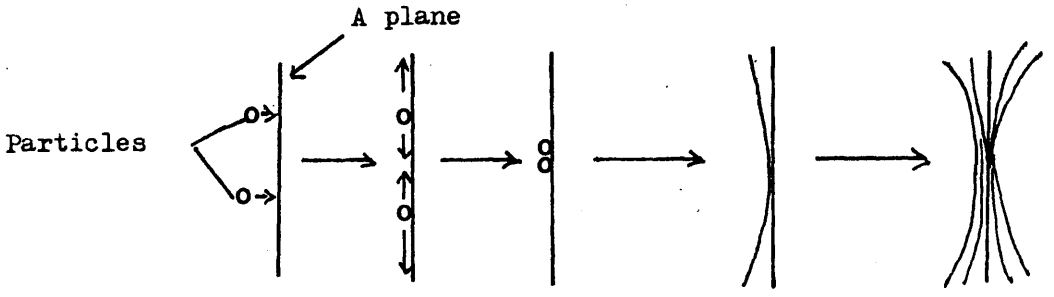

Fig.3.2.

Mechanism suggested for growth of new layer of ferrihydrite with gels; Sec. 3.1.1.6.

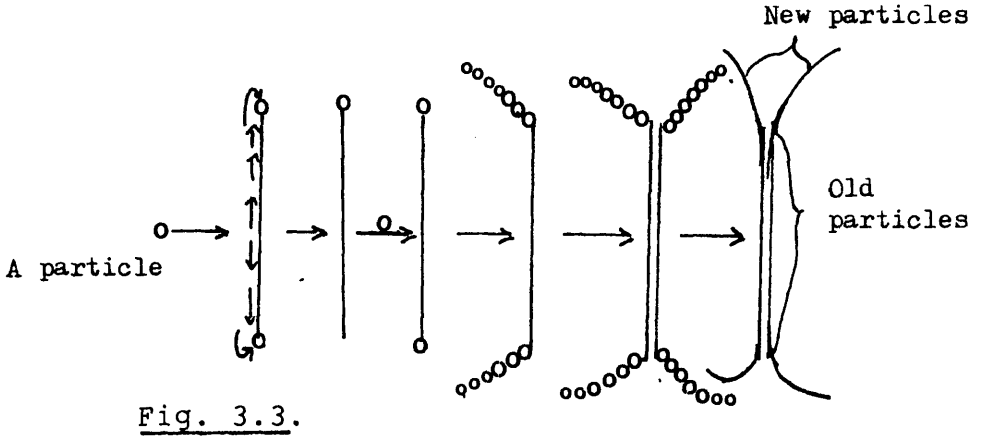

Fig. 3.3.

Mechanism suggested for tip growth of long fibril extending the ferrihydrite bundles within gels; Sec. 3.1.1.6.

3.1.1.7 Confirmation of Ferrihydrite's Morphology

The bundles of ferrihydrite observed by TEM probably represent their original morphology as formed by aging within gels.

Plate 3.12 from a sample prepared via the spray method (Chapter 2: 2.10.1.2) shows the bundles clearly - here the sample was examined without washing and disturbing the gel. Moreover, the micrograph from material prepared by the freeze-drying method (Chapter 2: 2.10.1.4) also shows similar bundles (Plate 3.13). Despite these fidings it might still be thought that the bundles could form when the sample was broken up with distilled water in specimen tubes.

However, another experiment was carried out by taking the sample within gel and embedding in resin with minimum disturbance of the sample (Chapter 2: 2.10.1.3). Here again (Plate 3.14) bundles of ferrihydrite could be seen; some bundles were distorted in shape which was caused while the sample was sectioned into thin slices.

It was also noticed that even under exceptionally high electron beam irradiation, bundles never formed from individual fibrils.

Thus, it seems that the bundles are the original morphology of ferrihydrite aging within gels. The different morphologies observed in 3 zones of the gel plug are probably due to:

(a) At very high supersaturation, fresh nuclei will form;

(b) At moderately high supersaturation, fresh fibrils will form on an existing nucleus; and

(c) At low supersaturation, growth of existing fibrils will result.

3.1.2 Effects of Aging on the Precipitates

3.1.2.1 In Carrageenan Gel

(a) After aging for 8 months in the double test tube the yellow-orange precipitate from the main precipitation zone, bundles of ferrihydrite transformed to small pod-shapes whose distribution followed the lines of the original fibrils (Plates 3.15, 3.17). The diffraction pattern was identified as that of goethite, α-FeOOH (Plate 3.16; Table 3.3). This pod-shaped goethite is similar to goethite, (M.Kassim, 1982) which was produced by aging ferrihydrite in solution at pH 6.4 for 20 days.

In Plate 3.15, and especially 3.17 it was observed that the pod-shapes formed almost at the identical angle of about 60 to each other (star-shaped twins). Plate 3.18 shows this angle in coarser material from the same section of the same gel plug. The single larger size of the star-shaped crystal is in part due to fact that the crystal consisted of several parallel twinned particles.

TABLE 3.3

Electron Diffraction Lattice Spacings from Aging Fe(III) in Carrageenan Gel for 8 Months & 26 days; Sec. 3.1.2.1a

Pl 3.16	Pl 3.19	A	Ferrihydrite		∝-FeOOH ASTM 17-536	
nm	nm	nm	nm	hkl	nm	hkl
0.412	...	...	...	...	*0.418	110
0.266	0.270	0.270	...	...	*0.269	130
0.247	0.247	0.248	...	...	0.249	040
0.243	...	...	0.246	111	*0.245	111
0.224	...	0.228	...	...	0.225	121
...	...	0.197	0.198	113	0.192	041
...	...	0.182	...	...	0.180	211
0.170	0.177	...	0.173	114	0.172	221
0.156	...	0.155	...	...	0.156	151,160
...	...	0.150	*0.147	300,213	0.147	320
0.143	0.145	...	...	...	0.142	112
...	...	0.138	...	...	0.139	330
0.131	...	...	...	...	0.132	321

* : Indicates the strong rings.
Pl3.16 : The spacings of pod and star-shaped crystals in Plate 3.15.
Pl3.19 : The spacings of small pod-shaped crystals grown on the fibrils in Plate 3.19.
A : d values of ∝-FeOOH reported by M.Kassim, plate 17b (1982).
Ferrihydrite : Standard d spacing (Towe & Bradley, 1967; Brown, 1953)

(Sudo et al., 1981; Petrovskaya, 1975). Such favored growth could have arisen from a high local concentration of growth species (fresh iron(III)).

Thus, the transformation of ferrihydrite to goethite has occurred by aging within carrageenan gel. This phenomenon probably occurs by a dissolution-reprecipitation mechanism (Feitknecht & Michaelis, 1962) under the influence of polysaccharide (carrageenan). This interpretation is supported by other report that some organic compounds can influence the transformation between the phases of iron oxyhydroxide (ferrihydrite, α, β and γ) (Taylor et al.,1987). Moreover, Cornell & Geovanoli (1985) reported that some simple sugars can influence the formation of goethite and hematite by hydrolysis and ageing of Fe(III) solutions.

These twinned particles are very similar to a single twinned α-FeOOH which was formed in solutions by Cornell et al. (1983) and Atkinson et al. (1968).

According to Cornell et al. (1974), such twinned crystals were always associated with other compounds. However, the material of Plate 3.17 formed several star-shapes along the bundle and was identified as goethite only. This morphology possibly occurred by transformation from ferrihydrite to pod-shaped goethite from the bundle's morphology as in Plate 3.20, followed by diffusion of fresh Fe(III). This process may represent the seeding of goethite within the gel;

freshly formed goethite will grow as parallel branches on the existing pod-shaped geothite (along the fibrils) at a constant angle of 60°, producing chains of star-shaped particles. Therefore, pod-shaped goethite probably occurred by dissolution and precipitation (aging). This morphology especially in Plate 3.17 is possibly to resemble the seeding of goethite within the gel which is similar to the seeding of ferrihydrite in Sec. 3.3.

In one case, goethite was observed growing on the fibrils of ferrihydrite after aging for only 26 days as indicated by the arrows in Plate 3.19. Diffraction data corresponded to ferrihydrite and goethite (Plate 3.19; Table 3.3). We do not know why goethite formed in this particular specimen at such a relatively early stage.

(b) Twenty six days old yellow-orange precipitate from the main precipitation zone was thoroughly washed and kept in distilled water at room temperature for more than 8 months, resulting in the production of pod-shaped crystals of α-FeOOH grown along the bundles as shown in Plate 3.20. This morphology can be explained if pod-shaped goethite was produced by dissolution and nucleation from ferrihydrite under the influence of carrageenan gel left in the tube. The lack of star-shaped twins in this sample is probably due to the absence of fresh Fe(III). The similar condition has been

explained that dissolution of ferrihydrite produces Fe(III) ions which give rise the formation of goethite in solution (Schwertmann & Murad, 1983).

3.1.2.2 In Silica Gel

(a) Aging ferrihydrite for six months resulted in silica gel almost separating out from the bundles. The bundles in Plate 3.21 gave the two strong diffractions, 0.257 nm (100) and 0.153 nm (115), of ferrihydrite.

(b) Two weeks old precipitate was washed free of gel and kept in distilled water for more than 8 months. The morphology was similar to that in Plate 3.2 and the material showed the 2 strong spacings of ferrihydrite.

Therefore, it appears that the silica gel blocked the transformation of ferrihydrite to goethite. A similar observation was made by Schwertmann & Taylor (1972) that soluble silica in soil was sufficient to retard the transformation of γ-phase to goethite or hinders nucleation of goethite. Brindley & Brown (1980) reported that the conversion of ferrihydrite to hematite in solution is inhibited by the presence of silica. Adsorbed silica species stabilise ferrihydrite (Carlson & Schwertmann, 1981). Similar factors are probably operating here.

3.1.2.3 In Mixed Gel

(a) Aging ferrihydrite for more than 8 months in the double test tube at room temperature produced the similar morphology and the same compound as in Plate 3.1; bundles of ferrihydrite.

(b) Two weeks old yellow-orange precipitate was thoroughly washed and kept in distilled water for more than 8 months at room temperature resulting the same compound and similar morphology as in Plate 3.1; identical as hair-like bundles of ferrihydrite.

Thus, it could be concluded that silica gel plays an important factor to inhibit the transformation of ferrihydrite to goethite although only a small proportion of silica gel is present.

3.1.3 Urea Added to the Silica Gel

It is known that urea hydrolyses at above 70° C, but this experiment was carried out at room temperature without hydrolysis in order to see if the morphology changed as a result of the presence of urea itself in solution (Chapter 2: 2.7.1.1). Transmission electron microscope studies of most areas showed very clear bundles (Plate 3.22) similar to those found in mixed gel (Plate 3.1). The diffraction pattern shows two broad bands characteristic of amorphous ferrihydrite.

In a few areas, small loosely aggregated particles were observed in addition to the bundles (Plate 3.23). Diffraction showed both ferrihydrite and α-FeOOH (Plate 3.23, Table 3.4).

Thus, in the presence of urea the bundle morphology was more clearly developed, and α-FeOOH was produced with a morphology not found elsewhere for this material in the present study. A complex may have formed between urea and Fe(III); this could speed up the conversion of ferrihydrite to goethite by a dissolution-precipitation mechanism.

3.1.4 $NaClO_4$ Solution Added to $NaHCO_3$ Solution

Transmission electron microscopy of 26 days aged yellow-orange precipitate within mixed gel, prepared as mentioned in Chapter 2: 2.7.1.3, showed bundles and its diffraction pattern showed 2 strong rings, 0.150 nm (115) and 0.257 nm (100), due to ferrihydrite.

One sample showed pod-shaped goethite forming from the fibrils of ferrihydrite after aging 26 days (Plate 3.24). Its diffraction data were identified as a mixture of the both two compounds (Plate 3.24, Table 3.5). It has been reported that pod-shape goethite was produced after aging iron(III) perchlorate solution at room temperature for 2 1/2 years (Feithnecht & Michaelis, 1962).

TABLE 3.4

Electron Diffraction Result of Urea Added to the Gel; Sec. 3.1.3

P13.23	Ferrihydrite		∝-FeOOH ASTM 17-536	
nm	nm	hkl	nm	hkl
0.444	...	...	*0.418	110
0.268	...	...	*0.269	130
0.229	*0.224	112	0.225	121
0.191	*0.198	113	0.192	041
0.146	*0.147	300,213	0.1467	320
0.136	...	...	0.1357	311
0.118	0.118	223,008& 312	0.1198	341
...	...		...	...

* : Indicates the strong rings.
P13.23 : The spacings from loosely aggregated particles in Plate 3.23.
Ferrihydrite : Standard d spacing (Towe & Bradley,1967; Brown, 1953).

TABLE 3.5

Electron Diffraction Data for Ferrihydrite and α-FeOOH, Sec. 3.1.4

P13.24	Ferrihydrite		α-FeOOH ASTM 17-536	
nm	nm	hkl	nm	hkl
0.418	...	...	*0.418	110
0.257	*0.254	100	0.258	021
0.227	*0.224	112	0.225	121
0.174	0.173	114	0.172	221
0.154	*0.151	115	0.151	250, 002

* : Indicates the strong rings.
P13.24 : The spacings from pod-shaped crystals in Plate 3.24.
Ferrihydrite : Standard d spacing (Towe & Bradley, 1967; Brown, 1953).

3.1.5 NaCl Solution Added to $NaHCO_3$ Solution

Yellow-orange precipitate prepared as described earlier (Chapter 2: 2.7.1.4) showed the morphology as bundles and its electron diffraction data were identified only as ferrihydrite. Thus, chloride ion addition gave no effect in morphology or the composition of the materials formed within gels. Gildawie, p.72 (1977) reported that cigar-shaped crystals of β-FeOOH could be obtained by hydrolysis of 0.1M ferric chloride solution at room temperature for 14 days. Other workers have reported that if the solution contains fluoride or chloride ions at the ratio for Cl^-/Fe^{3+} was 0.55 (Matashige & Yusuke, 1979), or that on hydrolysis at room temperature of concentrated $FeCl_3$ solution with Na_2CO_3 or NaOH solution (Pechenyuk et al.,1985), β-FeOOH could be produced. Feitknecht et al. (1975) reported that the transformation of the amorphous iron(III) oxide hydroxide to β-FeOOH occurred at high concentration of chloride ions; Fe^{3+}:Cl^-, 0.026M:0.34M left for one year reaction or 0.0064M:0.085M left for 13 years.

It seems that the beta form can be produced only at fairly high concentration of chloride ion or by aging for years at low concentration. Thus, it is no wonder that β-FeOOH was never been observed in this study; Fe^{3+} (0.1M), Cl^- (0.083M).

Chloride ion is essential for the formation of the beta form of the oxyhydroxide (Paterson & Rahman, 1983, 1984) because chloride ion is included tightly within β-FeOOH crystal (Matashige & Yusuke, 1979) and if chloride ions have been washed from the crystals α-FeOOH would be formed instead (Mackay, 1960).

3.1.6 Effect of Heat

All the precipitates (within the gel) were washed before the heating process was carried out as described in Chapter 2: 2.8.1.

3.1.6.1 In Silica Gel

When samples of the yellow-orange precipitate of ferrihydrite were heated at 85° C and 98-100° C for 2 or 5 hours, neither their morphology nor their compounds changed and the diffraction data corresponded to 0.253 nm (100) and 0.150 nm (115) spacings of ferrihydrite. The morphology was similar to Plate 3.1.

This indicates that silica gel is an inhibitor of morphological transformation and a stabilizer of the original compound of the materials.

As described earlier (Chapter 2: 2.3.1) silica gel became mobile at about 95° C, therefore, after heating the sample at 98-100° C the bundles could be seen clearly without interference from the gel.

3.1.6.2 In Mixed Gel

Electron microscope studies of ferrihydrite after heating for 5 hours at 98-100° C, showed pod-shaped particles but still arranged in bundles (Plate 3.25). Its diffractions indicated mainly goethite but are consistent also with the presence of some ferrihydrite (visible as fibrils at arrow `a´); also present are weak spots, corresponding to a spacing of 0.362 nm, and assigned to $\alpha$-$Fe_2O_3$ (Plate 3.25; Table 3.6, shown at arrow `b´). This spherical aggregated particles are possibly α-Fe_2O_3 particles which are similar in morphology to those reported by Matijević (1981) and Towe & Bradley (1967).

As described in Chapter 2: 2.3.3, mixed gel became mobile at 60-65° C, but some of the ferrihydrite evidently still remains as fibrils holding the bundles in shape. The transformation of iron oxyhydroxide to α-Fe_2O_3 by heating is a well-known process (Nobuoka & Ado, 1966; Zolotovskii et al., 1977; Watari et al., 1983).

Moreover, there is evidence that ferrihydrite will transform to hematite in an aqueous medium at 92° C (Johnston & Lewis, 1983) and goethite will form after heating ferrihydrite suspensions at 70° C in alkali medium at pH 11.2-14 (Cornell & Gioivanoli, 1985).

TABLE 3.6

Electron Diffraction Data for α-FeOOH (by Heating Ferrihydrite;) Sec. 3.1.6.2

P13.25	α-FeOOH ASTM 17-536		α-Fe_2O_3 ASTM 13-534		Ferrihydrite	
nm	nm	hkl	nm	hkl	nm	hkl
0.446	*0.418	110	...	...	...	...
0.364	...	...	*0.366	012	...	...
0.260	*0.269	130	*0.269	104	...	...
0.242	*0.245	111	...	...	*0.246	111
0.185	0.180	211	0.184	024	...	...
0.167	0.169	240	*0.169	116	...	...
0.161	0.161	231	0.160	018	...	...
0.154	0.156	151,160	...	...	*0.151	115

* : Indicates the strong rings.
P13.25 : the spacings from the pod-shaped crystals in Plate 3.25
Ferrihydrite : Standard d Spacings (Towe & Bradley, 1967; Brown, 1953).

3.2 IRON OXYHYDROXIDE IN MOBILE SOLUTIONS

Yellow-orange precipitate from two types of preparation (Chapter 2: 2.7.2.1 & 2.7.2.2) were examined in the electron microscope. Both samples gave a similar morphology of loosely aggregated particles of different sizes (Plate 3.26). This observed morphology is similar to that in Plate 3.11 which was grown above the gel plug and also to the results of other work (Sutherland, 1970; Saleh & Jones, 1984; Jones & Saleh, 1986).

These two experiments were carried out in order to confirm the interpretation offered for the morphology of ferrihydrite in Plate 3.11; Sec. 3.1.1.5.

Its diffraction pattern showed 2 broad bands corresponding to spacings of 0.153 nm and 0.255 nm, characteristic of ferrihydrite.

Furthermore, on aging the yellow-orange precipitate in the solution for 7 days, its morphology changed as in Plate 3.27; needle crystals grew outwards from aggregated particles which possibly would transform to goethite crystals by further aging. The diffraction data were still identified as ferrihydrite (spacings of 0.153 nm (115) and 0.256 nm (100)).

It is reported that a mixture of goethite and hematite will form by storing ferrihydrite in an aqueous solution at 24° C and pH 2.5-12.0 for < 3 years (Schwertmann & Murad, 1983).

3.3 IRON OXYHYDROXIDE IN MIXED GEL; EFFECT OF FERRIHYDRITE SEEDS

3.3.1 Metal Ion Rich Zone; Seeded

First generation of seeding precipitation from this zone shows long fibrils extending from ferrihydrite seed (Plate 3.28). The seed is indicated by an arrow.

Plate 3.29, second generation of seeding precipitation which was prepared from the first generation precipitate shows only long fibrils which are similar to Plate 3.10. These long fibrils possibly form from seeded ferrihydrite by extending existing fibrils. In addition, some areas show the formation of small bundles which are similar to Plate 3. 5. The long fibrils are probably new ferrihydrite extending on seeded ferrihydrite, whereas the small bundles are probably new ferrihydrite which form in parallel with long fibrils.

3.3.2 Main Precipitation Zone; Seeded

Plate 3.30 shows long fibrils extended from bundles. The fibrils are probably the freshly formed ferrihydrite and the bundles (arrowed) are the seeds.

3.3.3 Low Concentration of Fe(III) Solution (0.05, 0.01M); Unseeded

There was only one band of yellow-orange precipitate (similar to main precipitation zone). This was formed after 22 days aging in mixed gel. Examination in the electron microscope, reveals large bundles which are identical with Plate 3.1.

Therefore the finding in Sec.3.3.1 that long fibrils and small bundles existed is the result of the presence of seeds and is not due to lowering the concentration of Fe(III) solution which might be used up by the upper zone in the gel plug during the seeding process (Sec. 2.7.3).

Therefore in the seeding experiment (the real experiment of Sec 2.7.3) it could be concluded that few fresh nuclei hardly form even at the main precipitation zone but long fibrils extending on the existing seeds are formed instead of new bundles.

From these morphologies the growth of ferrihydrite within gels can be explained as follows:

(a) In the absence of seeds, the growth of the particles depends on the concentration. Nuclei will start to form at a critical concentration as in curve `a´ shown in Fig. 3.4. Therefore, nuclei will form at the main precipition zone and hydroxide ion rich zone and develop into bundles.

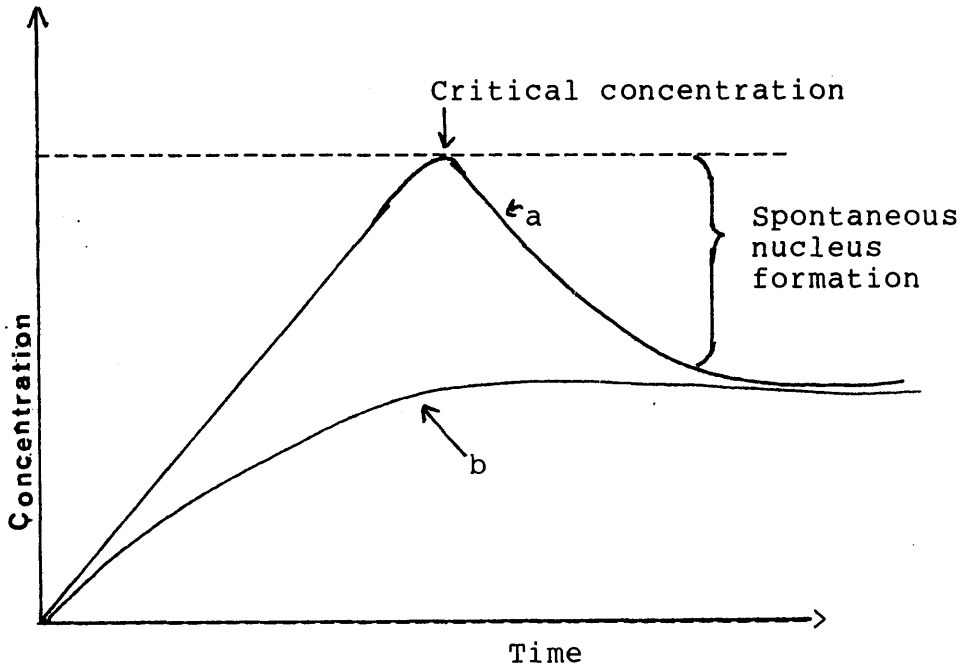

Fig. 3.4.

Role of ferrihydrite seeds on the particle growth of iron oxyhydroxide within gels.

Curve a : Absence of seeds.
Curve b : Presence of seeds.

(b) In the presence of seeds, the growth of the particles will form below the critical concentration point as in curve `b´ shown in Fig. 3.4. Therefore, the particles will grow on the existing seeds by extending their fibrils.

In addition, the morphology from the main precipitation zone from the control experiment (test of null hypothesis) which was run parallel with the real one revealed large bundles identical with those of Plate 3.1, so that the possibility of spurious effects, due to such factors as gel aging, can be excluded.

3.4 IRON OXYHYDROXIDE IN CARRAGEENAN GEL CONTAINING KAOLINITE

3.4.1 Kaolinite, $Al_2Si_2O_5(OH)_4$

A fine suspension of kaolinite in distilled water was examined in the electron microscope. It shows a pseudo-hexagonal morphology with thin plates and sharp edges as in Plate 3.31. Electron diffraction patterns (Plate 3.31) gave spacings as in Table 3.7 which are similar to kaolinite (ASTM 6-221, 12-447 and 14-164). This morphology is quite similar to which was observed by Sudo et al. (1981).

TABLE 3.7

Electron Diffraction Spacings from Standard Kaolinite

Sec. 3.4.1

P13.31	ASTM 6-0221		ASTM 12-447		ASTM 14-164	
nm	nm	hkl	nm	hkl	nm	hkl
0.466	...	...	...	...	...	...
0.435	...	...	0.434	110	0.437	110
0.266	...	...	...	...	...	...
0.242	0.239	003	0.248	131	0.239	003
0.231	0.234	202,131	0.233	202,113	0.234	131,113
0.174	0.179	004	0.178	004	...	...
0.170	0.167	204,133	0.1698	222	...	...
0.154	0.154	134,203	0.154	...	...	...
0.152	0.149	060,331	0.148	...	0.149	...
0.132	0.131	204	...	...	...	...
0.128	0.129	261,401	...	...	...	...
0.126	0.127	334,062,	...	...	...	...
...	...	332	...	...	...	...

Plate3.31 : Standard kaolinite from Georgia, USA.
A.S.T.M 6-0221 : Sample from Pugu, Tanganyika.
A.S.T.M 12-447 : Sample from Banska Bela, Czechoslovakia.
A.S.T.M 14-164 : Sample from Scalby, Yorkshire, England.

3.4.2 Nine Days Diffusion

It was noticed that the precipitate formed rapidly in the presence of kaolinite (9 days diffusion) Examination in the electron microscope showed large, thick, irregularly-shaped particles of collective pseudo-hexagonal kaolinite among the bundles in all 3 zones (or perhaps some other layer silicate).

It is suggested that various morphologies of kaolinite containing interlayer water can be formed; tubes, laths, ball, scrolls, and plates with rolled edges (Cairns-Smith, 1982).

(a) Metal Ion Rich Zone (Plate 3.32)

Thin bundles consisting of a few fibrils were sometimes apparently associated with large particles. Diffraction patterns from a large particle which was chosen at the thinest part from this zone are shown in Plate 3.33. The spacings correspond to some of the spacings of standard kaolinite (Table 3.8). Therefore, the large particles are aluminosilicate possibly containing a kaolinite-ferrihydrite complex. Cronstedtite, 1:1 layer silicate is a very iron-rich layer silicate containing ferric ions at tetrahedral sides (Geiger et al., 1983). The small bundles are identified as ferrihydrite ; 0.256 nm (100), 0.221 nm (112), 0.198 nm (113) and 0.155 nm (115). These bundles seem to be more crystalline than before (4 spacings not just 2). This

TABLE 3.8

Electron Diffraction Spacings from Iron Oxyhydroxide in the Carrageenan Gel Containing Kaolinite, Secs. 3.4.2, 3.4.3 & 3.4.4

P13.33 nm	P13.37 nm	P13.38 nm	P13.31 nm
0.621	...	...	...
...	0.424	0.406	...
0.353	0.355	...	...
0.306	0.302	...	...
0.287	0.289	...	...
0.221	...	0.230	0.231
0.217	0.213	...	...
...	0.208	...	...
0.204	0.203	0.204	...
0.189	0.189	...	...
...	0.184	...	...
0.176	...	...	0.174
0.171	0.171	...	0.170
...	0.167	...	...
0.154	...	0.154	0.154
...	...	0.152	0.152
...	...	0.137	0.132

P13.31 : Standard kaolinite from Georgia, USA.
P13.33 : Spacings from a large particle from metal ion rich zone, after 9 days aging.
P13.37 : Spacings from metal rich zone after 8 months diffusion.
P13.38 : Spacings from main precipitation zone, after 9 days diffusion followed by 8 months in distilled water.

crystallinity is probably due to the presence of kaolinite. It has been reported that better diffraction data of ferrihydrite is provided when kaolinite is coated with ferrihydrite (Jones & Saleh, 1986).

(b) Main Precipitation Zone (Plate 3.34 and 3.35)

Fully developed ferrihydrite bundles are formed after only 9 days diffusion and are comparable to those in Plate 3.3 formed after 26 days aging. Thus rapid growth of the particles is probably due to the presence of kaolinite within carrageenan gel.

(c) Hydroxide Ion Rich Zone (Plate 3.36)

Small bundles form and some associate with the large particles.

3.4.3 Eight Months Diffusion

Plate 3.37 shows clearly hexagonal kaolinite crystals associated with iron oxyhydroxide on the surface (and possibly between the layers of kaolinite). This can arise because the surface of clay layers carries negative charges, whereas the edges carry positive charges and clay has the unique property of expanding its lattice in presence of water (Bahadur & Ranganayaki, 1981). This electron micrograph (Plate 3.37) was taken from the red-brown precipitate at the metal ion rich zone. Diffraction pattern spacings (Plate 3.37) correspond to kaolinite (Table 3.8), with one

basal spacing 0.424 nm (110) characteristic of α-FeOOH. Therefore, probably dissolution and precipitation from ferrihydrite bundles have occurred.

Therefore, goethite was formed by dissolution and subsequent growth of nuclei; it is effected by carrageenan gel (Sec. 3.1.2.1) rather than kaolinite. Hence, kaolinite accelerates the growth of ferrihydrite.

The morphology and diffraction pattern of the yellow-orange precipitate in the main difraction zone were similar.

An other possible explanation is that `kaolinite´ after 8 months diffusion has re-formed into hexagons and that these may contain some Fe(III) substituted for Al(III).

3.4.4 Nine Days Diffusion Followed by Eight Months in Distilled Water

The sample was taken from the main precipitation zone. Plate 3.38 shows bundles and a large particle similar to that in Plate 3.34. It can be seen that some bundles appear to be associated with the large particle which is believed to be kaolinite. The bundles are identified from the diffraction spacings as ferrihydrite, 0.154 nm (115) and 0.259 nm (100). The large particle in Plate 3.38 gave the diffraction pattern shown in Plate 3.38 and its spacings correspond to the standard kaolinite and are similar to the large particle in Plate 3.33 (Table 3.8).

The possible explanation is that at the early stage of precipitation it would produce only ferrihydrite and the phase transformation was inhibited by the presence of silicate species in kaolinite even though carrageenan gel was present. It has been observed in model soils that adsorbed silica may retard the transformation of ferrihydrite to the more stable goethite (Carlson & Schwertmann, 1981).

Thus, the ferrihydrite-kaolinite complex formed at the early stage of diffusion at about pH <7.0 and the goethite-kaolinite complex formed after about 8 months of diffusion ; pH at about > 7.0 but < 9.0.

Concerning the above results, it has been reported that the formation of ferrihydrite- kaolinite complex occurred at pH 4.1 leading to a reduction of the total net negative charge of the kaolinite particles. Hence, positively charged particles of ferrihydrite are retained on the negatively charged kaolinite surface by a Coulombic force (Yong & Ohtsubo, 1987). Such effects have been observed in model soils (Jones & Saleh, 1986).

3.5 DISSOLVING GOETHITE from a SAMPLE CONTAINING KAOLINITE

An attempt was made to dissolve goethite from the sample discussed in Sec. 3.4.3 in acid oxalate for 15 minutes. An electron micrograph of the resulting material was similar to that of Plate 3.37.

This negative result is probably due to insufficient time in dissolving process, because it was reported that once the ferrihydrite-kaolinite complex formed it is extremely stable (Yong & Ohtsubo, 1987). It is known that freshly formed ferrihydrite is a reactive material with a high isoelectric point and is predominantly positively charged up to a pH of about 8 (Parks, 1965).

3.6 HOMOGENEOUS PRECIPITATION OF IRON OXYHYDROXIDE WITHIN SILICA GEL BY HYDROLYSIS OF UREA

The yellow-orange precipitate prepared by Dr. M.Kaya according to this technique (Sec. 2.9; Table 2.2) is illustrated in Plate 3.39 as pod-shaped particles associated with silica gel. The electron diffraction spacings correspond to α-FeOOH (Table 3.9). The experiment was repeated (by me) several times giving the morphological results similar to Plate 3.39 on every occasion, but sometimes the electron diffraction spacings corresponded to ferrihydrite rather than goethite. It has been reported previously that α-FeOOH, α-Fe_2O_3 and $NH_4Fe_3(OH)_6(SO_4)_2$ were formed by hydrolysis of urea with ferric sulphate salt solution (Lorenz & Kempe, 1984). Thus, again, silica gel retarded the morphological and phase transformations.

TABLE 3.9

Electron Diffraction Spacings of ∝-FeOOH by Hydrolysis of Urea (Sec. 3.6)

P13.39 nm	∝-FeOOH ASTM 17-536 nm	hkl
0.346	0.338	120
0.265	*0.269	130
0.244	*0.245	111
0.215	0.219	140
0.164	0.166	060
0.140	0.142	112

* : Indicates the strong rings.
P13.39 : The spacings from small pod-shaped particles associated with silica gel in Plate 3.39.

	Conditions	Silica gel	Mixed gel	Carr gel	Carr + Kao
Age Result	gel only R.T	54d ferri	54d ferri	54d ferri	9d ferri, kao,+ferri
Age Result	gel only R.T	6m ferri	8m ferri	8m goethite	8m goethite+ kao
Age Result	gel,then dist.H_2O, R.T	14d+8m ferri	14d+8m ferri	26d+8m goethite	9d+8m ferri,kao+ ferri
Age Result	gel,heated at 89-100°C	5 hrs ferri	5 hrs goethite+ +ferri+αF_2O_3	...	...

Fig. 3.5: Summary of iron oxyhydroxide obtained by diffusion of ferric ion solution in gels.

Key words: Carr : carrageenan, d : day, ferri : ferrihydrite, hrs : hours, kao : kaolinite, m : month and R.T : room temperature.

Plate 3.1:

26 days old hair-like bundles of ferrihydrite formed within mixed gel using $NaHCO_3$ solution as alkali source (Sec. 3.1.1).

Plate 3.2:

26 days old poorly crystalline hair-like bundles of ferrihydrite formed within silica gel using $NaHCO_3$ solution as alkali source (Sec. 3.1.1).

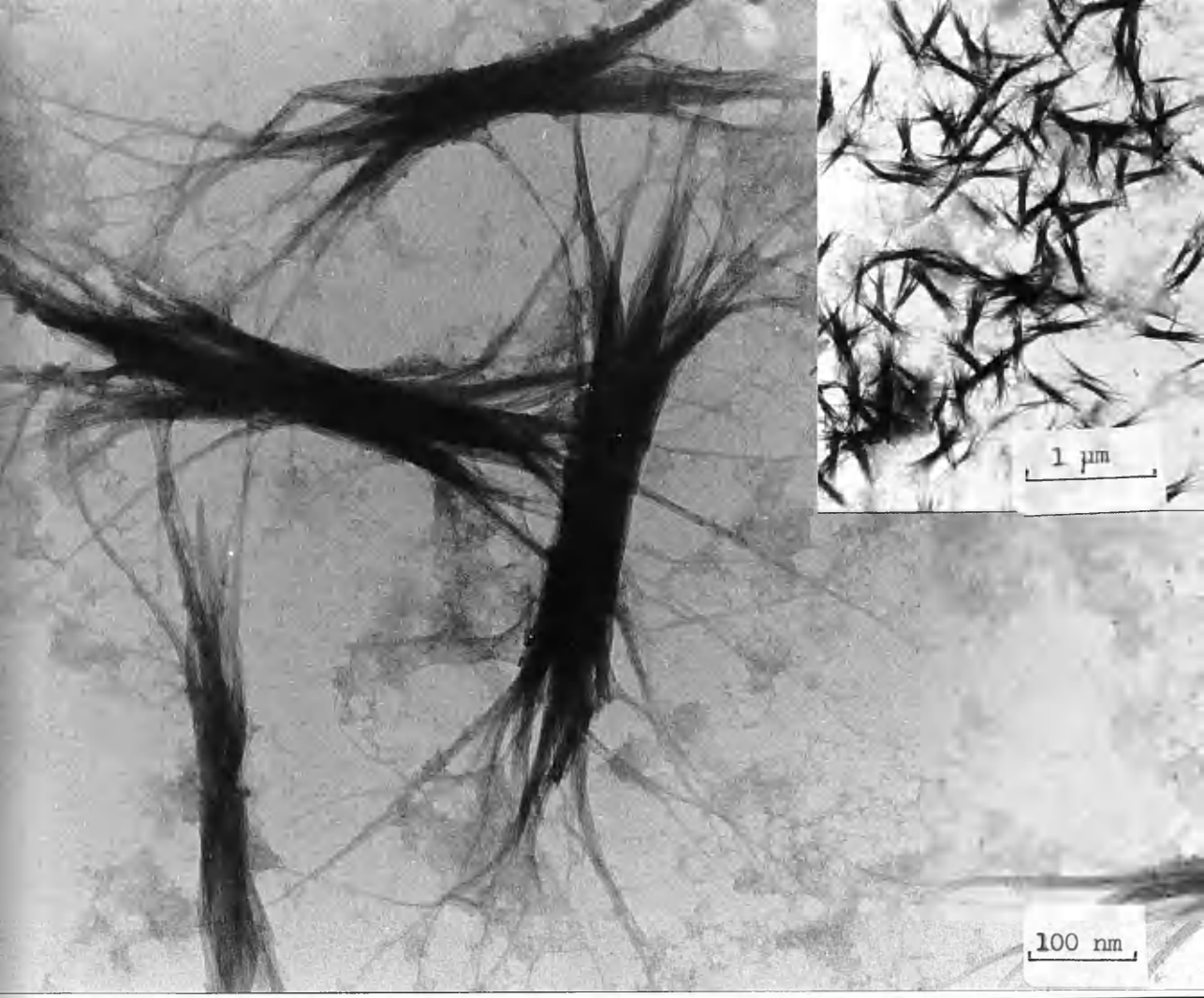
1 µm
100 nm


100 nm

Plate 3.3:

26 days old slowly developed hair-like bundles of ferrihydrite produced within carrageenan gel using $NaHCO_3$ solution as alkali source (Sec. 3.1.1).

Plate 3.4:

Electron diffraction pattern of ferrihydrite shown in Plate 3.3; Table 3.1.

Plate 3.5:

Small hair-like bundles of ferrihydrite formed within milxed gel at hydroxide-rich zone after 47 days aging (Sec.3.1.1.2).


100 nm

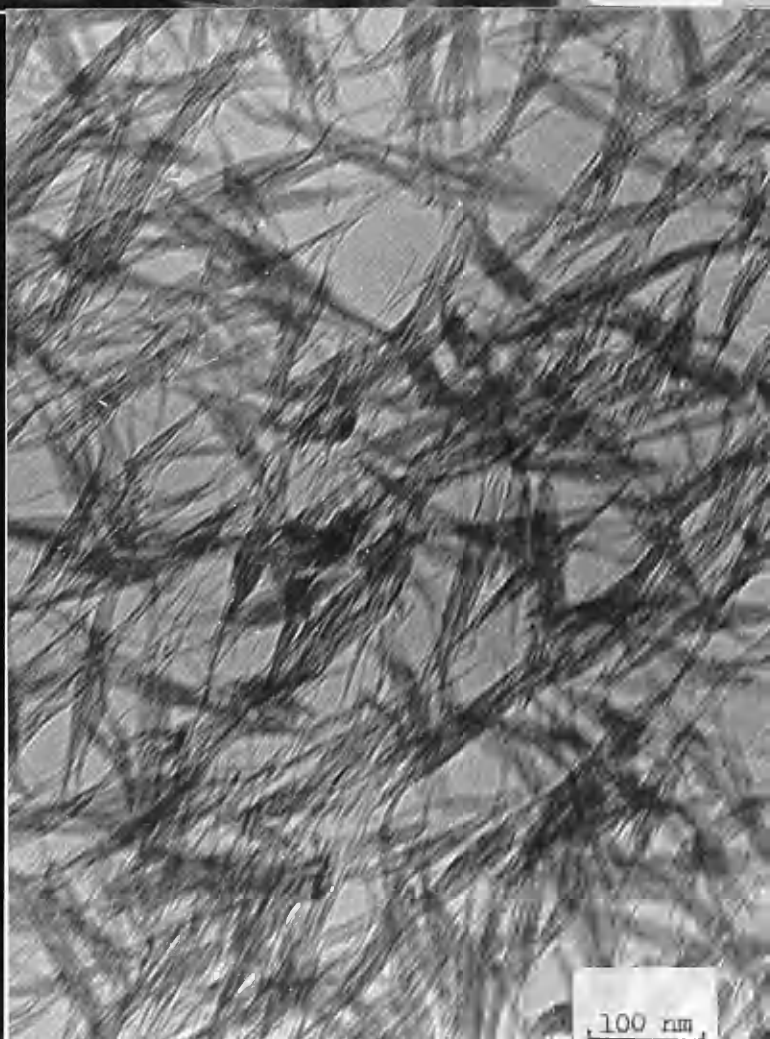
100 nm

Plate 3.6:

Ferrihydrite from main precipitation zone within mixed gel after 8 days aging (Sec. 3.1.1.3).

Plate 3.7:

Ferrihydrite from main precipitation zone within mixed gel after 47 days aging (Sec. 3.1.1.3).

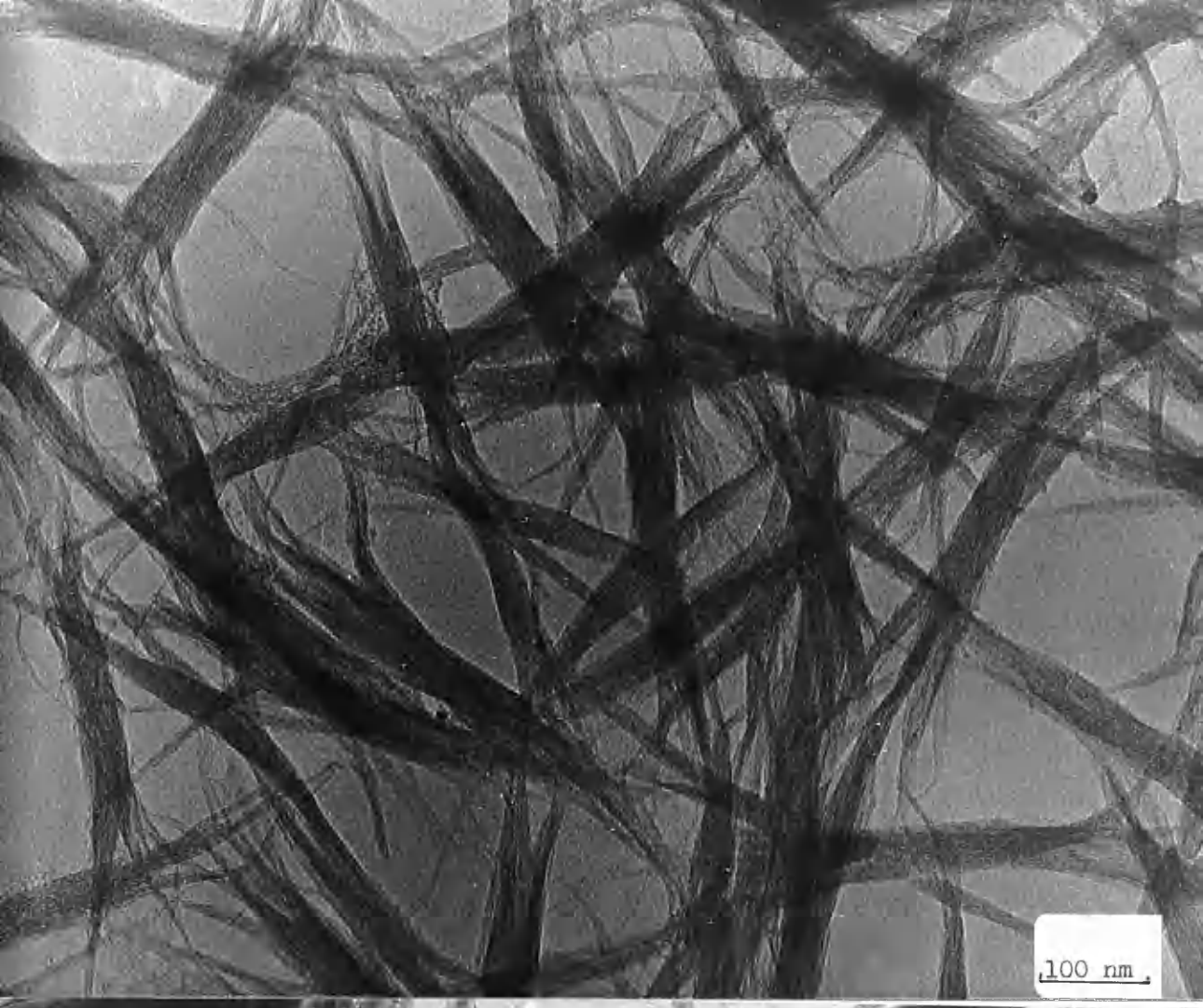
100 nm


100 nm

Plate 3.8:

Material prepared as in Plate 7 showing single fibrils at high magnification at about 0.7 nm diameter.

Plate 3.9:

Ferrihydrite (and mixed gel medium) formed within mixed gel from main precipitation zone; examined by SEM (Sec. 3.1.1.6).

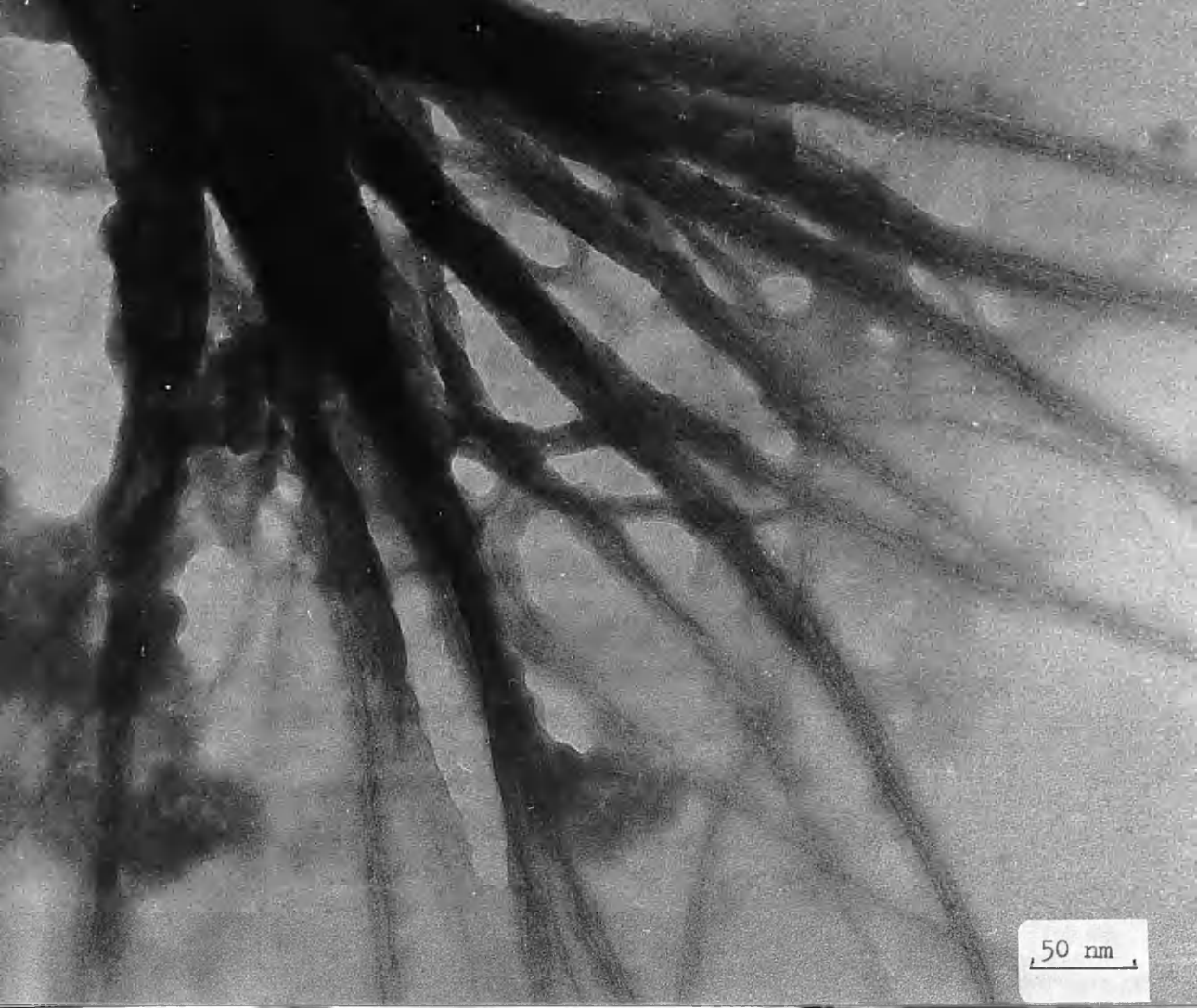
50 nm


4 µm

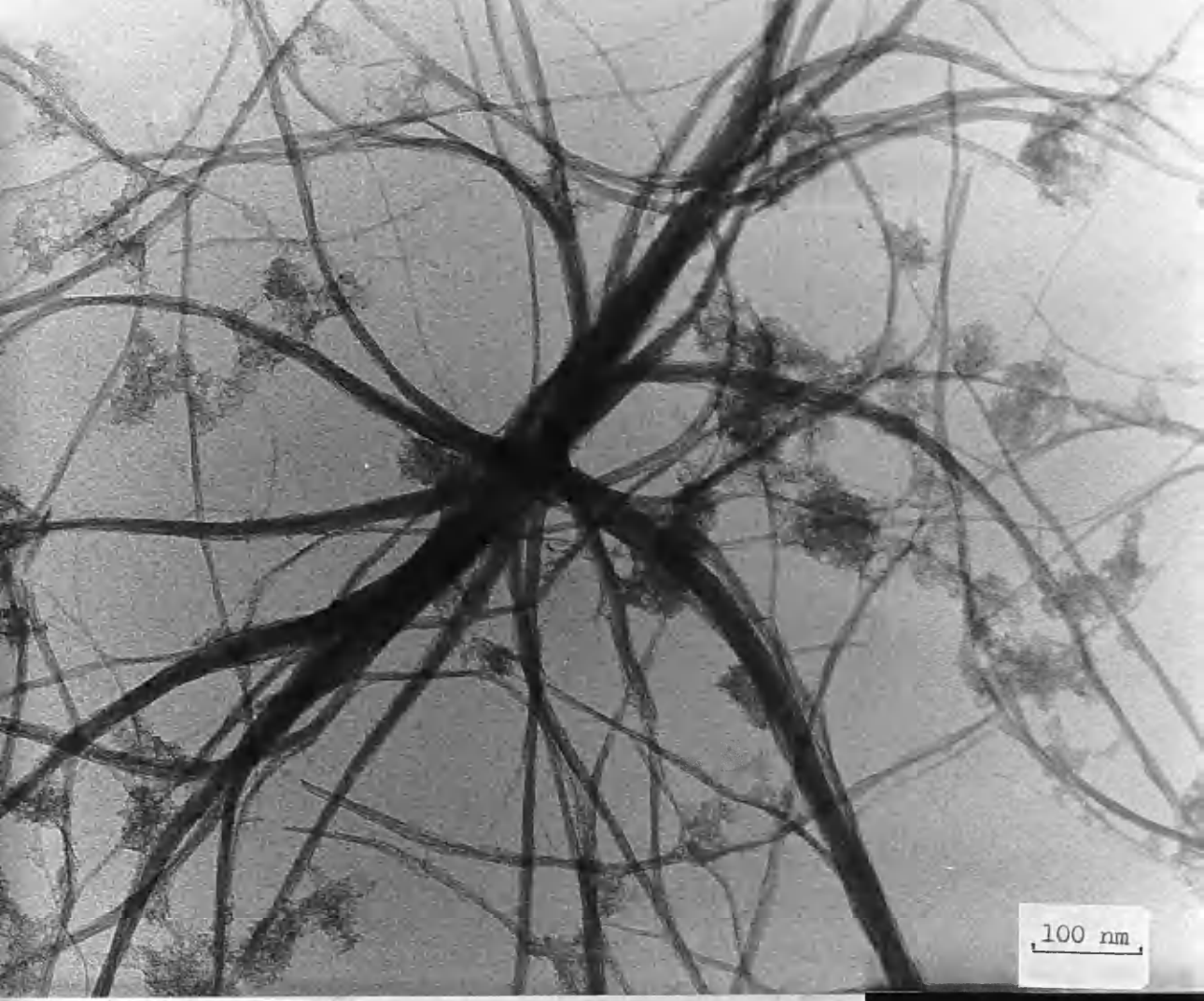
100 nm

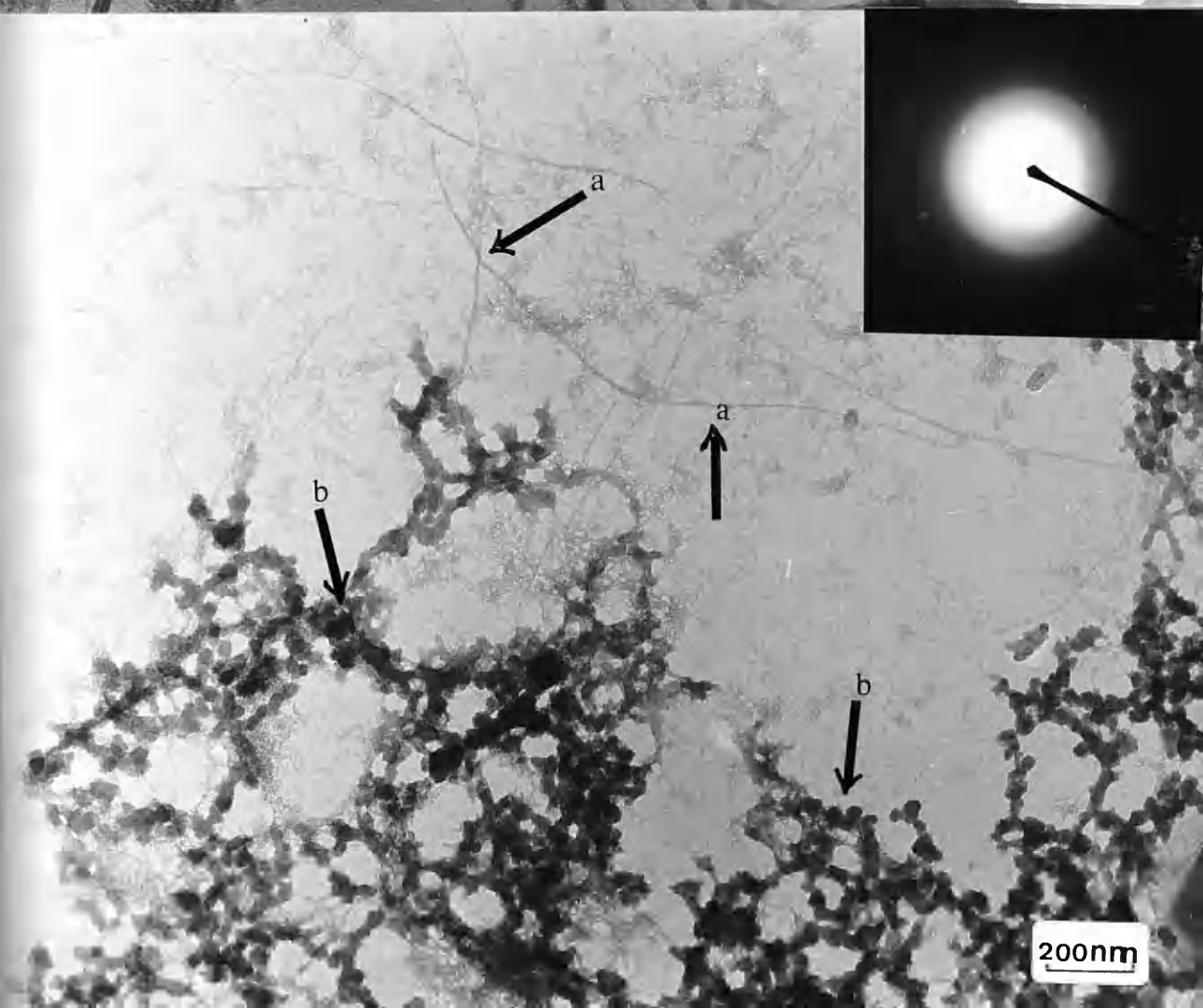
a
a
b
b
200nm


70 nm

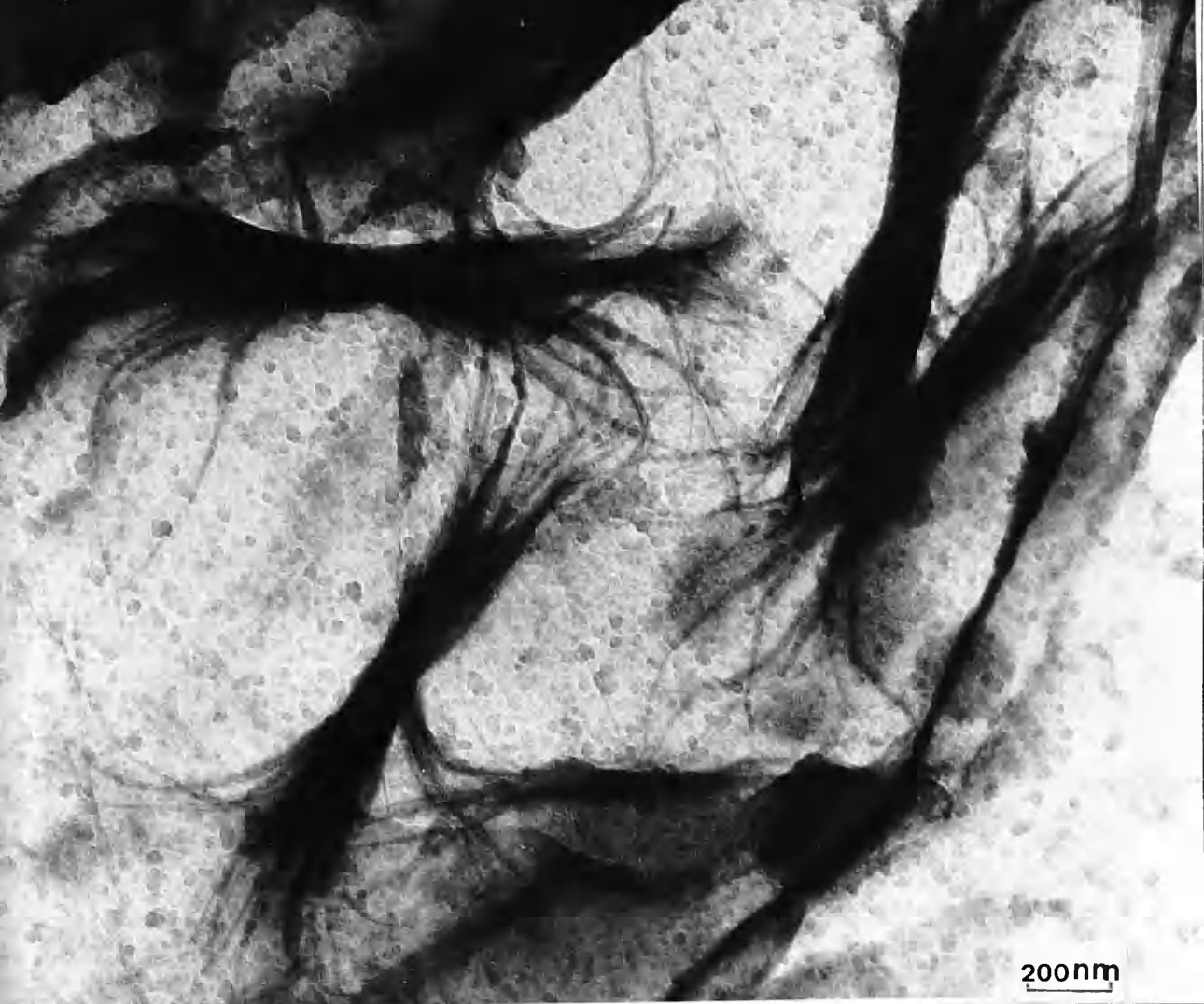
200nm

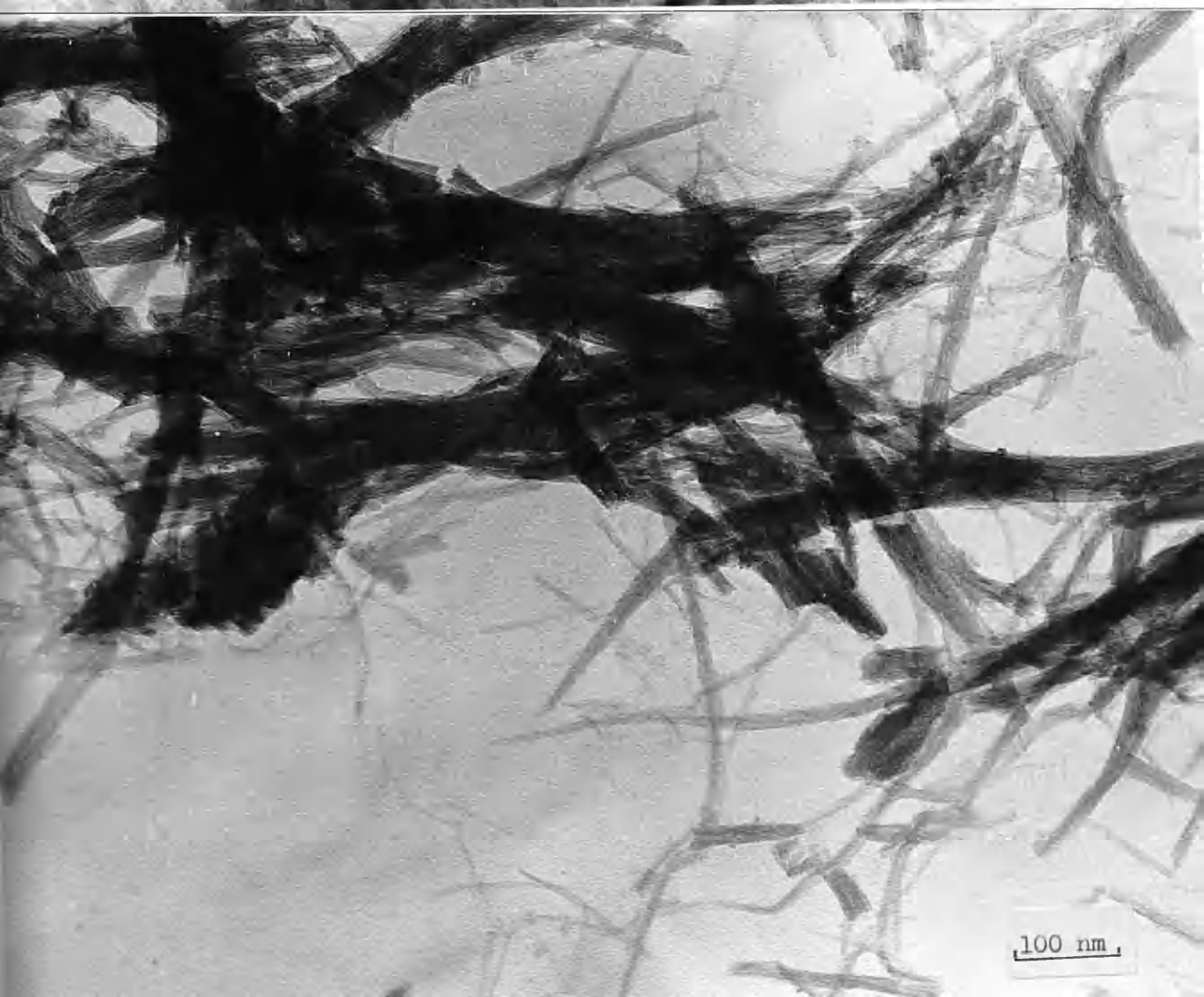
100 nm

Plate 3.15:

Pod-shaped and star-shaped crystals of α-FeOOH (from main precipitation zone) produced on aging the precipitate within carrageenan gel for 8 months at room temperature (Sec. 3.1. 2.1a).

Plate 3.16:

Electron diffraction pattern from the pod-shaped crystals shown in Plate 3.15; Table 3.2.


100 nm

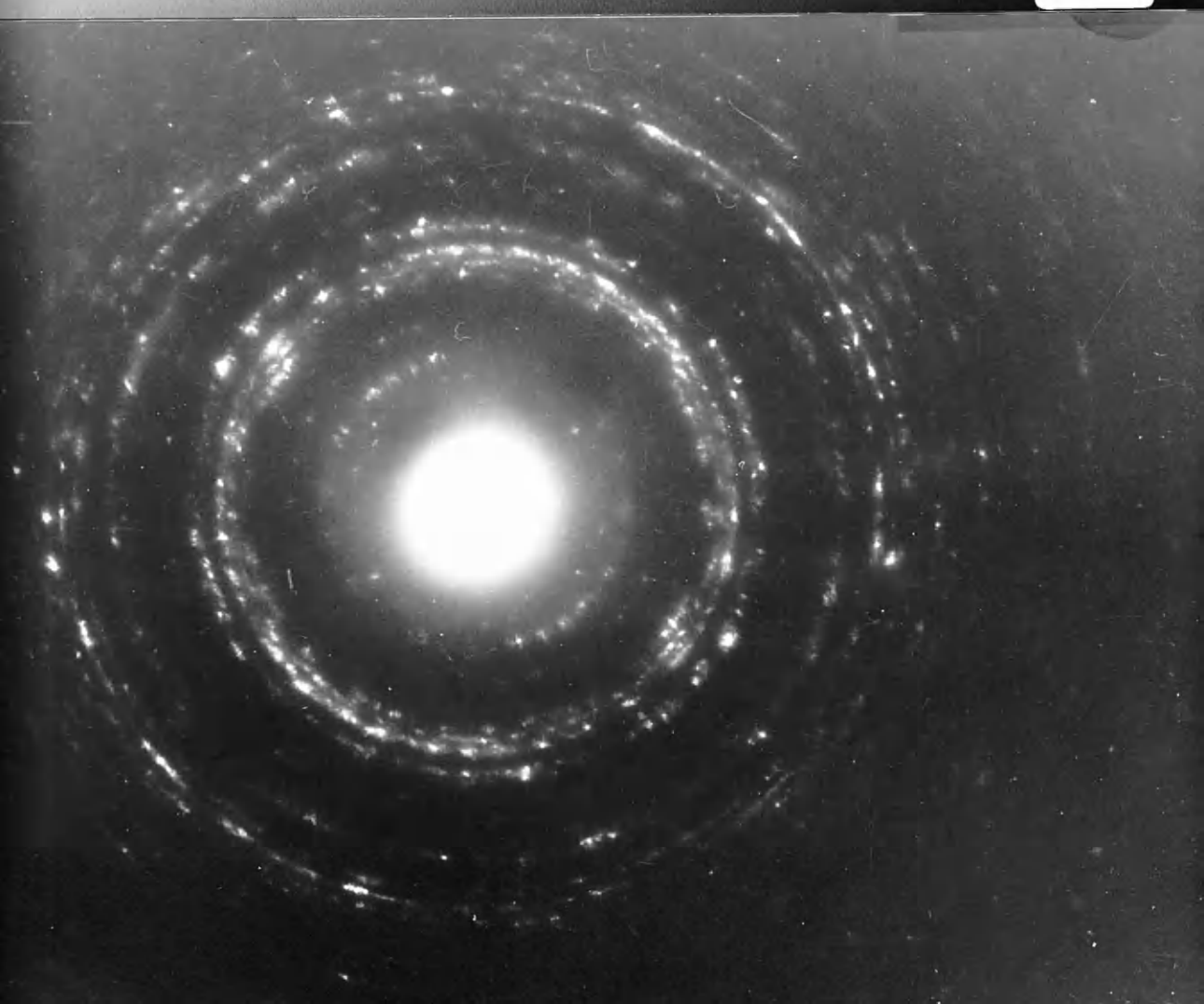

Plate 3.17:

α-FeOOH showing 60 angles between star-shaped twins from main precipitation zone produced on aging within carrageenan gel for 8 months at room temperature (Sec. 3.1.2.1a). Electron diffraction pattern is similar to Plate 3.16.

Plate 3.18:

Coarser material from same sample as Plate 3.17. Electron diffraction pattern is similar to Plate 3.16.

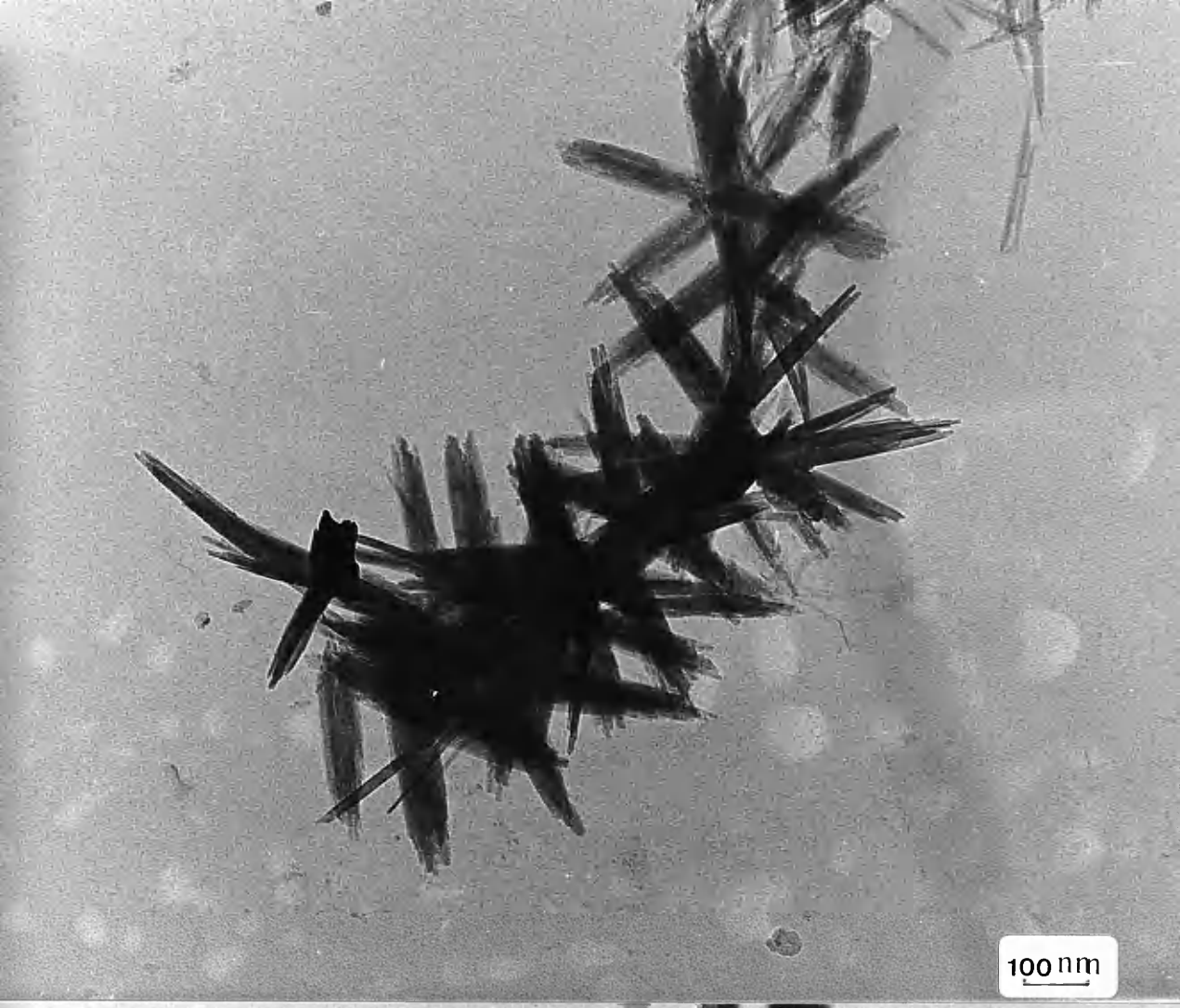
100 nm

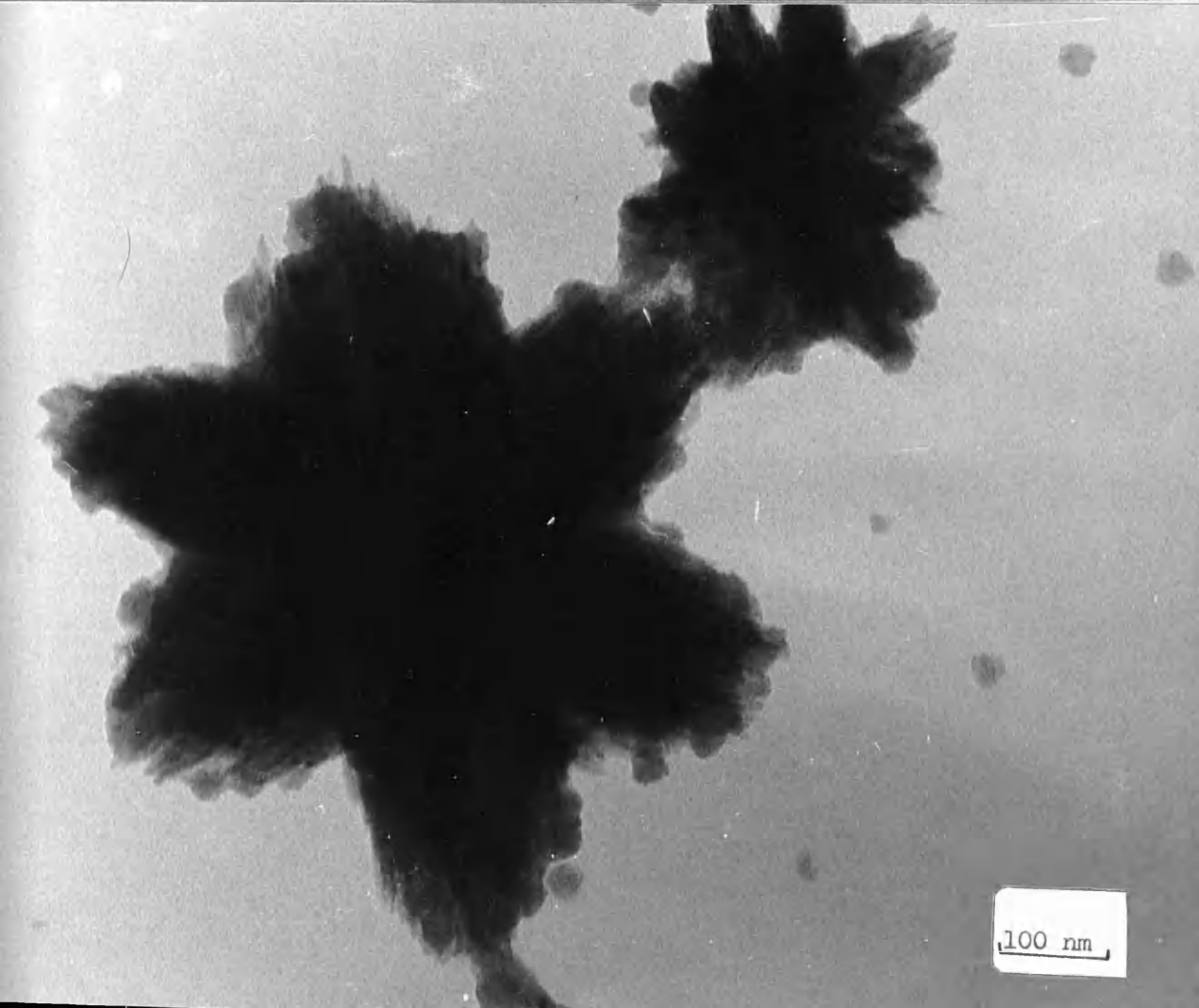
100 nm

Plate 3.19:

Small pod-shaped crystals of α-FeOOH (arrowed) grown on the fibrils of ferrihydrite from main precipitation zone produced from aging Fe(III) within carrageenan gel for 26 days at room temperature (Sec. 3.1.2.2a).

Plate 3.20:

Pod-shaped particles along the bundles formed after diffusion of Fe(III) solution in carrageenan gel for 26 days and then in distilled water for 8 months, at room temperature.

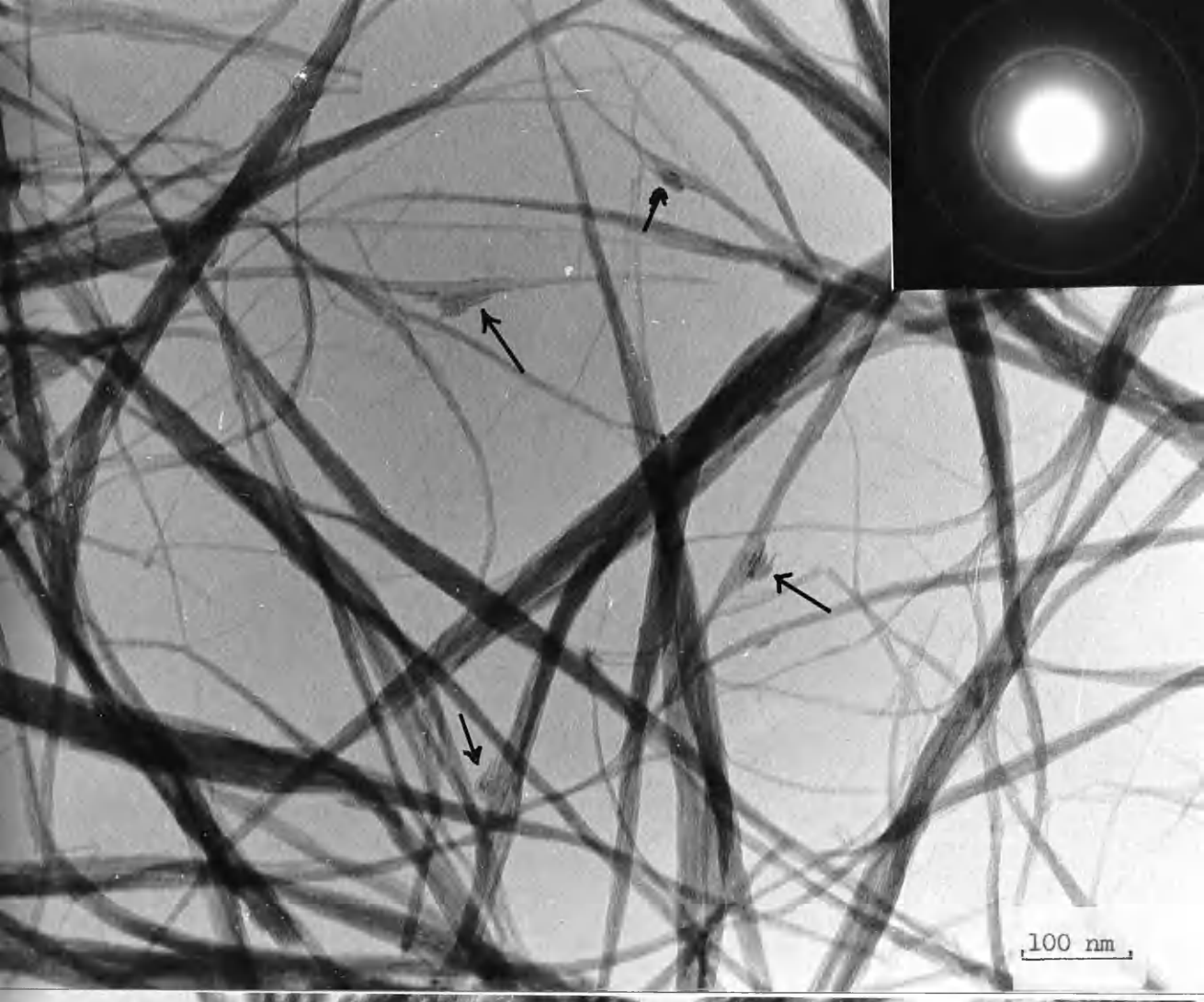
100 nm


100 nm

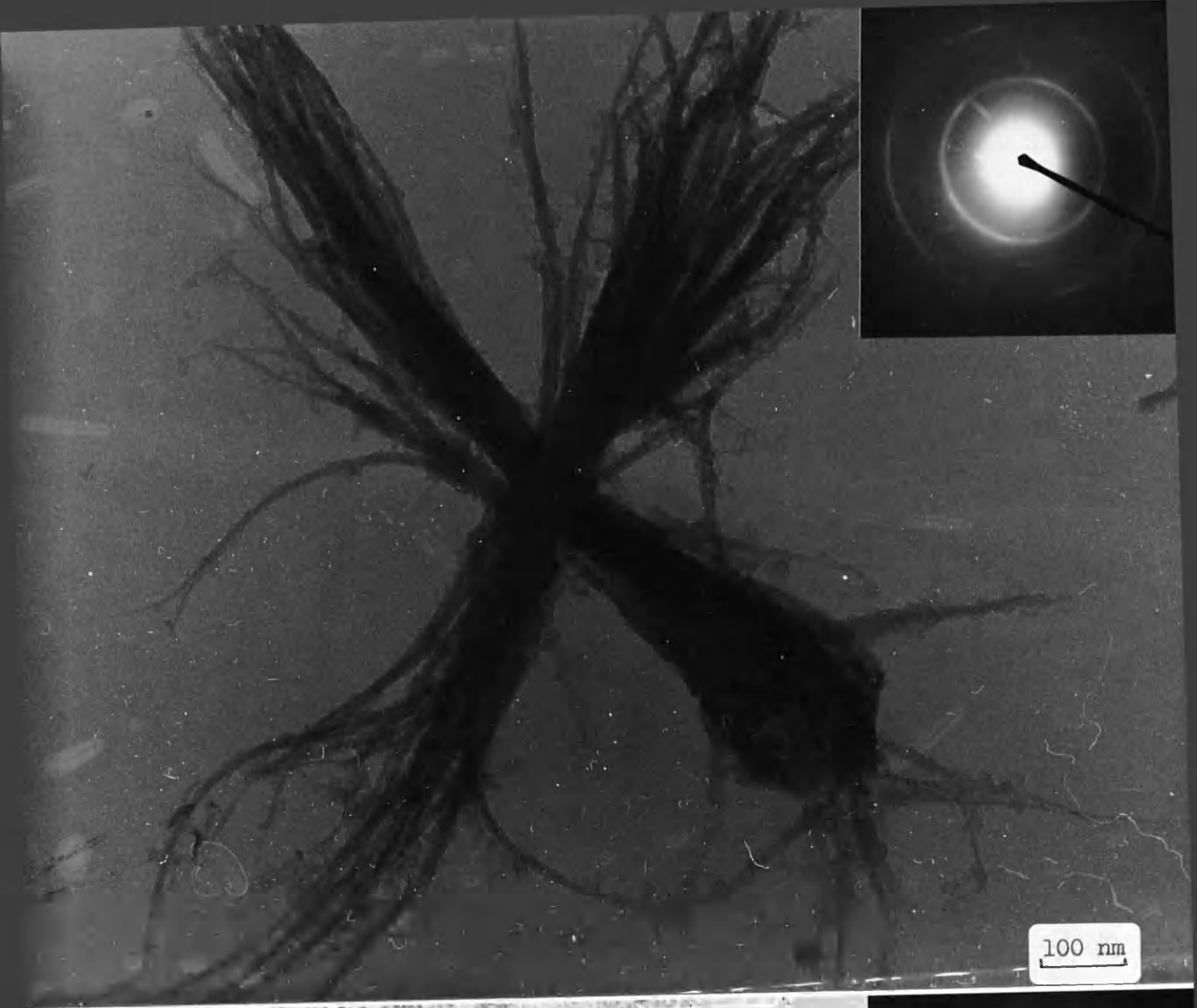
100 nm

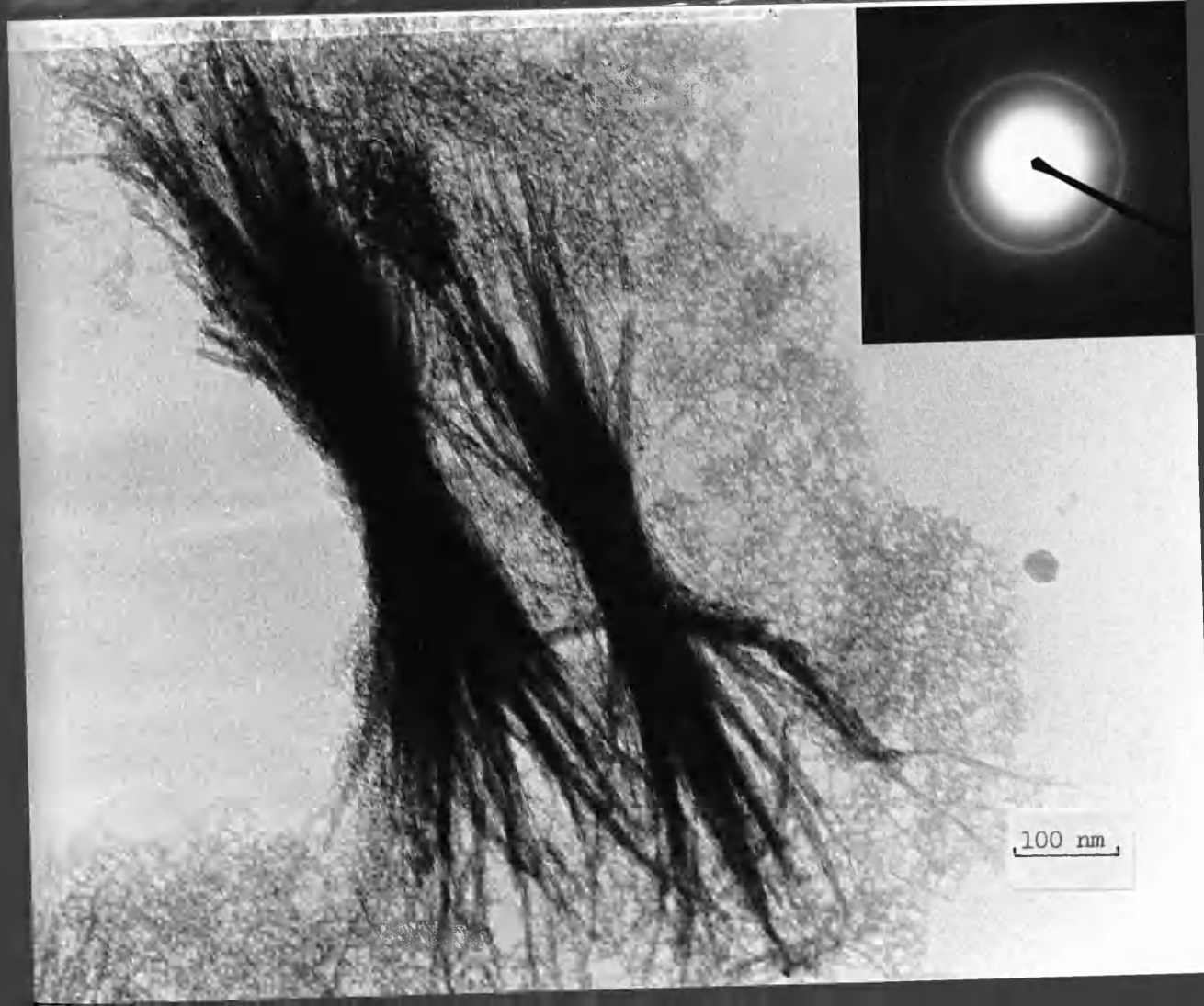
100 nm

Plate 3.21:

Large hair-like bundles of ferrihydrite from main precipitation zone formed from aging Fe(III) within silica gel for 8 months at room temperature (Sec. 3.1.2.2a).

Plate 3.22:

Hair-like bundles from main precipitation zone of ferrihydrite obtained within silica gel containing urea after 26 days aging (Sec. 3.1.3).

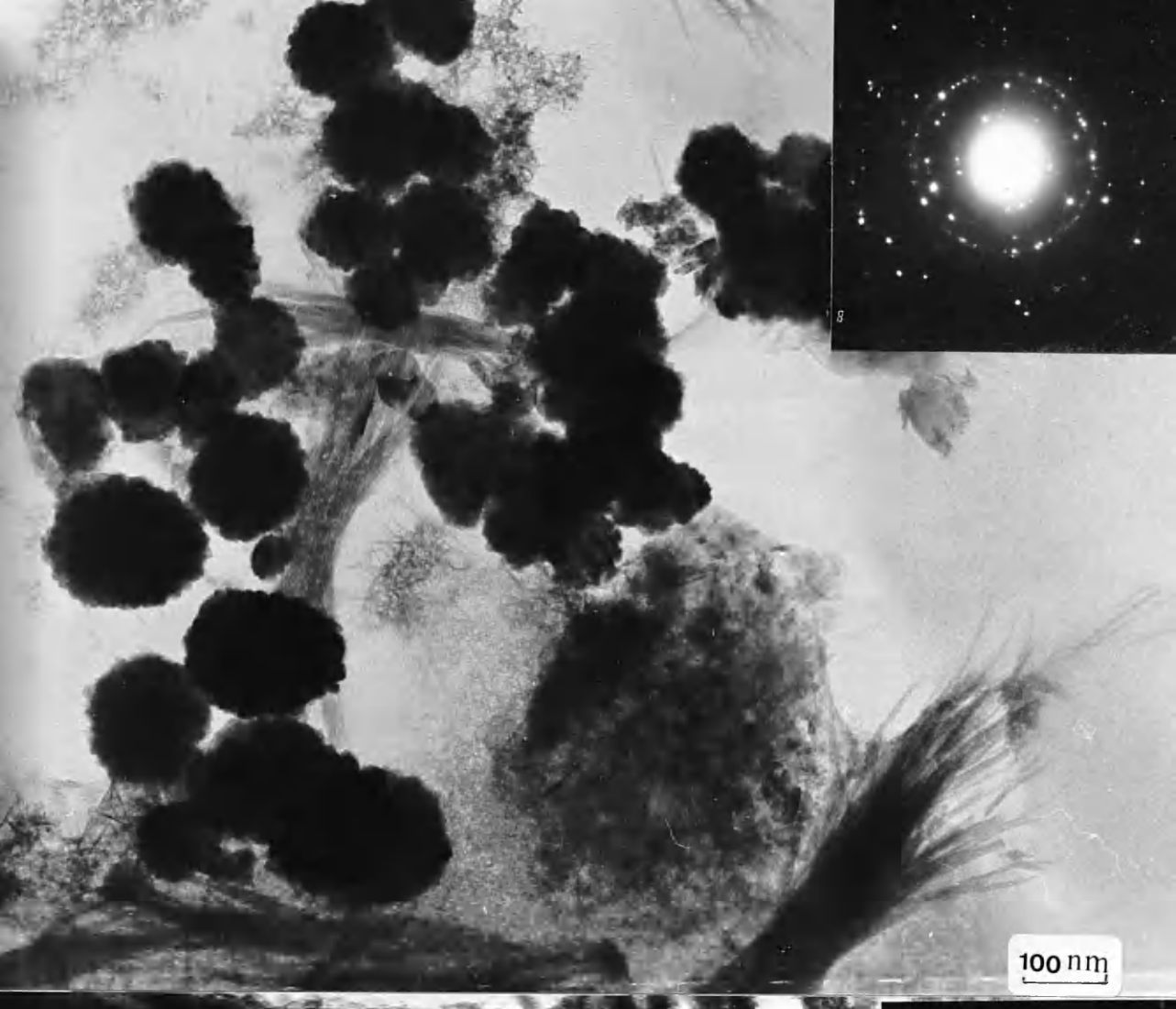
100 nm

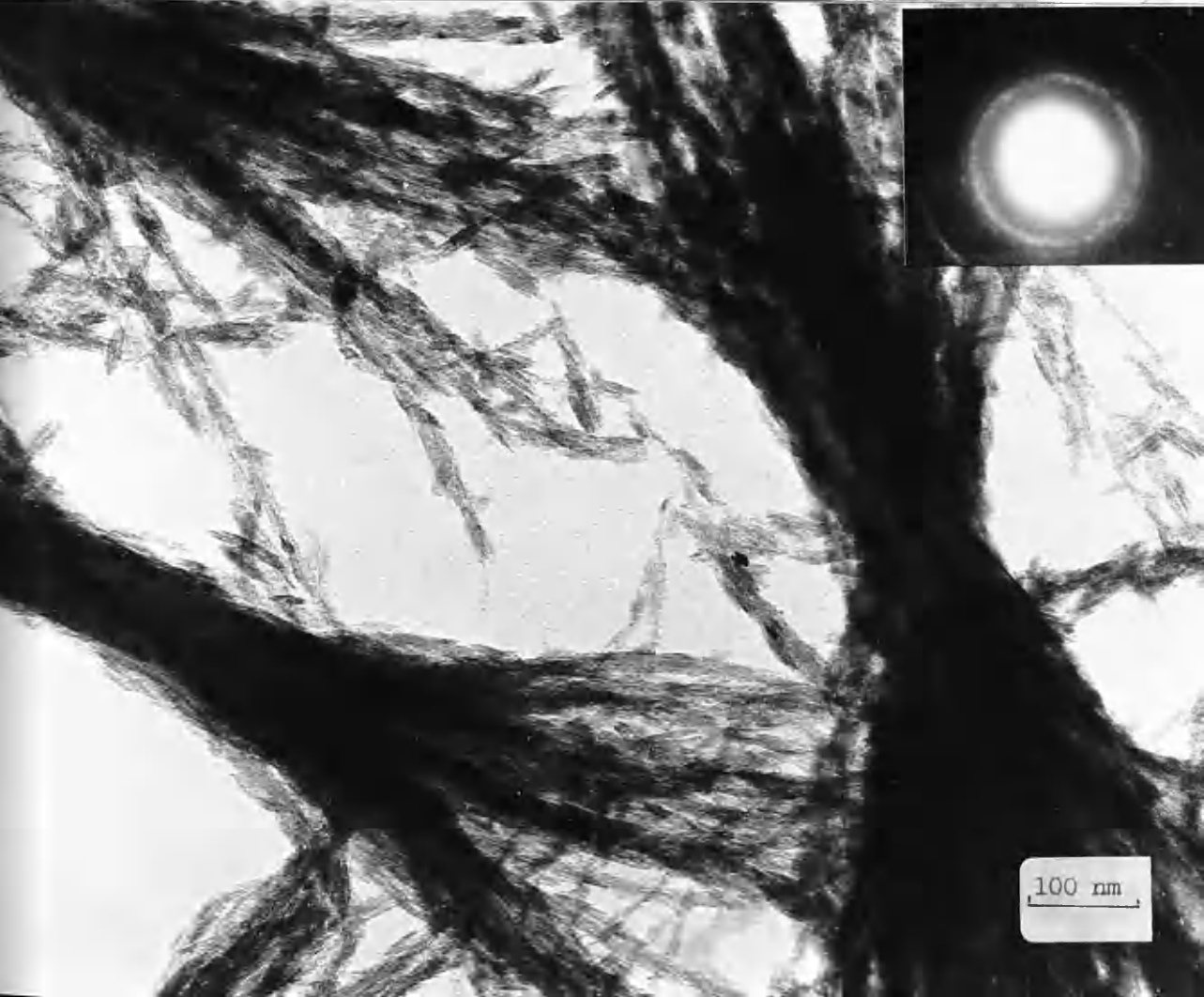
100 nm

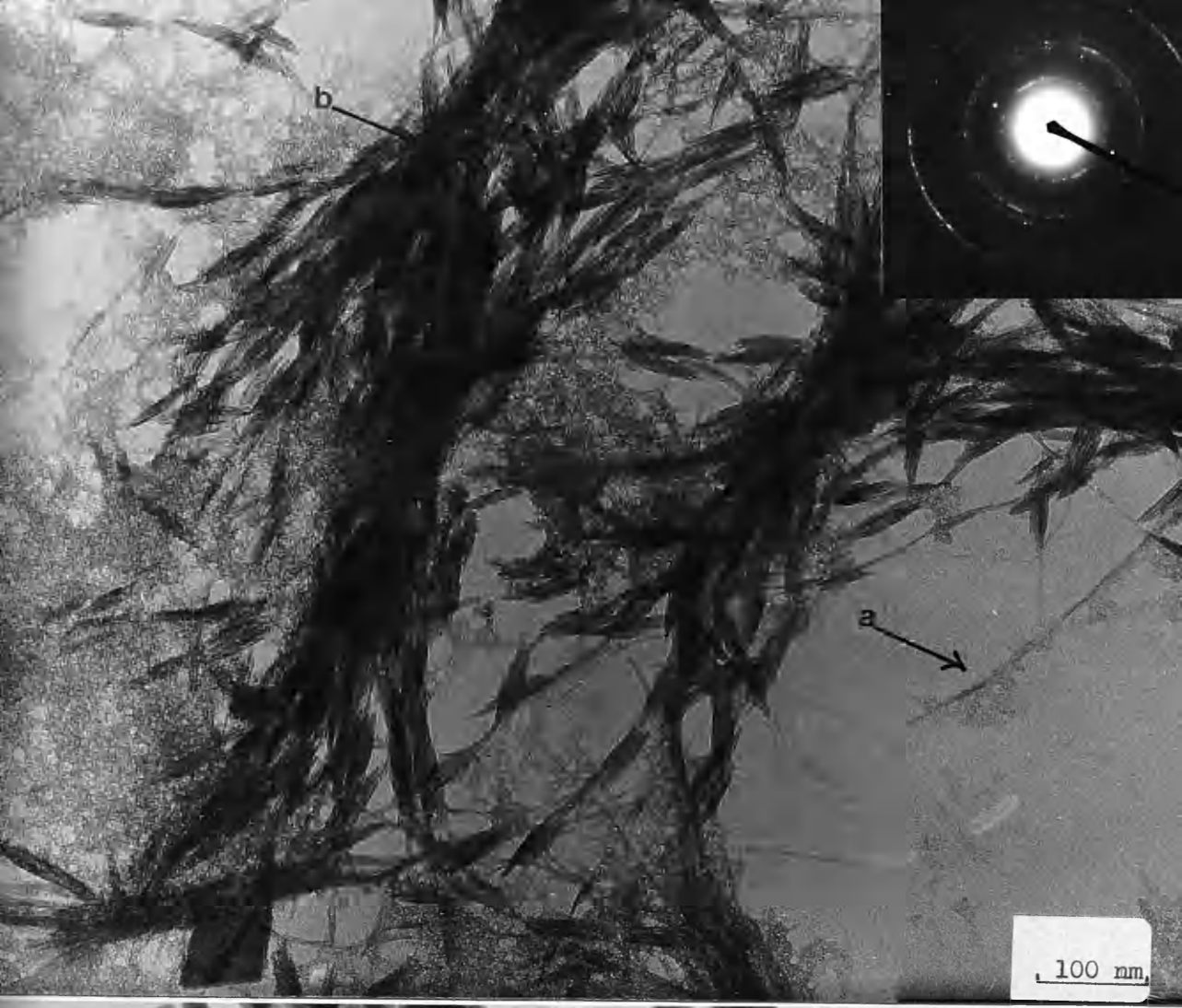
b
a
100 nm

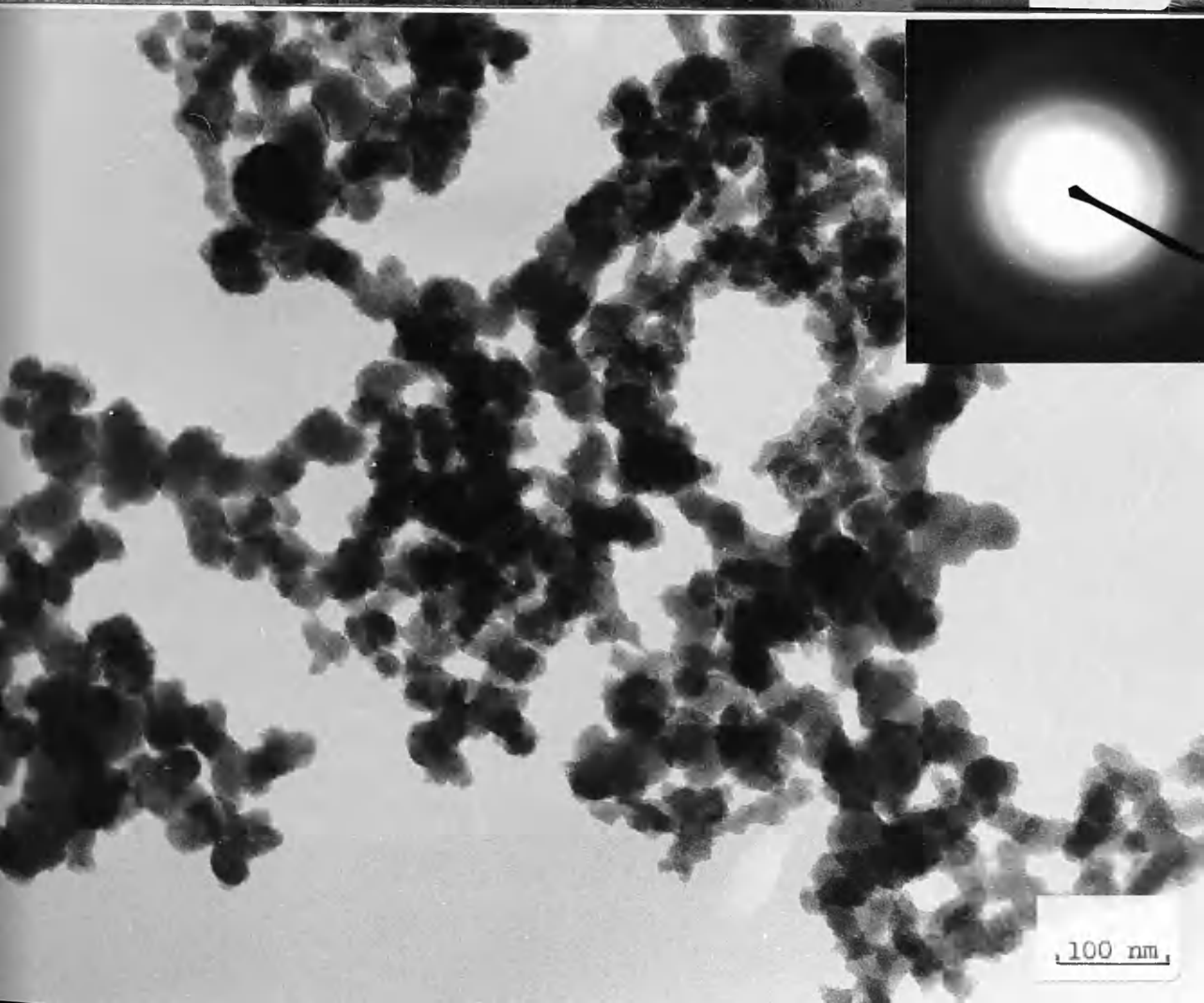
100 nm

Plate 3.25:

Pod-shaped α-FeOOH along the bundles from main precipitation zone after heating bundles of ferrihydrite within mixed gel at 89-100^{o} C for 5 hours (Sec.3.1.6.2; Table 3.5). (Visible as fibrils of ferrihydrite `a', and small aggregate of $\alpha$-$Fe_2O_3$ `b').

Plate 3.26:

Loosely aggregated particles of ferrihydrite freshly formed in $NaHCO_3$ solution (Sec. 3.2).

Plate 3.27:

Material prepared as in Plate 3.26, after 7 days aging.

Plate 3.28:

First generation of seeding from metal ion rich zone. Seeded ferrihydrite is indicated by an arrow (Sec. 3.3.1).

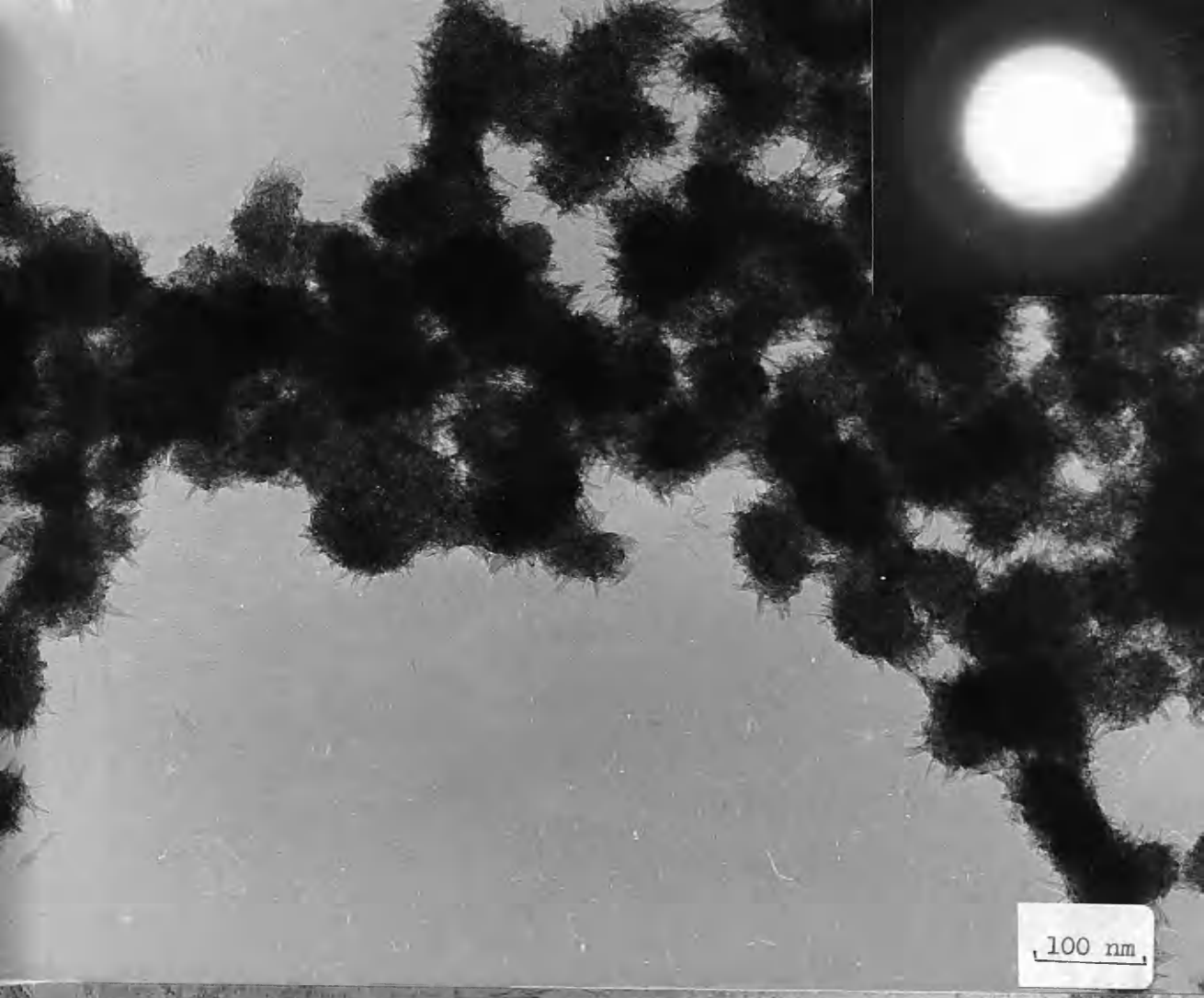
100 nm

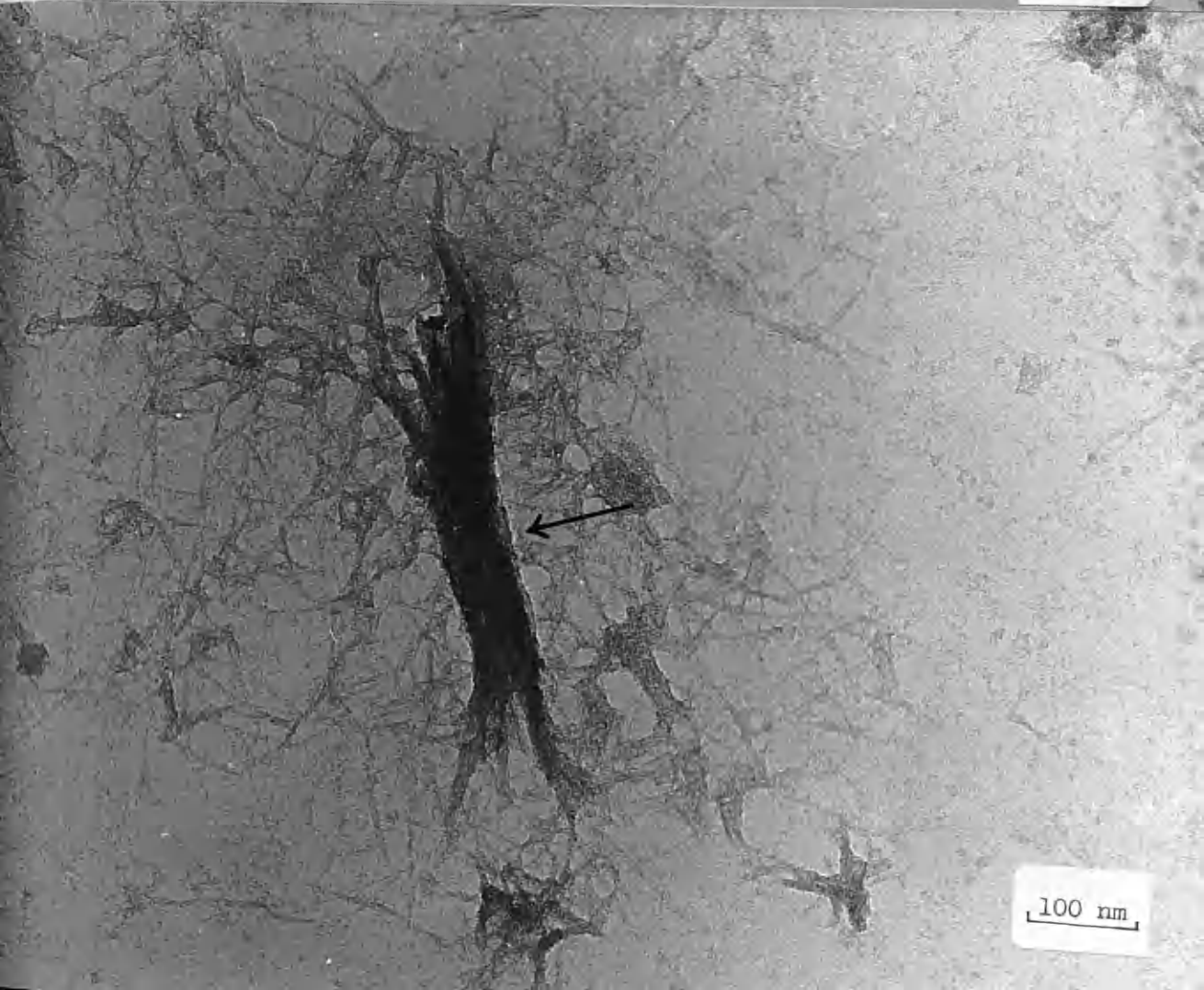
100 nm

Plate 3.29:

Second generation of seeding from metal ion rich zone. (Sec. 3.3.1).

Plate 3.30:

First generation of seeding from main precipitation zone. Seeded ferrihydrite is indicated by arrows. (Sec. 3.3.2).

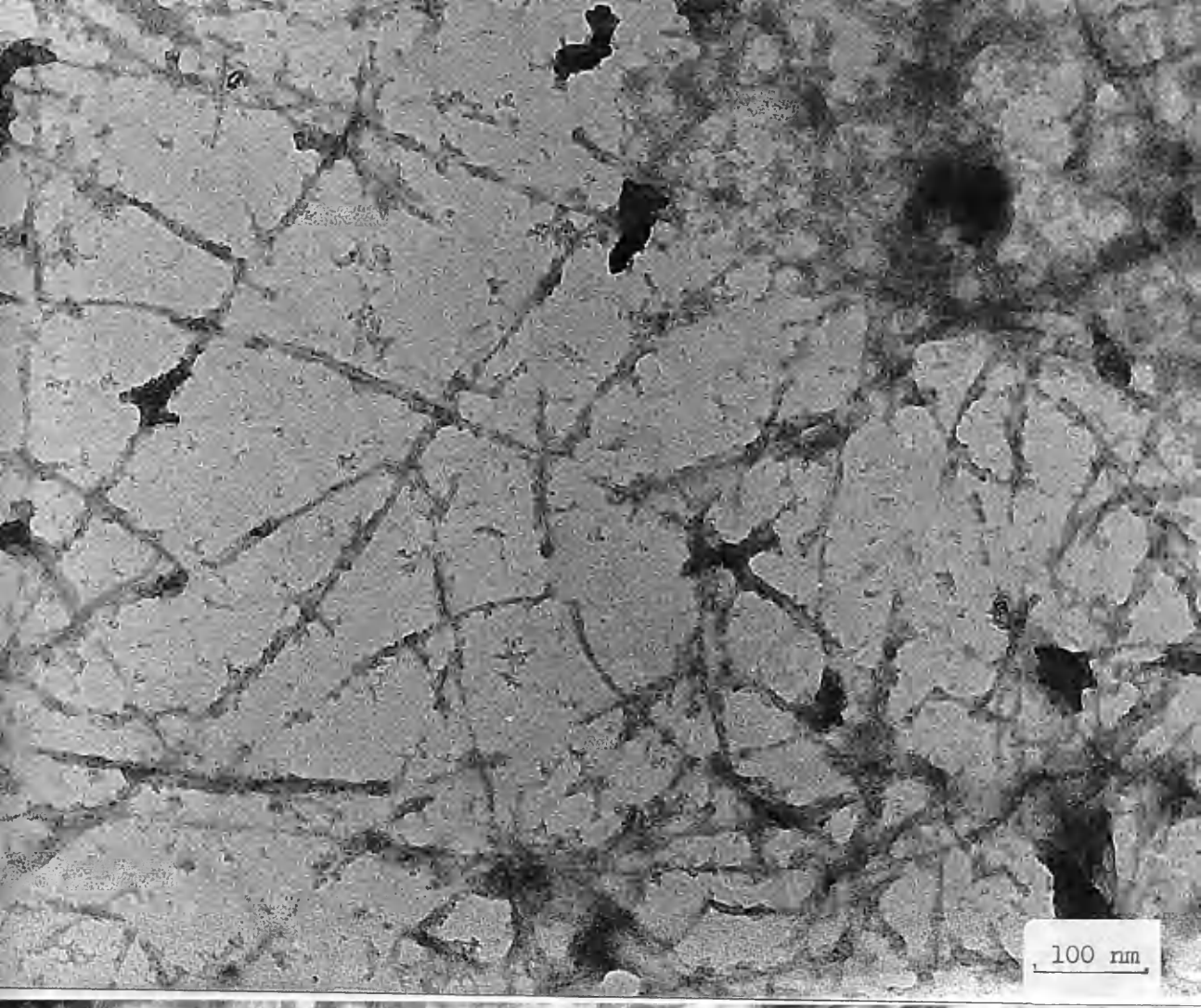
100 nm

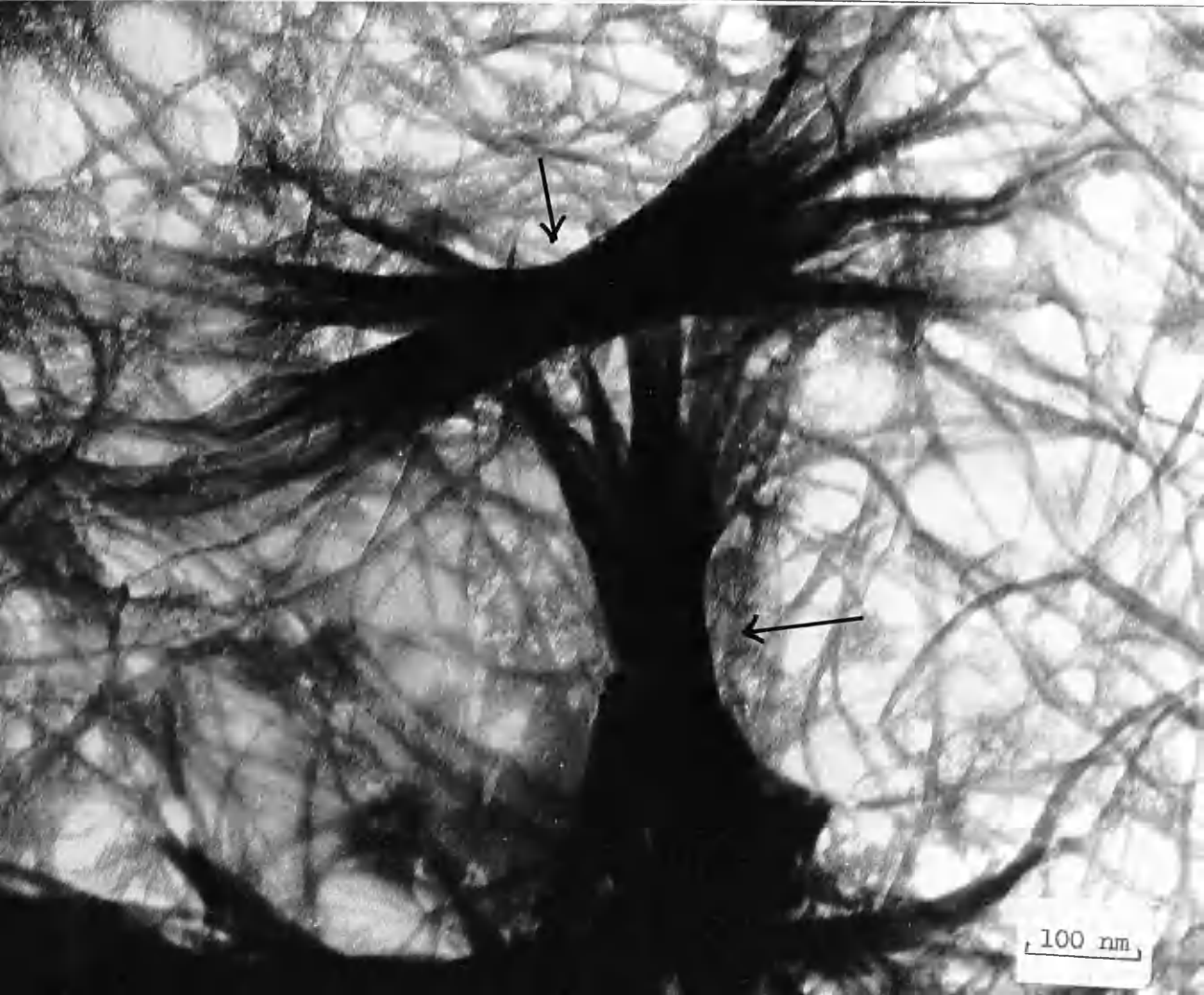
100 nm

Plate 3.31:

Electron micrograph of pseudo-hexagonal plates with sharp edges in variable sizes, from standard kaolinite suspension (Sec. 3.4.1).

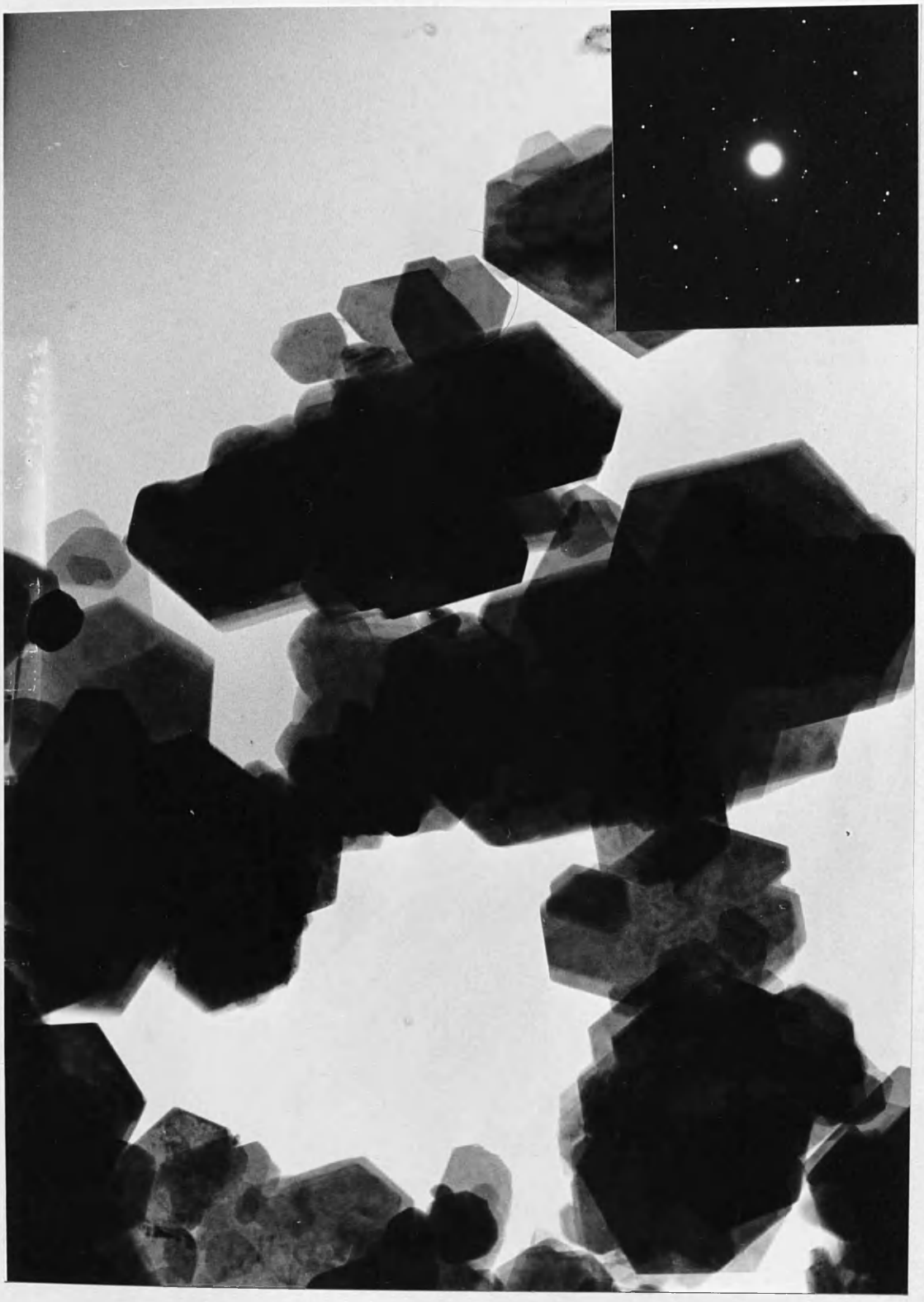

Plate 3.32:

Nine days old precipitate from metal ion rich zone of Fe(III) in the carrageenan gel containing kaolinite (Sec. 3.4.2).

Plate 3.33:

Electron Diffraction pattern of a large particle in Plate 3.32; Table 3.7.


1 µm

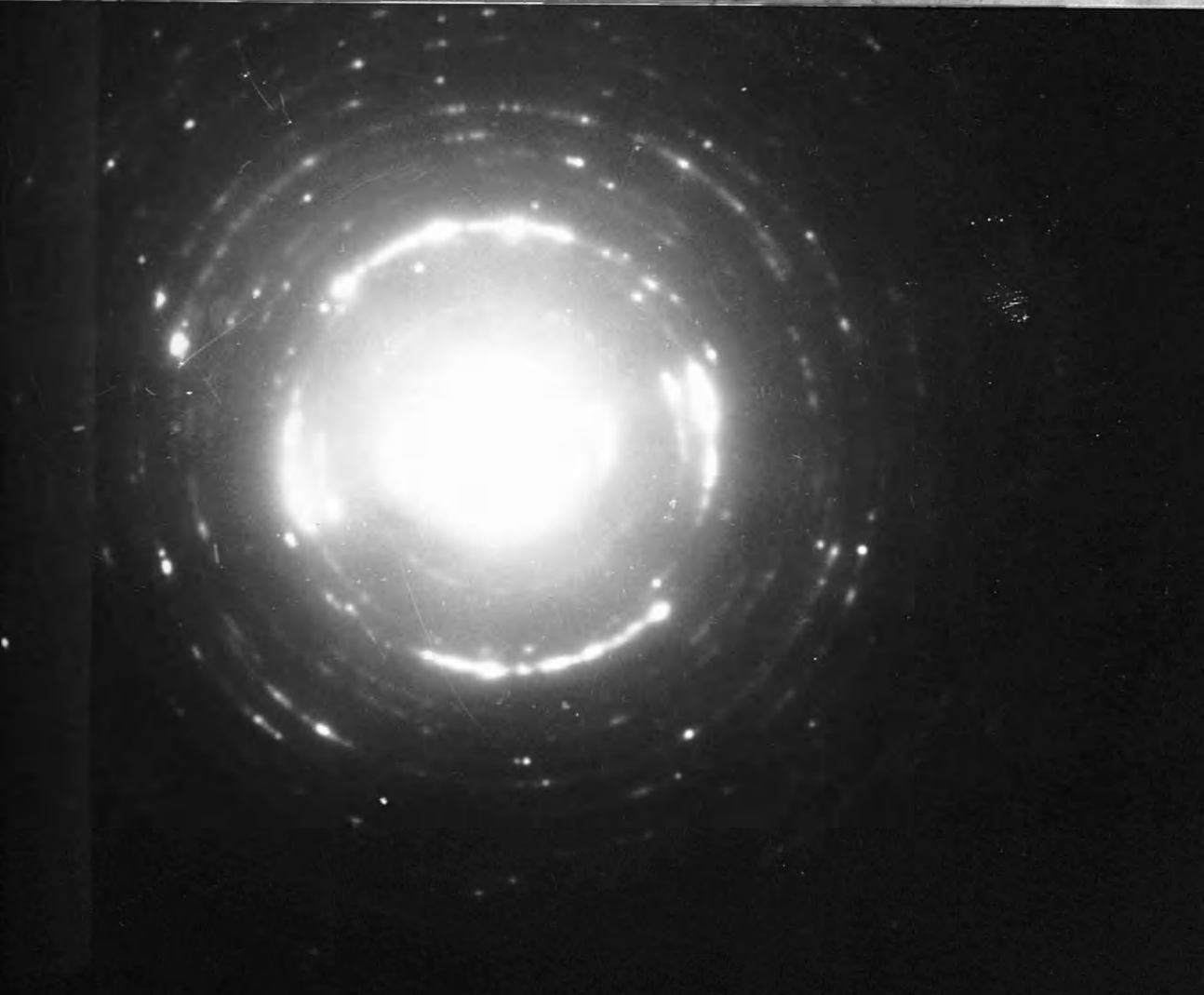

Plate 3.34:

Nine days old precipitate from main precipitation zone of Fe(III) in the carrageenan gel containing kaolinite (Sec. 3.4.2).

Plate 35:

Enlarged detail (small bundles) from Plate 3.34.

Plate 36:

Nine days old precipitate from hydroxide ion rich zone of Fe(III) in the carrageenan gel containing kaolinite (Sec. 3.4.2)

Plate 3.37:

Eight months old precipitate from metal ion rich zone of Fe(III) in the carrageenan gel containing kaolinite (Sec. 3.4.3). The attached electron diffraction pattern of the whole area of hexagonal particles.

Plate 3.38:

Electron micrograph of 9 days old precipitate from main precipitation zone of Fe(III) in the carrageenan gel containing kaolinite and followed by 8 months in distilled water (Sec. 3.4.4). The attached electron diffraction pattern of a large particle as indicated by an arrow (Sec. 3.4.4; Table 3.7).

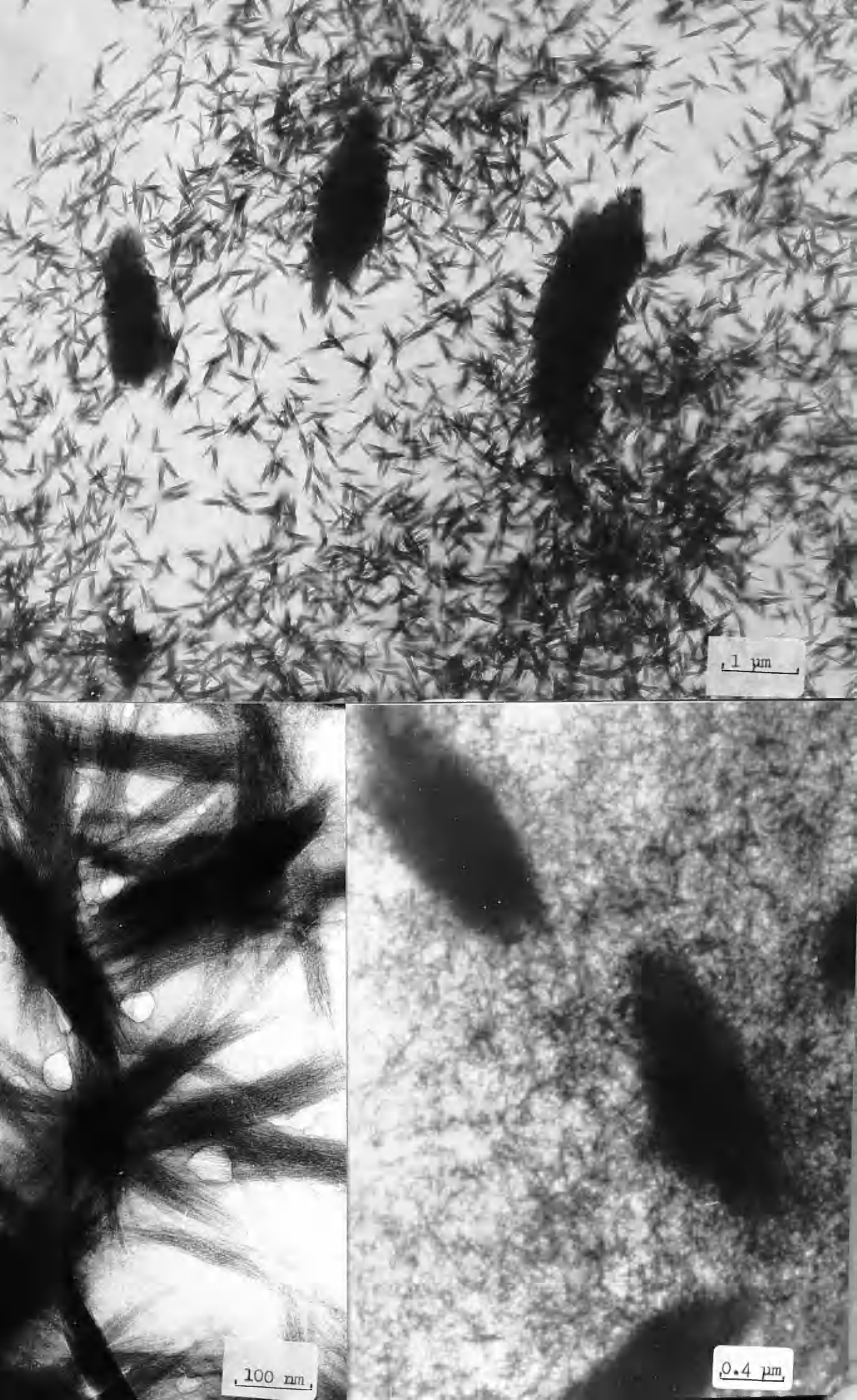
1 µm
100 nm
0.4 µm

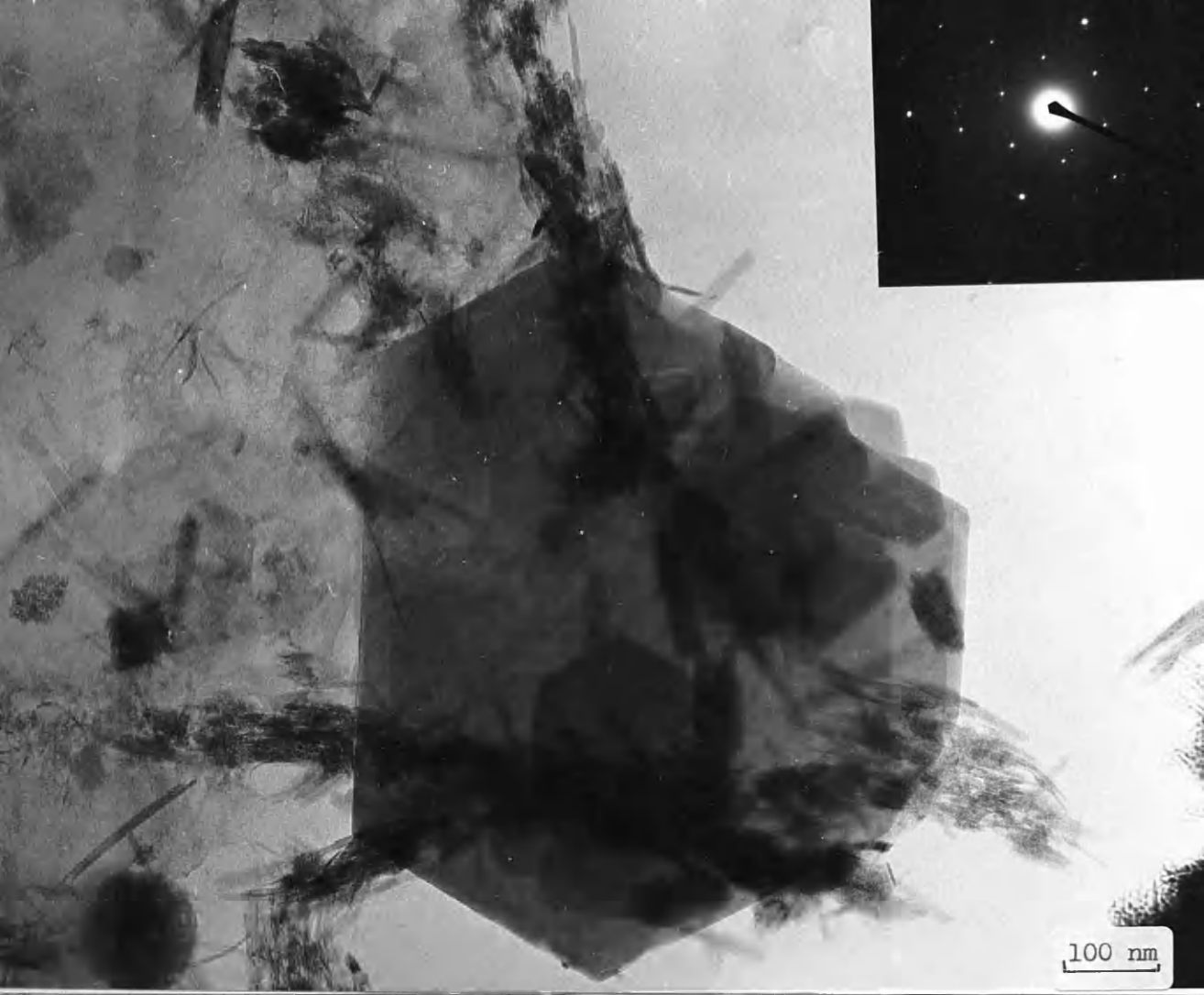
100 nm


100nm

Plate 3.39:

Small pod-shaped particles of α-FeOOH associated with silica gel formed on heating for 2 hours of Fe(III) solution with urea within silica gel (Sec. 3.6). Electron diffraction spacings are shown in Table 3.8.

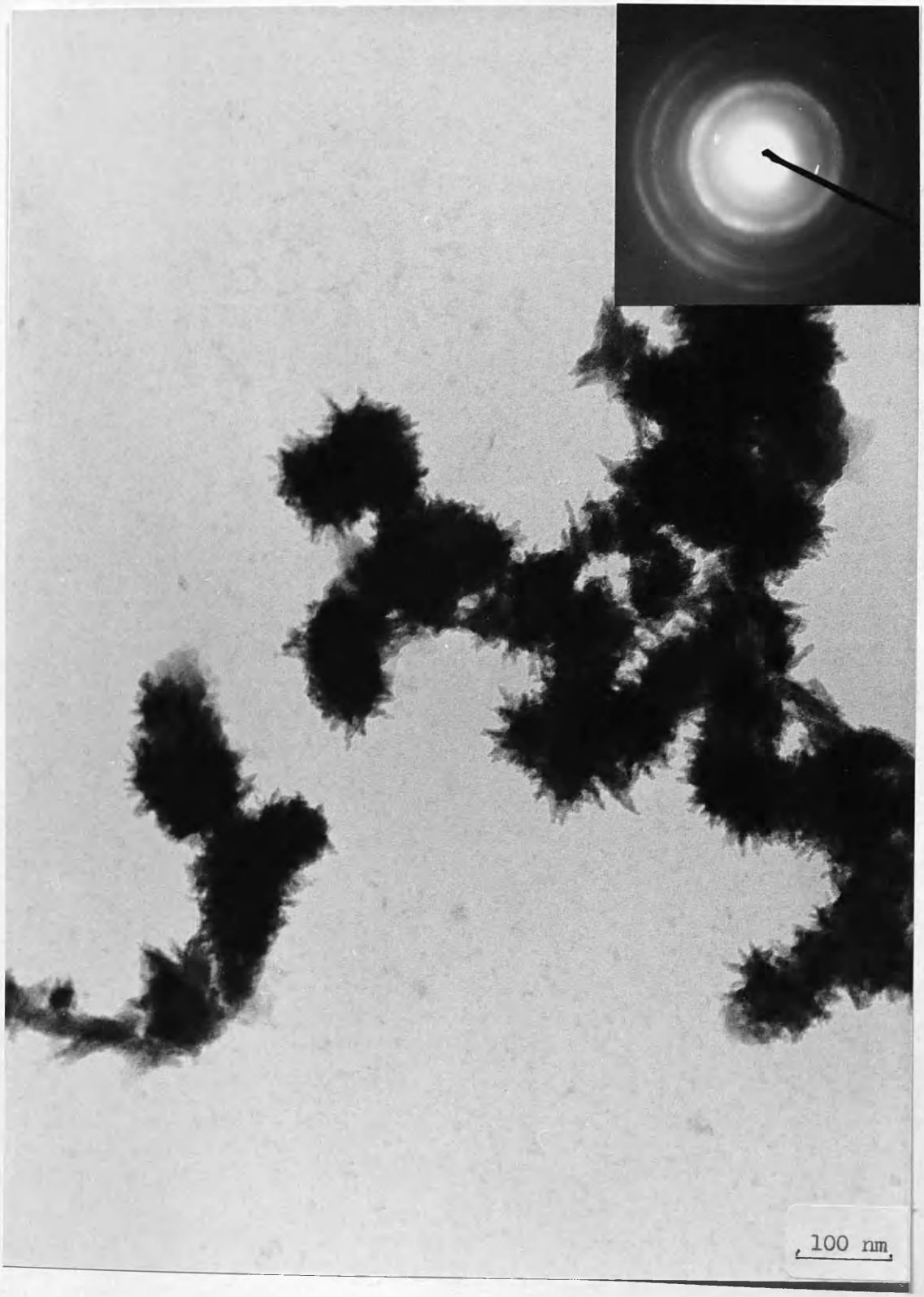
100 nm

CHAPTER FOUR

Precipitation of Copper Compounds

page

4.1 Precipitation in Carrageenan Gel 84

4.2 The Morphology Formed within the Gel ... 85

4.2.1 Rod-Like Morphology 85

4.2.2 Crumpled Sheets Morphology 86

4.2.3 Bowtie Morphology Formation 87

(a) Copper (II) Sulphate and HEPES Solutions (Sec. 2.7.6) 87

(b) Copper (II) Sulphate and HEPES Solutions Containing Kaolinite (Sec. 2.7.7) 88

(c) Mechanism Suggested for Bowtie 89

4.2.4 Dendritic Morphology 90

4.3 Copper (II) Perchlorate in NaOH Solution ... 91

4.1. PRECIPITATION IN CARRAGEENAN GEL

The precipitate was formed after 2 days diffusion in the carrageenan gel. Different phenomena of precipitate in the tubes are shown below:

TABLE 4.1

Precipitation from Copper Compounds in Carrageenan Gel

Alkali Source Soln.	Age (days)	P P T 1		P P T 2	
		F band Ppt.	T band Ppt.	F band Ppt.	T band Ppt.
HEPES or HEPPS	after26	turquoise	blue	pale blue	blue
NaOH	after26	red-brown	blue	blue and blue-green Liesegang rings throughout the band	

Key word:

PPT1 : Copper(II) sulphate solution as a metal ion.
PPT2 : Copper(II) perchlorate solution as a metal ion.
F : Front (metal-rich).
T : Tail (hydroxide-rich).

(For concentrations see Section 2.7.6; 2.7.7).

The blue and turquoise precipitates are probably due to the formation of copper(II) hydroxide or basic copper sulphates. The red- brown precipitate that formed at the front band probably contained copper (I) oxide material. But it can not be explained why it forms at the front band instead of the tail band. The Liesegang rings observed formed after aging of the blue bands.

4.2 THE MORPHOLOGY FORMED WITHIN THE GEL

The main theme of interest in this section is the morphologies developed by copper compounds grown in gels. Copper(II) sulphate and perchlorate were used as metal ion solutions and various alkali sources were used as described in Sec.2.7.6. Only the interesting morphologies will be reported; others formed as aggregated particles of Cu(I) and Cu(II) oxides of various sizes.

The similar morphologies will be reported as one group regardless of different material used as follows:

4.2.1 Rod-Like Morphology

This morphology was observed from front band precipitate containing copper perchlorate and NaOH or HEPPS solutions. Fresh precipitate two days old using NaOH solution shows as fine rod-like particles, and it develops (longer and thicker) to some extent after 7 days of aging as in Plate 4.1. Its diffraction pattern corresponds to copper(II) hydroxide, ASTM 13-420; the spacings match to the standard strong spacings at 0.373nm (021), 0.266nm (002) and 0.226nm (130).

On the other hand, the turquoise precipitate from sulphate ion is probably from basic copper sulphate but it decomposed to copper(I or II) oxide in the electron

beam. Moreover, the similar morphology and the same compound (Cu(I), Cu(II) oxides) were observed even after 60 days of diffusion.

4.2.2 Crumpled Sheet Morphology

Plate 4.2 was obtained from the front band precipitate of copper(II) sulphate and HEPPS solution after aging 9 days in the gel. The diffraction pattern corresponds to CuO, ASTM 5-0661. The spacings which correspond to the strong standard spacings are 0.277nm (110) and 0.236nm (111). Furthermore, a similar morphology and compound were obtained from the sample containing copper(II) perchlorate, kaolinite and HEPES solutions within the gel after 3 days of diffusion. Its diffraction spacings approximate to CuO, ASTM 5-0661 and the spacings that match to the strong standard spacings are 0.237nm (111) and 0.184nm (202). The crumpled sheet morphology probably arises from drying out and folding of very thin sheets as shown clearly in Plate 4.2. The CuO (black) is presumably formed by beam damage of the blue material.

A similar morphology was observed from precipitate prepared by Dr. M. Kaya; hydrolysis of copper(II) sulphate with hexamine in silica gel (Sec.2.8 Table, 2.3). Plate 4.3 shows some areas of isolated crumpled sheets and others that are associated with silica gel.

Diffraction data from the latter consist of rather diffuse rings indicative of poorly ordered material. Measurements corresponds fairly well to copper silicate hydrate, $3CuSiO_3.H_2O$, ASTM 11-248 (Table 4.2).

4.2.3 Bowtie Morphology

This morphology is the most interesting structure grown in gels. It could be found only under certain conditions as shown below:

(a) Copper(II) Sulphate and HEPES Solutions (Sec. 2.7.6)

The optimum of bowtie formation was observed from the sample obtaining at the front band of the gel plug after 8 days of diffusion (Plate 4.4). Moreover, it could not be observed within 6 days of diffusion. Hence, the bowtie morphology subsequently grows rapidly from the fresh copper ion. A close examination on Plate 4.4 reveals that the layers forming in the bowtie are at around the same angle (50°-60°). The textured diffraction pattern (Plate 4.4) the bowties are single crystal-like entities. The diffraction in Plate 4.4 corresponds to copper (II) sulphate hydroxide, Brochantite, $Cu_4SO_4(OH)_6$ as in Table 4.3. This compound, $CuSO_4.3Cu(OH)_2$, is probably the original compound comprising the blue precipitate; it is subsequently affected by electron beam damage.

TABLE 4.2

Electron Diffraction Spacings from a Copper Silicate Compounds Grown in Silica Gel by Hydrolysis of Hexamine

Pl4.3 nm	$3CuSiO_3.H_2O$ ASTM 11-248 nm
0.411	0.410
0.302	0.306
0.240	0.238
0.158	0.158
0.139	0.136
0.137	0.133

Pl4.3 : Electron diffraction spacings from the area of crumpled sheets associated with silica gel in Plate 4.3.

In addition, small half bowties grew on the individual discs of bowties by aging rather than forming a new nucleus (Plate 4.5). Thus, the nucleus of a bowtie is probably formed only at a certain age and at specific areas within the gel plug.

Plate 4.5 shows 2 morphologies from copper compounds; a very thick bowtie containing branches of small half bowties and the crumpled sheets which are similar to Plate 4.2 as indicated with an arrow. The diffraction pattern from a thin area at the edge of a bowtie (Plate 4.5) corresponds roughly to CuO, ASTM 5-0661 and the diffraction data from crumpled sheets also corresponds roughly to the standard CuO.

Plate 4.6 taken on an SEM shows clearly the morphology of bowtie and branches of secondary bowties on the edge of the discs.

(b) Copper(II) Sulphate and HEPES Solutions Diffusing in Carrageenan Gel Containing Kaolinite (Sec.2.7.7)

It was noticed that when kaolinite was added to the gel, the particles grew rapidly within 3 days of diffusion as shown in Plate 4.7. Therefore, kaolinite behaves as an activator for the bowtie formation. The diffraction data corresponds to copper (I & II) oxide (6 $CuO.Cu_2O$), ASTM 3-0879; the spacings which correspond to the standard strong spacings are 0.292nm (200), 0.248nm (004), 0.205nm (220,213), 0.165nm (224) and

0.145nm (323,400). The copper oxide is possibly formed by beam damage to the blue precipitate.

(c) Mechanism Suggested for Bowtie Formation

Concerning the bowtie morphology in three dimensions (Plate 4.6), it is assumed that they consist of uneven edge form discs of changing diameter stacked together to form a column. The irregular discs probably develop from the discs which form at the early stage of bowtie formation as shown in Plate 4.4; straight line at the both ends of the bowtie as indicated by arrows suggested that there are consisting from perfect discs. Thus, the secondary bowties are probably due to the particle growth by aging which shows as petal-like morphology (Plate 4.6).

It was suggested that the nucleus started to form at the centre "knot" of a bowtie from a small aggregate of atoms. The new arriving particles grew on the surface of a nucleus either to expand the diameter of the circular-like disc or to form the next parallel disc on the existing one as shown in Fig. 4.1. which can be explained as follows:

At a&b : Arrival of particles on the surface of the disc, and randomly moving around until they reach a stable site which is probably at the edge of the disc, which continues to grow outwards.

At c&d : Once the diameter of the disc became large, the possibility is the aggregation of the particles on the disc would occur.

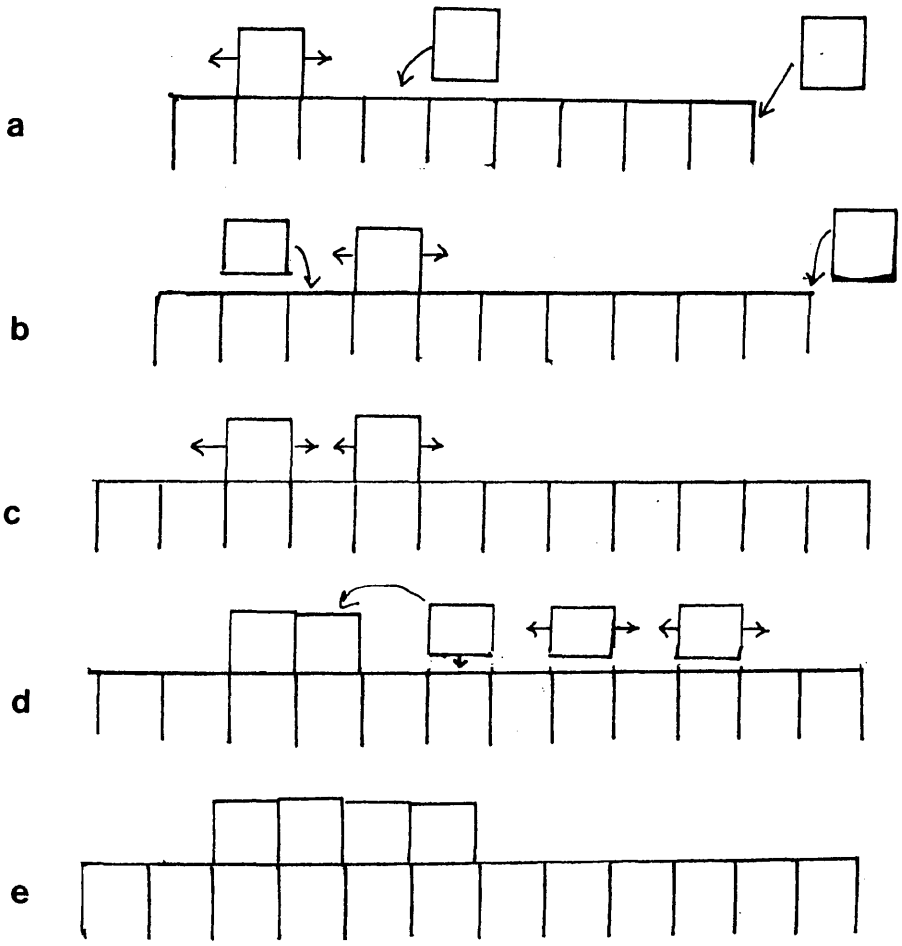

Fig.4.1.

Mechanism suggested for layered Perovskite growth in a half bowtie structure of $Cu_4SO_4(OH)_6$ within the gel (Sec. 4.2.3).

At e : Thus it was expected a new disc to form on the surface of the original one, and the same mechanism would be happening on the opposite face of the original disc. It was predicted that lower supersaturation would give greater disc size.

This mechanism is similar to the argument about the growth of ferrihydrite as bundles or as fibres (Sec.3.1. 1.6).

The phenomenon which can not so far be explained is why the discs appear to grow at a specific angle.

Occasionally half bowties were also observed which is probably due to breakage while the sample was being prepared.

4.2.4 Dendritic Morphology

In this section dendritic structure was observed from the blue sample prepared from copper(II) sulphate in HEPES solution within carrageenan gel containing kaolinite at the tail band after aging 10 days (Sec. 2.7.7) as shown in Plate 4.8. Dendrites grow at different rates giving rise to different sizes of dendrites, secondary arms and so forth. For example, notice the bacterium (arrow) has deflected growth.

The diffraction pattern in Plate 4.8 corresponds to copper metal, ASTM 4-0836; the spacings which correspond to the strong spacings are 0.200nm (111), 0.180nm (200)

and 0.126nm (220). This was an unexpected result because the sample was blue, corresponding to copper(II) hydroxide. The copper metal dendrites probably formed during specimen preparation by reduction on the carbon film. The bacterium would likely be on the grid and hence affected growth at that stage.

4.3 COPPER (II) PERCHLORATE IN NaOH SOLUTION

This experiment (Sec.2.7.8) was carried out in order to compare the morphologies of copper compounds grown in gels and in the solution.

Plate 4.9 shows the rod-like structure obtaining from the fresh blue precipitate. Thin single rods can also be seen in this micrograph; these are probably formed at the first stage of growth. This phenomena could also account for the rod-like structure in Plate 4.1 which has a similar morphology. The electron diffraction pattern of Plate 4.9 corresponds to copper (I) oxide, ASTM 5-0667; the spacings correspond very well to the standard strong spacings and they are 0.297nm (110), 0.246nm(111), 0.213nm (200) and 0.149nm (220). This compound probably results from decomposition in the beam.

Plate 4.10 shows thin sheets with serrated edges which probably developed from the rod-like structure after aging one day in the alkali solution. This sample was a dark brown precipitate, whose diffraction data correspond to copper (II) oxide, ASTM 5-0661; 0.279nm

(110) and 0.230nm (111 or 200) and other spacings correspond to the weak spacings.

A different morphology of CuO has been reported by Matijević (1981) who prepared it as polyhedra by heating $Cu(NO_3)_2$ with NaOH solutions at 100° C for 70 minutes.

Copper (I) oxide and copper metal, and perhaps even copper(II) oxide in some cases, are possibly due to decomposition in the electron beam as follows:

$$Cu(OH)_2 \longrightarrow CuO \longrightarrow Cu_2O \longrightarrow Cu \text{ metal}$$

Each compound will be obtained according to the degree of irradiation damage that is influenced by:

1. Time of irradiation;
2. Intensity of beam;
3. Position of sample with respect to the carbon support film; and
4. Size of condenser aperture.

Furthermore, it was noticed that perchlorate and sulphate ions had not much effect on morphology ; Plate 4.2 taken from product using sulphate ion shows a similar morphology with the one using perchlorate ion.

Concerning the results from this section, there is no evidence that kaolinite particles are associated with any specific morphology of copper compounds grown in carrageenan gel containing kaolinite. This may be due to the lower positive charge of copper ion (+2 as opposed to +3 for iron).

Plate 4.1:

Rod-like morphology of a Cu compound formed within carrageenan gel from front band precipitate after 7 days aging; using $Cu(ClO_4)_2$ and NaOH solutions (Sec. 4.2.1).

Plate 4.2:

Crumpled sheets of a Cu compound produced within carrageenan gel from front band precipitate after 9 days aging; using $CuSO_4$ and HEPPS solutions (Sec. 4.2.2).


100 nm

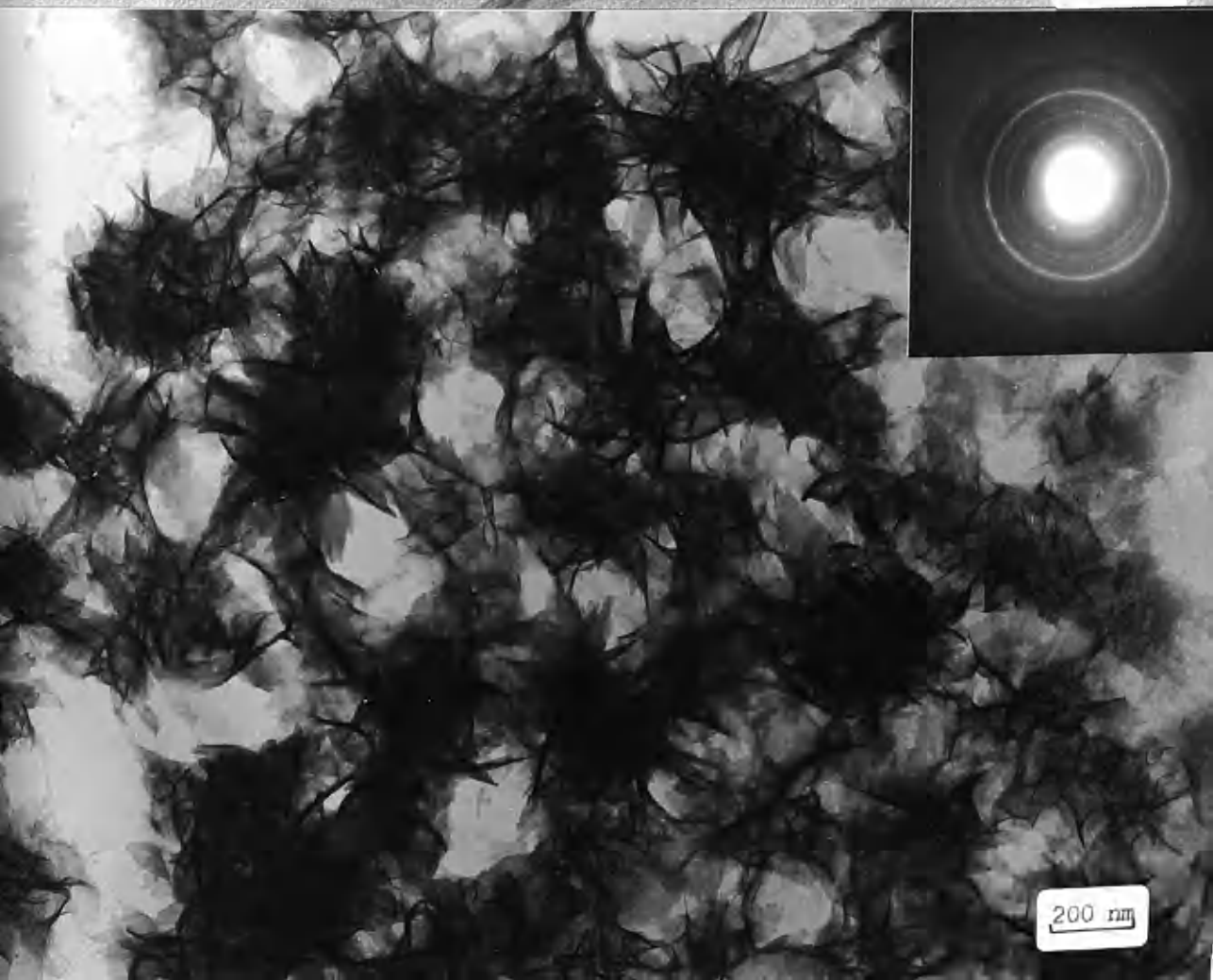
200 nm

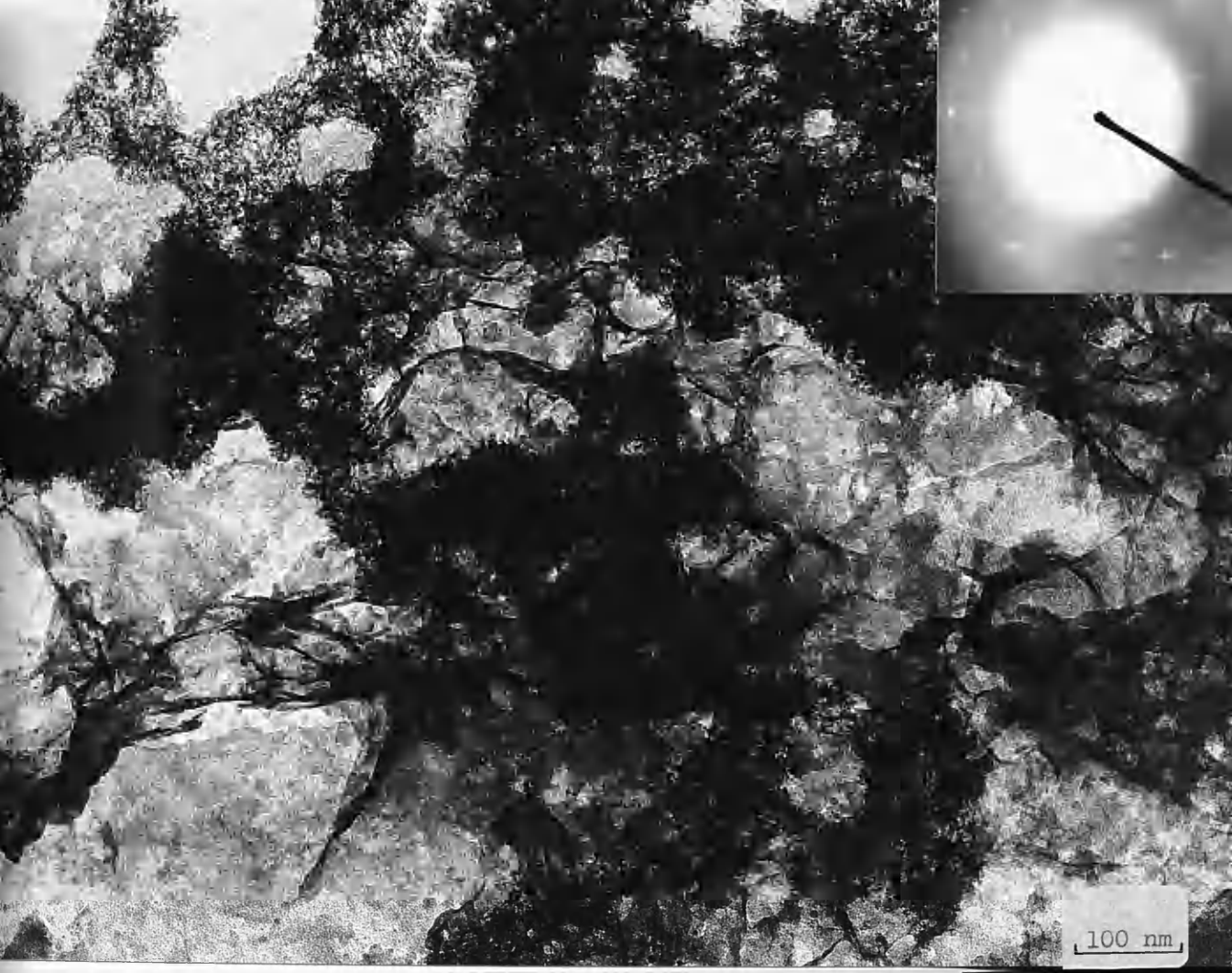
100 nm

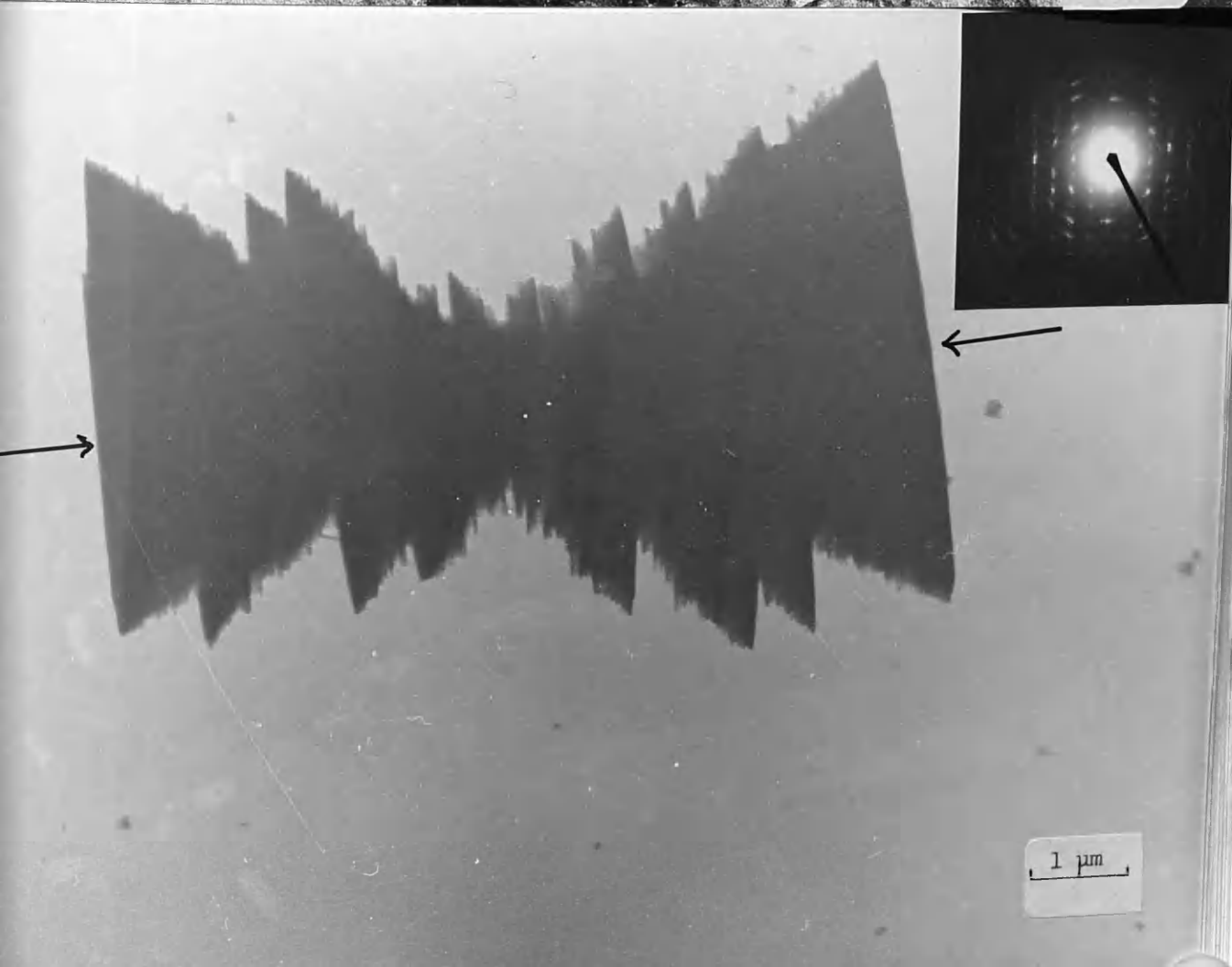
1 µm

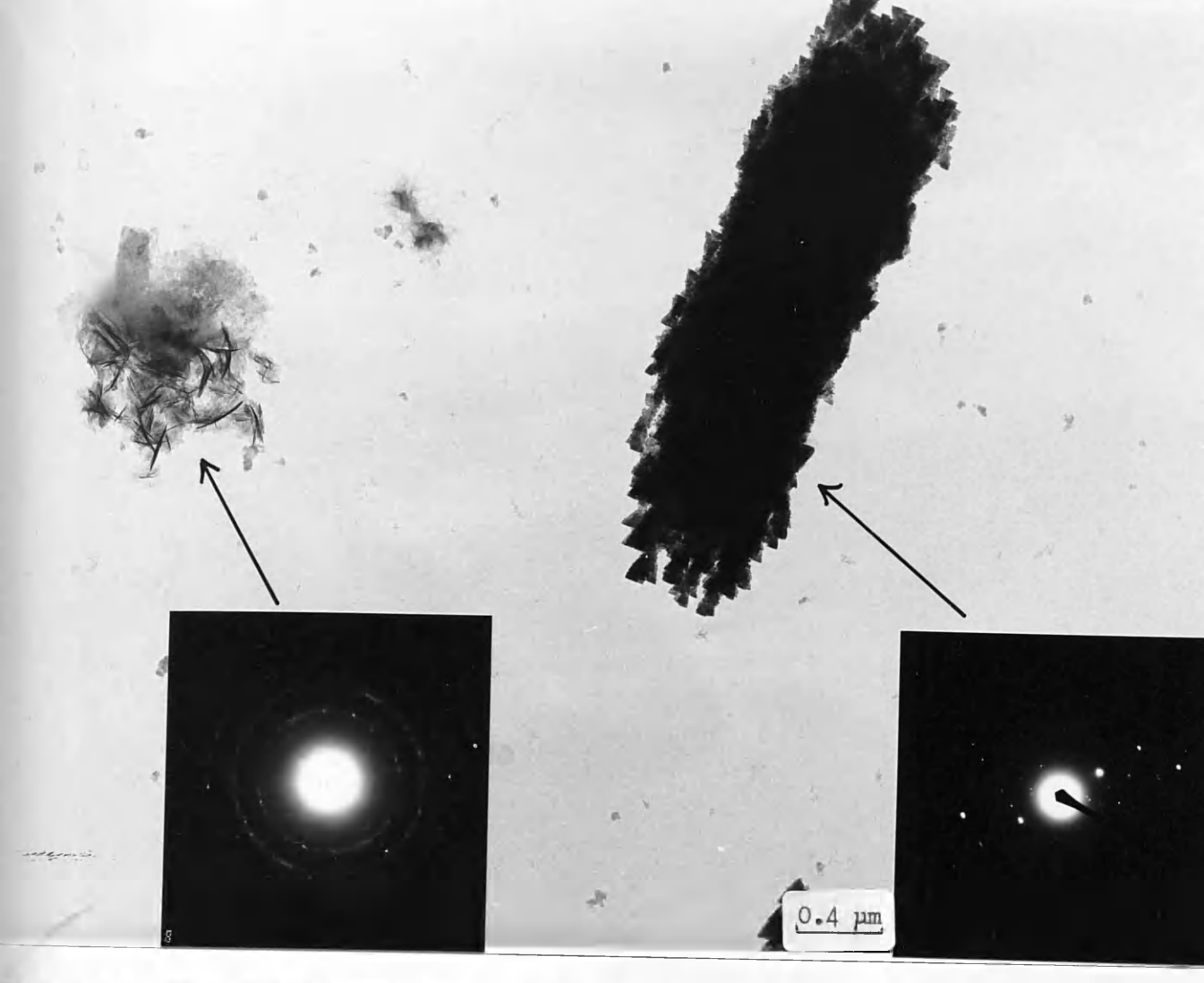
0.4 µm

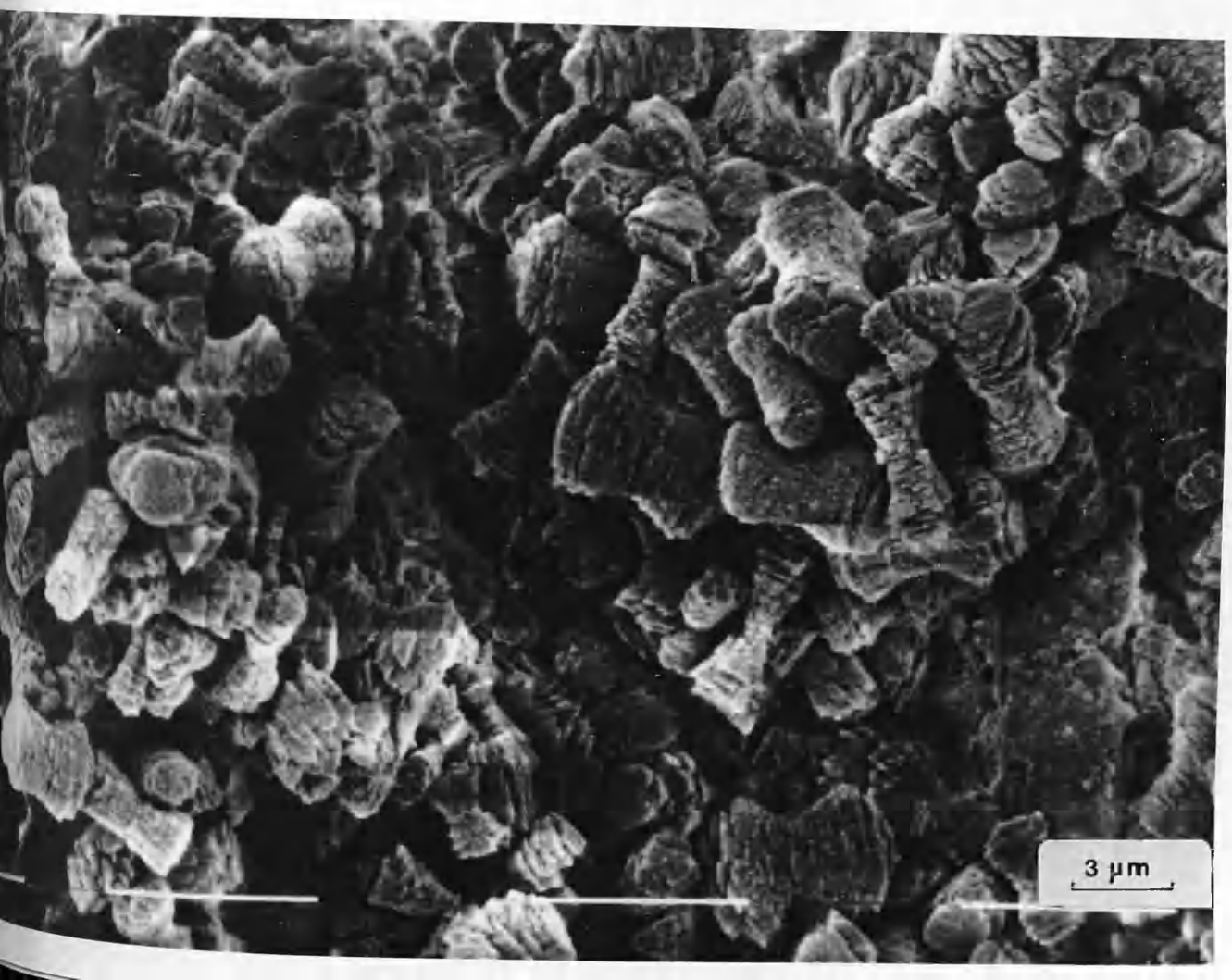
3 µm

Plate 4.3:

Crumpled sheets of a copper silicate produced within silica gel by hydrolysis of hexamine with $CuSO_4$ solution (Sec. 4.2.2).

Plate 4.4:

The early stage of bowtie morphology from a Cu compound produced within carrageenan gel from the front band precipitate after 8 days aging; using $CuSO_4$ and HEPES (Sec. 4.2.3a).

Plate 4.5:

8 months old bowtie-like morphology of a Cu compound formed within carrageenan gel from same sample as Plate 4.4 (Sec. 4.2.3 a).

Diffraction Pattern:

Left: Crumpled sheets. Right: Bowtie morphology.

Plate 4.6:

Scanning electron micrograph of a Cu compound showing the three-dimensional structure of the bowtie morphology; from same sample as Plate 4.5 (Sec. 4.2.3b).

Plate 4.7:

3 days old fully developed bowtie morphology of a Cu compound formed within carrageenan gel containing kaolinite; using $CuSO_4$ and HEPES solutions (Sec. 4. 2.3.b, Table 4.5).

Plate 4.8:

Dendritic structure of metallic copper produced within carrageenan gel containing kaolinite from tail band precipitate after 10 days aging; using $CuSO_4$ and HEPES solutions (Sec. 4.2.4).

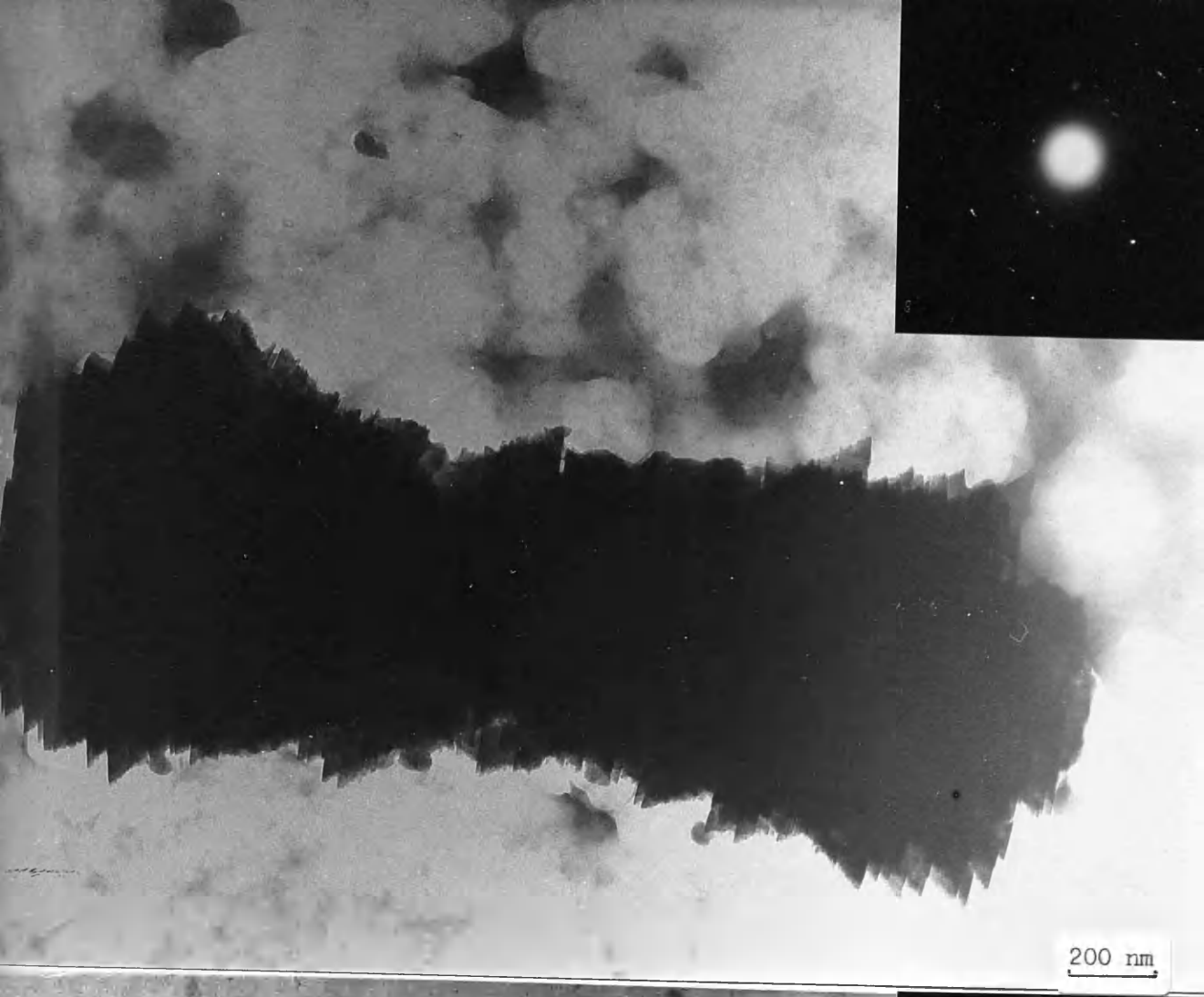
200 nm

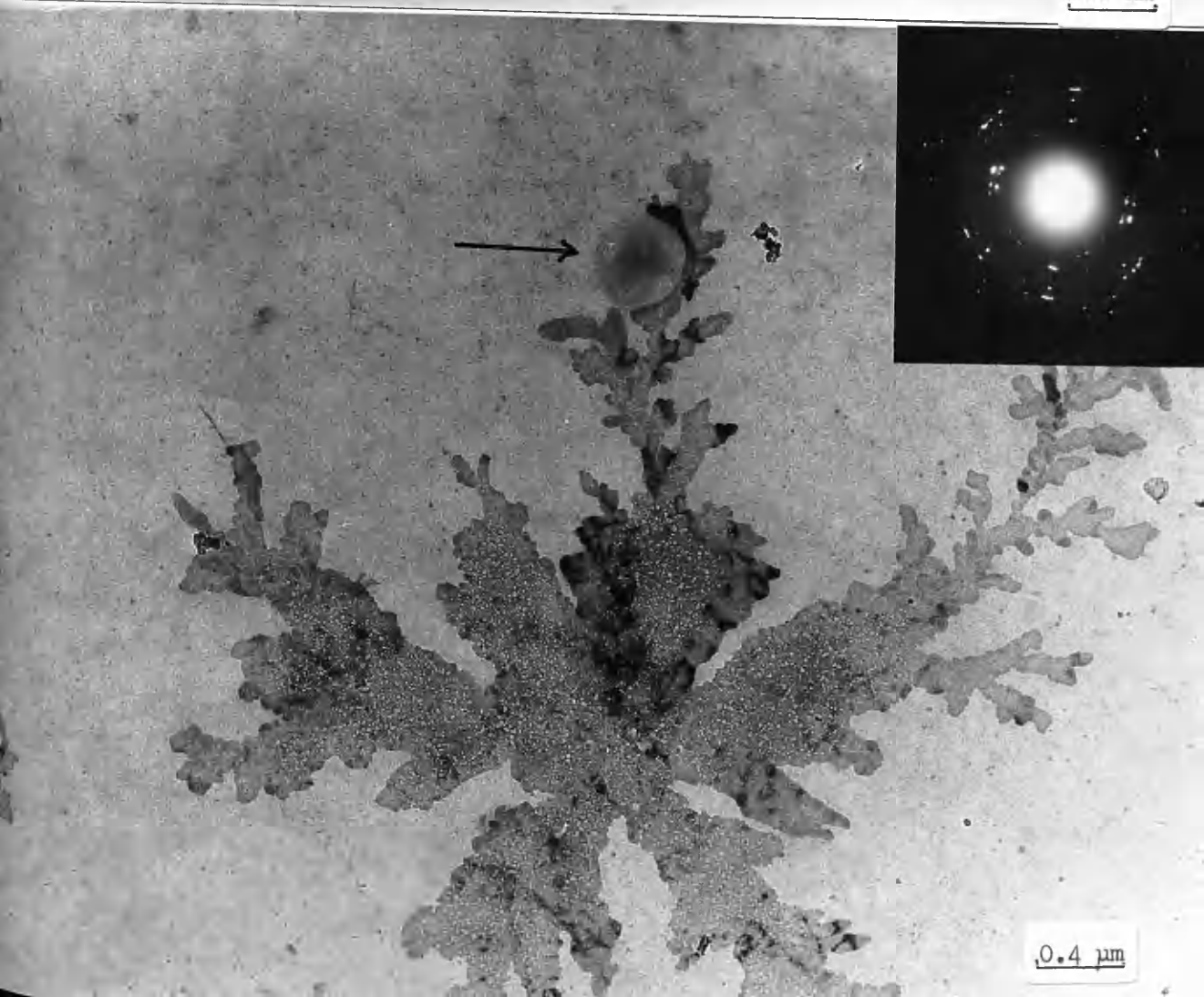
0.4 µm

Plate 4.9:

Rod-like morphology of a Cu compound from immediate precipitate formed by adding solid $Cu(ClO_4)_2$ to NaOH solution (Sec.4.3).

Plate 4.10:

Serriform morphology of Cu (II) oxide formed after one day aging from same sample as Plate 4.9 (Sec. 4.3).

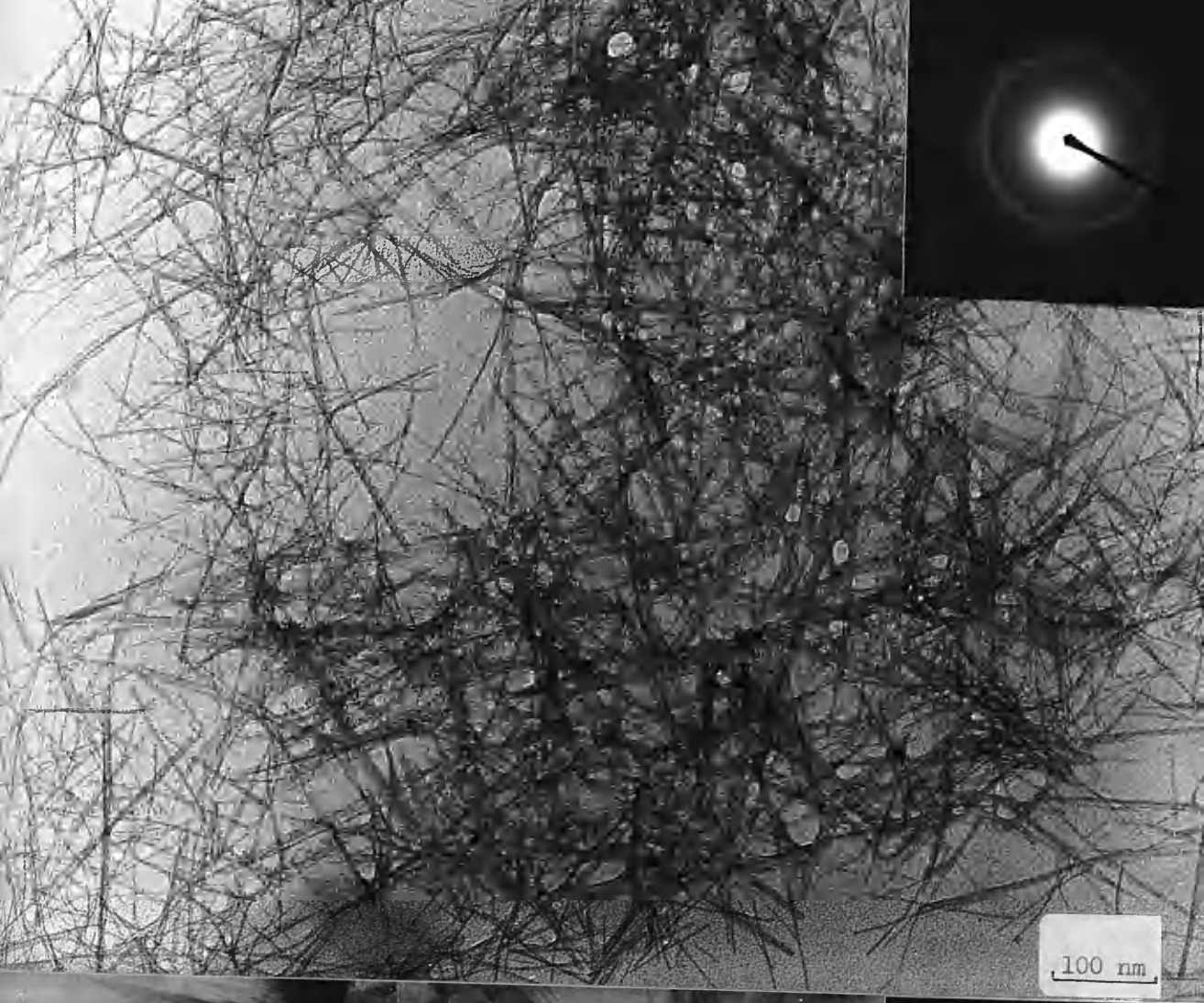
100 nm


0.4 μm

CHAPTER FIVE

Precipitation of Ag, Pt and Pd Metals

		page
5.1	Silver Particles in Silica Gel	93
5.2	Silver Particles in NaOH Solution	94
5.3	Platinum Particles in Gels	95
5.4	Palladium Particles in Gels	98

5.1 SILVER PARTICLES IN SILICA GEL (Sec.2.7.9)

The initially formed dark brown precipitate turned black by aging in different alkali source solutions. The dark brown precipitate is probably silver(I) oxide, whereas the black precipitate is silver metal. The ready reduction of the oxide to the metal is well known (Cotton and Wilkinson, 1980). Ten days old precipitate was examined in the electron microscope, showing small circular particles dispersed on the carbon film support when HEPES solution was the precipitating agent (Plate 5.2). These circular or spherical particles resemble those of Anderson (1975) and Berry and Skillman (1971); grown in mobile solutions. The diffraction pattern corresponds to silver metal as expected. On the other hand, when HEPPS solution was used instead, dendritic morphology was observed after 10 days aging (Plate 5.1). Close examination of the micrograph (Plate 5.1) shows that the dendritic object is probably nucleated at the centre and then the particles grew gradually in 3 dimensions as branches or secondary and tertiary arms and so forth as described earlier in Chapter I (Fig. 1.19). The diffraction pattern from a single dendritic object shows polycrystalline material which gives the six diffraction spacings characteristic of silver metal (Plate 5.1, Table 5.1). This dendritic morphology (Ag metal) is similar to the fractal structures (zinc metal leaves) grown electropositionally by Matsushita et al. (1984).

5.2 SILVER PARTICLES IN NaOH SOLUTION (Sec.2.7.10)

Plate 5.3 shows the irregular shapes of aggregated particles formed from fresh grey precipitate in the solution. Two strong diffuse rings and other lattice spacings correspond to silver(I) oxide (Table 5.2).

After 10 days aging, the grey precipitate had adopted a strikingly different morphology, with cubic structures overlapping at the edges (Plate 5.4). The diffraction pattern from the whole area shows a collection of spots whose spacings correspond to silver metal, as shown in Table 5.1.

In contrast, in this study there is no evidence of the pentagonal and icosahedral multiply twinned particles of silver metal described by Burton (1975) and Marks et al.(1980).

Nevertheless, this study produced marvellous dendritic forms (Plate 5.1) which to our knowledge have not been reported in the literature previously although somewhat similar forms have been observed by Fryer (1984) by reduction of dissolved $AgNO_3$ with coal at room temperature.

TABLE 5.2

Diffraction Spacings of Silver Compounds in NaOH Solution (Sec.2.7.10; 5.2)

P15.3	Ag_2O ASTM 12-793	
nm	nm	hkl
0.337	0.335	110
0.275	*0.273	111
0.238	*0.237	200
0.203	...	...
0.167	*0.167	220
0.144	*0.143	311
0.136	0.137	222
0.120	0.118	400

* : Indicates the strong ring.

P15.3 : Diffraction spacings of aggregated particles in Plate 5.3.

5.3 PLATINUM PARTICLES IN SILICA GEL (Sec. 2.7.12)

The reaction expected from platinum metal ion solution is as follows:

$$PtCl_4^{2-} + 2OH^- \longrightarrow PtO + H_2O + 4Cl^-$$

$$PtO \xrightarrow[\text{or heat}]{\text{reducing agent}} Pt \text{ (metal)}$$

It was reported by Hegenberger et al. (1987) that metal oxide particles are more easily reduced on carbon-based support.

Preliminary precipitation of platinum particles was carried out with different alkali solutions within silica gel or without it by diffusion in the double test tube method resulting as follows:

(a) A Black precipitate was formed within the silica gel by using all alkali solutions which have been described previously (Sec. 2.7.12).

(b) In the absence of the gel, a black precipitate was obtained only with $NaHCO_3$ solution but was not seen with HEPES or HEPPS solution.

Thus, the gel plays an important role in producing the precipitate which could not be obtained in the solution reactions.

A preliminary experiment within silica gel was carried out in the double test tube using HEPES solution as the precipitating agent. Ten days old black precipitate was examine in the electron microscope and it shows small loosely aggregated particles (Plate 5.5). The average aggregate size is about 25 nm. The diffraction data from the broad rings pattern correspond very well to platinum metal as shown in Table 5.3.

Homogeneous precipitation in gel containing HEPPS was chosen to precipitate platinum and palladium particles in order to provide stable conditions for reaction. The precipitation was carried out at various concentrations, but 0.025M K_2PtCl_4 will be discussed for comparison with palladium particles in Sec. 5.4 below. It was observed that all particle shapes of platinum metal in all 3 types of alkali solutions and at various concentrations show a similar morphology as in Plate 5.6. This micrograph shows random aggregates of platinum particles of different sizes. Small microcrystals are also observable as indicated by arrows `a´. This micrograph was taken after 1 day aging the precipitate. Close examination of the micrograph reveals that the larger semi-regular objects are probably composed of smaller microcrystals. There is no evidence of formation of larger aggregates in the electron microscope even at high beam irradiation. Thus, this formation occurred due to aging the precipitate in the tube. It seems that the

TABLE 5.3

Diffraction Spacings from Platinum Compounds in Silica gel Containing HEPPS

(Sec.2.7.12.1; 5.3)

P15.5 nm	P15.6 nm	Pt Metal ASTM 4-802 nm	hkl
0.227	0.224	*0.227	111
0.196	0.197	*0.196	200
0.138	0.136	*0.139	220
0.118	0.119	*0.118	311

* : Indicates the strong ring.
P15.5 : Diffraction spacings from loosely aggregated particles in Plate 5.5.
P15.6 : Diffraction spacings from aggregated particles in Plate 5.5.

aggregates attempted to form geometric shapes (the average of the large particles size ~60nm across) which are discernable in Plate 5.6 indicated by arrows as follows:

Pentagonal (b), triangular (c), hexagonal (d), square (e), rhombohedral (f) and poly-icosahedron (g). The latter shape was described by Marks et al. (1980) as a combination of two icosahedra. It was expected that these geometric-like shapes would rearrange towards the sharp geometric shapes by aging. But any such process is incomplete even after one year aging the precipitate in the tube and the large particles remain the same size at about 60 nm across (Plate 5.7). It was noticed that similar morphologies were formed in the absence of silica gel . Other workers have reported that platinum particle form hexagonal and triangular shapes; the particles size were observed 10nm after heating at 850° C (Domínguez & Yacamán, 1980) and 4nm-50nm at 700° C (Harris, 1985). Moreover, White (1982) reported that platinum particle size was about 68 nm after heating at 600° C for one hour.

It seems that the larger size (~60nm) of the particles will be obtained only at higher temperature; due to fusion of the microcrystalline particles, whereas in the present study the aggregated platinum (~60nm) was obtained only by aging homogeneously in silica gel, at room temperature.

Electron diffraction data from the platinum particles in Plate 5.6 correspond to platinum metal (Table 5.3).

5.4 PALLADIUM PARTICLES IN SILICA GEL (Sec. 2.7.12)

The reaction expected is similar to platinum particles as described previously as follows:

$$PdCl_4^{2-} + 2OH^- \longrightarrow PdO + H_2O + 4Cl^-$$

$$PdO \xrightarrow{\text{reducing agent or heat}} Pd \text{ (metal)}$$

Preliminary precipitation of palladium particles was carried out in the same procedure as in platinum Section. Furthermore, similar precipitates were obtained, although the black precipitate formed more slowly in the gel using $NaHCO_3$ solution.

Three micrographs (Plate 5.8, 5.9 and 5.10) are from the sample preparing by homogeneous precipitation in silica gel containing HEPPS at different ages. These precipitates were taken from the concentration of 0.025M K_2PdCl_4 (Sec.2.7.12.1, Table 2.1). It was noticed that this concentration gave the best result in terms of precipitation reaction (time) and producing the

geometric shapes. For example, the precipitate from 0.05M K_2PdCl_4 formed only after about after one year aging in the gel, and the geometric shapes are not observable from the sample prepared from of 0.04 molar solution.

Plate 5.8 shows similar aggregated palladium particles rather similar to those shown for platinum in Plate 5.6. But the palladium particles rearranged towards more geometric shapes, and some very sharply defined particles can be seen even though the sample was only aged for 1 day.

Close examination of the higher magnification micrograph of Plate 5.9 shows that the loosely circular particles tend to rearrange towards a regular geometric shape; triangular (a), pentagonal (b) and hexagonal (c).

After 21 days aging of the precipitate, it was noticed that all the particles developed very sharp geometric structures as in Plate 5.10. It was observed that the particles of the same shape were formed in different sizes; for example the different triangles (a). Presumably each of these particles corresponds to one of the loosely circular aggregates at the earlier stage of growth, with its material rearranged towards the most stable state which is in closed packing atoms i.e., one of the geometric structures. Plate 5.10 shows the striking change in particle morphology towards the sharp facets. Several distinct forms of these particles

can be seen ; triangular (a), square (b), rhombohedral (c), pentagonal (d), and hexagonal (e). Diffraction contrast effects are evident due to twinning and thickness variations in particles (f). The possible explanation of these shapes are as follows:

Two distinct shapes of these particles are pentagonal and hexagonal shapes, the so-called multiply twinned particles or MTPs (Ino & Ogawa, 1967; Allpress & Sanders, 1967). Pentagonal projections are obtained from pentagonal bipyramid particles, Fig. 5.1a, (Burton, 1975) which are built up from 5 tetrahedra. The formation of a decahedral MTP from 5 tetrahedra necessitates strains, dislocations or misfits, because the tetrahedra are not completely space filling, Fig. 5.1b, (Marks et al., 1980).

On the other hand, hexagonal projections are obtained from 20 tetrahedra combining to give an icosahedral MTP, Fig.5.1c.

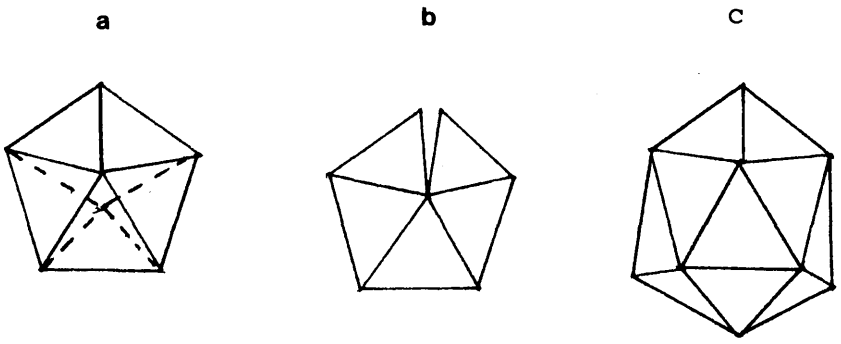

Fig. 5.1. Multiply-twinned particles forming from tetrahedra, (a) ideal pentagonal bipyramid; (b) distorted structure from twinning of five tetrahedra; (c) icosahedral structure forming from twenty tetrahedra.

The nucleation and growth mechanism of MTP's are complex and a detailed discussion can be found in a review article by Gillet (1977).

Square particles commonly arise from materials with a face centred cubic structure and rhombohedral projections are a special view of a pentagonal particle, (Burton 1975).

Finally, trigonal plane shapes presumably arise from structures in which the close-packed {111} planes lie parallel to the support film.

It was reported that the expected equilibrium shape is of the form of a polyhedron with markedly rounded corners (Anderson, 1975). These rounded corner particles also can be seen clearly in Plate 5.9 and 5.10.

The electron diffraction spacings in Plate 5.9 are characteristic of palladium metal, as shown in Table 5.4. In addition, the electron diffraction spacings resulting from crystals in Plate 5.8 and 5.10 show the similar pattern and are also characteristic of palladium metal.(Table 5.4.).

TABLE 5.4

Diffraction Spacing from Palladium Compounds

in Silica Gel Containing HEPPS

(Sec.2.7.12.1, 5.4)

P15.9	Pd Metal ASTM 5-0681	
nm	nm	hkl
0.225	*0.225	111
0.194	*0.195	200
0.137	*0.138	220
0.116	*0.117	311

* : Indicates the strong ring.
P15.9 : Diffraction spacings from aggregated particles in Plate 5.9.

Plate 5.1:

Dendritic forms of Ag metal produced after 10 days aging in silica gel using HEPPS solution (Sec. 5.1).


100 nm

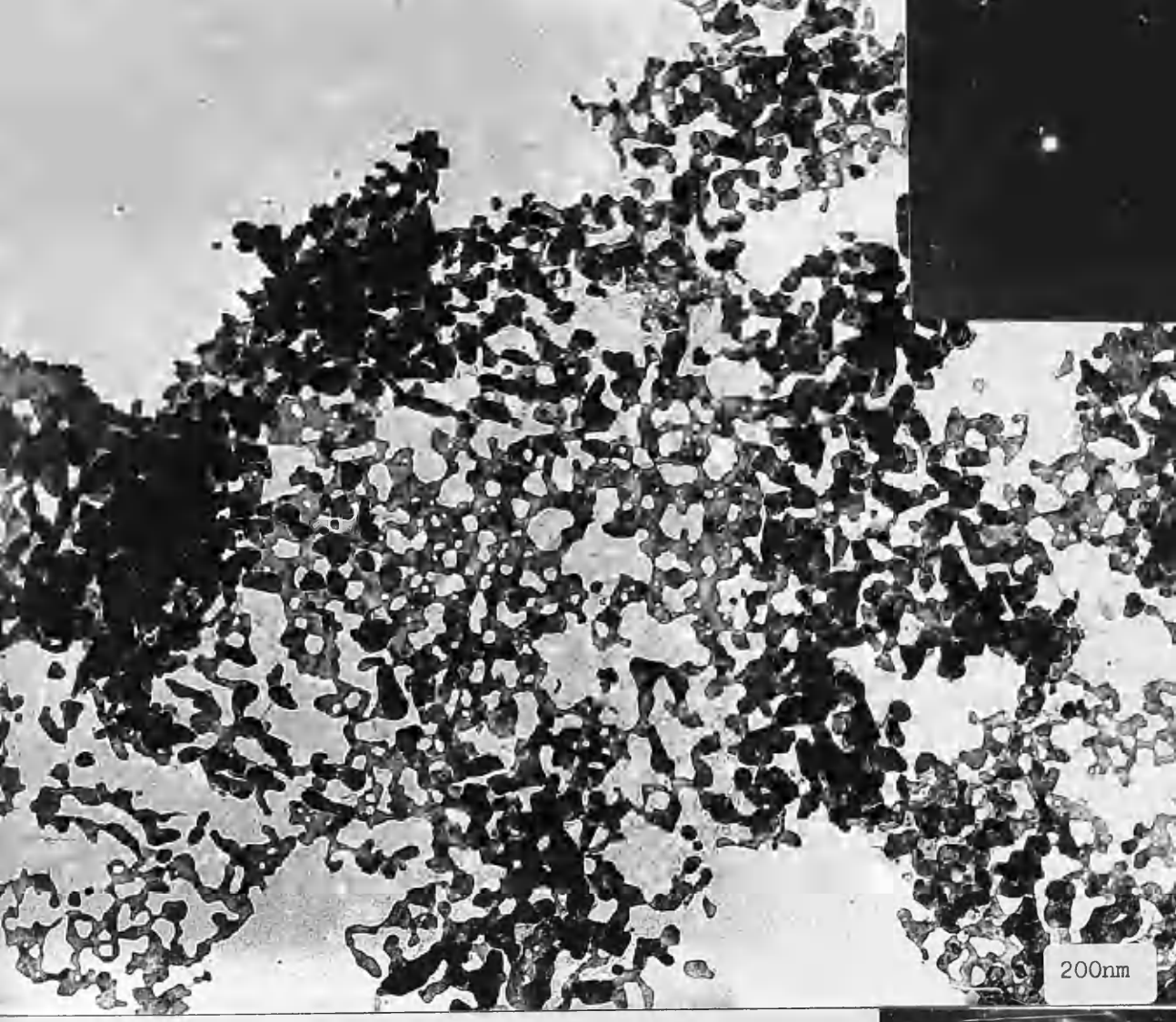
200nm

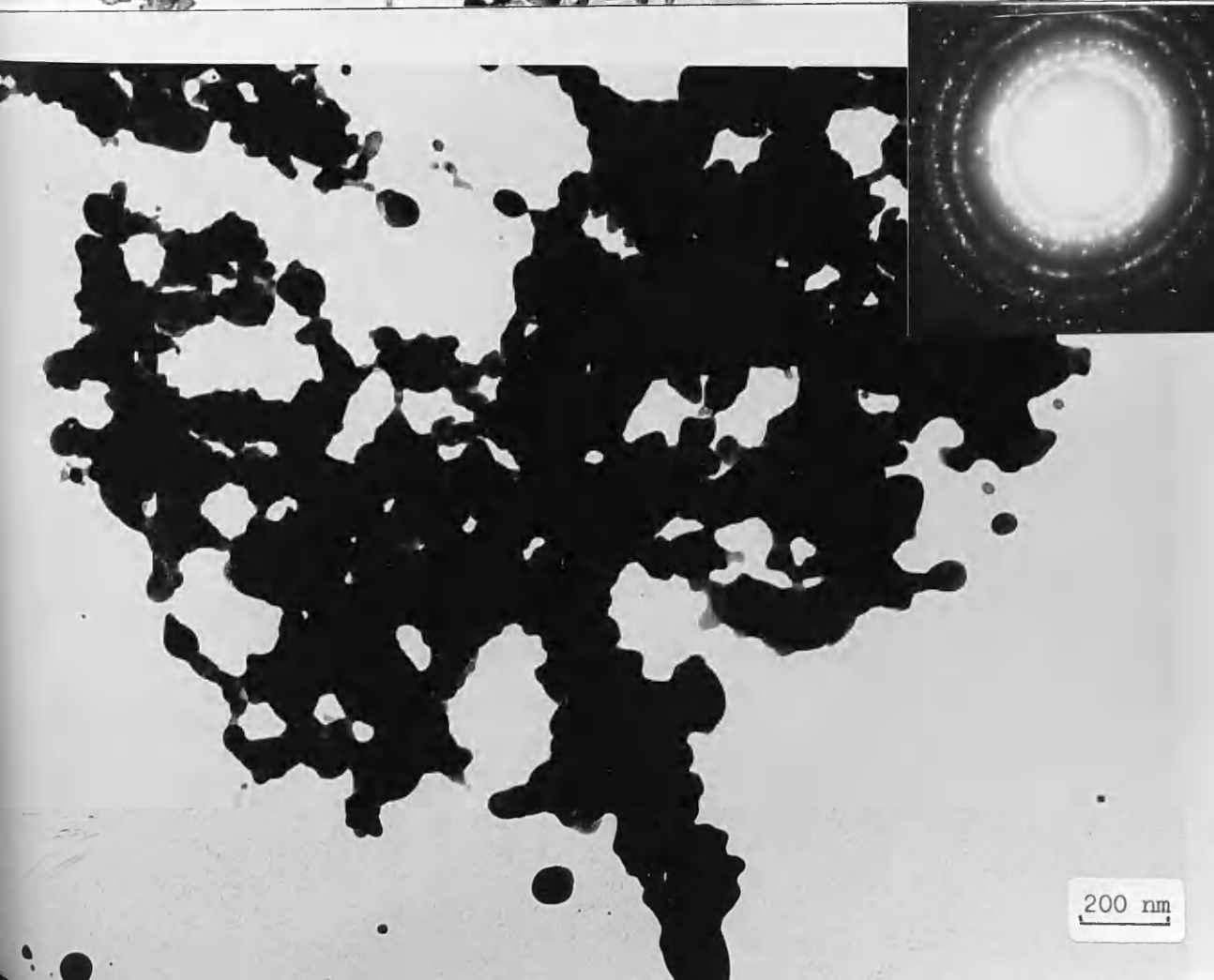
200 nm

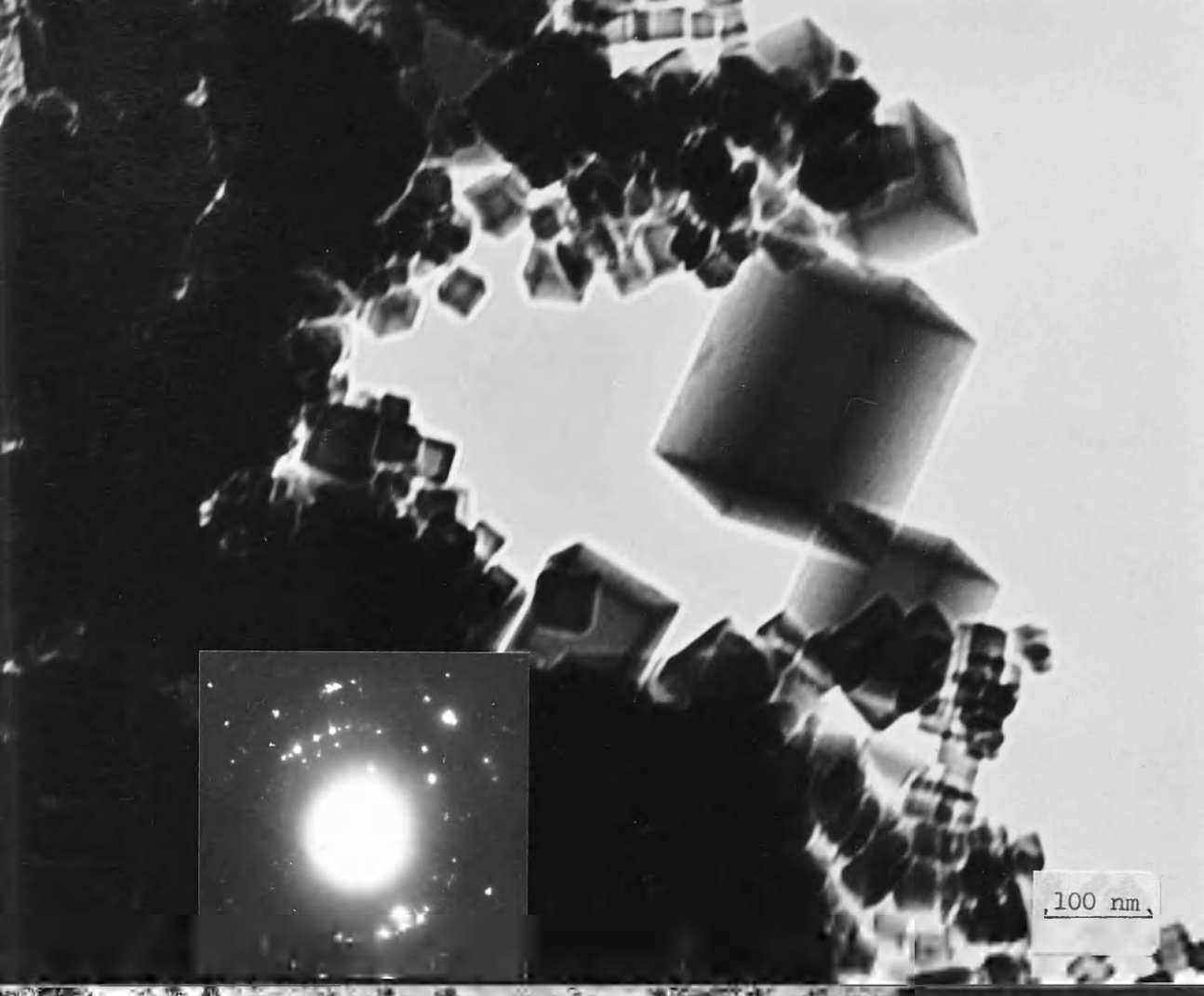
100 nm

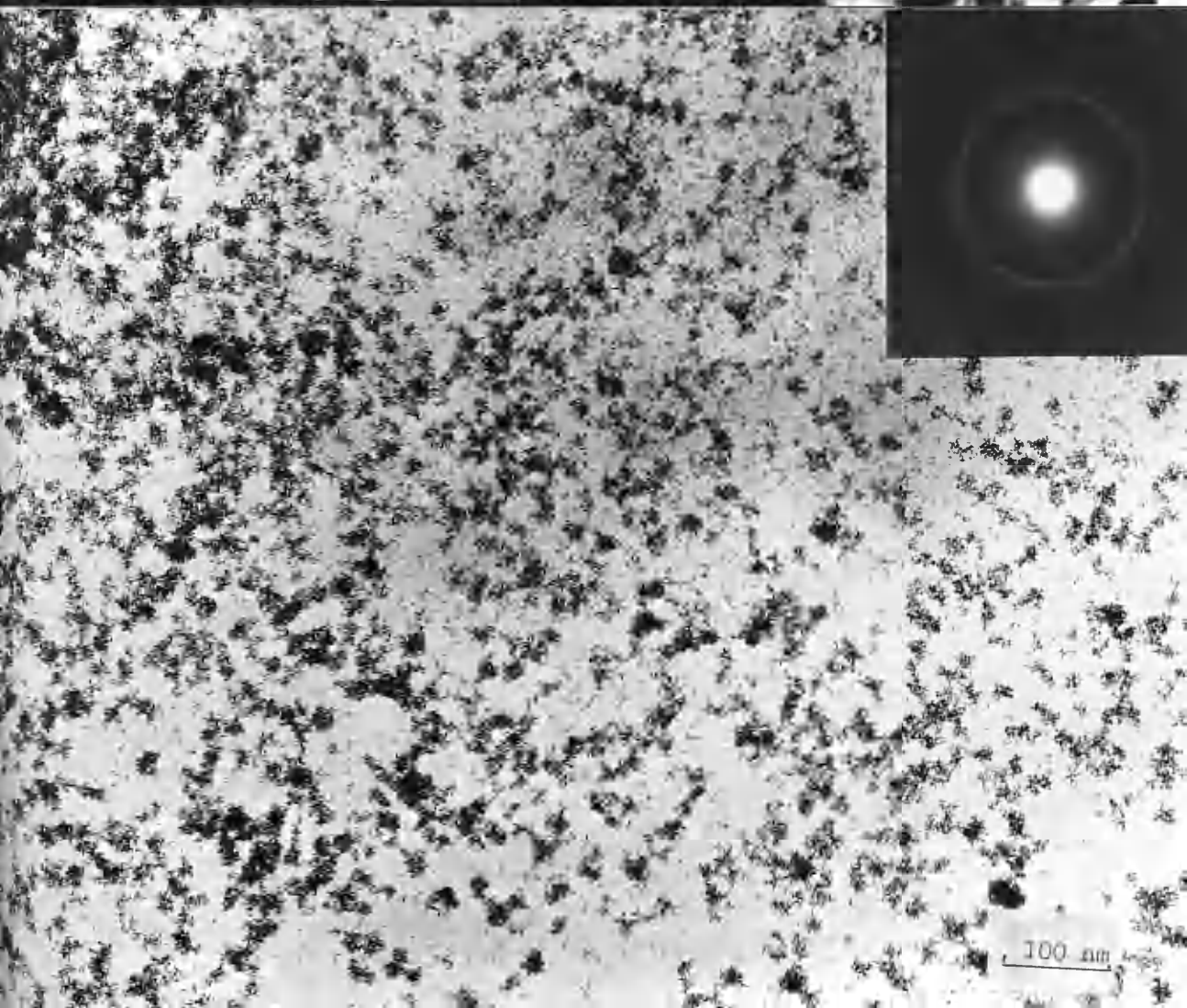
100 nm

Plate 5.6:

Aggregated small Pt particles obtained homogeneously in silica gel containing HEPPS after 1 day aging (Sec.5.3).

Plate 5.7:

Aggregated Pt particles same sample as Plate 5.6; after 1 year aging.

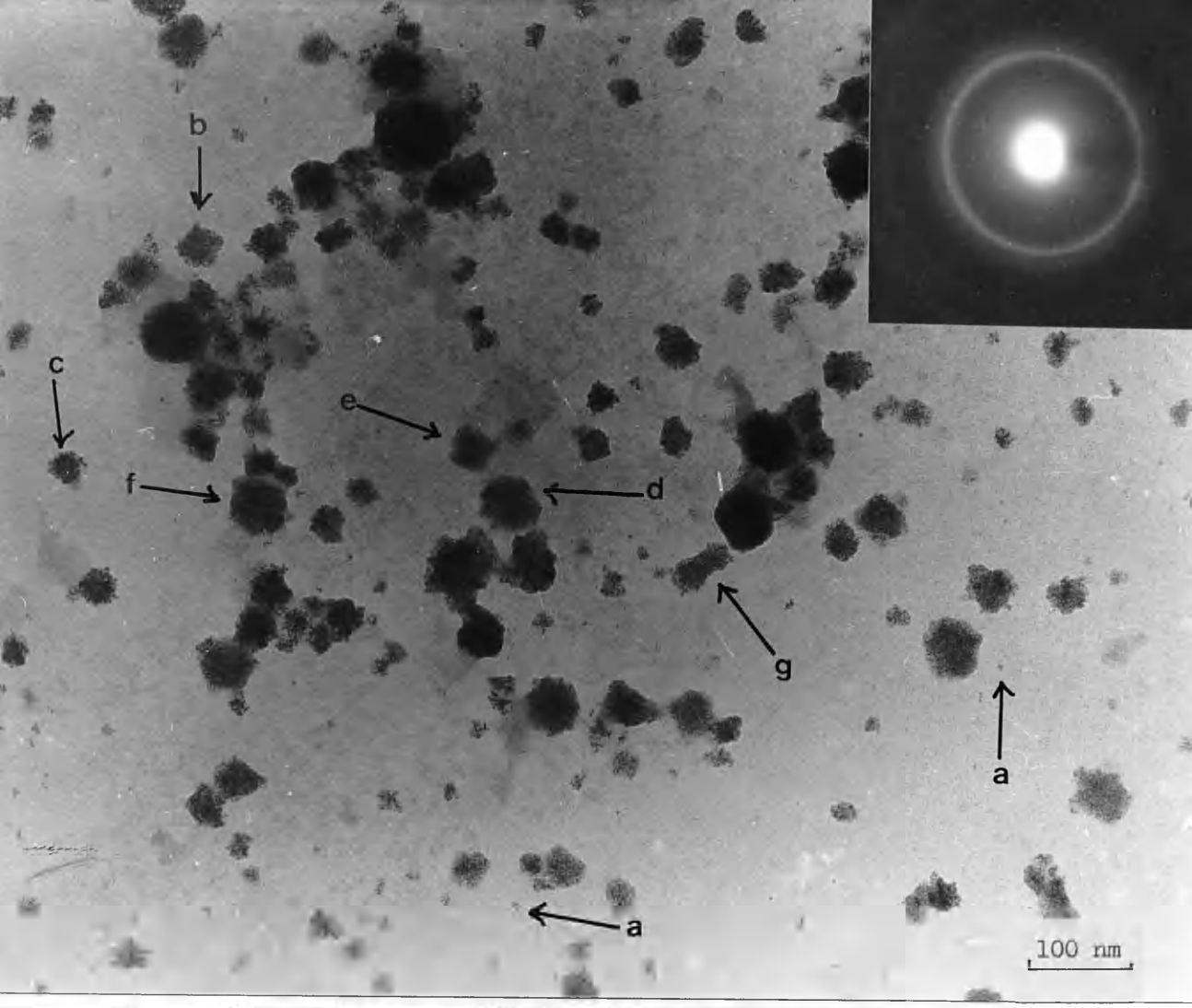
b
c
e
f
d
g
a
a
100 nm

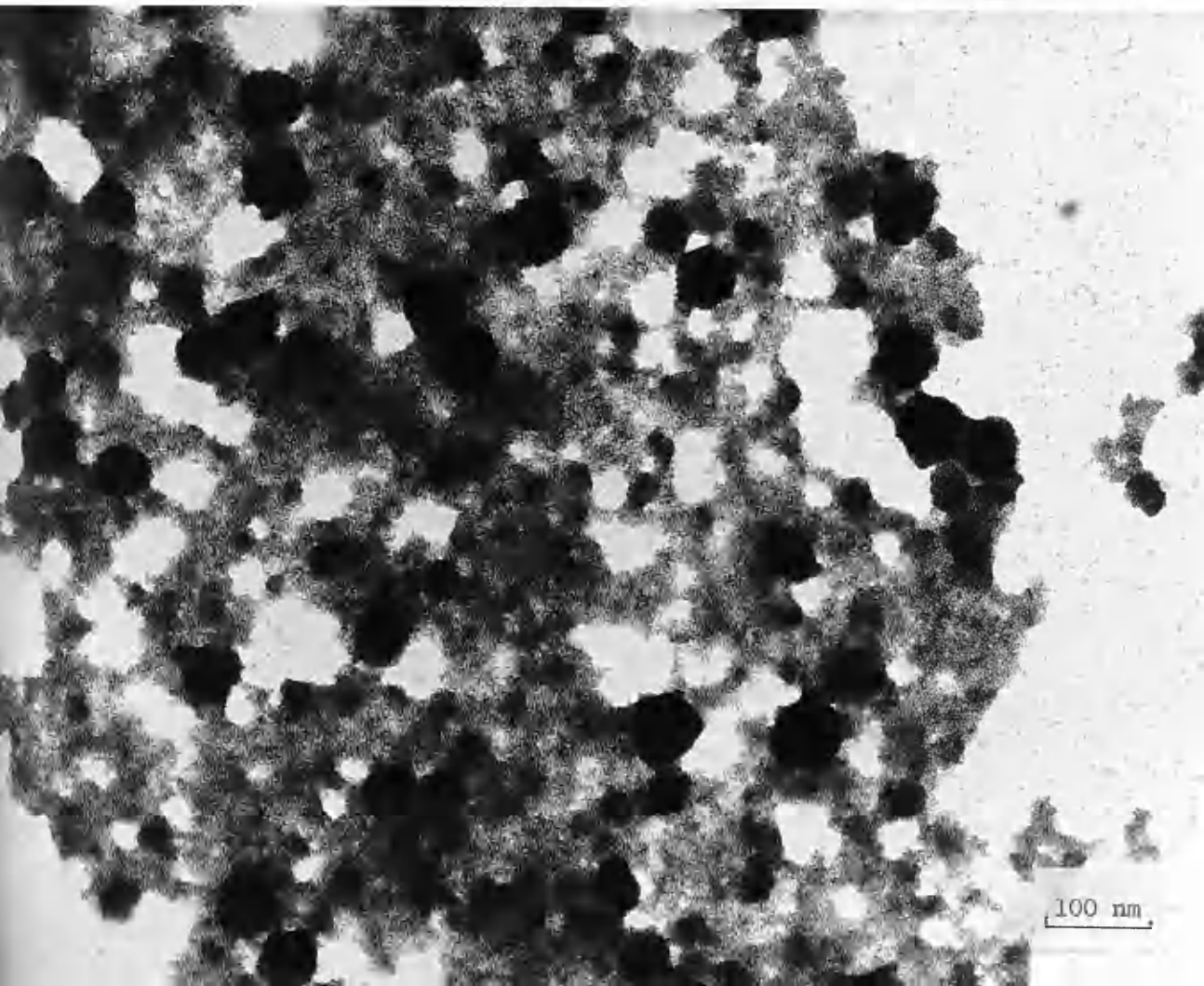
100 nm

Plate 5.8:

Aggregated small Pd particles formed homogeneously in silica gel containing HEPPS after 1 day aging (Sec.5.4).

Plate 5.9:

Aggregated Pd particles formed homogeneously in silica gel containing HEPPS after 4 days aging (Sec.5.4). Same sample as Plate 5.8.

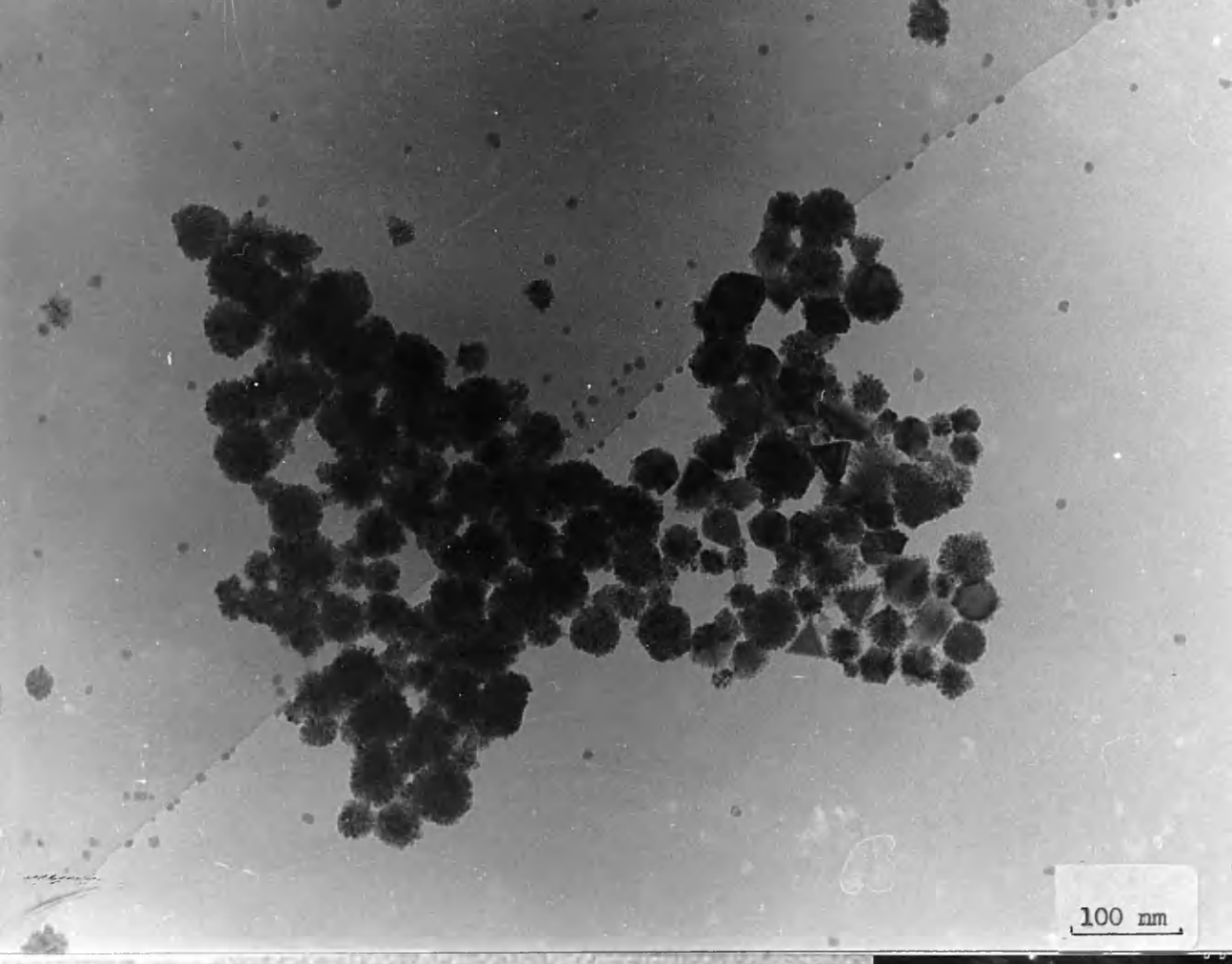
100 nm

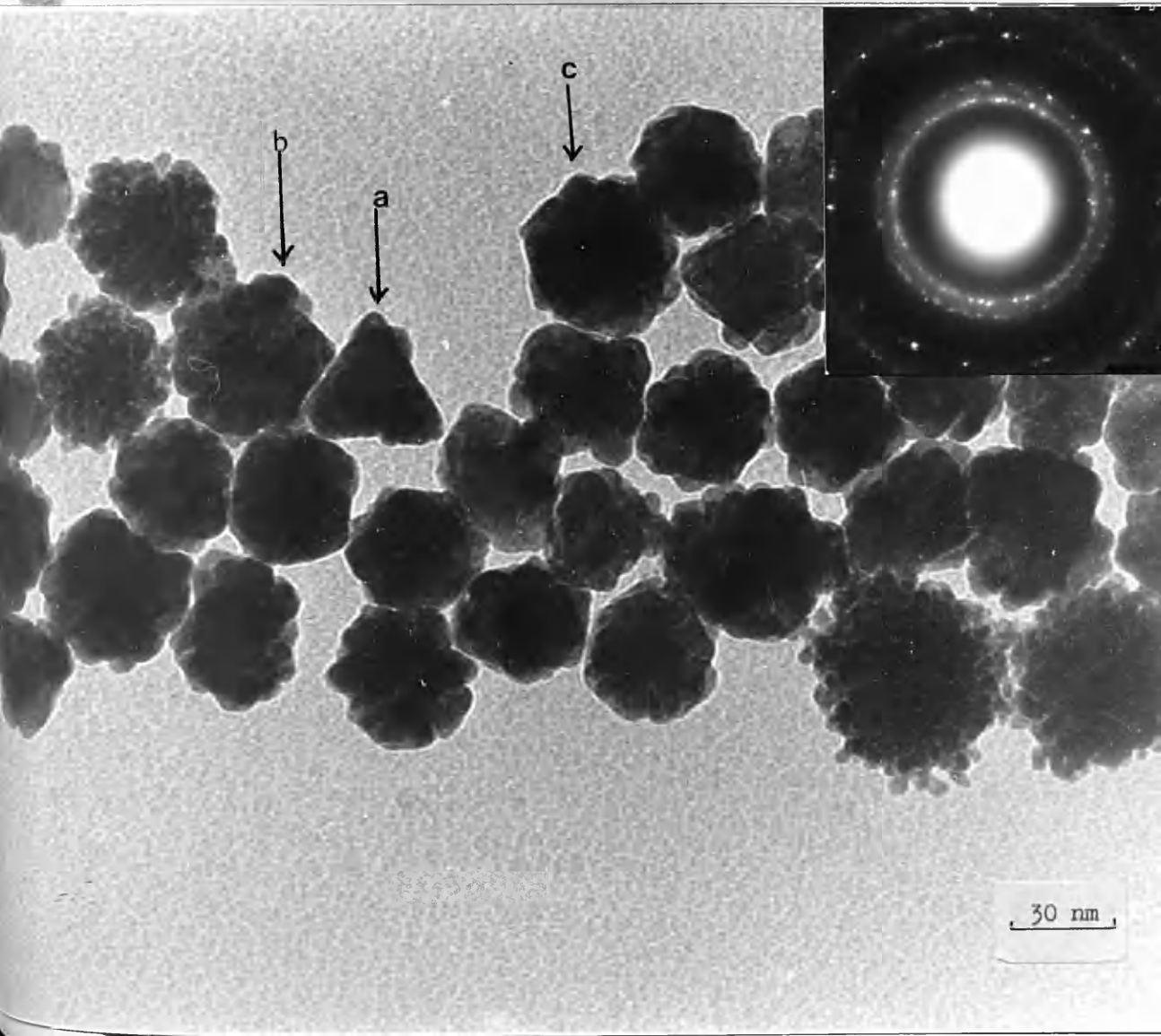
c
b
a
30 nm

Plate 5.10:

Crystalline Pd particles obtained homogeneously in silica gel containing HEPPS after 21 days aging (Sec.5.4). Same sample as Plate 5.7.

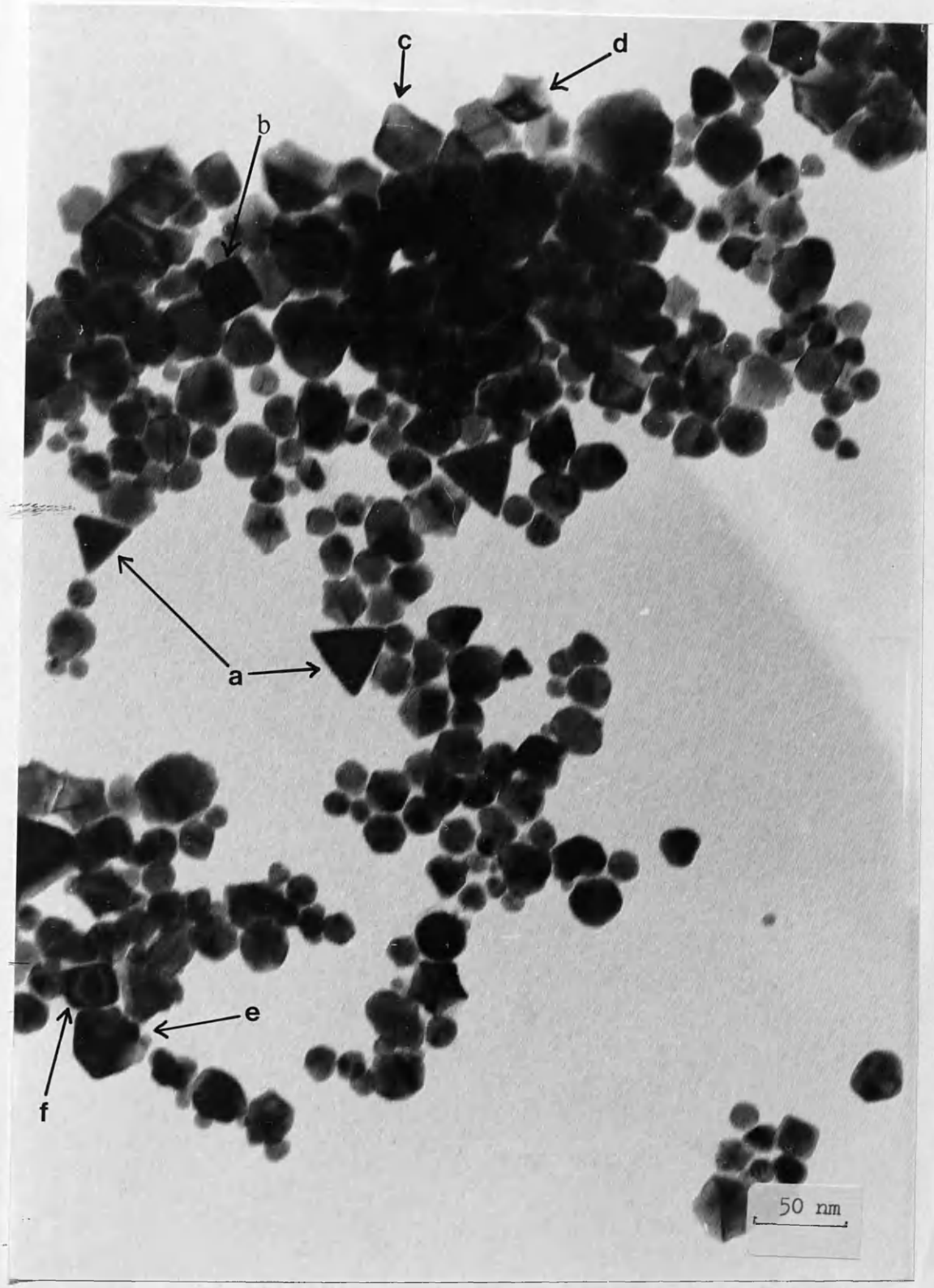
c
d
b
a
e
f
50 nm

CHAPTER SIX

MISCELLANEOUS PRECIPITATION IN SILICA GEL

page

6.1 PRECIPITAION OF METAL CARBONATES WITHIN THE GEL BY HYDROLYSIS OF UREA 102

6.1.1 $BaCO_3$ Crystals Grown in Gel 102

6.1.2 $SrCO_3$ Crystals Grown in Gel 103

6.1.3 $CaCO_3$ Crystals Grown in Gel 104

6.1.4 $CdCo_3$ Crystals Grown in Gel 105

6.1.5 Basic Lead Carbonate Crystals Grown in Gel 106

6.2 PRECIPITATION OF METAL SILICATE WITHIN THE GEL

6.2.1 Pb-Silicate Crystals Obtained by Hydrolysis of Hexamine 107

6.2.2 Co-Silicate Crystals Obtained by Hydrolysis of Hexamine 107

6.2.3 Ni-Silicate Crystals Obtained by Hydrolysis of Hexamine 108

6.2.4 Al-Silicate Crystals Obtained by Hydrolysis of Hexamine 108

6.2.5 Mg-Silicate Crystals Obtained by Hydrolysis of Hexamine 109

6.2.6 Zn-Silicate Crystals Obtained by Hydrolysis of Urea 109

6.2.7 Zn-Silicate Crystals Obtained by Hydrolysis of Hexamine 109

6.3 PRECIPITATION OF MnO_2 WITHIN SILICA GEL ... 110

6.3.1 MnO_2 Crystals Obtained by Hydrolysis of Urea or Hexamine 110

6.3.2 MnO_2 Crystals Obtained by Oxidation of $KHSO_5$ or $NaIO_4$ 112

6.1 PRECIPITATION OF METAL CARBONATES WITHIN THE GEL BY HYDROLYSIS OF UREA

The expected reactions from metal ion solution by hydrolysis of urea (Ch.2; Table 2.2) are as follows:

$$(H_2N)_2\ CO + 3H_2O \xrightarrow{85\text{-}90^{\circ}C} CO_2 + 2NH_4^+ + 2OH^-$$

a) $M^{n+} + nOH^- \longrightarrow M(OH)n$ or M-silicate (at high temperature)

heat → M_2O_n

reduction → MO_x ($x<n/2$) or M (metal)

or

(b) $CO_2 + H_2O \rightleftharpoons H_2CO_3 \rightleftharpoons H^+ + HCO_3^- \rightleftharpoons 2H^+ + CO_3^=$

or $CO_2 + OH^- \longrightarrow HCO_3^-$

$CO_3^= + M^{2+} \rightleftharpoons MCO_3$ or $M_2(OH)_2(CO_3).\ nH_2O$ basic carbonate

heat → $MO + CO_2$

The general formula of basic carbonate:

$[M(OH)_2]_x\ [MCO_3]_y.\ nH_2O$

6.1.1 $BaCO_3$ Crystals Grown in Silica Gel (Sec. 2.9; Table 2.2)

White dendritic crystals of barium carbonate can be seen clearly in a test tube as shown in Plate 6.1. The crystals were observed in a light microscope and were typically about 3 mm long with opened branches of about 1 mm long, similar to those grown in silica gel at PH 10.2 and 20°C by García-Ruiz & Amorós (1981); 3mm long.

Other morphologies of barium carbonate (the snow-flake like and the polycrystalline ball aggregated crystals) by Cho et al. (1977) were obtained in a test tube containing 0.6M barium chloride, 0.6M potassium carbonate and silica gel mixture at pH 6.0, 1 day aging.

The electron micrograph in Plate 6.2 shows a branch of the dendritic forms with rough surface, and holes (marked by arrows). The holes were probably caused by electron beam damage. This morphology was totally different from that grown in solution. Takiyama (1981) has reported that barium carbonate produced in solution has a rod-like structure.

The diffraction shows very diffused spots making it difficult to measure its lattice spacings. However, the spacings correspond roughly to barium carbonate as shown in Table 6.1, as expected. It has been reported that the barium carbonate structure will not change up to 1000^{o} C (Cork & Gerhard, 1931) and will decompose to barium oxide at above 1300^{o}C (Lander 1949).

6.1.2 $SrCO_3$ Crystals Grown in Silica Gel (Sec. 2.9; Table 2.2)

A similar morphology to barium carbonate was observed in the test tube and in light microscope but the forms are slightly shorter in length, about 2.7 mm long.

The electron micrograph of Plate 6.3 shows only a segment from the dendritic crystals and displays a rough surface. The polycrystalline diffraction pattern corresponds to strontium carbonate as shown in Table 6.2; no evidence of strontium oxide was observed. This carbonate is fairly stable; it would decompose to oxide at above 1300 ^{o}C (Lander 1949).

6.1.3 $CaCO_3$ Crystals Grown in Gel (Sec. 2.9; Table 2.2)

Well-shaped smooth-faced rhombohedral crystals were observed in the light microscope. The edge length of crystals are about 0.2mm and the angle is about 77^{o}. The morphology is similar to calcite as prepared by diffusing $CaCl_2$ and $(NH_4)_2CO_3$ solutions in a silicate acid gel at pH 7-8 at 22^{o} C, but in that work the crystals were about 2.5mm long (Nickl & Henisch, 1969; Barta et al. 1971). Calcite has also been grown in Zero-G by diffusing chemicals ($CaCl_2$, $(NH_4)_2CO_3$) through opposite ends of a compartment containing pure water, giving smaller crystals which are about 0.5mm across. Besides the rhombohedra, some irregularly-shaped crystals of different sizes were obtained under microgravity (NASA 1977), but not in the present work.

Plate 6.4 shows irregular shaped and very thick particles which did not give detailed lattice spacings.

TABLE 6.1

Electron Diffraction Spacings from Barium Carbonate Particles Formed Homogeneously in Silica Gel by Hydrolysis of Urea. (Sec. 2.9; 6.1.1)

P16.2	$BaCO_3$ ASTM 11-697	
nm	nm	hkl
0.413	*0.402	111
0.350	*0.348	200
0.248	*0.246	220
0.213	0.211	311
0.207	0.201	222
0.162	0.160	331
0.154	0.156	420

* : Indicates the strong rings.
P16.2 : The lattice spacings from a segment of the dendritic forms in Plate 6.2.

TABLE 6.2

Electron Diffraction Spacings from Strontium Carbonate Formed Homogeneously in Silica Gel by Hydrolysis of Urea (See, 2.9; 6.1.2)

Pl6.3	$SrCO_3$ ASTM 5-0418	
nm	nm	hkl
0.303	0.301	002
0.284	0.284	012
0.266	0.260	102
0.227	0.227	211
0.191	0.191	132
0.156	0.157	241
0.135	0.131	332

Pl6.3 : The lattice spacings from a segment of the dendritic form in Plate 6.3.

Nevertheless, the diffraction spacings correspond to calcite only (Table 6.3) (there was no evidence of aragonite, (ASTM 5-0453), vaterite (ASTM 13-192), or calcium oxide (ASTM 4-0777)). Calcium carbonate will decompose at about 900^{0}C (Lander 1949). It has been reported that almost 100 % aragonite would form at high temperature (>80^{0}C) by adding Na_2CO_3 to $CaCl_2$ solutions (de Keyser & de Gueldre, 1950) and only aragonite will be formed at 70-90^{0}C by bubbling calcium bicarbonate solution with CO_2 gas (Kitano, 1962). In this study, the sample (in gel) was prepared at 85-90^{0}C but there is no evidence of aragonite being present.

Furthermore, it has been reported that calcium silicate would form in the gel at pH below 6 (Armington & O´Connor, 1980). But in this work the pH started off at 2.5 but there is no evidence that the silicate was formed.

6.1.4 Crystals of $CdCO_3$ Grown in Gel (Sec. 2.9; Table 2.2)

Plate 6.5 shows small crystals dispersed within the gel; the polycrystalline diffraction pattern matches very well to the strong lattice spacings of cadmium oxide, ASTM 5-0640; 0.279 nm (111), 0.234 nm (200) and 0.161 nm (220). Undoubtedly the material was originally cadmium carbonate (it was a white) but this decomposed

in the electron beam to give CdO (brown). It is well known that cadmium carbonate will decompose to cadmium oxide at 500°C (Dean, 1985).

6.1.5 Basic lead Carbonate Grown in Gel (Sec.2.9; Table 2.2)

Large (~4 μm) thin, crystals were observed consisting of thin platelets which allowed the electron beam to pass through. Single crystal diffraction patterns were commonly observed as shown in Plate 6.6. A close examination of Plate 6.6 shows a twin boundary as indicated by an arrow and many intensities contour lines within the platelet. The spacings are characteristic of basic lead carbonate, $Pb_3(CO_3)_2(OH)_2$, as shown in Table 6.4.

6.2 PRECIPITATION OF METAL SILICATES WITHIN THE GEL

The expected reactions from metal ion solution by hydrolysis of hexamine (Chapter 2; Table 2.3) are as follows:

$$C_6H_{12}N_4 + 6H_2O \rightleftharpoons 4NH_3 + 6CH_2O$$

$$NH_3 + H_2O \rightleftharpoons NH_4^+ + OH^-$$

TABLE 6.4

Electron Diffraction Spacings From lead Carbonate Hydroxide Obtained by Hydrolysis of Urea

(See, 2.9; 6.1.5)

P16.6 nm	$Pb_3(CO_3)_2(OH)_2$ ASTM 13-131 nm	hkl
0.419	0.425	012
0.330	*0.329	015
0.267	*0.262	110,009
0.242	0.249	018
0.203	0.205	205
0.186	0.186	119
0.174	0.170	$10\underline{1}3$
0.163	0.161	125
0.155	0.153	217
0.152	0.151	300
0.140	0.139	$21\underline{1}0$
0.120	0.125	$312,21\underline{1}3$

* : Indicates the strong rings.
P16.6 : The lattice spacings of a large particle in Plate 6.6.

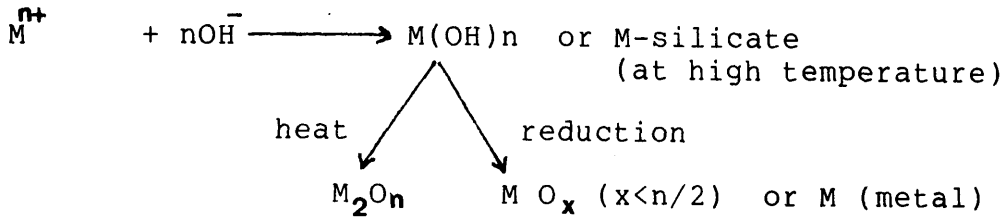

Strom & Wonjun (1980) reported that rate of conversion of hexamine to formaldehyde depended on pH in the buffers of constant ionic strength, the reaction half life decreasing from 13.8 hours at pH 5.8 to 1.6 hours at pH 2.0. For this reason, various ranges of pH were carried out in preliminary precipitation.

6.2.1 Pb-Silicate Crystals Obtained by Hydrolysis of Hexamine (Sec. 2.9; Table 2.3)

Plate 6.7 shows the morphology of lead silicate particles as circular arrays of dendritic objects.The particles seem to be poorly crystalline forms which show only diffuse diffraction rings (Plate 6.7), corresponding to the strong spacings of $PbSiO_3$, ASTM 20-594. These are 0.230 nm ($\bar{4}21$,130), 0.267nm ($\bar{3}21$) and 0.323nm (202).

6.2.2 Co Silicate Crystals Obtained by Hydrolysis of Hexamine (Sec.2.9; Table 2.3)

The very thin crumpled sheets of cobalt compound are observed in Plate 6.8.The crumpling is probably caused by stress on the large thin sheets or may be an artefact of drying down during specimen preparation. The diffraction pattern (Plate 6.8) shows very broad rings but it matches very well with the strong lattice spacings

TABLE 6.5

Electron Diffraction Spacing From Aluminum Silicate Obtained in Silica Gel by Hydrolysis of Hexamine (See, 2.9; 6.2.4)

P16.10 nm	Al_2SiO_5 ASTM 11-46 nm	hkl
0.335	*0.335	200
0.306	*0.318	$02\bar{1}$,111+
0.303	0.302	021,$1\bar{2}1$
0.270	0.270	$2\bar{1}1$
0.222	0.223	300
0.151	0.151	050,$1\bar{3}\bar{3}$+
0.134	*0.138	$3\bar{5}1$,$4\bar{4}\bar{2}$, $40\bar{3}$,$23\bar{3}$, 142

* : Indicates the strong rings.
P16.10 : The lattice spacings from the particles in Plate 6.10.

of cobalt silicate, Co_2SiO_4, in the standard ASTM 15-497; these are 0.245 nm (311), 0.199 nm (400) and 0.153nm (333,511).

6.2.3 Ni-Silicate Crystals Obtained by Hydrolysis of Hexamine (Sec. 2.9; Table 2.3)

Plate 6.9 shows the nickel compound consisting of very thin sheets which are crumpled in places.This material is probably poorly crytalline, and shows broad diffraction rings (Plate 6.9). The spacings correspond very well with the strong standard lattice spacings of nickel orthosilicate, Ni_2SiO_4, ASTM 15-255; they are 0.242nm (311), 0.213nm (400) and 0.139 nm (440).

6.2.4 Al-Silicate Crystals Obtained by Hydrolysis of Hexamine. (Sec.2.9; Table 2.3)

This compound was very difficult to observe in the electron microscope, probably due to lack of material on the microgrid or only a very small amount of this material being available for study. A close examination in Plate 6.10 shows a large particle that contains small network particles. Nevertheless, these particles diffracted very sharply, showing a spotty pattern which corresponds to aluminum silicate, Al_2SiO_5, (Table 6.5).

6.2.5 Mg-Silicate Crystals Obtained by Hydrolysis of Hexamine (Sec. 2.9; Table 2.3)

Plate 6.11 shows a rhombus platelet particle which in some parts is very thin so that the carbon film can be seen beneath it. The diffraction pattern consists of a scattered spotty pattern but corresponds to magnesium metasilicate, $MgSiO_3$, as shown in Table 6.6.

6.2.6 Zn-Silicate Crystals Obtained by Hydrolysis of Urea (Sec. 2.9; Table 2.2)

Plate 6.12 shows the morphology of crumpled sheets. The diffraction patterns consisted of very diffuse rings, whose lattice spacings could not be calculated. Nevertheless, zinc silicate was expected in this hydrolysis because the experiment was carried out at high temperature (85 ^{o}C) and the pH of the medium increased as the hydrolysis of urea was carrying on. Thus, the experimental conditions seem to be suitable for the formation of zinc silicate.

6.2.7 Zn-Silicate Crystals Obtained by Hydrolysis of Hexamine (Sec. 2.9; Table 2.3)

Plate 6.13 shows a rough surface of parallelogram morphology of a zinc compound. Its diffraction pattern shows clearly that the particles formed as a single

TABLE 6.6

Electron Diffraction Spacings From Magnesium Meta-Silicate formed in Silica Gel by Hydrolysis of Hexamine (See, 2.9; 6.2.5)

P16.11	$MgSiO_3$ ASTM 7-216	
nm	nm	hkl
0.318	*0.317	420,221
0.283	0.283	511
0.250	*0.249	202
0.215	0.211	630
0.157	0.159	931
0.142	0.147	...
0.133	Plus 8 lines to 0.123	
0.126		

* : Indicates the strong rings.
P16.11 : The lattice spacings from a parallelogram particle in Plate 6.11.

crystal. Beside the single crystal pattern, a ring pattern is also observed which is probably due to the decomposition of the original crystal in the electron beam. The spotty pattern corresponds to zinc silicate, Zn_2SiO_4, as shown in Table 6.7. On the other hand, the ring pattern did not match to any of the following compounds: ZnO, Zn metal, SiO_2 or Si metal. Thus, this ring pattern corresponds to an unidentified material.

Therefore, it was evident that using different alkali sources can produce totally different morphologies as well as different compounds; for example, the results obtained from lead and zinc compounds.

6.3 PRECIPITATION OF MnO_2 CRYSTALS WITHIN THE SILICA GEL

6.3.1 MnO_2 Crystals Formed by Hydrolysis of Urea or Hexamine

(a) By Hydrolysis of Urea

The main reactions are:

$$(H_2N)_2CO + 3H_2O \xrightarrow{85\text{-}90^{\circ}C} CO_2 + 2NH_4^+ + 2OH^-$$

$$M^{2+} + 2OH^- \longrightarrow M(OH)_2 \text{ or M-silicate}$$

$$\text{or } CO_2 + H_2O \rightleftharpoons H_2CO_3 \rightleftharpoons H^+ + HCO_3^- \rightleftharpoons 2H^+ + CO_3^=$$

$$CO_3^= + M^{2+} \rightleftharpoons MCO_3 \text{ or basic carbonate}$$

TABLE 6.7

Electron Diffraction Spacings from Zinc Silicate Obtained in Silica Gel by Hydrolysis of Hexamine (See, 29; 6.2.7)

Pl6.13a nm	Zn_2SiO_4 ASTM 20-1454 nm	Pl6.13b nm
0.351	0.348	0.276
0.289	0.287	0.242
0.251	0.251	0.172
0.220	0.222	
0.200	*0.203	
0.178	0.222	
0.143	0.144	

* : Indicates the strong rings.
Pl6.13a : Diffraction lattice Spacings from single crystal pattern of parallelogram form (Plate 6.13).
Pl6.13b : Diffraction spacings from the polycrystalline ring pattern in Plate 6.13.

For manganese compound:

$$Mn(OH)_2 + \tfrac{1}{2}O_2 \longrightarrow MnO_2 + H_2O$$

(b) By Hydrolysis of Hexamine

$$C_6H_{12}N_4 + 6H_2O \rightleftharpoons 4NH_4^+ + 6CH_2O$$

$$NH_3 + H_2O \rightleftharpoons NH_4^+ + OH^-$$

$$M^{n+} + nOH^- \rightleftharpoons M(OH)n \text{ or M-silicate}$$

For manganese compound:

$$Mn(OH)_2 + \tfrac{1}{2}O_2 \longrightarrow MnO_2 + H_2O$$

The expected result in this section was $Mn(OH)_2$, $MnCO_3$ or Mn-silicate by hydrolysis of urea, and $Mn(OH)_2$ or M-silicate by hydrolysis of hexamine. But the product was manganese(IV) oxide even though the reaction was carried out in a stoppered quick-fit test tube (see Ch.2; Sec.2.10). The oxidation of manganese hydroxide to manganese oxide occurs in alkali medium in the presence of air especially at high temperature (Szigeti et al., 1972). The oxygen may have been present in the gel before the heating process was carried out.

However, the morphology of manganese(IV) oxide was observed as small aggregated particles from both the hydrolysis systems used and this is shown in Plate 6.14 and 6.15. The spotty diffraction patterns correspond only roughly to ρ-MnO_2, as shown in Table 6.8.

6.3.2 MnO_2 Crystals Obtained by Oxidation with $NaIO_4$ and $KHSO_5$

The oxidation of Mn(II) aqua ions using periodate in strong acidic solutions occurs autocatalytically at room temperature to give as products permanganate and colloidal manganese(IV) oxide. In this case Mn(II) is oxidised quantitatively to permanganate only on heating the reaction solutions to boiling point.

It was known that the autocatalytic reaction can occur by bringing the media close to neutral solution which gives as final product manganese(IV) oxide and permanganate. On the other hand, if the pH and periodate concentration are adjusted and the reaction carried out at room temperature, the final product would only be manganese(IV) oxide. It was reported that the colloidal manganese(IV) oxide is stable for several months at pH 5.0-8.0 and at around 293^{o} K; it would not be oxidized to higher valence states even in the excess of periodate. (Tiginyanu et al., 1983).

TABLE 6.8

Electron Diffraction Spacings From Rho-Manganese(IV) Oxide Formed in Silica Gel by Hydrolysis and Oxidation (Sec. 2.9, 2.10; 6.3.1-6.3.4)

P16.14 nm	P16.15 nm	P16.16 nm	P16.17 nm	ρ-MnO_2 ASTM 12-714 nm
0.400	...	0.411	...	*0.400
0.268	...	...	0.269	0.260
...	...	0.245	0.253	*0.243
0.236	0.220	0.236	...	0.235
0.214	0.205	0.217	0.220	*0.212
0.169	...	0.166	0.168	0.165
0.144	0.145	...	0.145	0.143
0.138	...	...	...	0.136
0.124	...	...	...	0.125
0.111	...	...	...	0.107

* : Indicates the strong rings.
P16.14 : Diffraction lattice spacings in Plate 6.14.
P16.15 : Diffraction lattice spacings in Plate 6.15.
P16.16 : Diffraction lattice spacings in Plate 6.16.
P16.17 : Diffraction lattice spacings in Plate 6.17.

Therefore, in this study a similar preparation was carried out (see Ch.2; Sec.2.10) which could be described as an autocatalytic reaction.

The main autocatalytic reaction using $KHSO_5$ solution is:

$$Mn^{2+} + HSO_5^- + H_2O \longrightarrow MnO_2 + SO_4^{=} + 3H^+ \text{ (acidic medium).}$$

The result from the both reactions show the morphology of manganese(IV) oxide as microcrystals. Plate 6.16 shows the wide range of crystal size and arrangement formed; I shall not attempt to interpret it in terms of crystal growth mechanism resulting from the autocatalytic reaction (it is very complex). The polycrystalline diffraction pattern (Plate 6.16) matches very well to the standard spacings of ρ-MnO_2 as shown in Table 6.8.

A close examination of Plate 6.17 shows microcrystals associated with silica gel in which it is very difficult to see the crystal forms. However, the diffuse polycrystalline diffraction pattern (Plate 6.17) corresponds also to ρ-MnO_2 as expected.

Plate 6.1:

A photograph of dendritic forms from the same sample as in Plate 6.2.

Plate 6.2:

Dendrite of $BaCO_3$ produced homogeneously in silica gel by hydrolysis of urea.(Sec.6.1.1; Table 6.1).

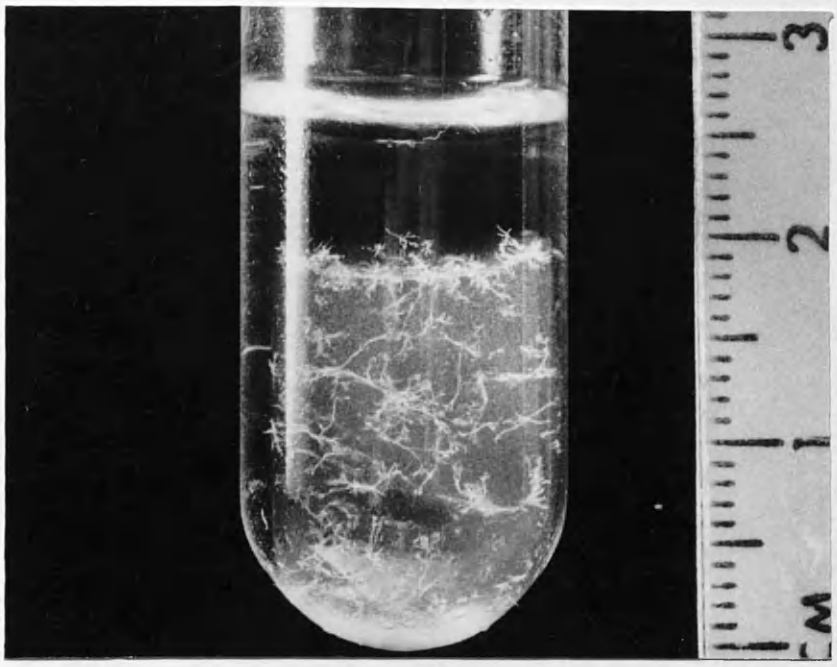
3
2
1
CM

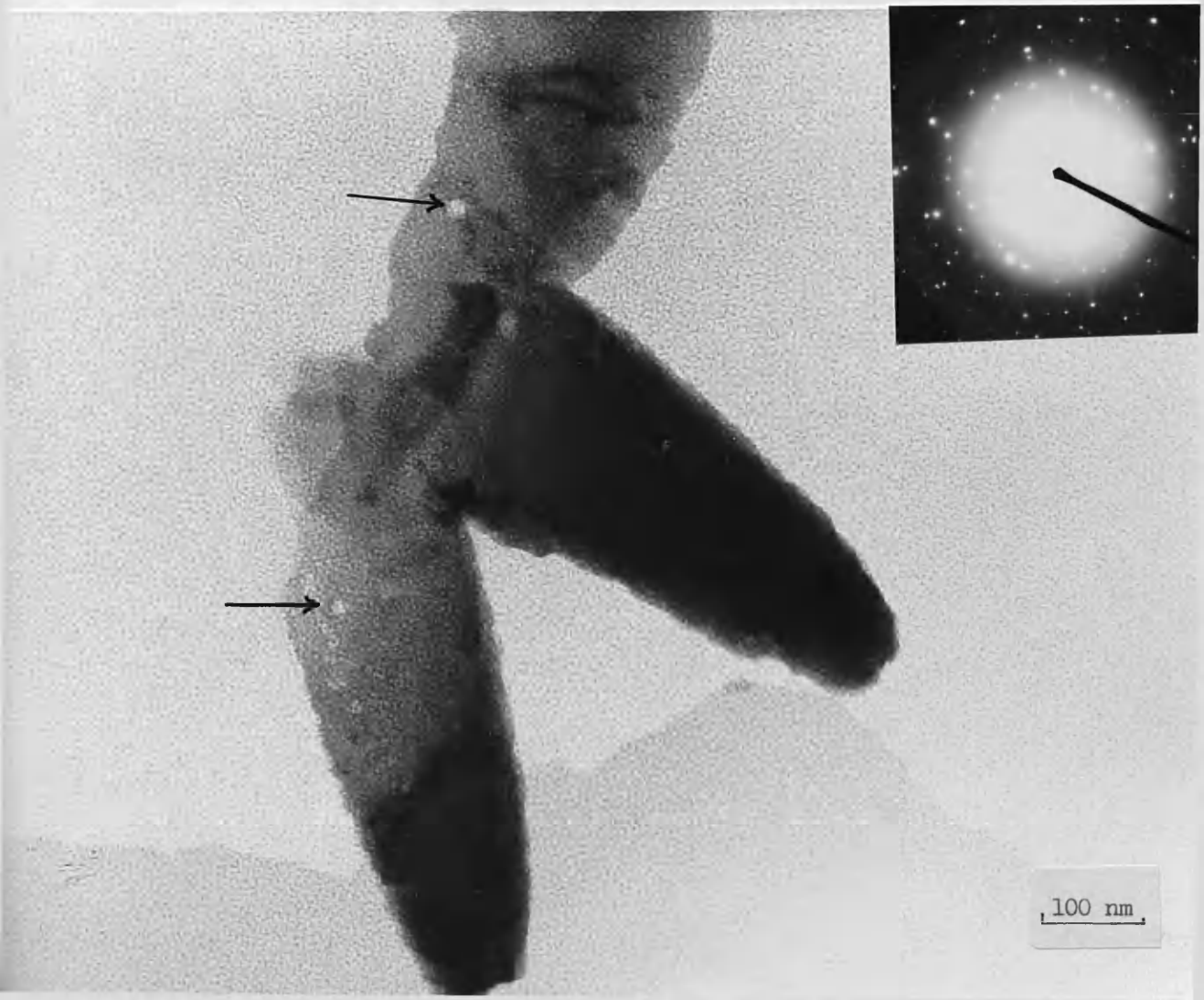
100 nm

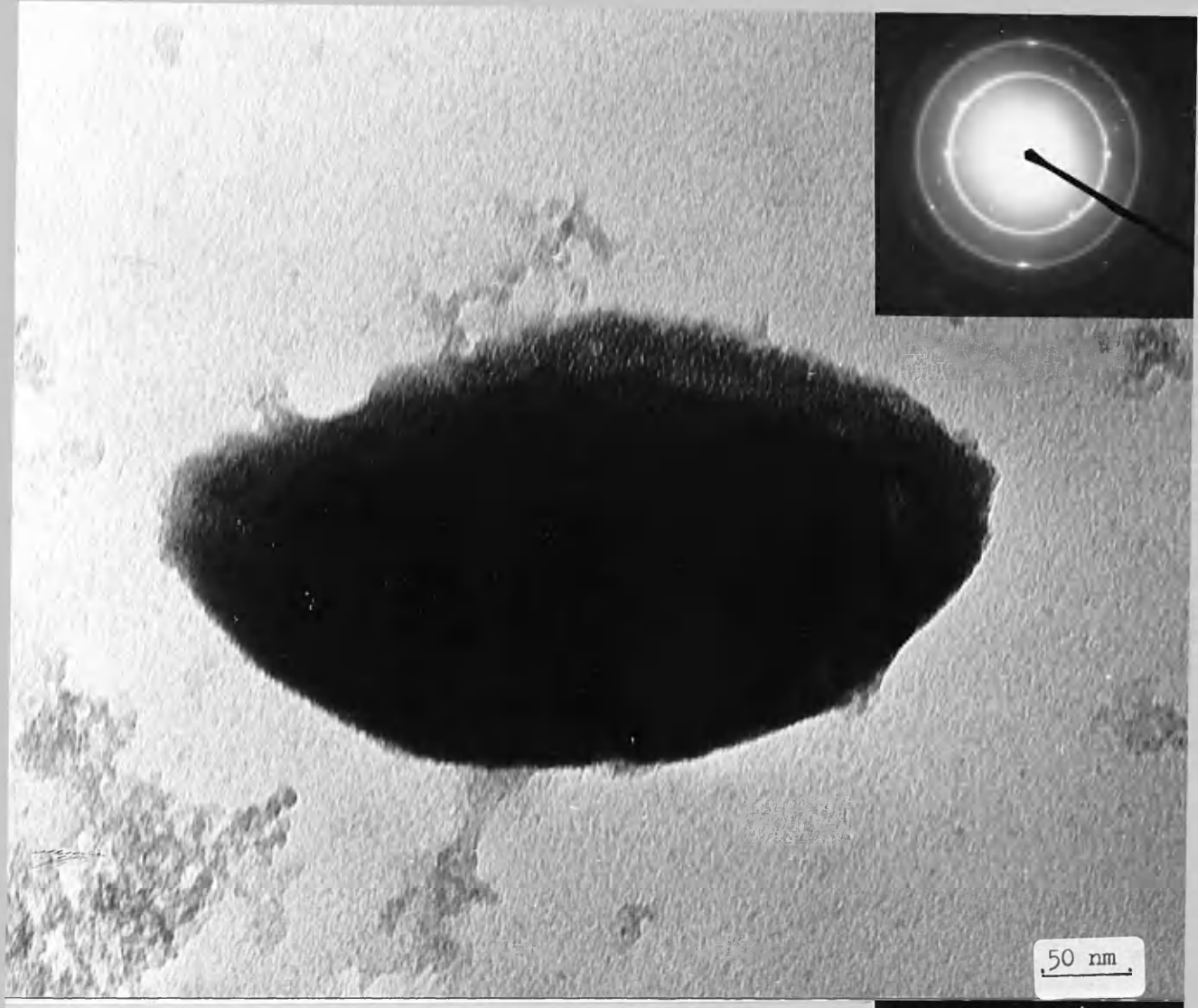
50 nm

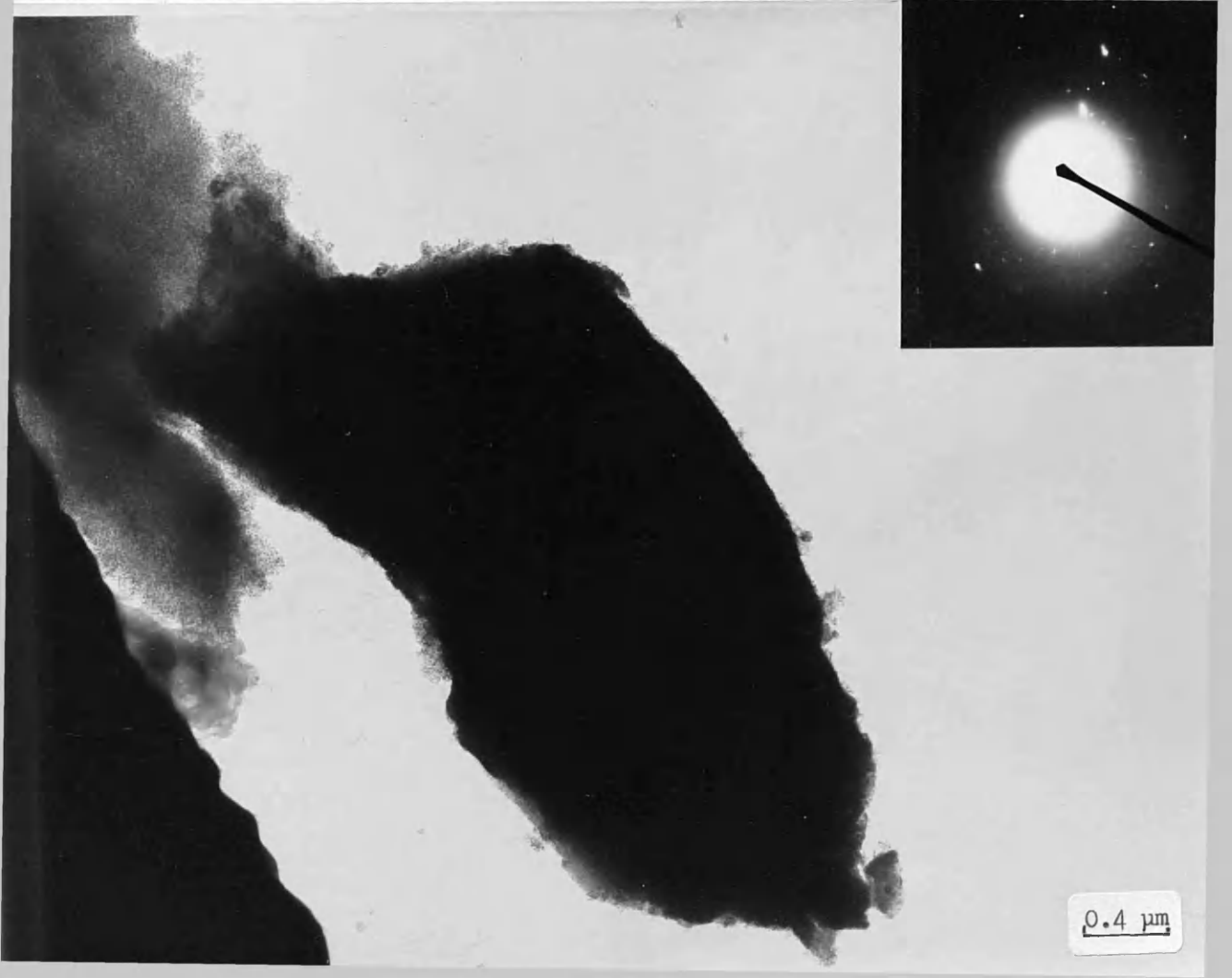
0.4 µm

Plate 6.5:

Small particles CdO formed homogeneously in silica gel by hydrolysis of urea.(Sec. 6.1.4).

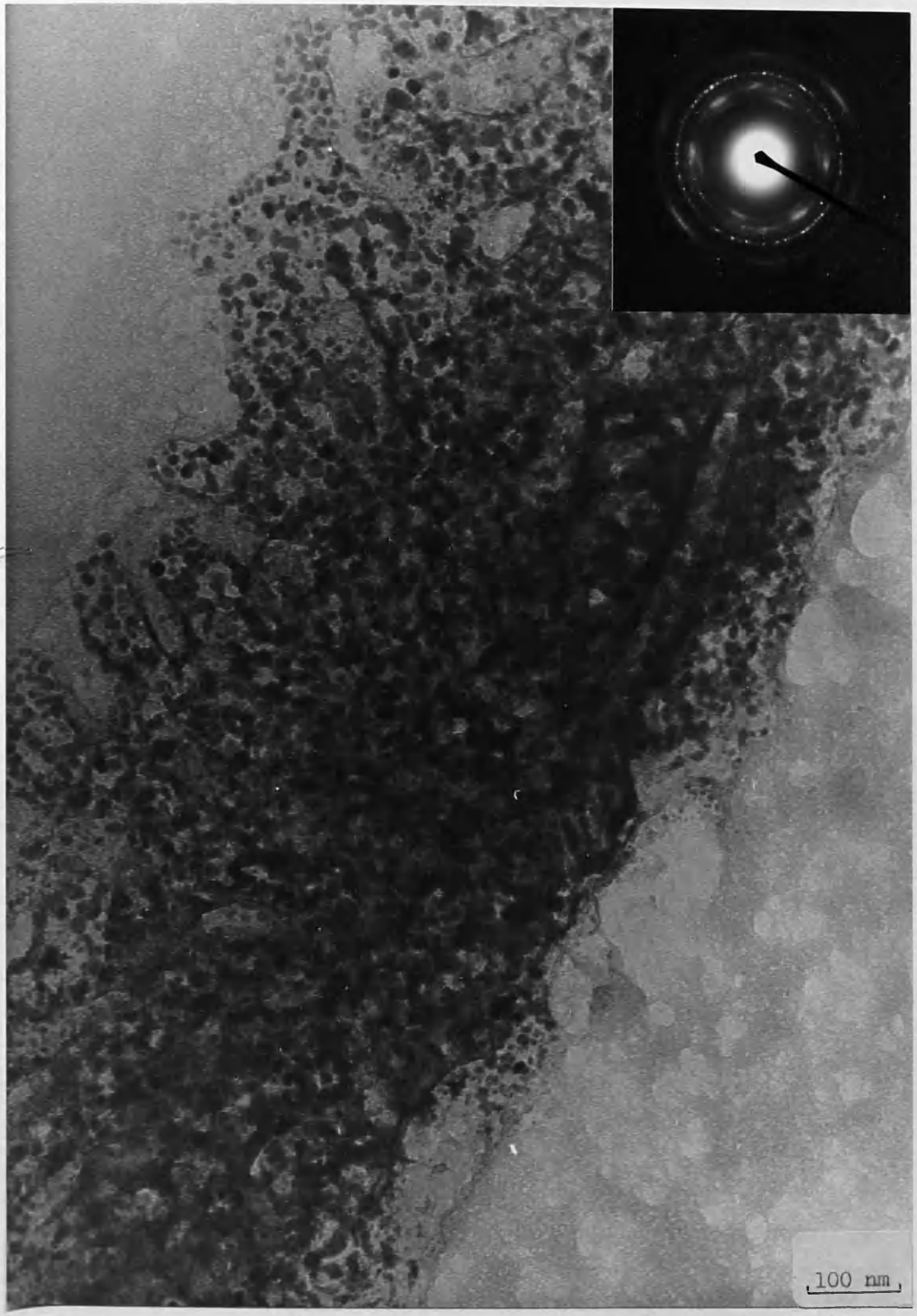
100 nm

Plate 6.6:

Large thin particle of $Pb_3(CO_3)_2(OH)_2$ Produced homogeneously in silica gel by hydrolysis of urea. (Sec. 6.1.5; Table 6.4).

Plate 6.7:

Circular arrays of dendritic $PbSiO_3$ formed in silica gel homogeneously by hydrolysis of hexamine. (Sec. 6.2.1).

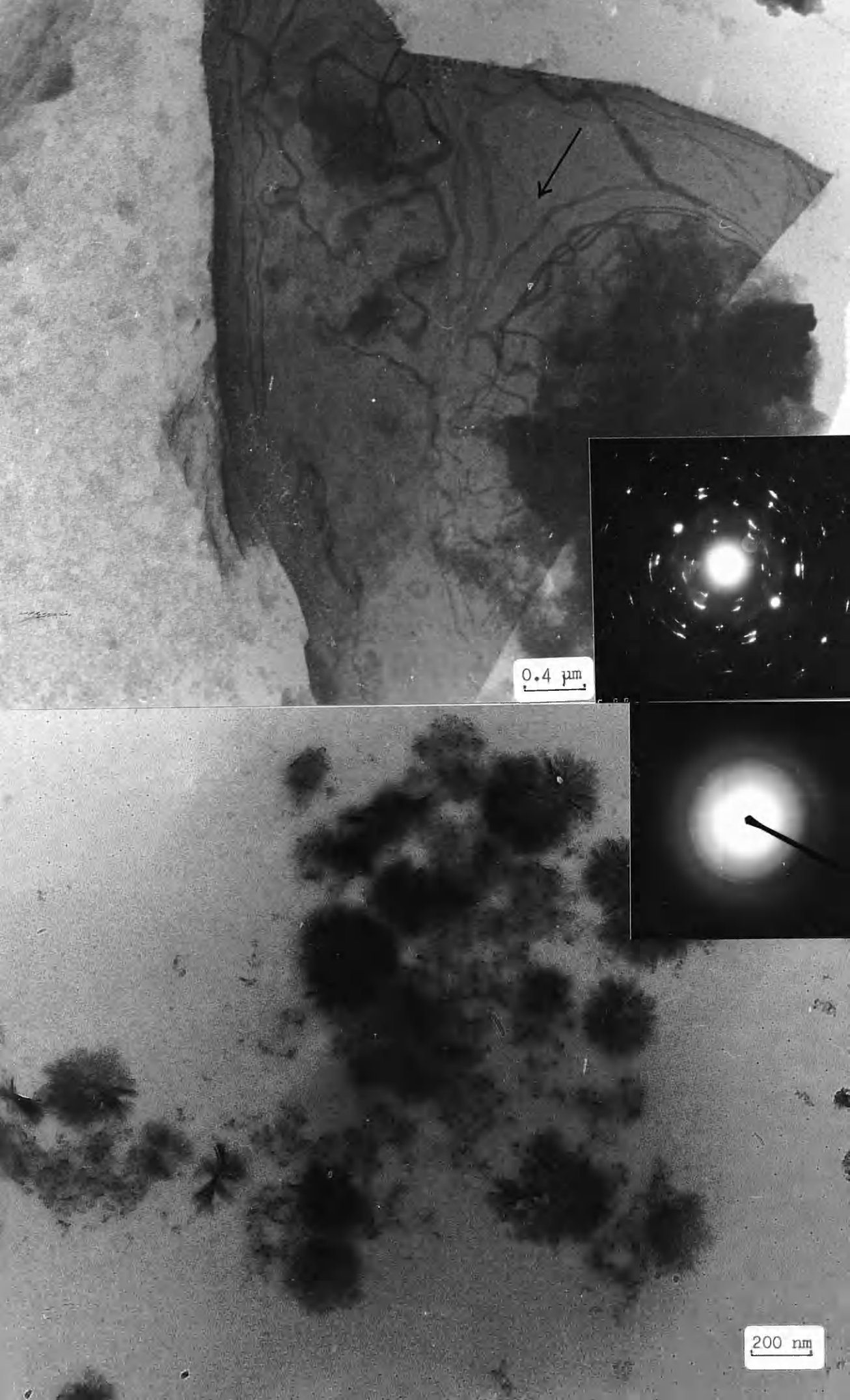
0.4 µm
200 nm

Plate 6.8:

Crumpled sheets Co_2SiO_4 produced homogeneously in silica gel by hydrolysis of hexamine.(Sec.6.2.2).

Plate 6.9:

Crumpled sheets Ni_2SiO_4 formed homogeneously in silica gel by hydrolysis of hexamine.(Sec.6.2.3).


100 nm

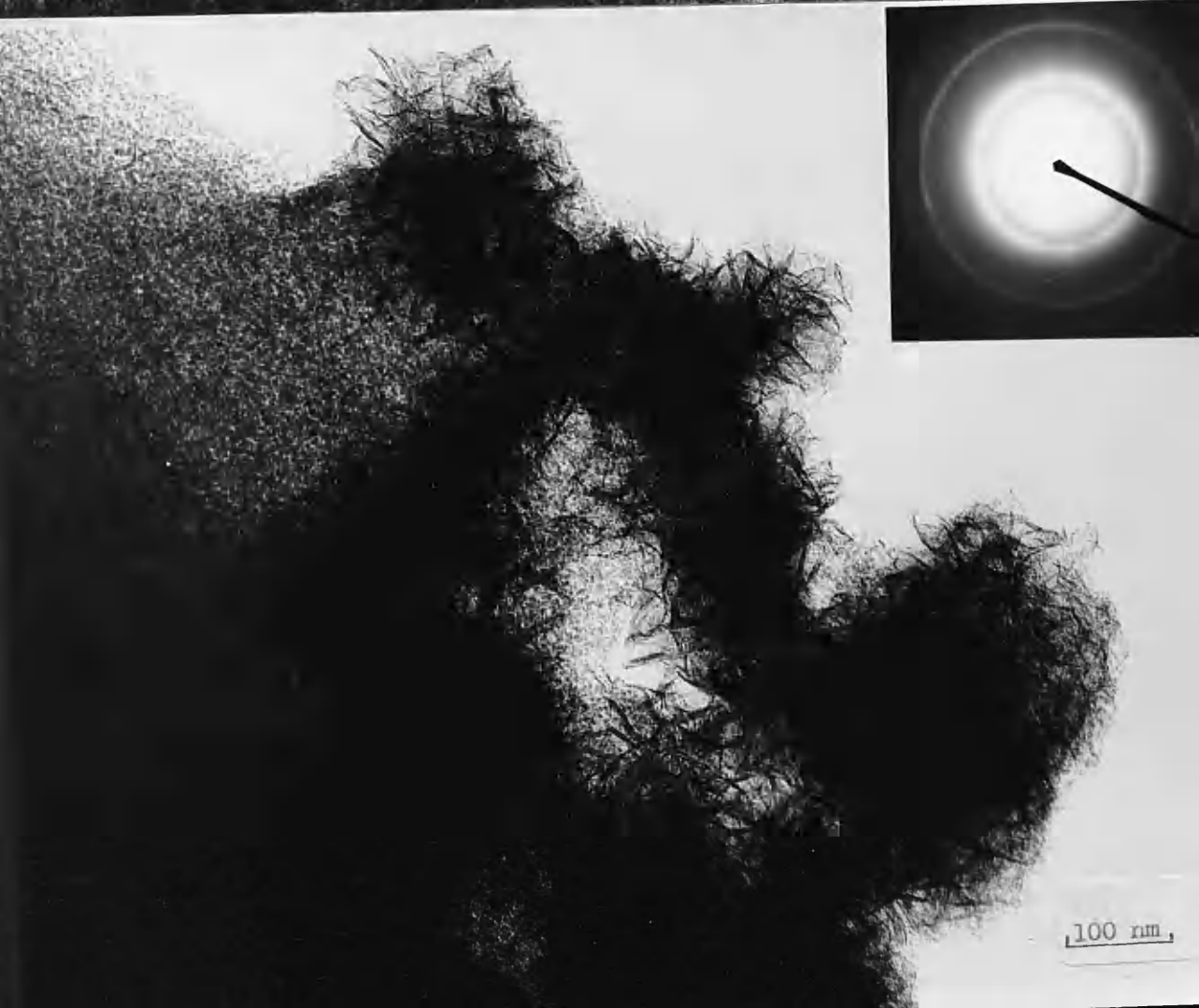
100 nm

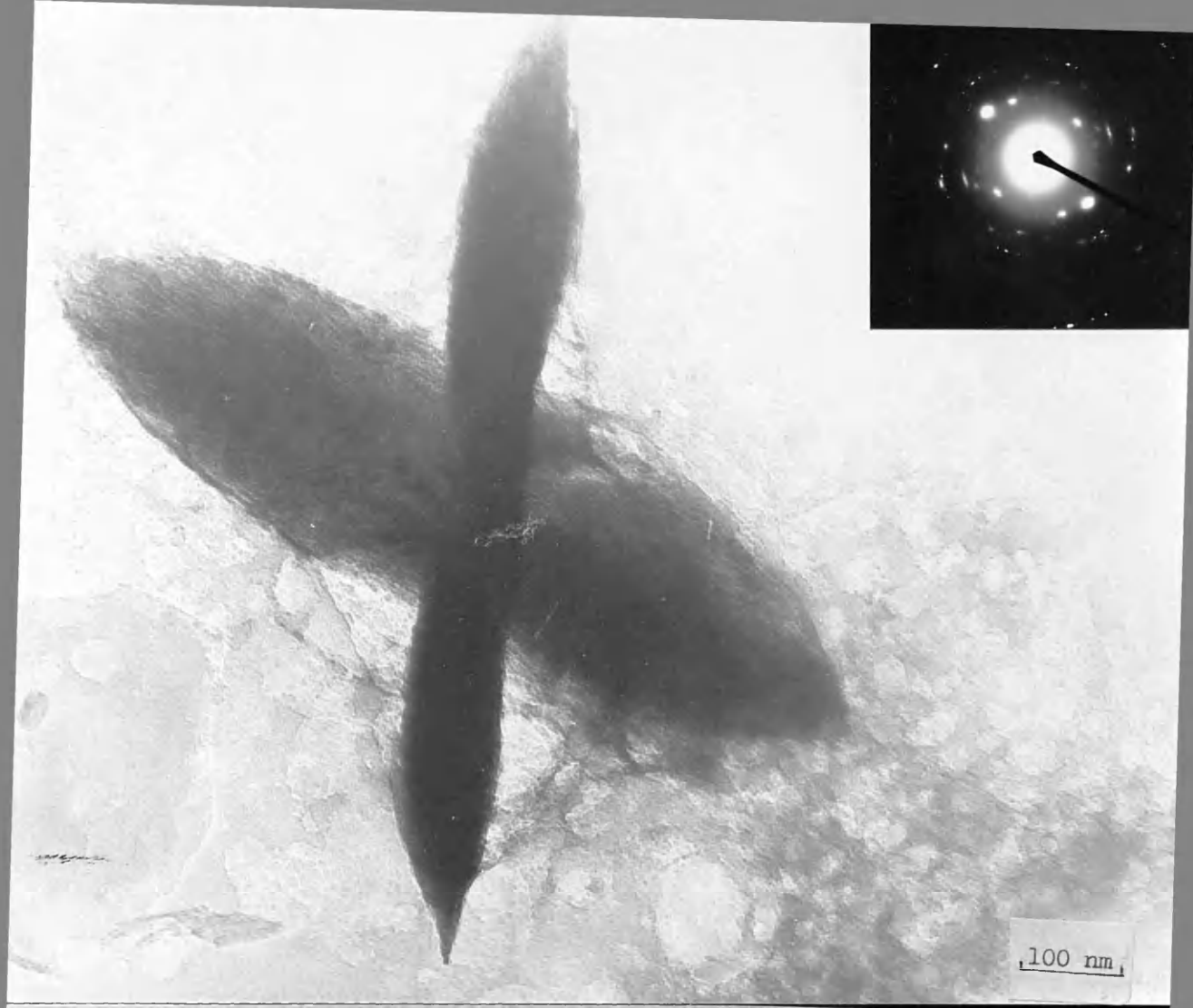
100 nm

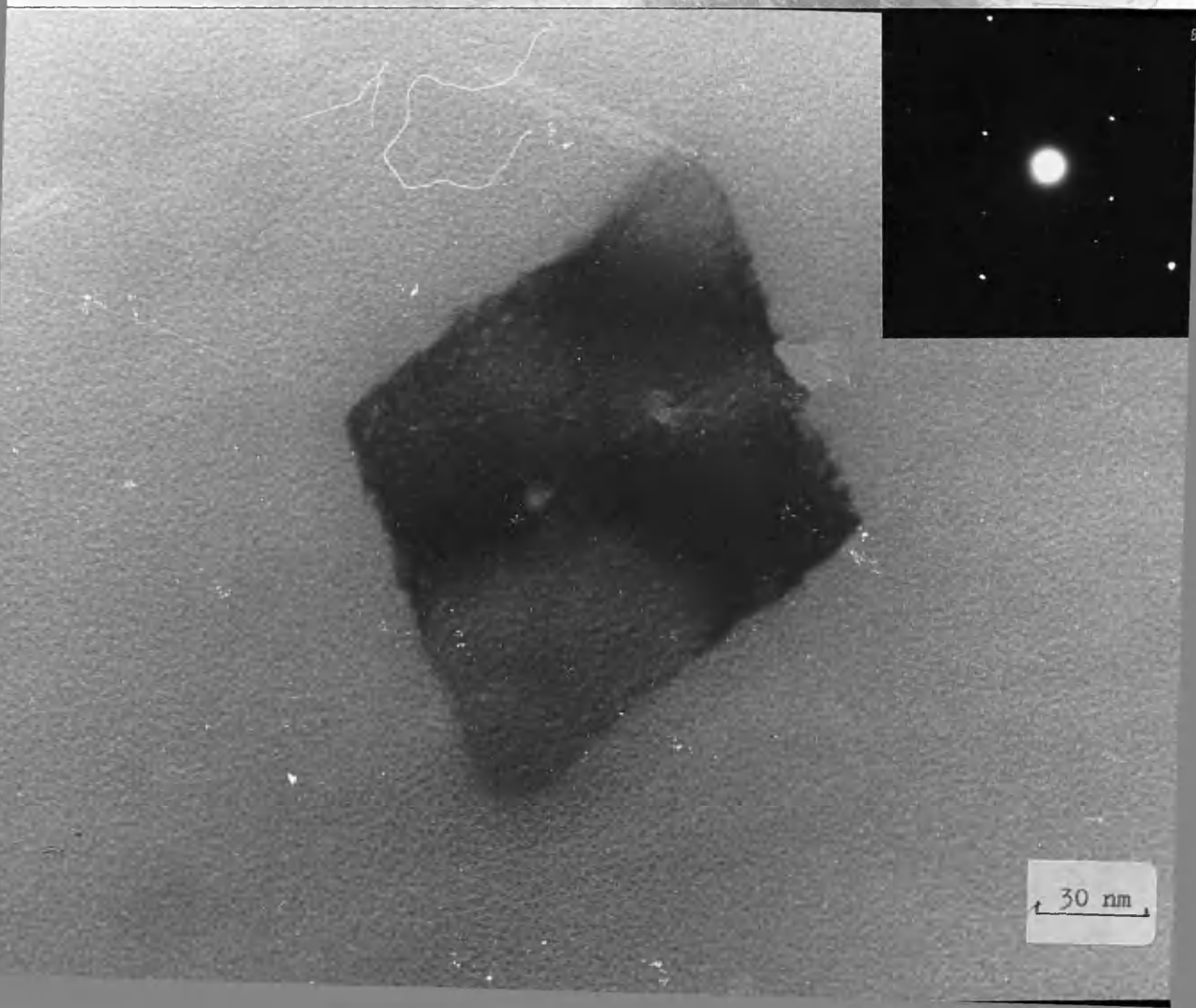
30 nm

Plate 6.12:

Crumpled sheets of Zn-silicate formed homogeneously in silica gel by hydrolysis of urea.(Sec.6.2.6).

Plate 6.13:

Single crystal of parallelogram form of Zn_2SiO_4 produced homogeneously in silica gel by hydrolysis of hexamine.(Sec.6.2.7;Table 6.7).

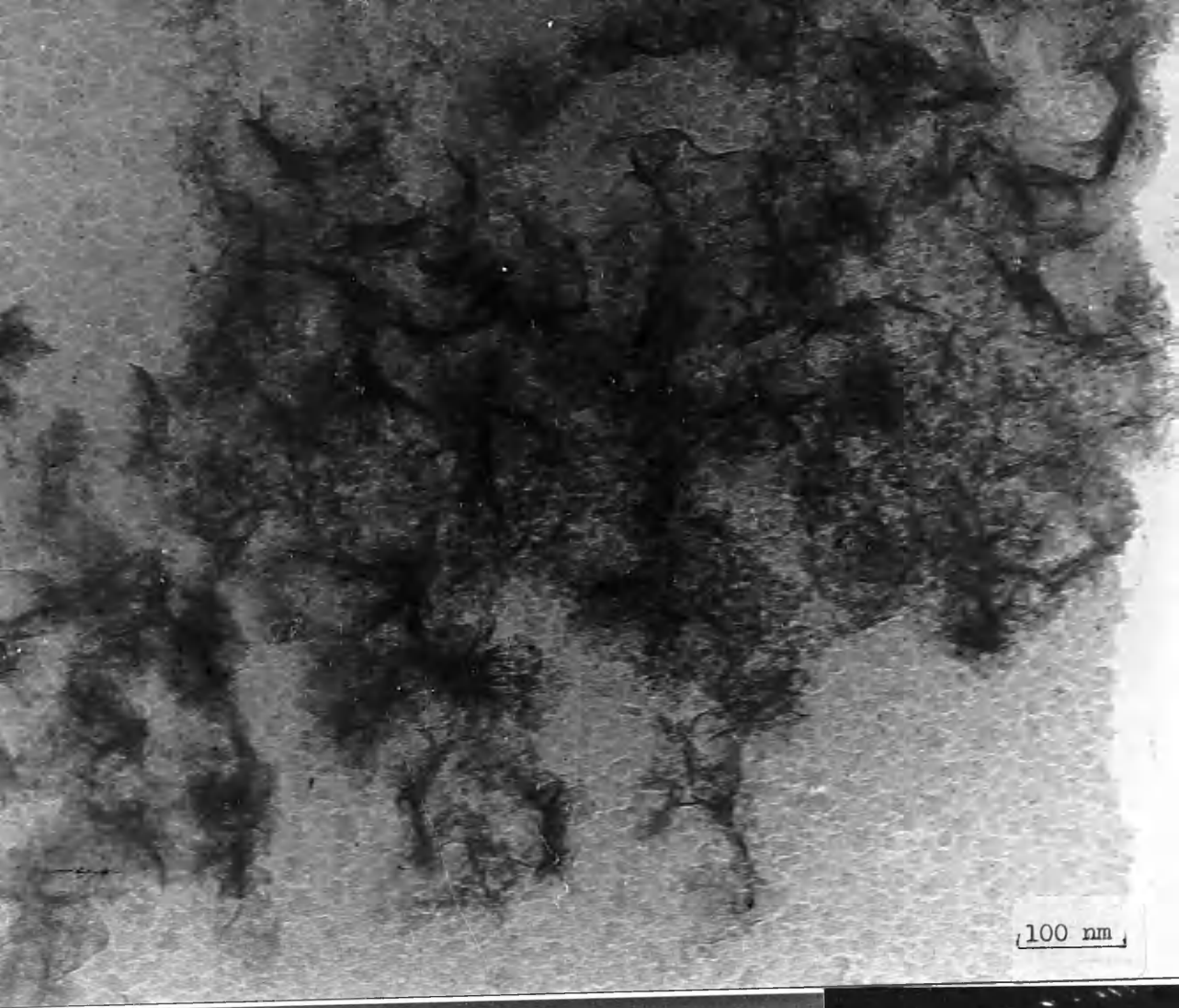
100 nm

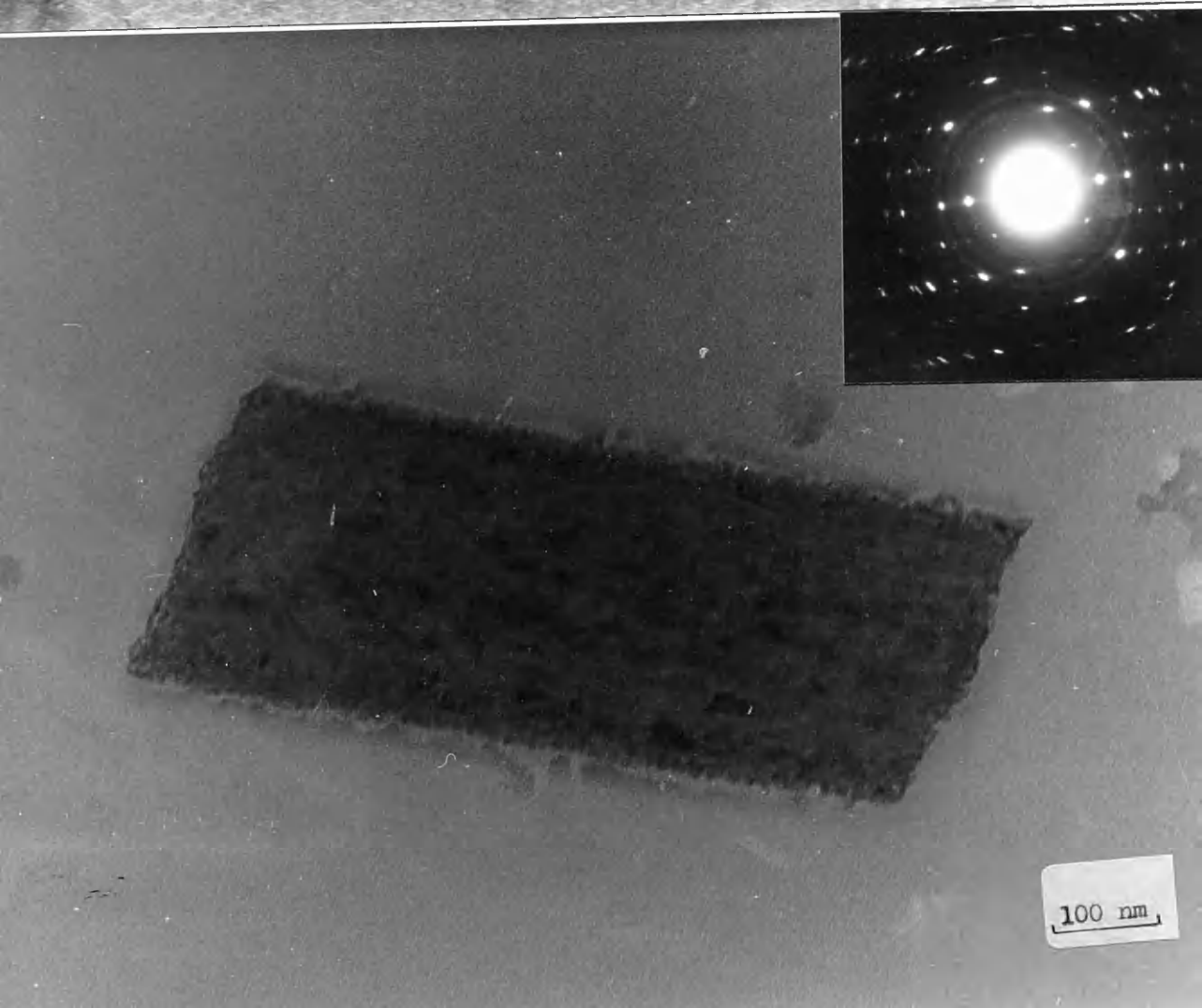
100 nm

Plate 6.14:

A large plate containing small particles of ρ-MnO_2 produced homogeneously in silica gel by hydrolysis of urea.(Sec.6.3.1; Table 6.8).

Plate 6.15:

Aggregates of irregular shaped ρ-MnO_2 formed homogeneously in silica gel by hydrolysis of hexamine (See, 6.3.4; Table 6.8).

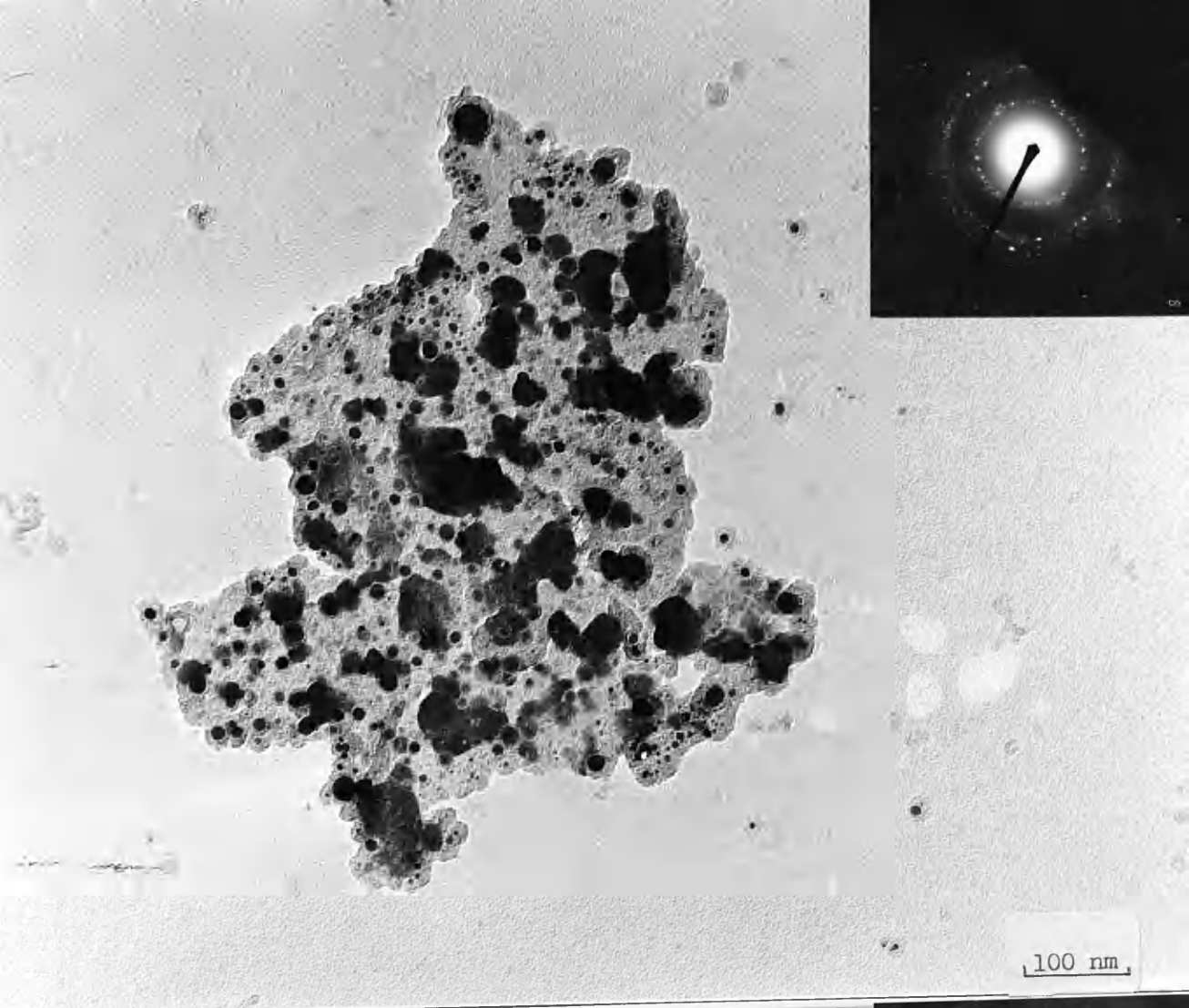
100 nm

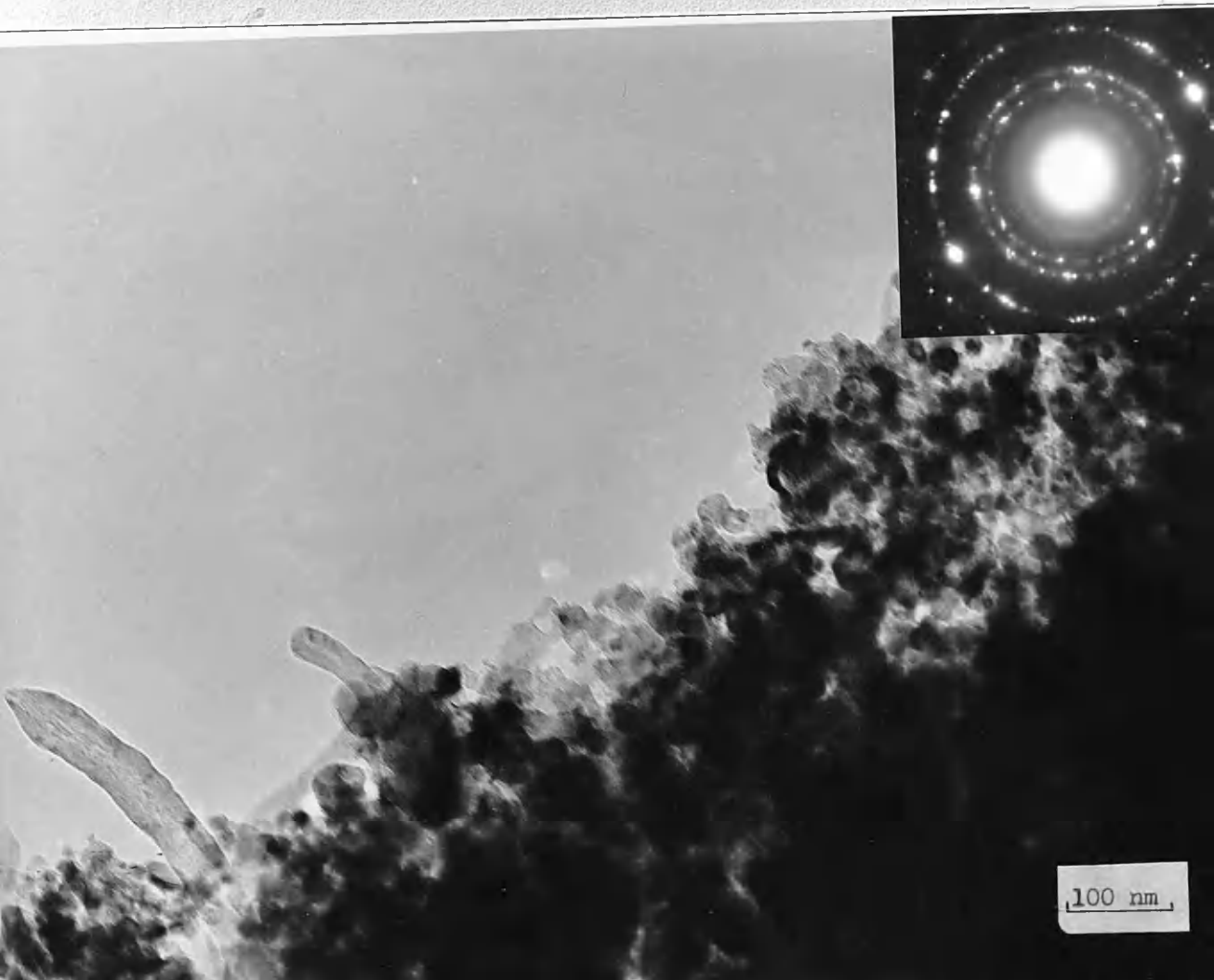
100 nm

Plate 6.16:

Irregular shaped crystals of ρ-MnO_2 produced homogeneously in silica gel by oxidation of $KHSO_5$ solution. (See, 6.3. 2; Table 6.8).

Plate 6.17:

Small particles of ρ-MnO_2 formed homogeneously in silica gel by oxidation of $NaIO_4$ solution. (See. 6.3.3; Table 6.8).

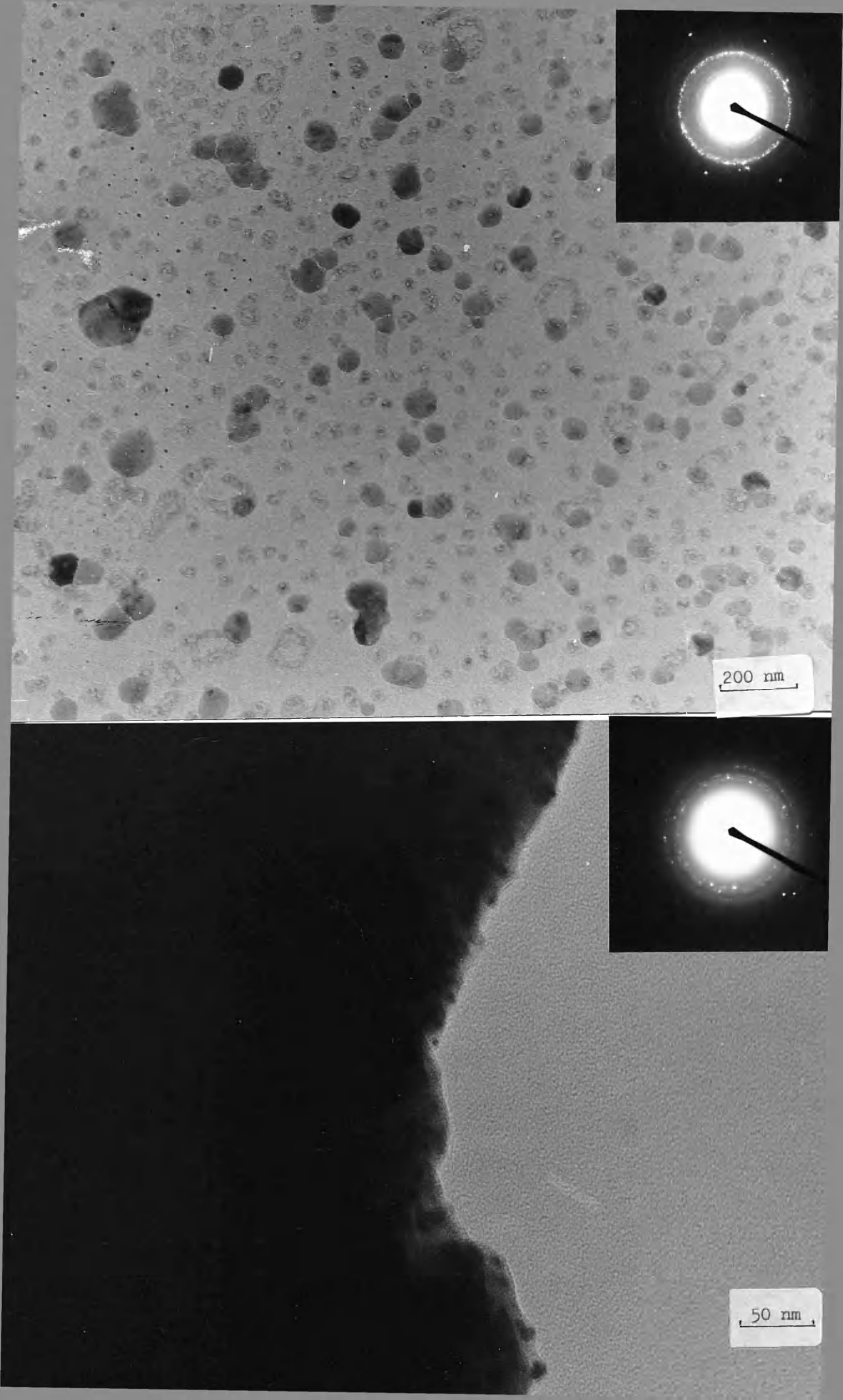
200 nm
50 nm

CHAPTER SEVEN

page

Conclusion 114

Further Work in Gels 119

References 120

CONCLUSION

Silica gel at room temperature acted as a retarder for the phase transformation (ferrihydrite to goethite) and as stabilizer for the morphology as well as the compound (ferrihydrite) on aging nearly a year or on heating at 89-90° C for 5 hours.

Carrageenan gel at room temperature acted as activator or promoter for the conversion of the less stable phase to the more thermodynamically stable phase (ferrihydrite to goethite).

Mixed gel is the best gel media for growing the long fibrillar particles (ferrihydrite).

Ferrihydrite can be grown in all types of gels (used in this study) and in all alkali source solutions (used in this study) by diffusion in the double tubes.

The original morphology of ferrihydrite grown in gels at room temperature is suggested as hair-like bundles (unlike that grown in solution). A mechanism of growth is suggested that the small bundles will nucleate at the early stage of the precipitate formed. The bundles will continue to grow larger to some extent by the mechanism of tip and new plane growths. On further diffusion, long fibrils will grow as extensions on the existing bundles. These fibrils would occur at metal ion rich zone and in the seeding process; the growth is probably more important than the nucleation.

In all cases in this study, the first formation of iron oxyhydroxide in gels by diffusion in double test tubes, at room temperature is ferrihydrite. It will transform to goethite by aging for nearly a year in the tube using carrageenan gel or carrageenan gel containing kaolinite or storing nearly a year in distilled water from 26 days old ferrihydrite grown in carrageenan gel. These phenomena are probably due to the presence of carrageenan gel.

Goethite will also be obtained after heating ferrihydrite within the mixed gel or by hydrolysis of urea at 85^{o}C for 2 hours. Star-shaped goethite crystals form by diffusion in carrageenan gel for nearly a year.

Large semi-oval crystals associated with ferrihydrite formed at the early stage of growth in carrageenan gel containing kaolinite are possibly a kaolinite-ferrihydrite complex or Al substituted by Fe in kaolinite. Hexagonal kaolinite associated with goethite and possibly between the layers formed after aging at room temperature and further diffusing in the gel.

β-FeOOH did not form in the diluted concentration of chloride ion (0.083M) within the mixed gel.

Copper compounds were shown to be unstable in the electron beam. It was observed that different and similar morphologies and compounds when using perchlorate or sulphate anion and NaOH, HEPPS or HEPES solution as alkali source.

The most interesting morphology is the bowties ($Cu_4SO_4(OH)_6$) which resulted from copper (II) sulphate and HEPES solution at the early stage of diffusion.

Rod-like morphology ($Cu(OH)_2$) was obtained from perchlorate anion and NaOH or HEPPS solution.

A Crumpled sheet morphology was observed from sulphate anion and HEPPS solution ; perchlorate anion containing kaolinite and HEPES solutions. In addition, a similar morphology was observed for $CuSiO_3.H_2O$ obtained by hydrolysis of sulphate anion with hexamine solution.

The blue precipitate formed from perchlorate and sulphate anions was probably copper sulphate hydroxide or copper hydroxide but this rapidly decomposed in the electron beam to give copper (I or II) oxide. Occasionally, dendritic copper metal was observed, from samples from the tail band.

Beautiful dendritic silver metal was formed by aging silver nitrate and HEPPS solutions within silica gel. On the other hand, cubic crystal were obtained by aging silver nitrate in sodium hydroxide solution.

Large (average dimension $\sim$ 60nm) loosely geometrical shaped platinum particles with rough surfaces were produced by homogeneous precipitation in silica gel at the early stage of formation and were still present after one year aging. About 30 nm loosely aggregated particles by diffusion method.

Palladium particles exhibited similarities to platinum particles but more geometrical shapes were observed. Some particles from the one day old black precipitate formed by homogeneous reaction within silica gel were already transformed to regular geometrical structures with sharp edges. Among various concentrations (0.05M-0.01M) from the ratios between K_2PtCl_4 :KCl, 0.025M K_2PtCl_4 + 0.1M KCl is the one that showed more geometrical shapes and faster precipitation than the others.

Metal carbonates were precipitated by hydrolysis of urea at 85-90^{o}C in silica gel; their morphologies are as follows:

Barium and strontium carbonates appeared as large (~3mm long) dendritic objects.

Well-shaped rhombohedral crystals of calcium carbonate (calcite) were observed, about 0.2 mm long with an angle of about 77^{o}.

Small (~3nm) irregular shaped particles of cadmium oxide were observed. This compound undoubtedly resulted from decomposition of cadmium carbonate in the beam.

The product with zinc appeared in TEM as crumpled sheets and showed very broad diffuse electron diffraction patterns. Data suggested that the compound is not zinc carbonate but probably zinc silicate.

A large (~4μm), thin plate of basic lead carbonate was observed with many contour lines and twin boundaries.

Metal silicates were obtained from hydrolysis by hexamine at 85-90^{o}C as follows:

Circular arrays of dendritic $PbSiO_3$ formed in silica gel.

Cobalt and nickel silicates appeared as crumpled sheets which probably arise from drying out and folding of thin sheets.

Oval shaped particles consisting of small network was identified as aluminium silicate, Al_2SiO_5.

Magnisium silicate formed as rhombus platelet particles.

With zinc, a parallelogram morphology was obtained. Electron diffraction gave a single crystal pattern identified as zinc silicate (Zn_2SiO_4), together with unidentified rings (not Zn-silicate ZnO, Zn metal, SiO_2 or Si metal).

Small aggregated particles of rho-manganese(IV) oxide were obtained from Mn^{2+} by hydrolysis of urea and hexamine, whereas small ($\sim$65 nm) regular shaped crystals of rho-manganese(IV) oxide by oxidation with sodium periodate or peroxomonosulphuric acid.

Much remains to be studied in this new field but it is hoped that the results and the observations in this thesis will open up the subject to further study in many aspects.

FURTHER WORK IN GELS

This study can be carried out in more details in various aspects in order to examine the effect of gels in the growth of particles as follows:

Precipitation from iron(III) solution in the double tubes at varied temperatures and times.

Precipitation from iron(III) solution in seeded goethite by diffusion in the double tube technique.

Growth of β-FeOOH in the double tube method by use of chloride ion at different concentrations and times.

Precipitation from iron(III) solution under the influence of suitable organic compounds by diffusion in the double tubes.

Precipitation from iron(III) solution homogeneously by hydrolysis of urea and hexamine for different times.

Precipitation of silicates from mixed metals (Al+Mg, Al+K and Mg+K) homomgeneously by hydrolysis of hexamine in silica gel.

Precipitation of metal carbonates at different pH with different alkali sources in silica gel at room temperature.

REFERENCES

Abdulkhadar, M; and Ittyachan, M.A.(1981) J. Crystal Growth, 55, 398.

Abdullah, J.; Baird, T. and Braterman, P.S. (1986) J. Chem. Soc. Chem. Commun., 256.

Agar, A.W. (1960) Brit. J. Appl. Phys., 11, 504.

Agar, A.W. (1965) J. Am. Soc., 109, 67.

Agar. A.W. (1965) in "Techniques for Electron Microscopy", (Kay, D.H. ed.), 2nd. edn., Blackwell Scientific Publications, Oxford, p. 1.

Agar, A.W.; Alderson, R.H.; and Chescoe, D. (1974) "Principles and Practice of Electron Microscope Operation", North Holland, Amsterdam, vol., 2.

Ahmed, H. and Broers, A.N. (1972) J. Appl. Phys., 43, 2185.

Alderson, R.H. and Halliday, J.S. (1965), in "Techniques for Electron Microscopy", (Kay, D.H. ed.), 2nd. edn., Blackwell Scientific Publications, Oxford, p. 478.

Alexandra, S.; Jan, S., Jaroslav, V., Jaroslav, T., and Viadimir, Z. (1984) Chem. Prum., 34(8), 407.

Allpress, J. G. and Sanders, J.V. (1967) Surface Science, 7, 1.

Anderson, J.R.(1975) "Structure of Metallic Catalyst Catalysts", Academic Press, London, p. 259.

Andrews, K.W.; Dyson, D.J. and Keown, S.R. (1967) "Interpretation of Electron Diffraction Patterns", Adam Hilger, Ltd., London, p. 14.

Arend, H. and Connelly, J.J. (1982) J. Crystal Growth, 56, 642.

Armington, A.F. and O´Conner, J.J. (1968) J. Crystal Growth, 3(4), 367.

Armington, A.F. and O´Conner, J.J. (1980) in "Inorganic Synthesis" (Busch and Daryle H. ed.), 20, 4.

A.S.T.M. index, "X-Ray Powder Data File", American Society for Testing Materials, Philadelphia, (revised annually).

Atkinson, R.j.; Posner, A.M. and Quirk, J.P. (1968) J. Inorg. Nucl. Chem., 30, 2371.

Bahadur, K. and Ranganayaki, S. (1981) "Origin of Life A Functional Approach",Allahabad, India, pp.46,47, and 255.

Biedermann, G. and Schindler, P. (1957) Acta Chem. Scand., 11, 731.

Blank, Z. and Brenner, W. (1971) J. Crystal Growth, 11, 255.

Barta, Č.; Žemlička, J. and René, V. (1971) J. Crystal Growth, 10, 158.

Berry, C.R. and Skillman, D.C. (1971) J. Appl. Phys.,42, 2818.

Biedermann, G.; Schindler, P. (1957) Acta Chem. Scand., 11, 731.

Bolland, M.D.A.; Posner, A.M.; and Quirk, J.P. (1980) Clays Clay Miner., 28, 412.

Borggaard, O.K. (1984) J. Siol Sci., 35, 71.

Boulin, D. and Ellis, W.C. (1970 J. crystal Growth, 6, 290.

Brady, R.M. and Ball, R.C. (1984) Nature, 309, 225.

Braterman, P.S. and Baird, T. (1984) Private Communication, Department of Chemistry, University of Glasgow.

Brice, J.C. (1986) "Crystal Growth Processes", John Wiley & Sons, New York, p. 258.

Brindley, G.W. and Brown, G. (eds.) (1980) "Crystal Structures of Clay Minerals and Their X-Ray Identification", Monograph No. 5, Mineralogical Society, London, p. 374.

Britz, D. and Nancollas, G.H. (1969) J. Inorg. Nucl. Chem., 31, 3861.

Broers, A.N. (1972) in "Proc. 5th Int. Conf. on Ion and Laser Beam Science and Technology", (Bakish, R. ed.), Electrochemical Soc., N.Y., p.3.

Brown, G. (1953) J. Soil Sci., 4, 220.

Burton, J.J. (1970) J. Chem. Phys., 52, 345.

Busch, H. (1926) Ann. Phyzik, 81, 974.

Cairns-Smith, A.G. (1982) "Genetic Takeover and the Mineral Origins of Life", Cambridge University Press, Cambridge.

Campbell, A.S. and Schwertmann, U. (1984) J. Soil Sci., 35, 569.

Carlson, L. and Schwertmann, U. (1981) Geochim. Cosmochim. Acta., 45(3), 421.

Caslavsky, J.L. and Suri, S.K. (1970) J. Crystal Growth, 6, 213.

Cho, S.A.; Gomez, J.A.; Camisotti, R. and Ohep, J.C. (1977) J. Materials Sci., 12, 816.

Chukhrov, F.V.; Zvyagin, B.B.; Gorshkov, A.I.; Ermilova, L.P.; and Balashova, V.V. (1973) Izvest. Akad. Nauk. SSSR., 23.
(See Fleischer, M.; Chao, G.Y.; and Kato, A. (1975) Am. Miner., 60, 485).

Chukhrov, F.V.; Zvyagin, B.B.; Gorshkov, A.I.; Ermilova, L.P.; Korovushkin, V.V.; Rudnitskaya, E.S.; and Yakubovskaya, N. YU. (1976) Izvest. Akad. Nauk. SSSR. Ser. Geol., 5, 5.
(See Fleischer, M. et al., Am. Miner. (1977) 62, 1057).

Cody, R.D. and Shanks, H.R. (1974) J. Crystal Growth, 23, 275.

Cornejo, J.; Serna, C.J. and Hermosin, M.C. (1984) J. Colloid Interface Sci., 102, 101.

Cork, J.M. and Gerhard, S.L. (1931) Am. Min., 16, 71.

Cornell, R.M.; Posner, A.M. and Quirk, J.P. (1974) J. Inorg. Nucl. Chem., 36, 1937.

Cornell, R.M.; Mann, S. and Skarnulis, A.J. (1983) J. Chem. Soc., Faraday Trans. 1, 79 (III), 2679.

Cornell, R.M.; Giovanoli, R. (1985) Clays Clay Miner., 33 (5), 424.

Cornell, R.M. (1985) Clays Clay Miner., 33(3), 219.

Cornell, R.M.; Giovanoli, R. and Schindler, P.W. (1987) Clays Clay Miner., 35(1), 21.

Cornell, R.M.; and Giovanoli, R. (1987) J. Chem. Soc. Chem. Commun., 6, 413.

Cosslett, V.E. (1978) J. Microsc., 113, 1113.

Cotton, F.A. and Wilkinson, G. (1980) "Advanced Inorganic Chemistry, 4th edn., John Wiley & Sons, New York, p. 969.

Dean, J.A. (ed.), (1985), "Lang's Handbook of Chemistry", 13th edn., McGraw-Hill Book Company, New York, p. 4.

Doherty, R., (1975) in "Crystal Growth", (Brian. R. Pamplin, ed.), Pergamon Press, Oxford, p. 576.

Domínguez, J.M. and Yacamán, M.J. (1980) in "Growth and Properties of Metal Clusters", Bourdon, J., (ed.), Elsevier Scientific Publishing Co., Amsterdam, p. 496.

Ennos, A.E. (1954) Brit. J. Appl. Phys., 5, 27.

Feitknecht, W.; and Michaelis, W. (1962) Helv. Chim. Acta., 45, 212.

Feitknecht, W.; Giovanoli, R.; Michaelis, W. and Muller, M. (1975) Z. Anorg. Allg. Chem., 417(2), 114.

Fleischer, M.; Chao, G.Y. and Kato, A. (1975) Am. Miner., 60, 485.

Fleischer, M.; Pabst, A.; Mandarino, J.A. and George, Y. Chao, (1977) Am. Miner., 62, 1057.

Fox, L.E. (1988) Nature, 333, 442.

Franke, W.; Lenk, K.; Ittyachen, M.A. and Mohananpillai, K. (1981) J. Crystal Growth, 51, 309.

Freundlich, H. (1909)
(See Mullin, J.W. (1961) "Crystallization", Butterworths, London, p. 33.

Fryer, J.R. (1979) "The Chemical Applications of Transmission Electron Microscopy", Academic Press, London, p. 11.

Fryer, J.R. (1984) Private Communication, Department of Chemistry, University of Glasgow.

García-Ruiz, J.M. and Amorós, J.L. (1981) J. Crystal Growth, 55, 379.

Geiger, C.A.; Henry, D.L. and Bailey, S.W. (1983) Clays Clay Minerals, 31(2), 97.

Gildawie, A.M.(1977) Ph.D. Thesis, Department of Chemistry, University of Glasgow.

Gillet, E.; Roux, J.F. and Gillet, M. (1965) Bull. Soc. Franc. Mineral. Crist., 90, 54.

Gillet, M. (1977) Surf. Sci., 67, 139.

Glauert, A. (1974) "Principles and Practice of Electron Microscope Operation".

Halberstadt, E.S. and Henisch, H.K. (1968) J. Crystal Growth, 3,4, 363

Halliday, J.S. (1965) in "Techniques for Electron Microscopy", (Kay, D.H. ed.), 2nd. edn. Blackwell Scientific Publications, Oxford, p. 525.

Harris, P.J.F. (1985) Applied Catalysis, 16, 440.

Hashimoto, H.; Endoh, H.; Tanji, T.; Kumao, A.; Ono, A. and Watanage, E. (1977) J. Phys. Soc. Japan, 42, 1073.

Hart, R.K.; Kassner, T.F. and Maurin, J.K. (1970) Phil. Mag., 21, 453.

Hatschek, E. (1912a) Z. Chem. Ind. Kolloide, 10, 77.

Hatschek, E. (1912b) Z. Chem. Ind. Kolloide, 10, 124.

Hatschek, E. and Simon, A.L. (1912) Z. Chem. Ind. Kolloide, 10, 265.

Hegenberger, E.; Wu, N.L. and Phillips, E. (1987) J. Phys. Chem., 91, 5067.

Henisch, H. K. (1970) "Crystal Growth in Gels", Pennsylvania State University Press, Pa.

Henisch, H. K. (1988) "Crystals in Gels and Liesegang Rings", Cambridge.

Hibi, T. (1954) "Proc. 3rd Int. Conf. Electron Microscopy", London, 636.

Hirsch, P.B.; Howie, A.; Nicholson, R.B.; Pashley, D.W. and Whelan, M.J. (1965) "Electron Microscopy of Thin Crystals", Butterworths, London, p. 2.

Holmes, H.N. (1917) J. Phys. Chem., 21, 709.

Holmes, H.N. (1926) in "Colloid Chemistry", (Alexander, J., ed.), 796.

Hren, J.J. (1979) Ultramicroscopy, 3, 375.

Iler, R.K. (1979) "The Chemistry of Silica", John Wiley & Sons, New York, p. 173.

Ino, S. and Ogawa, S. (1967) J. Phys. Soc. Japan, 22, 1365.

Isaacson, M.S. (1977) in "Principles and Techniques of Electron Microscopy", (Hayat, M.A. ed.), Van Nostrand Reinhold, New york, p. 1.

Johnston, J.H. and Lewis, D.G. (1983) Geochim Cosmochim. Acta., 47(11), 1823.

Jones, Angela, A. and Saleh, A.M. (1986) Clay Miner., 21(1), 85.

Jullien,R. and Botet, R. (1987) "Aggregation and Fractal Aggregates", World Scientific, Singapore, p. 1.

Kassim, M.J.N., (1982) Ph.D. Thesis, Department of Chemistry, University of Glasgow.

De Keyser, W. L. and Degueldre, L. (1950) Bull. Soc. Chim. Belges, 59, 40.

Kitano, Y. (1962) Bull. Chem. Soc. Japan, 35, 1980.

Knoll, M. and Ruska, E. (1932) Ann. Physik, 12, 607.

Kume, S.; Aikami, T.; Kodera, E. and Kakinoki, J. (1972) J. Crystal growth, 12, 316.

La Mer, V.K. and Dinegar, R.H. (1950) J. Am. Chem. Soc., 72(17), 4847.

Lamb, A.B. and Jacques, A.G. (1938) J. Am. Chem. Soc., 60, 1217.

Lander, J.J. (1949) J. Chem. Phy., 17(10), 893.

Le Geros, Racquel Zapanta and Le Geros, John P. (1972) J. Crystal Growth, 13/14, 476.

Lendvay, E. (1971) J. Crystal growth, 10, 77.

Le Poole, J.B. (1947) Phillips Tech. Rev., 9, 33.

Lewis, D.G. and Schwertmann, U. (1979) Clay. Miner., 14, 115.

Lewis, D.G. and Schwertmann, U. (1980) J. Colloid Interface Sci., 78, 543.

Liaw, H.M. and Eaust, J.W. Jr. (1972) J. Crystal Growth, 13\14, 471.

Liesegang, R.E. (1912) Z. Chem. Ind. Kolloide, 10, 273.

Liesegang, R.E. (1914) Z. Physik. Chem., 88, 1.

Liesegang, R.E. (1926a) in "Colloid Chemistry", (Alexander, J. ed.), Chemical Catalogue Co., New York, p. 783.

Liesegang, R.E. (1926b) in "Colloid Chemistry", (Alexander, J. ed.), Chemical Catalogue Co., New York, p. 251.

Lim, C.H.; Jackson, M.L.; Koons, R.D. and Helmke, P.A. (1980) Clays Clay Miner., 28, 223.

Lorenz, M. and Kempe, G. (1983) J. Signalau f zei chnungsmater, 11(1), 69.

Lorenz, M. and Kempe, G. (1984) J. Signalau f zei chnungsmater, 12(4), 269.

Luft, J.H. (1961) J. Biophys. Biochem. Cytol., 9, 409.

Mackay, A.L. (1960) Mineral Magn., 32, 545.

Mackenzie, R.C.; Follett, E.A.C. and Meldau, R. (1971) in "The Electron-Optical Investigation of Clays", (Gard, J.A. ed.), Mineralogical Soc., London, p.315.

Mandelbrot, B.B. (1982) "The Fractal Geometry of Nature", Freeman, San Francisco.
(See also Jullien & Botet (1987) "Aggregation & Fractal Aggregates", World Scientific, Singapore, p. 24).

Manning, P.G.; Lum, K.R. and Birchall, T. (1983) Can. Mineral., 21, 121.

Maoloe, O. and Birch-Andersen, A. (1956) Symp. Soc. Gen. Microbiol., 6, 261.

Marks, L.D. Howie, A. and Smith, D.J. (1980) Inst. Phys. Conf. Ser., 52, 397.

Marriage, E. (1981) Wied. Ann., 44, 507.
(See Henisch, 1970)

Matashige, O. and Yusuke, U. (1979) Nippon Kagaku Kaish, 5, 624.

Matijević, E.; Sapiesko, R.S. and Melville, J.B. (1975) J. Coll. Interface Sci., 50(3), 578.

Matijević, E.; and Scheiner, P. (1978) J. Coll. Interface Sci., 63(3), 509.

Matijević, E. (1981) Acc. Chem. Res., 14(1), 22.

Matsushita, M.; Sano, M.; Hayakawa, Y. Honjo, H. and Sawada, Y. (1984) Phys. Rev. Letters, 53, 286.

Mattock, G. (1954) Acta Chem. Scand., 8, 777.

Meakin, P. (1983) Phys. Rev., A27, 604.

Miller, E.B. (1931) in "Colloid Chem.", (Alexander, J. ed.), The Chemical Catalog Co., New York.

Mulay, L.N. and Selwood, P.W. (1955) J. Am. Chem. Soc., 77, 2693.

Mullin, J.W. (1961) "Crystallization", Butterworths, London.

Mullin, J.W. (1975) in "Crystal Growth", (Pamplin, B.R. ed.), Pergamon Press, Oxford, Vol. 6.

Murad, E. and Schwertmann, U. (1980) Am. Mineral., 65, 1048.

NASA, (1977) "Zero-G Technology", in Apollo-Soyuz Pamphlet, US. Govt. Printing Office, Washington, D.C., 8, 41.

Nicholas, J.F. (1968) Austral. J. Phys., 21, 21.

Nickl, H.J. and Henisch, H.K. (1969) J. Electrochem. Soc., 116, 1258.

Nobuoka, S. and Ado, K. (1966) Kogyo Kagaku Zasshi, 69 (10), 1899.

Nobuoka, S.; Ado, K. and Takahashi, A. (1967) Kogyo Kagaku Zasshi, 70(2), 212.

O´Conner, J.J.; Di Pietro, M.A.; Armington, A.F. and Rubin, B. (1966) Nature, 212, 68.

O´Conner, J.J. and Armington, A.F. (1967) J.crystal Growth, 1, 327.

Ostwald, W. (1897) "Lehrbuch Allgemeine Chemie", 2 ii, 444.
(See Mullin, J.W. (1961) "Crystallization", Butterworths, London, p. 26).

Ostwald, W. (1900) Z. Phys. Chem., Leipzig, 34, 295.
(See Mullin, J.W. (1961) p. 33).

Parker,S.G. and Pinnell, J.E. (1968) J. Crystal Growth, 3/4, 490.

Parks, G.A. (1965) Chem. Rev., 65, 177.

Patel, A.R. and Bhat, H.L. (1972) J. Crystal Growth, 12, 288.

Paterson, R. and Rahman, H. (1983) J. Colloid Interface Sci., 94, 60.

Paterson, R. and Rahman, H. (1984) J. Colloid Interface Sci., 97(2), 423.

Pechenyuk, S.I.; Rogachev, D.L.; Kasikov, A.G.; Popova, R.A.; Zalkind, O.A. and Kuz´mich, L.F. (1985) Zh. Neorg. Khiw., 30(2), 311.

Petrovskaya, N.B. (1975) "Hypergene Iron Oxides in Geological Processes", Nauka, Moscow, Fig. 74,77, p. 186.

Plank, C.J. (1947) J. Colloid Sci., 2, 413.

Prasad, S.V.S. and Rao, V. Sitakara (1984) J. Mater. Sci., 19(10), 3266.

Riecke, W.D. (1961) Optik, 18, 373.

Russell, J.D. (1979) Clay Miner., 14, 109.

Saleh, A.M. and Jones, A.A. (1984) Clay Miner., 19(5), 745.

Schneider, W. (1984) J. Comments Inorg. Chem., 3(4), 205.

Schugar, H.; Walling, C.; Jones, R.B. and Gray, R.B. (1967) J. Amer. Chem. Soc., 89, 3712.

Schwertmann, U. and Taylor, R.M. (1972) Clays Clay Miner., 20, 159.

Schwertmann, U. and Fechter, H. (1982) Clay Miner., 17(4), 471.

Schwertmann, U. and Murad, E. (1983) Clays Clay Miner., 31(4), 277.

Smith, C.S. (1965) "A History of Metallography", The University of Chicago Press, Chicago.

Smith, D.J.; Cosslett, V.E. and Stobbs, V.M. (1981) Inter. Sci. Rev., 6, 155.

Šolcová, A.; Šubrt, J.; Vinš, J.; Hanousek, F.; Zapletal, V. and Tlaskal, J. (1981) Collect. Czech. Chem. Commum., 46(3), 3049.

Spence, J.C.H. (1981) "Experimental High-Resolution Electron Microscopy", Clarendon Press, Oxford.

Steinberger, I.T.; Alexander, E.; Brada, Y,; Kalman, Z.H.; Kiflawai, I. and Mardix, S. (1972) J. Crystal Growth, 13/14, 285.

Strom, J.G. and Wonjun, H. (1980) J. Pharm. Sci., 69(11), 1261.

Strong, C.L. (1962) Sci. Am., 206, 155.

Sudo, T.; Shimoda, S.; Yotsumoto, H. and Aita, S. (1981) "Developments in Sedimentology, Electron Micrographs of Clay Minerals", Kodansha Ltd., Tokyo, Vol. 31.

Suri, S.K.; Henisch, H.K. and Faust, J.W. Jr. (1970) J. Crystal Growth, 7, 277.

Sutherland, D.N. (1970) Nature, 226, 1241.

Sylva, R.N. (1972) Rev. Pure Appl. Chem., 22, 115.

Takiyama, K. (1981) Bunseki Kagaku, 30, 32.

Takiyama, K. (1987) in " Proceedings Electron Microscopy Society of America", (Bailey, G.W. ed.), 45th Annual Meeting, Baltimore, 2-7 August, 1987.

Taylor, R.M.; Self, P.G. and Fitzpatrick, R.W. (1987) Applied Clay Science, 2, 41.

Tiginyanu, Ya.D; Moravskii, A.P.; Shuvalov, V.F.; and Berdnikov, V.M. (1983) Kinet. Katal., 24(1), 11.

Towe, K.M. and Bradley, W.F. (1967) J. Colloid Interface Sci., 24, 384.

Trendelenburg, P. (1919) Biochemische Z. Band, 95, 146.

Trimm, D.L. (1978) Pure Appl. Chem., 50, 1147.

Tschernoff, D.K. (1879) "Investigations on the Structure of Cast Ingots." Zapinski Imperatorskago Russkago Tekhnicheskago Obshestva, Eng. Trans. W. anderson, Proc. Inst. Mech. Engrs., 1880.

Van Rheenen, P.R.; McKelvy, M.J. and Glaunsinger, W.S. (1987) J. Solid State Chem., 67, 151.

Venables, J.A. and Price, G.L. (1975) in " Epitaxial Growth", (Matthews, J.W. ed.), Academic Press, New York, p. 383.

Von Borries, B. and Ruska, E. (1939) Z. wiss Mikroscop, 56, 317.

Von Weimarn, P.R. (1925) Chem. Rev., 2, 217.

Walton, A.G. (1963) Anal. Chim. Acta., 29, 434.

Watari, F.; Delavignette, P.; Van Landuyt, J. and Amelinckx, S. (1983) J. Solid State Chem., 48(1), 49.

Weiser, H.B. and Milligan, W.O. (1935) J. Phys. Chem., 39, 25.

Werner, A. and Pfeiffer, P. (1907) Ber., 40, 272.

White, D. (1982) "Electron Microscope Studies of Redispersion Reactions." Ph.D. Thesis, Department of Chemistry, University of Glasgow.

Witten, T.A. and Sander, L.M. (1981) Phys. Rev. Lett., 47, 1400.

Witten, T.A. (1983) Phys. Rev., B27, 5686.

Wolf, R.J. and Joy, D.C. (1971) in "Proc. 25th Anniv. Meeting EMAG, (Nixon, W.C. ed.), Inst. Phys. Conf. Ser., London, 10, 34.

Woodhead, J.L. (1980) Sci. Ceram., 10, 169.

Woodhead, J.L. and Segal, D.L. (1984) Chem. Br., 20, 310.

Yong, R.N. and Ohtsubo, M. (1987) Appl. Clay Sci., 2(1), 63.

Zolotovskii, B.P.; Krivoruchko, O.P. and Buyanov, R.A. (1977) in "Tezisy Dokl. Soveshch. Kinet. Mekh. Reakts. Tverd. Tele, 7th", (Lyakhov, N.Z. ed.), Akad. Nauk. SSSR, 3, 36.
(Chem. Abst. 89: 31371P).

Zworykin, V.K.; Morton, G.A.; Ramberg, E.G.; Hillier, J. and Vance, A.W. (1945) "Electron Optics and the Electron Microscope", John Wiley & Sons, New York.